THÈSE

En vue de l'obtention du

DOCTORAT DE L'UNIVERSITÉ DE TOULOUSE

Délivré par **l'Institut Supérieur de l'Aéronautique et de l'Espace**
Spécialité : Traitement du signal

Présentée et soutenue par **Paul THEVENON**
le 19 novembre 2010

Interface air pour systèmes de navigation en bande S : étude détaillée des signaux OFDM

S-band air interfaces for navigation systems : a focus on OFDM signals

---

JURY

M. Jean-Claude Belfiore, président, rapporteur
M. Michel Bousquet, co-directeur de thèse
M. Olivier Julien
M. Marco Luise, rapporteur
M. Christophe Macabiau, directeur de thèse
M. Gérard Pousset

École doctorale : **Mathématiques, informatique et télécommunications de Toulouse**

Unité de recherche : **Équipe d'accueil ISAE-ONERA SCANR**

Directeur de thèse : **M. Christophe Macabiau**
Co-directeur de thèse : **M. Michel Bousquet**

Abstract

Positioning in urban or indoor environment is a hot topic, either due to regulations such as the E911 requiring US mobile telecommunication operators to be able to locate their subscribers in case of emergency, or due to the market development, with the extension of location-based services targeting the mass market concentrated in metropolitan areas. In urban or indoor areas, it is generally recognized that satellite-based positioning systems are not suitable (alone) to provide a continuous, reliable and accurate position to the user. Therefore, alternative positioning techniques may be useful to complement or replace satellite positioning in these environments. This PhD study has studied the possibility of using a mobile TV system based on the DVB-SH standard as system of opportunity for positioning.

The advantages of using a DVB-SH system for positioning are multiple. First, such system has a good availability in metropolitan areas, including indoor. Secondly, the emitters are synchronized and their density should be sufficient to track signals from several emitters simultaneously. This opens the possibility of using timing measurements from several emitters to find a position by tri-lateration. Also, the large bandwidth of the TV signal, required for the transmission of video content, should be beneficial for the accuracy of the timing measurements and for the robustness against multipaths. Therefore, DVB-SH system seems to be an interesting candidate as system of opportunity for positioning.

However, several challenges are to be solved for such a solution to be relevant. First, the signals propagate in the urban environment, which creates challenging conditions for positioning such as strong power fading, blockage of the desired line-of-sight signal or large echoes. Secondly, the DVB-SH standard uses an OFDM modulation, which has not been studied for positioning purpose. Therefore, techniques for fine tracking of the first received signal replica will have to be developed. Finally, a particularity of modern broadcast system is the use of a Single Frequency Network, in which all emitters send the same signal on the same carrier frequency. Therefore emitter identification in a Single Frequency will be another issue to be solved.

This PhD study has proved the feasibility of positioning using DVB-SH signals. The main contributions of this work are the propositions of (1) an OFDM signal delay tracking method working in urban propagation channels, and (2) a modification to the network deployment permitting emitter identification and (3) a first assessment of the position accuracy using the proposed algorithms. These two methods have very low impact on the initial TV broadcasting service if the right set of signal parameters is chosen: no signal modification is required and the network deployment modification uses a feature already present in the DVB-SH standard.

The positioning method was simulated using real urban propagation channel measurements. The obtained position has root mean square error of 40m. The main error contribution comes from tracking a non-line-of-sight signal. Further work would be required to deal with this issue, which would lower the position root mean square error to 7m, which has been locally observed in the simulation for good tracking conditions.

Index

Table of acronyms

3GPP	3rd Generation Partnership Project
8VSB	8-level Vestigial Sideband Modulation
ANFR	Agence Nationale des Fréquences (French Regulatory Agency)
ARNS	Aeronautical Radionavigation Service
ATSC	Advanced Television Systems Committee
BPSK	Binary Phase Shift Keying
CEPT	Conférence Européenne des Administrations des Postes et des Télécommunications (European Conference of Postal and Telecommunications Administrations)
CIR	Channel Impulse Response
cCIR	Combined Channel Impulse Response
CTF	Channel Transfer Function
DAB	Digital Audio Broadcasting
DLL	Delay-Lock Loop
DMB	Digital Multimedia Broadcast
DoP	Dilution of Precision
DVB	Digital Video Broadcast
DTV	Digital Television
EIRP	Equivalent Isotopically Radiated Power
EMLP	Early Minus Late Power
ESA	European Space Agency
ETSI	European Telecommunications Standards Institute
FER	Frame Error Rate
FFT	Fast Fourier Transform
GNSS	Global Navigation Satellite System
HDoP	Horizontal Dilution of Precision
iFFT	Inverse Fast Fourier Transform
IP	Internet Protocol
ISDB	Integrated Services Digital Broadcasting
ISI	Inter-Symbol Interferences
ITU	International Telecommunication Union
LOS	Line of Sight
ME-DLL	Multipath Estimating Delay Lock Loop

MIMO	Multiple Input Multiple Output
NLOS	Non Line of Sight
NLS	Non-linear Least Square
OFDM	Orthogonal Frequency Division Multiplexing
QAM	Quadrature Amplitude Modulation
QPSK	Quadrature Phase-Shift Keying
PRBS	Pseudo-Random Binary Sequence
RDSS	Radiodetermination-Satellite Service
RNSS	Radionavigation-Satellite Service
SFN	Single Frequency Network
SNR	Signal to Noise Ratio
SNIR	Signal to Noise and Interference Ratio
ToA	Time of Arrival
TPS	Transmission Parameter Signaling
UMTV	Unlimited Mobile TV
WRC	World Radiocommunication Conference

Table of figures

1 Introduction

1.1 Thesis background and motivations: urban and indoor navigation using signals of opportunity

As of the time of this study (2007-2010), the positioning market is truly exploding thanks to mass-market urban positioning. The number of GPS receivers sold in smart phones between 2006 and 2009 was greater than any other types of GPS receivers since the beginning of GPS[1]. However, the urban and indoor environments are still a challenge for satellite navigation systems, due to the frequent signal blockage by buildings or due to the intense multipath encountered in metropolitan areas. The performance degradations due to the urban or indoor environment affect positioning in terms of availability, accuracy, continuity and reliability.

Several leads have been followed by researchers in order to permit positioning for urban and indoor users:

- **Modification to GNSS.** This category comprises (1) receiver-side signal processing, such as longer integration period, new multipath-resistant modulation (BOC), adaptive DLL noise bandwidth, etc. and (2) system-level GNSS upgrades, such as the Assisted-GNSS, multi-constellation receivers, the presence pilot channels in the modernized GNSS, introduction of new satellite signals in new bands (on this topic, please refer to Annex A), etc. A good overview of this field is available in [Lachapelle 2004].
- **Other sources of positioning sensors**:
    - **Inertial sensors (gyro, accelerometers), magnetometers, vision-based sensors.** This type of sensor is complementary to GNSS and can provide aiding in GNSS signal tracking and/or position calculation. They can also increase positioning continuity in case of short GNSS signal outage.
    - **Dedicated radiolocation systems**. These systems are deployed in order to provide a positioning service on a given coverage. Among the wide range of existing solutions, there exist GNSS pseudolites, Ultra-Wideband (UWB) emitters, fixed RFID tags, etc. The main drawback of this type of solution is its high *cost* due to the deployment of extra infrastructure for a limited service coverage.
    - **Systems or signals of opportunity.** This type of solution consists in exploiting existing systems or signals, which have not been initially deployed for positioning. These are typically radio-communication systems, such as mobile communication systems or broadcast systems.

The field of this PhD study is set in the last quoted category.

Positioning using signals of opportunity has been a hot topic in the last years, especially since the E-911 regulation was adopted [E911 2000]. This US regulation requires that the telecommunication operators can locate their subscribers with an accuracy and reliability summarized in the table besides. Similar regulations have been adopted in the EU, but with no quantified accuracy targets yet [E112 2003].

[1] ION GNSS 2009 Plenary Session. Van Diggelen, F. Broadcom Corp.

Table 1 - FCC requirements for E911 due by September 2012 [E911 2000]

Required reliability	Required accuracy
For 67% of calls	50m
For 95% of calls	150m

The advantages of this solution are listed below. A similar analysis is available in [Raquet 2007]:

- **Availability**: Signals of opportunity are largely available in urban centers - including indoor - which is where most mass market users are located (pedestrian, urban vehicular). This could potentially reduce the **cost** for providing a positioning service since most infrastructure would already be available to provide the telecommunication service. Also, from a system deployment point of view, terrestrial networks are more accessible, ie. they can be more easily updated, modified and/or tested. Finally, most systems of opportunity are designed in order to provide their service indoor.
- **Variety of systems**: systems of opportunity use a wide variety of signals (modulation, bandwidth, carrier frequency) and network deployment (UHF networks for TV or radio, cellular network, indoor access points, etc.). If the sources of positioning data are not correlated, this can potentially provide some kind of diversity gain. For example, if a satellite path is blocked at a particular location, it may not be the case for the path taken by a Signal of Opportunity coming from a terrestrial emitter.
- **Integration of positioning and telecommunication services**: as a receiver would be able to provide both kind of services, one could imagine innovative service hybridization where telecommunication would help navigation (through the efficient transfer of data, similar to Assisted GPS) and conversely (location-assisted hand-offs or radio resource management, fine synchronization of terminals, etc.). This could also enable a cheap location-based service platform thanks to the use of a common RF front-end or signal processing functions for both the telecommunication and positioning service.

Finally, systems of opportunity are complementary with GNSS. Indeed, GNSS will remain the main positioning solution for terrestrial users in peri-urban or rural areas where systems of opportunity are less present. On the contrary, in urban areas, systems of opportunity will be able to take advantage of their attractive availability in order to provide a positioning service. In other words, systems of opportunity are not competing directly with GNSS, but will rather provide a complementary positioning solution.

Drawbacks, or rather challenges of using signals of opportunities are:

- **Design is not optimized for positioning**: the performances of the positioning service will be obtained through a "best effort" approach, making the most of the existing systems that have not been designed for positioning purpose. This can be illustrated at the signal level (CDMA codes with short length, OFDM modulation, etc.) or system level (only one emitter covering a given zone, no synchronization between the emitters, etc.).
- **Multipath/masking**: most considered systems of opportunity are using terrestrial emitters. Consequently, the transmission between those emitters and a receiver in an urban environment will be affected by intense multipath, local heavy signal fading and probably non-line-of-sight propagation. This could be a problem if geometric positioning principles such as trilateration are used.

- **Constraints wrt the telecommunication services**: Modifications to the systems should be kept at minimum so as not to interfere with the telecommunication signals, and also to keep the additional cost of the positioning service provision at a minimum.

Several systems of opportunity have been studied or are currently being studied for positioning. The following sections will provide a brief overview of the State of the Art in this domain.

1.1.1 mobile communication systems

The E911 regulation has initiated the research on positioning using a mobile telecommunication networks. Three techniques of user terminal positioning have been standardized in the 3G mobile systems [Zhao 2002]:

- Cell ID,
- Observed Time Difference of Arrival, and
- A-GPS.

The first two techniques uses state variables that are measured within the mobile telecommunication system. Therefore, using them for positioning is done at very low additional cost.

The **Cell ID** positioning technique consists in using the information of the currently serving emitter for location. Indeed, a mobile phone - even if idle - regularly exchanges information with the nearest emitter in order to be able to rapidly respond to a call. By knowing the coverage of each cell, which is an information required for efficient network deployment, the operator knows the approximate position of its users. The Cell ID accuracy depends on the size of the 2G / 3G cell, which can vary between 150 m in cities and 30 km in rural areas.

The **Observed Time Difference of Arrival** technique consists in estimating the relative time difference between the reception of a specific data packet from different emitters. These time differences can be converted into an hyperbolic position locus, and with enough time differences, a non-ambiguous position can be obtained. Issues associated to this technique are hearability of several emitters and absence of emitters' synchronization.

The hearability issue can be solved by introducing coordinated idle periods of transmission at neighboring emitters. Emitters successively interrupts their emission, so that in the vicinity of this emitter, the signal from the other emitters can be received. However, this results in some system capacity loss.

If the emitter are not synchronized, this technique requires some reference station to measure the synchronization of the emitters and provide some correcting data. These reference stations have limited coverage (generally 1 station is required for every 4 or 5 emitters), so deploying this solution over large areas is a heavy additional cost.

The accuracy obtained by the Observed Time Difference of Arrival depends on the emitters' configuration and on the multipath environment. In urban scenarios, the 67% position error varies between 30m and 2000m depending on the multipath intensity scenario [Ludden 2000] [Porcino 2001].

The performances obtained by using these techniques are not sufficiently accurate, which has led to the standardization of A-GPS as the unique means to comply with the FCC E-911 regulations.

The work achieved for locating a user in the 3G standards will carry on in future mobile communication systems and is an integrated part of the definition next generation mobile communication standards, such as LTE or WiMax [Venkatachalam 2009]. Similar techniques to the existing ones provisioned for 3G can be used. The results presented in this manuscript may also contribute to some alternative solutions.

1.1.2 WiFi

For indoor positioning, WiFi positioning has been considered due to the increasing ubiquity of WiFi signal inside buildings. The most successful WiFi positioning technique is called **fingerprinting** [Bahl 2000]. It consists in comparing the signal strength of nearby WiFi hotspots to a large up-to-date database created during a calibration phase. Generally, this principle is limited to a limited area such as a building, due to the database creation cost. This solution is put at risk if the WiFi hotspot database is not up-to-date, for example, if a WiFi router has been moved or removed.

An example of the use of this technique is the Ekahau Positioning Engine, a commercial service. The mean error achieved by the Ekahau Positioning Engine in indoor environment is 2.5m during quiet period or 12.8m during busy period (people moving around). During 95% of the trials, the error was respectively below 8.8m and 16.5m [Gallagher 2009].

WiFi positioning in ***outdoor*** urban environment has also achieved widespread adoption through the introduction of such service in the iPhone[2] and major mobile phone operating systems, thanks for example to the commercial Skyhook Wi-Fi Positioning Service. The cost for updating the database for whole cities on a worldwide scale is quite expensive: [Geomode 2002] assesses this cost between 3 to 10 man.hours/km² depending on the level of accuracy wanted for the measurements, but commercial interest seems to be able to compensate such costs. The error was measured to have a mean around 50m and a standard deviation between 40 and 60m during trials in urban canyons [Gallagher 2009].

The advantage of this fingerprinting technique is that the measurement is not dependent on geometry, and therefore, will not be affected by multipath. On the contrary, fading or multipath propagation will improve the accuracy of the positioning, by making the local signature of the measurement more correlated to a particular location.

However, the main disadvantage of this technique is the requirement of costly database, which has to be updated regularly. In addition, in this kind of system using large databases, the position calculation is often done in a remote location server, meaning that a communication link must exist between the sensor and the server.

1.1.3 Digital broadcast systems

Another class of positioning method using signals of opportunity is the use of broadcast systems.

Digital broadcast systems often employ powerful emitters and a relatively-low carrier frequency in order to have a large coverage with few emitters. For example, the TV emitter at the Pic du Midi in the Pyrenean mountains at the border between France and Spain, is emitting with a maximum

[2] http://www.skyhookwireless.com/press/skyhookapple.php

power of 13 kW EIRP[3] (50 kW is planned after the digital switch-over), and is expected to service users up to Bordeaux, 200 km away. With adequate signal processing, several TV emitters may be visible from a given location. This was demonstrated in [Rabinowitz 2005], with a field study in the San Francisco area.

Timing-based measurements can be derived for estimating a pseudo-range measurement between the receiver and several emitters, by applying correlation-based techniques using some pilot sequences already present in the signal for synchronization.

Timing-based positioning requires having a common system clock between all emitters and the receiver. This can be achieved by two ways: (1) the emitters are synchronized to a common system clock, or (2) some reference stations are required in order to measure the emitter clock corrections, which will then have to be transmitted to the receiver. The latter solution has been adopted by Rosum, which uses digital TV signals from the ATSC standard and reference stations to obtain a position estimate with a bias of about 25m and a standard deviation of 20m in an indoor environment in San Francisco [Rabinowitz 2005]. The use of reference stations adds complexity to the system and is quite costly to deploy over a large area.

Synchronized networks begin to appear in some broadcast systems, which, depending on the synchronization level of the emitters may remove the need of a reference station for positioning, or at least reduce the error due to this issue. This is for example the case for the digital radio standard DAB, which uses a Single Frequency Network (SFN) of emitters, in which every emitter transmits the same signal on the same carrier frequency and in a synchronized way. Trials with simple signal processing have led to a mean position error of 150m, in a location where the HDOP condition was poor [Palmer 2009]. DAB signals also have a limited bandwidth of 1537 kHz.

Beside the 2 presented broadcast systems (ATSC and DAB), a number of other broadcast standards exist all over the world, such as the European DVB-x family and the competing DMB-x family, or the Japanese ISDB standard for digital TV systems. A similar list could be drawn for digital radio systems. All these systems may be used as a system of opportunity in order to provide a positioning service.

1.1.4 Choice of DVB-SH system

In this study, the choice of the system of opportunity used for positioning is a system based on the **DVB-SH** standard (**Digital Video Broadcasting - Satellite to Handheld**).

DVB-SH is a European standard for mobile TV broadcasting to handheld terminals [DVB-SH 2008-1]. In comparison with the other broadcast systems presented in the previous section, one particularity is that the signals are transmitted at a carrier frequency of 2.2 GHz. This frequency is much higher than traditional broadcast system usually using carrier frequencies below 1 GHz. This permits to reduce the receivers' antenna size, which is required to provide a mobile service. In turn, the use of this carrier frequency requires a denser network of emitters due to higher free space and in-building penetration signal power losses.

At the beginning of the PhD study (2007-2008), DVB-SH was not fully standardized, but showed good promises for addressing the mobile handheld market. At the end of the PhD study (2010), the

[3] http://www.csa.fr/infos/autorisations/gabarits.php?plan=trans

DVB-SH is fully standardized, but pains to reach wide acceptance. This may be due to the difficulties encountered by the DVB-SH "flagship" satellite W2A payload [Forrester 2009], or due to the network operators defiance towards the unproven mobile TV service. However, even with these commercial uncertainties, DVB-SH is well representative of a new generation of broadcasting network. Even if such standard is not widely deployed in the future, it is a good basis for studying the possibilities proposed by such systems, and results found in this study may be applicable to other communication standards sharing similarities with DVB-SH.

The DVB-SH standard uses a network of emitters working in Single Frequency Network configuration, meaning that the emitters are synchronized. This opens the way to using a tri-lateration positioning technique, using timing-based measurements to calculate a pseudo-range between the receiver and the emitters. Also, SFN are designed so that the coverage of individual emitter overlaps, thus providing potentially several visible emitters at any point of the service coverage. This means that there may be sufficiently enough emitters to allow position calculation (3 emitters required for 2D positioning).

As video transmission requires large data throughput, the signal bandwidth is large: several MHz. This will be profitable for timing-based measurements, whose accuracy depends on the signal bandwidth. Also, large bandwidth may permit fine multipath mitigation techniques.

However, several challenges are identified for the use of such system for opportunitistic positioning. First, the urban propagation channel between a terrestrial emitter and a terrestrial receiver creates large fading, echos of the received signal and masking of the line-of-sight channel. This last point is particularly problematic, since the tri-lateration technique assumes a pseudo-range measurement following the line-sight path.

Then, the signal uses the Orthogonal Frequency Division Multiplexing technique. This technique is well-suited for data transmission in multipath environment. In particular, it works in loose time synchronization conditions, while fine time synchronization is required for pseudo-range estimation based on timing measurement.

Another challenge is that the use of a SFN means that emitters will be difficult to identify, since they all emit the same signal on the same carrier frequency and in a synchronized way. Emitter identification is essential in order to position the receiver with a tri-lateration technique.

From this short introduction on DVB-SH, it can be seen that a system based on this standard will provide interesting features for geometric positioning via tri-lateration technique. However, it also raises challenges requiring further investigations. It seems therefore an ideal candidate for the basis of a PhD study.

The choice of DVB-SH as System of Opportunity for positioning can be summarized by the following reasons:

- ***Synchronized network of emitters*** thanks to the use of SFN. This enables timing-based pseudo-range measurements without the need of costly reference stations.
- ***Coverage in urban centers and indoor*** targeting mass market audience (handheld and in-vehicle terminals) thanks to a dense network of emitters composed of a geostationary satellite for continent-wide rural or sub-urban areas, completed by terrestrial gap-fillers in urban areas.

- ***Convergence with other telecommunication systems*** at the receiver design level thanks to the carrier frequency at 2.2 GHz, close to other telecommunication bands (e.g. 3G band at 2.1 GHz, WiFi band at 2.45 GHz). Indeed, such "convergence receiver" could share the RF front-end and/or some signal processing functions (synchronization, data demodulation, etc.) between both services.
- ***Wideband signals***. Signal bandwidth up to 8 MHz are foreseen, which should be beneficial for positioning accuracy and multipath mitigation.
- ***OFDM modulation*** is used as air interface. This modulation is used in many new or upcoming telecommunication standards and has not yet been studied for positioning purpose (at least, at the beginning of the PhD study, except for an announcement from Rosum made in June 2008[4]). There is a strong chance of reuse of this work in other OFDM-using standards.

The work done in this study may be re-used without modifications, or with minor adaptations to other communication standards using an OFDM air interface and/or SFN.

Almost all recent terrestrial broadcasting standards for TV or radio use OFDM as air interface, except for the US digital TV standard ATSC which uses an 8VSB modulation. The main OFDM-using broadcasting standards are DAB, DVB-T/H/SH, DMB-T/H (Korea), ISDB (Japan). Every one of them has provisioned the use of SFN, as it is a spectrally efficient method to cover large service area. Interestingly, ATSC also provisions the use of SFN.

Other mobile communication standards use OFDM as air interface, such as WiMAX or 3GPP Long Term Evolution. In addition, modern mobile communication standards usually provision the use of ***soft handovers***, which consists in emitting the same signal from several emitters when a receiver move between those emitters [Viterbi 1994]. This allows providing increased signal power in the cell range limit. This soft handover may create a local, temporary single frequency network for a dedicated user, in which our positioning method could be used.

1.2 Thesis objectives

The overall objective of the thesis is to investigate the feasibility of positioning using a DVB-SH-based system as system of opportunity, and to assess the reachable performances.

About the decided positioning principle, the trilateration technique was chosen over the fingerprinting technique (e.g. used with WiFi systems) since it seemed to us that such technique required a too costly database to be reliable.

The foreseen positioning technique is based on a tri-lateration technique, using several pseudo-range measurements between the receiver and emitters and the knowledge of the emitters' position, to compute the receivers position. The pseudo-range measurements are estimated from Time of Arrival (ToA) measurements. This requires that the emitters are synchronized (or equivalently, that the emitter asynchronicity is monitored and transmitted to the receiver), which we assume is the case in the Single Frequency Network encountered in the DVB-SH system. Also, this principle assumes that the receiver is able to identify the signals it receives, ie associate a pseudo-range measurement with its emitter of origin.

From this short review of the tri-lateration principle, several objectives arise:

[4] http://www.rosum.com/pdfs/Rosum_NationalGridWireless_DVB-H_TechnologyTrial.pdf

- First, the received signal has to be modelled. This requires to understand the OFDM modulation and to model the effects of the urban propagation model;
- Secondly, some acquisition and tracking methods have to be derived in order to obtain the ToA measurements. These signal processing methods will have to be adapted to the OFDM air interface and to the particularities of the urban propagation model;
- Thirdly, an emitter identification technique has to be implemented.

Once a solution has been proposed for each of this issue,

- a complete simulator of the proposed positioning technique will be used in order to assess the performances of this technique. In particular, the simulator will be able to generate the received DVB-SH signal and to process it in order to obtain a pseudo-range and identify it. A particular attention will be brought to the modelling of the multipath, since we expect the in Non-Line-of-Sight (NLOS) bias to be the main error contributor.
- Finally, the feasibility of the overall positioning solution will be assessed, with a first overview of the reachable positioning performances. Also, the dependency of these performances with the signal parameters or network deployment of the DVB-SH will be studied.

The objective of this thesis is quite exploratory: no previous study of precise positioning using OFDM signals and SFN have been found during the literature review. This thesis focuses on proving the feasibility of such positioning service by finding some solutions to all the foreseen issues. In particular, two major challenges inherent to the choice of DVB-SH as system of opportunity have to be solved:

1. **Fine delay estimation of OFDM signals in urban or indoor environment**. This is particularly challenging since one of OFDM advantages - as telecommunication modulation - is its ability to work under loose synchronization conditions. Also, the urban and indoor environments are difficult propagation environments, where intense multipaths occur. The signal processing methods will have to try identifying and tracking the first incoming signal replica, which would yield the closest pseudo-range to the Line-Of-Sight (LOS) path. Yet, this first signal replica may be greatly attenuated compared to other replicas or absent due to the reception of the signal in NLOS conditions.
2. **Emitter identification in an SFN**. The principle of an SFN is to create artificial signal replicas coming from several emitters, that the receiver is able to combine in order to increase the useful signal power. For the receiver, the origin of the signal is unknown (and unnecessary for telecommunication purpose), since every emitter transmit exactly the same signal on the same carrier frequency and in a synchronized way. Yet, in order to calculate a position from different pseudo-range, the receiver has to know to which emitter each pseudo-range is associated.

As with every positioning system of opportunity, some modifications may be required in order to provide a positioning service. These modifications should be kept at minimum in order to limit the potential degradation brought by the positioning service on the telecommunication service, but also to remain as close as possible to the original system described in the DVB-SH standard, so that potential system operators can use the standardized processes and off-the-shelves equipments with minimum additional cost or risks.

1.3 Thesis Contributions

The 2 mentioned objectives of the thesis have been reached. More particularly:

- **A pseudo-range estimation method working in multipath environment**. This method uses the pilot sub-carriers that are already present in the DVB-SH signal to obtain an estimate of the channel impulse response (CIR). From this CIR estimate, the main peaks of delays of the main peaks are extracted and then finely tracked thanks to several delay-lock loops running in parallel. In order to maximize the chance of detecting the earliest signal replica (closest to the LOS path), the whole process is re-launched periodically. In order to keep the number of running DLL low, some DLL stopping schemes are also put in place.
- **An emitter identification method working in an SFN**. In order to be able to discriminate the origin of the incoming signal replicas, a system modification is proposed. It consists in introducing artificial delays between the emission of the emitters, so that the receivers does not receive signal replicas from 2 emitters at the same time. This does not hamper the telecommunication service as long as the delay does not exceed a duration associated to the DVB-SH signal parameters. This artificial delays will also permit to associate estimated delays with their emitters of origin from an approximate knowledge of the receiver position and emitter characteristics.

The pseudo-range estimation technique is mainly based on CIR measurements. Therefore, knowledge of the urban propagation channel is essential in order to define and optimize the pseudo-range estimation techniques. This thesis has therefore investigated several urban propagation channel models and used available channel-sounding measurements in order to validate the developed methods.

The combination of these 2 methods provides a full DVB-SH positioning method requiring no signal modification and a minor modification to the emitter's deployment (compatible with the DVB-SH standard). Assessments of the positioning method have been done in simulation using SFN channel sounding measurements done in urban environment. A root mean square position error of about 40m was simulated. This performance shall be improved by further researching many leads of improvements identified thanks to the experience gained in this study.

An extensive study has been done in order to assess every DVB-SH signal parameter sets provisioned in the standard, in order to see the compatibility of the positioning method with the telecommunication service and to identify the most interesting parameter sets and associated constraints. This will provide useful recommendations for DVB-SH operators wishing to assess the interest of providing a combined positioning and telecommunication service.

The work has been published in three communications in international conferences ([Thevenon 2008], [Thevenon 2009-1], [Thevenon 2009-2]). Also, this work has contributed to 2 other communications ([Serant 2010], [Mateu 2009]) and one technical article in Inside GNSS ("A Search for Spectrum, GNSS in S-Band", Sept-Oct 2010).

1.4 Thesis Outline

The current manuscript is structured as follows.

Chapter 2 describes the DVB-SH standard, both at system and signal level. The principles of Single Frequency Networks are presented, along with the model for the DVB-SH signal transmission that will be used in the rest of the study.

Chapter 3 describes the pseudo-range estimation method in the simplified case of a single emitter transmission. First, the specificities of the urban channel are modeled, since they will highly impact the choice of the techniques and the strategy used to estimate the pseudo-range. The method uses several different algorithms: a correlation to estimate the channel impulse response, the Matching Pursuit algorithm to obtain a rough estimate of several multipath delays in the CIR and a DLL to finely estimate the multipath delays. The strategy for using these 3 algorithms in the challenging urban multipath channel is described. This chapter ends with the presentation of simulation results.

Chapter 4 tackles the case of a multi-emitter system working in SFN configuration. Emitter discrimination requires a modification to the emitters' network by the introduction of different artificial delays at the emission of neighbor emitters. With this artificial delay introduced, it is then possible to use clustering algorithms to group the estimated delays by emitter. Simulations of pseudo-range estimation based on channel sounding measurements in an SFN are then presented.

Chapter 5 deals with the identification of emitters in SFN. Two identification techniques are compared: the emitter watermarking and the reverse positioning technique.

Chapter 6 presents conventional algorithms to calculate the position using the estimated pseudo-ranges. This will provide a hint of the reachable performances in the position domain.

Chapter 7 presents some recommendations to telecommunication operators to assist them in the provision of a positioning service using DVB-SH systems. First, guidelines for network deployments are provided. Then, the impact on the choice of the DVB-SH signal parameters on the positioning performances and the telecommunication service is provided.

Chapter 8 consists in the conclusion of this study and the interesting leads for further advancing this research topic.

2 Modelisation of a DVB-SH transmission

2.1 Introduction on DVB-SH

The DVB-SH (Digital Video Broadcasting - Satellite to Handheld) is an ETSI standard for broadcasting video content to mobile user using frequencies below 3 GHz. DVB-SH uses both geostationary satellite and terrestrial emitters in metropolitan areas in order to provide a continental coverage at lower deployment cost. The standard covers different sizes of signal bandwidth (1.7 MHz, 5 MHz, 6 MHz, 7 MHz and 8 MHz) to accommodate the different regulatory environments encountered all over the world. The standard is derived from the widely adopted DVB-T standard for fixed digital TV, and from the DVB-H standard for mobile digital TV.

DVB-SH has been supported by the French project TVMSL ("Télévision Mobile Sans Limites"), financed by the "Agence de l'Innovation Industrielle" and involving Sagem, Alenia, RFS, Philips, DiBcom, TeamCast, UDcast, CNRS, INRIA, CEA-LETI. Alcatel-Lucent has provided strong support to this standard and intends to deploy such system in the "Unlimited Mobile TV" (UMTV) project[5].

Since 2008, two standard documents are available [DVB-SH 2008-1] and [DVB-SH 2008-2], thus finalising all aspects of system definition, and opening the way to the commercial development of receiver chips.

As of 2010, 2 geostationary satellites have been launched with DVB-SH payload: ICO G1[6] over the USA and W2A[7] over Europe. Still, no DVB-SH terrestrial networks have been commercially deployed, although numerous test beds and demonstration have been done.

2.2 DVB-SH system architecture

2.2.1 System architecture

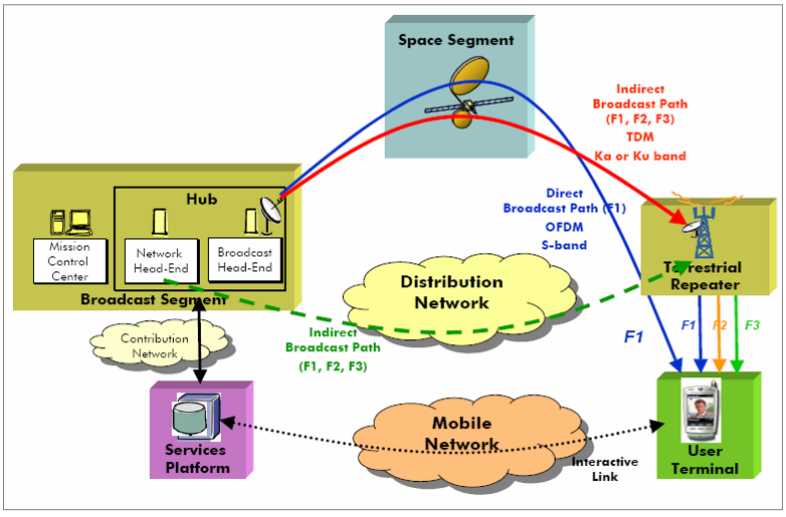

Figure 1 - System architecture of a DVB-SH system [Laine, 2007]

[5] http://www.alcatel-lucent.com/campaigns/mobileTV/
[6] http://investor.ico.com/releasedetail.cfm?ReleaseID=304683
[7] http://www.ses-astra.com/business/en/news-events/press-archive/2009/09-04-06/index.php

Figure 1 illustrates the architecture of a DVB-SH system. The system comprises:

- A **service platform**, which performs content adaptation and aggregates TV programs and rich multimedia services into IP service streams.
- A **broadcast segment**, which maps the IP service streams onto the satellite and terrestrial repeater radio resources
- A dedicated **GEO satellite** (e.g. W2A, 10°E, operated by Solaris Mobile Ltd, a joint venture between Eutelsat and SES Astra) that amplifies and convert the satellite radio signals from Ka/Ku band to S-band. These signals are transmitted directly to the terminals and provide a cost-effective continental coverage.
- A **network of terrestrial repeaters**, which receives service bundles from the broadcast segment either via satellite backhaul or via a terrestrial IP network and converts them onto the S-band terrestrial carriers for delivery to the terminals in zones where the satellite coverage is degraded, such as dense metropolitan areas and indoor environments. The terrestrial repeaters will also be able to broadcast additional local content, compared to the satellite stream.
- **User terminals**, which can decode the DVB-SH signals, and which are also likely to be compatible with 3G networks, thanks to the proximity between the frequency bands used by DVB-SH (2.2 GHz) and 3G networks (1.8 and 2.1 GHz).

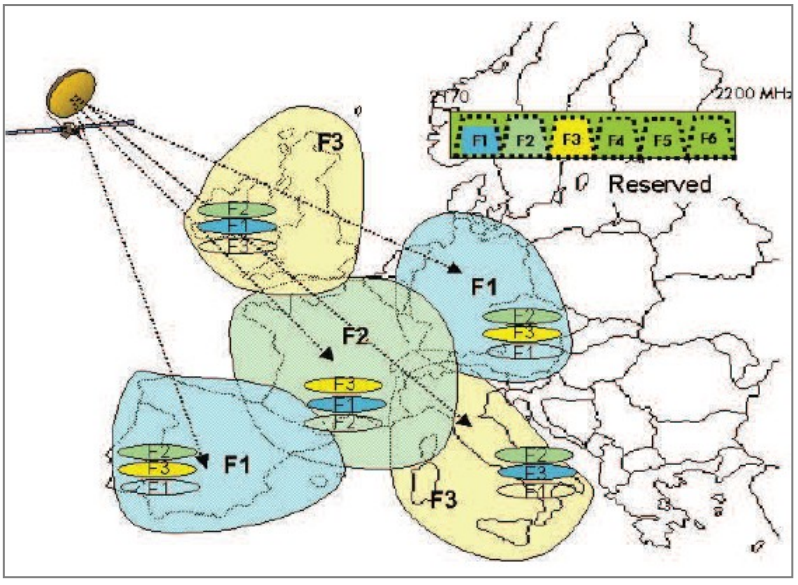

Figure 2 - Frequency sharing between satellite and terrestrial repeaters [Chuberre, 2006]

A European DVB-SH system intends to use the so-called “2 GHz MSS” downlink allocation (2170 - 2200 MHz), which will be available throughout Europe through a decision made by the European Commission in May 2009 [8]. This use of carrier frequency is much higher than traditional broadcasting system: for example, French digital TV uses carrier frequencies between 470 and 850 MHz. Using such higher carrier frequency permits to reduce the antennas, such favouring the integration of the DVB-SH receivers on handheld terminals. Also, thanks to the proximity of other telecommunication bands (3G at 1.8 and 2.1 GHz), mutualization of receiver sub-systems such as RF front-end or signal processing functions is foreseen.

[8] http://europa.eu/rapid/pressReleasesAction.do?reference=IP/09/770

In a classic scenario [Chuberre 2006], 15 MHz of this frequency allocation will be divided into 3 frequency channels of 5 MHz each. The satellite will use a 3-color frequency reuse pattern, so that each beam covering a given country will transmit 5 MHz of signals. Then, the terrestrial repeaters will use all 15 MHz (Figure 2). This means that the common channel of 5 MHz used simultaneously by the satellite and the terrestrial repeaters will achieve a Single Frequency Network (SFN), where both types of emitters transmit the same signal in a synchronized way. The receiver will therefore receive several delayed replicas of the same signal, and with the appropriate signal processing, will be able to combine them in order to improve the reception quality. This solution not only permits to prevent interferences between the satellite and the terrestrial repeaters, but also provides transmit diversity to the receiver.

A typical system capacity is 9 Mbps (2.3 Mbps transferred by a satellite link and 7 Mbps transferred by terrestrial links) [Chuberre 2006]. The 2.3 Mbps would have a large coverage (1 country or "language zone") and corresponds to 9 TV programs encoded at 256 kbps, which is adapted to typical handheld screen size and resolution.

2.2.2 Single Frequency Network principle

In a DVB-SH system, the emitters may work in a Single Frequency Network (SFN). An SFN is a network of emitters that broadcast:

- the same signal
- on the same carrier frequency
- in a synchronized way.

Therefore, a receiver in an SFN will receive several delayed replicas of the same signal. As long as the receiver is able to cope with those multipaths (through equalization techniques for example) this will increase the power of the useful signal. If the multipaths are too intense (for example the delays of the replicas are outside the equalizer range of the receiver), those replicas will create interferences. Therefore, the SFN deployment shall take into account the receiver's equalizer's performances in order to avoid self-interferences within the system.

[Mattsson 2005] describes the requirements and benefits of the SFN in a broadcast network.

Requirements:

- ***Equalization techniques in the receiver*** to combine the signal replicas arriving with different delays, as explained above. As we will see, OFDM is a modulation technique which makes equalization very simple.
- ***Frequency synchronization of the emitters.*** [DVB-SH 2008-2] quotes a carrier frequency stability requirement of about 1/1000th of the sub-carrier spacing. This would result in a frequency synchronization with a precision of a few Hz.
- ***Timing synchronization of the emitters.*** [Fernández 1999] quotes a maximum time synchronization offset requirement of ±1 µs. However, we would require a better time synchronization for our localization application. This can be achieved thanks to GPS-synchronized clock, such as the Symmetricon 4370A DVB Sync Source for example, with an

accuracy of ±50 ns[9] in terms of jitter to the UTC time. In this study, a perfect emitter timing synchronization is assumed.

- ***Data synchronization of the emitters.*** All emitters should transmit the same data. Therefore, the feeder link for distributing the data source to the emitters should be robust.
- ***Adequate transmitter spacing.*** In order to avoid interferences from different emitters, the different signal replicas shall arrive within the equalization range of the receiver. Therefore, the range of each emitter shall be chosen so that this constraint is respected. To this end, system using SFN generally provisions the introduction of artificial delays for certain emitters, in order to avoid such interferences. This feature will be used in this study.

Benefits:

- ***SFN require less total power.*** In an SFN, the overall service coverage is serviced by several low-power emitters, that require less power than a single high-power emitter for the same service coverage.
- ***Transmit diversity.*** Since the signal replicas coming from different emitters will follow a different path, they will be affected by uncorrelated fading. This provides a favorable case for data transmission.

2.3 DVB-SH air interface presentation

The DVB-SH standard is described extensively in the [DVB-SH 2008-1] and [DVB-SH 2008-2].

The DVB-SH comprises two modes of transmission:

- An **Orthogonal Frequency Division Multiplexing** (OFDM) mode based on DVB-T standard with enhancements. This mode can be used on both the satellite and terrestrial paths; the two signals are combined in the receiver to strengthen the reception in a Single Frequency Network (SFN) configuration.
- A **Time Division Multiplexing** (TDM) mode partly derived from DVB-S2 standard, in order to optimize transmission through satellite towards mobile terminals. This mode is used on the satellite path only. The system supports code diversity recombination between satellite TDM and terrestrial OFDM modes so as to increase the robustness of the transmission in relevant areas (mainly suburban).

The preferred mode of transmission is the first one, and this is the one that will be considered in this study. Its main advantage is a much simpler terminal, where only one demodulator is used to receive both the satellite and terrestrial signals.

The standard only specifies the DVB-SH transmitter and leaves the receiver's implementation free. The transmitter's block diagram for both transmission modes is shown below.

[9] http://www.symmetricom.com/media/files/downloads/product-datasheets/DS%5F4370.pdf

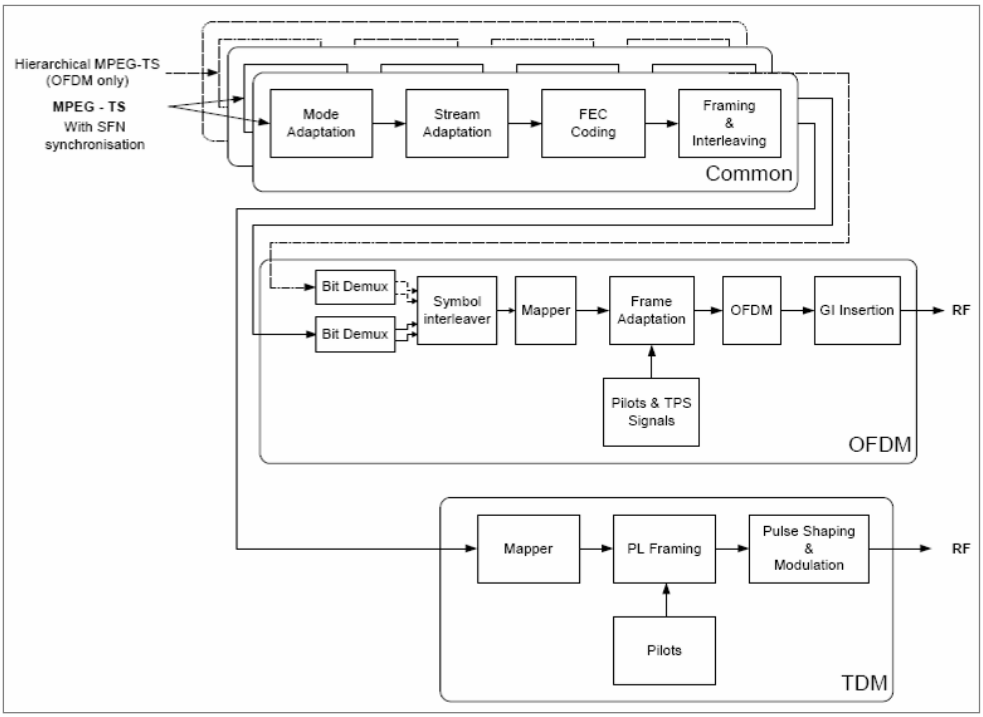

Figure 3 - Functional block diagram of the DVB-SH transmitter [DVB-SH 2008-1]

A large part of the [DVB-SH 2008-1] document is dedicated to the stream encapsulation, framing, coding and interleaving. Different data headers are included, and the channel coding is done using turbocoding with different rates from 1/5 to 2/3.

The rest of the section will describe the transmitted signal.

2.3.1 OFDM modulation principle

The Orthogonal Frequency Division Multiplexing (OFDM) modulation [Bingham 1990] is a telecommunication modulation technique that is robust in multipath environment. The following sections will explain how it combats 2 characteristics of the multipath propagation channel: (1) frequency selectivity and (2) time dispersivity.

2.3.1.1 Fighting against frequency selectivity

One issue affecting modern mobile wireless communication systems is frequency selectivity. Frequency selectivity appears when signal replicas arrive with a delay τ larger than the inverse of the signal bandwidth B, which corresponds roughly to the duration of one symbol.

This phenomenon is illustrated in Figure 4. On the upper figure, a signal replica arrives with a very short delay compared to the signal pulse width. In the frequency domain, this short multipath creates a slight degradation over the signal bandwidth considered as a flat fading. Flat fading can be easily corrected by dividing the received signal by a complex factor corresponding to the complex distortion affecting the signal bandwidth.

On the lower figure, the signal replica arrives with a larger delay than the signal pulse width. This is translated in the frequency domain by a distortion which is frequency-dependent, hence the term frequency-selective fading. In this case, the channel distortion can be corrected, but at the expense of complex and computationally-heavy signal processing involving adaptive techniques [Proakis 2006].

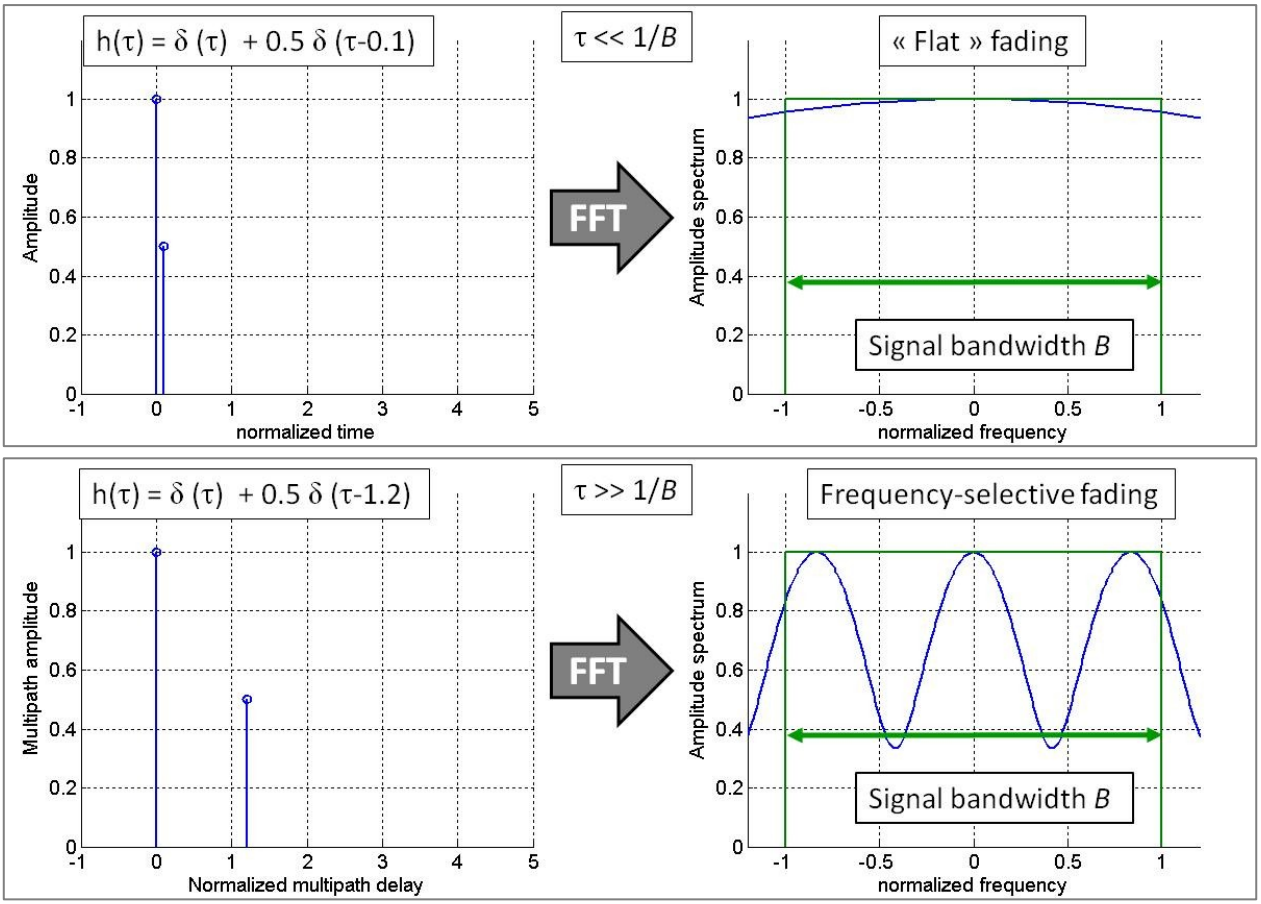

Figure 4 - illustration of frequency selectivity created by a multipath channel

Frequency selectivity is an issue for wideband telecommunication standards aiming at working in the urban or indoor environment, since they have large bandwidth B (required for high data throughput) and are transmitted in the presence of multipaths (large τ, created by the urban environment).

OFDM is a type of modulation that is well adapted to this kind of challenge. It combats frequency-selective fading by transferring in parallel several symbols on low-bandwidth sub-carriers. The bandwidth of each sub-carrier is low enough so as to consider the multipath channel as non-frequency selective (see Figure 5).

In this case, it will be simpler to correct the channel distortion by correcting each sub-carrier individually by the corresponding flat fading attenuation factor.

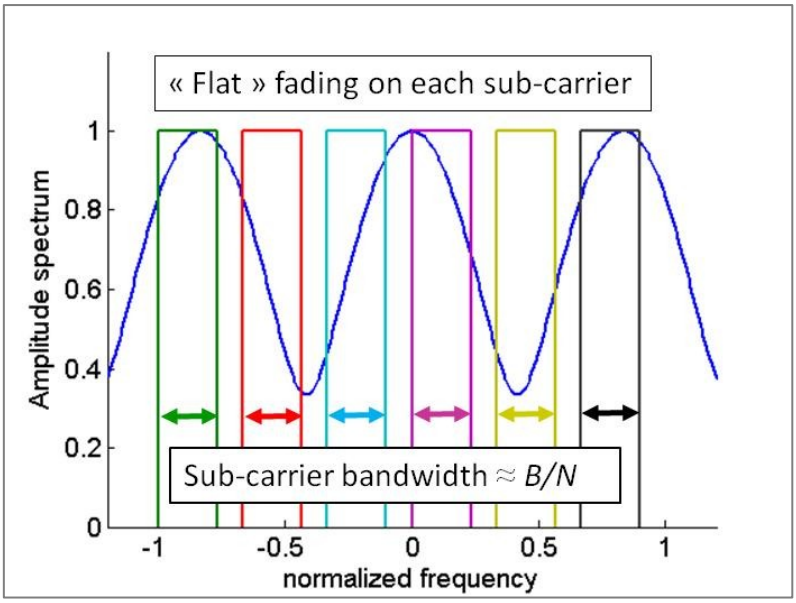

Figure 5 - Frequency division multiplexing to combat frequency selectivity

This solution could have been achieved by a simple frequency division multiplexing, as shown in Figure 5, but the use of guard bands would reduce the spectral efficiency of the transmission and hence decrease the data throughput of the transmission.

In OFDM, each sub-carrier is shaped by a rectangular pulse, which translates into a sinc-shaped spectrum. Each sub-carrier is spaced so that the zeros of one sub-carrier spectrum corresponds to the peaks of the neighboring sub-carriers. This permits to avoid inter-sub-carrier interferences - thus explaining the ***orthogonality*** concept used in the modulation name - while keeping a high spectral occupation and therefore spectral efficiency.

Figure 6 shows the spectrum of 8 orthogonal sub-carriers, while Figure 7 shows the spectrum of the sum of these 8 sub-carriers, ie the OFDM signal. We can note the rectangular shape of the OFDM spectrum, indicating an near optimum bandwidth usage for a telecommunication system. The shape of the spectrum would be even more rectangular with the increase of the number of sub-carriers.

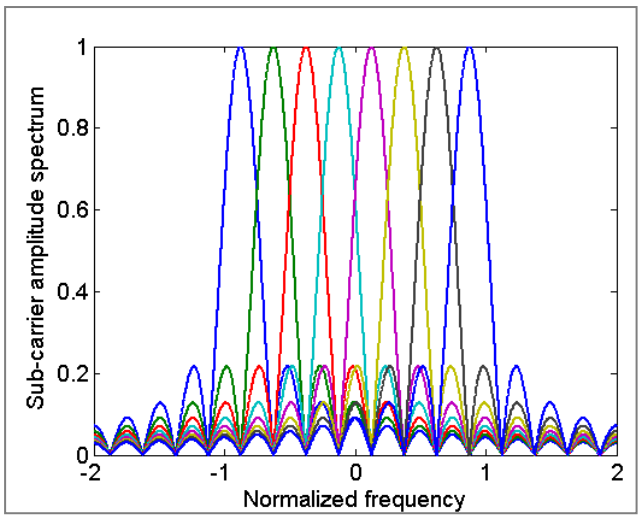

Figure 6 - Amplitude spectrum of 8 orthogonal sub-carriers

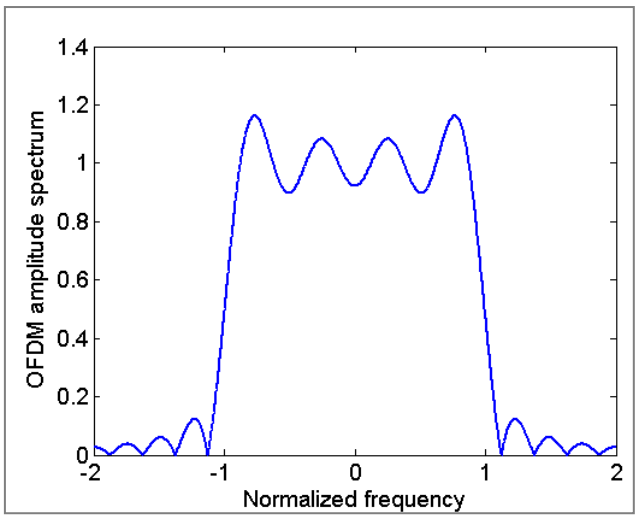

Figure 7 - Amplitude spectrum of an OFDM signal with 8 sub-carriers

In practice, the digital modulation is achieved by doing an inverse Fast Fourier Transform (iFFT) operation on the N_{FFT} symbols to be transmitted, while the demodulation is done with a direct FFT [Bingham 1990]. This requires that the number of symbols sent in one OFDM symbol is a power of 2. The use of the iFFT and FFT translates the fact that each symbols is carried on a particular sub-carrier, ie a slice of the total signal bandwidth occupied by the sub-carrier. Another way to explain the use of the iFFT / FFT in the OFDM modulation is to say that the transmitted symbols are distributed in the frequency space and turned into a signal to be transmitted in the time space.

The use of the FFT algorithm permits to have large N_{FFT} values, thanks to its computational efficiency and the improvement of chips' computational power. This allows OFDM to be applied to wideband transmissions by turning a large channel bandwidth B, affected by frequency selectivity, into a juxtaposition of N_{FFT} narrowband sub-carriers with a bandwidth B/N_{FFT}, only affected by flat fading.

2.3.1.2 Fighting against time dispersivity

The second issue brought by multipath channel is time dispersivity, ie the spreading of a symbol's power in time. This can be an issue for long symbols, or in other words, symbols carried by one narrowband sub-carrier in the OFDM modulation. Indeed, the time spreading of one symbol over the following one will degrade its demodulation by creating Inter-Symbol Interferences (ISI).

In order to avoid this, a guard interval is introduced, whose length is greater than the maximum delay of a significant echo in the multipath channel. Typical values of maxium mulitpath delay are of the order of a few micro-seconds in urban environments.

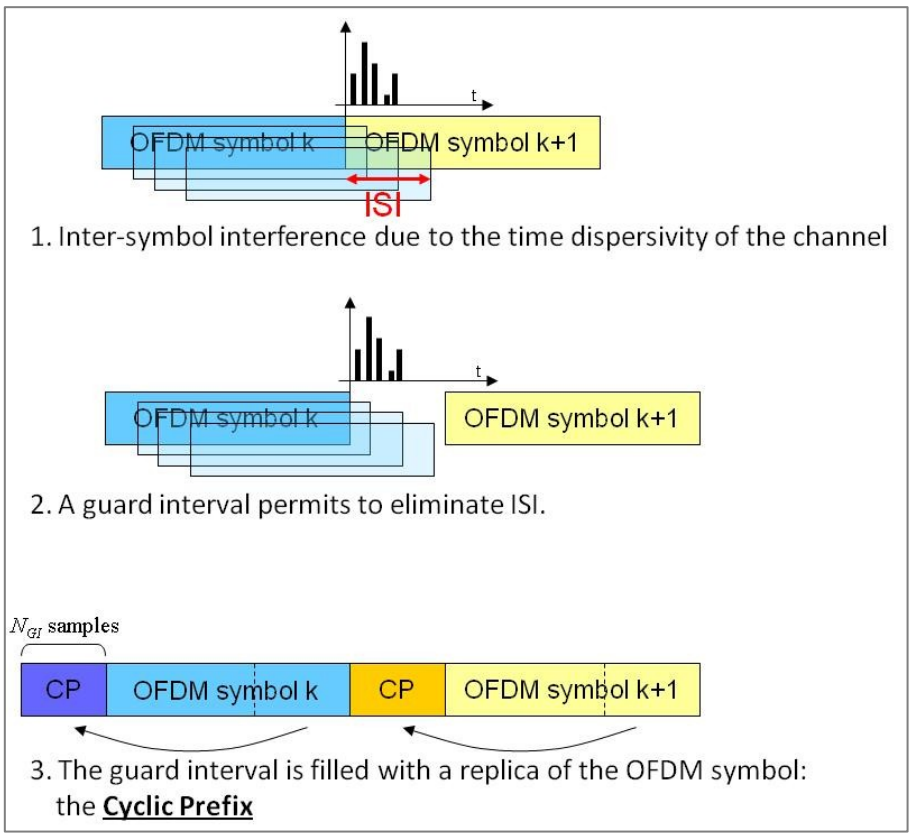

Figure 8 - Cyclic Prefix introduction to combat time dispersivity

Instead of leaving this guard interval empty, a replica of the signal is copied as shown in Figure 8. It is called the Cyclic Prefix (CP). The CP has several advantages:

- There are less variations of the signal power than if the guard interval was empty. This prevents some distortion due to the "memory effects" of some electronic components (amplifier, filter).
- The CP provides some margin on the synchronisation of the receiver. This is permitted thanks to the fact that the demodulation of an OFDM symbol is done by FFT. Even if the FFT window start is placed inside the CP instead of at the start of the useful symbol, all information will be present in the FFT window, and the delay will only result in a phase shift of the FFT output.
- Orthogonality between sub-carriers is kept in multipath environment.
- The CP adds redundancy to the signal, which can be used for synchronisation.

Including the CP between consecutive OFDM symbols, reduces the efficiency of the transmission link by introducing non-data, redundant information. Basically, if CP is the ratio of the CP duration and the total symbol length, the efficiency of the transmission is reduced by a factor $1/(1+CP)$. However, the benefits of using the CP largely outsize this transmission efficiency reduction.

2.3.2 DVB-SH modes: standardized sets of OFDM signal parameters

In DVB-SH, the OFDM signal waveform is defined by 3 parameters:

- $\boldsymbol{N_{FFT}}$ - the size of the FFT used for modulation and demodulation. N_{FFT} can take the following values {1024 , 2048 , 4096, 8192}.
- $\boldsymbol{CP}$ - the size of the so-called Cyclic Prefix, which is used as guard interval to avoid inter-symbol interferences due to the delay spread of the signal created by a multipath environment. CP can take the following values {1/4 , 1/8 , 1/16 , 1/32}
- $\boldsymbol{B}$ - the bandwidth of the transmission. B can take the following values {1.7 , 5 , 8} MHz.

The triplet formed by these parameters is called a DVB-SH signal mode. In this study, it will often be referred as "***DVB-SH mode***" in the following. The DVB-SH provisions several different DVB-SH modes, so as to provide flexibility for the telecommunication operators in the DVB-SH system deployment.

Other parameters are directly linked to these 3 main parameters.

- Sample duration T_{samp}. It is the duration of one sample, which depends on the signal bandwidth B. Values are given in Table 2.
- Useful symbol duration $T_U = N_{FFT}.T_{samp}$. The sub-carrier spacing is equal to $1/T_U$.
- Symbol duration $T_{symb} = T_U.(1+CP)$. This comprises the CP duration in addition to the useful symbol duration.

Table 2 - relation between B and T_{samp}

B	T_{samp}
1.7 MHz	7/12.8 µs
5 MHz	7/40 µs
8 MHz	7/64 µs

2.3.3 Overall signal illustration

In an OFDM transmission, symbols are transmitted in parallel over N_{FFT} sub-carriers. There are different types of symbols:

- **Null** symbols, which are located on sub-carriers on the edge of the transmission spectrum and have a zero value. They act as guard bands, used to limit the out-of-band emissions of the OFDM signal. Their number is determined by the FFT size N_{FFT}, by defining K as the number of non-null sub-cariers (see Table 3);

Table 3 - relation between N_{FFT} and K

N_{FFT}	K
1024	853
2048	1705
4096	3409
8192	6817

- **Data** symbols, which are modulated thanks to a Quadrature Amplitude Modulation (QAM), and contain the data payload to be transmitted (the DTV signal). QPSK, 16-QAM and non-uniform 16-QAM mapping are supported;
- **Transmission Parameter Signaling** (TPS) symbols, carrying information about transmissions, e.g. channel coding and modulation;
- **Pilot** symbols, that are modulated by a BPSK pseudo-random sequence. Their amplitude is boosted by a factor 4/3 compared to the data or TPS symbols. There are 2 kind of pilots symbols: continual pilots and scattered pilots. Pilots are mainly used for synchronization and channel equalization.

An example of the resulting complex demodulated constellation (without channel distortion and good SNR condition) is shown in Figure 9. In this example, a 2K DVB-SH mode was used.

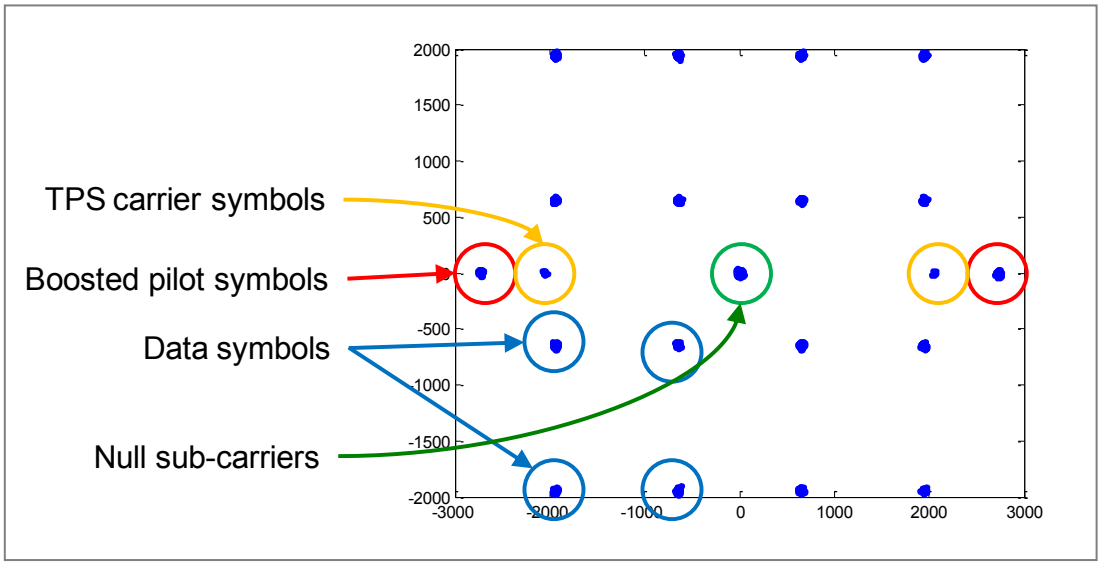

Figure 9 - Illustration of demodulated constellation

The 2048 symbols carried over the same number of sub-carriers are divided between:

- K = 1705 useful sub-carriers
  - 45 continual pilot symbols
  - 142 scattered pilot symbols (a number of scattered and continual pilots are on the same sub-carrier, thus reducing this number to 131 distinct scattered pilots)

- 17 Transmission Parameter Signalling symbols, which carry information about the signal parameters
- 1512 data symbols, modulated by 16-QAM

- 343 null sub-carriers, which are used as guard bands on the edges of the transmission spectrum.

2.3.4 Pilot locations

Two kinds of pilots exist in the DVB-SH standard: continual and scattered pilots.

- The continual pilots are always inserted on the same sub-carriers on every OFDM symbol.
- The scattered pilots are inserted every 12 sub-carriers, with a repeating pattern every 4 OFDM symbols.

The location of the pilots is illustrated in Figure 10.

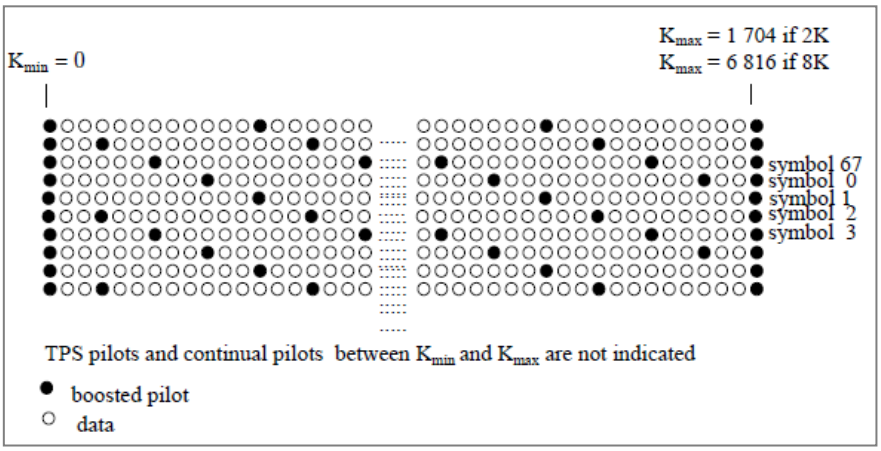

Figure 10 - Pilot location [DVB-SH 2008]

The value of the pilot symbols depends on the pilot sub-carrier index. It is determined from a pseudo-random binary sequence (PRBS) w_k, generated according to the following circuit:

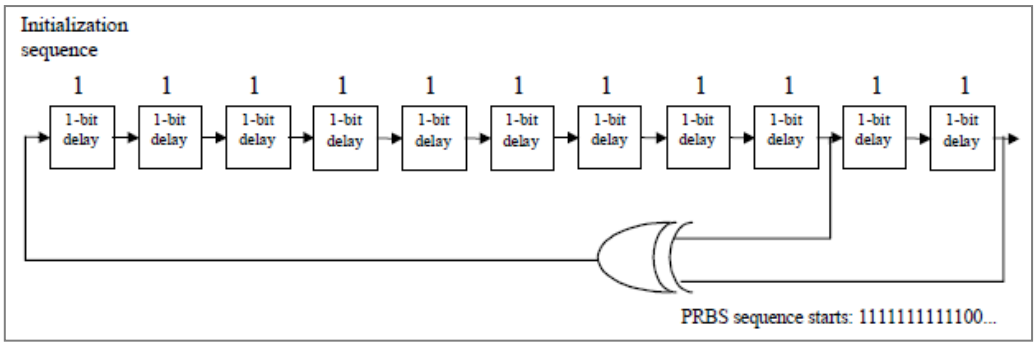

Figure 11 - Generation of the PRBS sequence [DVB-SH 2008]

The pilots are transmitted at boosted power on a BPSK modulation. The exact value of the symbol is given thanks to the following formulas: $4/3 * 2(1/2 - w_k)$.

2.3.5 Model of the baseband OFDM transmission chain

For the rest of this study, OFDM signals are modeled according to the block diagram shown in Figure 12.

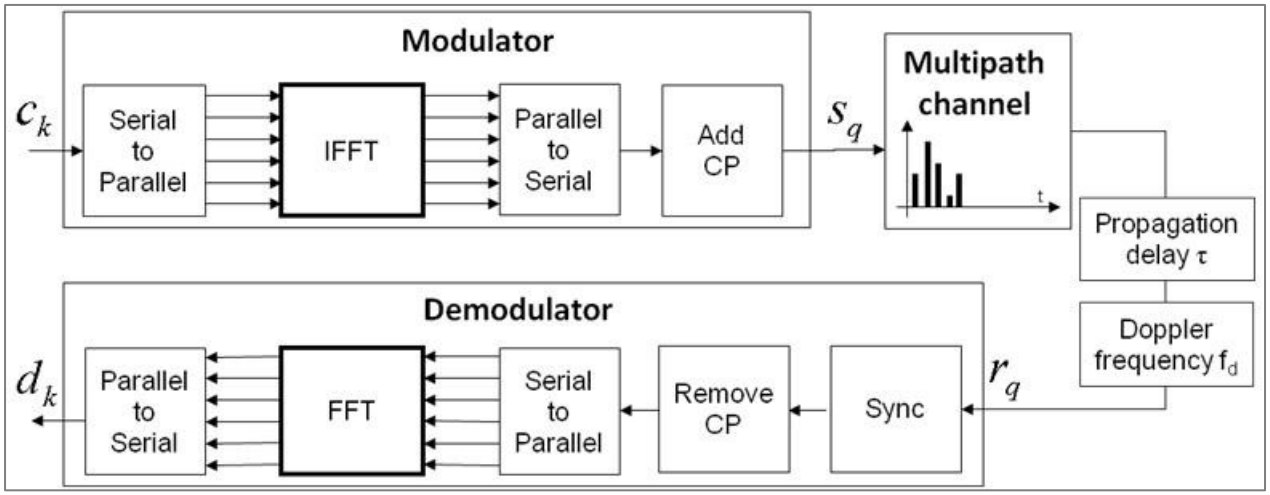

Figure 12 - Model of the baseband OFDM transmission chain

This model of the transmission chain makes some hypotheses:

- ***No sampling clock offset*** is present: the sampling of the received signal is perfectly done. Sampling clock offset is rarely mentioned in OFDM models, meaning that it has either little impact or that it is well corrected;
- ***No emission or reception filter***: it is considered that these 2 filters do not affect the transmitted signal. This hypothesis is quite realistic due to the presence of guard bands on the edge of the transmitted signal's spectrum. The useful part of the spectrum is in the middle of the band, where an emission or reception filter would have very little influence.
- ***No spectrum distortion due to the Doppler Effect***: the displacement of the receiver results in a Doppler effect, which creates an frequency offset different for each sub-carriers. For small values of speed, it is usual to consider that all the sub-carriers are affected by a single frequency offset.

2.3.5.1 Expression of the baseband emitted sampled signal

Let us assume that there are $N_{symb} * N_{FFT}$ symbols to be transmitted. They are put in a matrix shape with N_{symb} lines and N_{FFT} columns. One OFDM symbol will transmit all N_{FFT} symbols of a given line.

The expression of the emitted baseband sampled signal for one OFDM symbol is:

$$s_{l,q} = \sum_{k=0}^{N_{FFT}-1} c_{l,k} \exp\left(j2\pi \frac{kq}{N_{FFT}}\right) = IFFT\left[\left(c_{l,k}\right)_{k=0}^{k=N_{FFT}-1}\right](q \qquad \text{Eq. 2.1}$$

with l is the OFDM symbol index

q is the sample index. It covers both the useful signal and the Cyclic Prefix: $q \in [-CP.N_{FFT} \dots N_{FFT} - 1]$

$c_{l,k}$ is the modulated symbol transmitted over the k-th subcarrier of the l-th OFDM symbol. It corresponds to the symbol at the location (l, k) in the matrix of the transmitted symbols.

2.3.5.2 Expression of the baseband signal after channel filtering

The emitted signal goes through a multipath channel, which is defined by the baseband Channel Impulse Response (CIR) formed by the vector $\mathbf{h_l}$. In this section, the CIR vector is modelled by a filter with the same sampling rate than the signal. The elements of $\mathbf{h_l}$ therefore corresponds to tapped delay lines, with a complex amplitude $h_{l,n}$ corresponding to the signal replicas received at a delay $n.T_{samp}$.

An Additive White Gaussian Noise is also added to represent the receiver's thermal noise contribution, but will be dropped from expressions for simplicity.

The received signal after carrier removal is affected by a delay τ (normalised by the sampling period) and a carrier frequency offset f_{CFO} (normalised by the sub-carrier spacing).

The received signal at the receiver's input is

$$r_{l,q} = e^{j\left(2\pi f_{CFO}\frac{(q+lN_t)}{N_{FFT}}+\varphi_0\right)}(\mathbf{h_l} \otimes \mathbf{s_l})_{q-\tau} \quad \textbf{Eq. 2.2}$$

, with f_{CFO} the normalised carrier frequency offset,
φ_0 a random initial phase
τ the normalised delay introduced by the channel
$\mathbf{h_l}$ the vector composed by the sampled channel impulse response
$\mathbf{s_l}$ the the vector containing the emitted samples of the l-th OFDM symbol

2.3.5.3 Expression of the baseband signal after synchronization

The first operation done by the receiver is the synchronization, both for timing and frequency. Timing synchronization consists in placing the demodulator's FFT window at the correct time, ideally towards the end of the CP near the start of the useful part of the OFDM symbol. Frequency synchronization consists in removing the residual carrier which may subsist after carrier removal.

This synchronization step is usually done using the method detailed in [van de Beek 1997]. This method consists in using the auto-correlation of the received signal. The presence of the CP creates a peak in the correlation output, whose delay corresponds to the start of the useful part of the symbol and whose phase corresponds to the required frequency correction.

After this step, the received signal is only affected by a residual normalized timing offset $\Delta\tau$ and a normalized residual carrier frequency offset Δf:

$$r_{l,q}^{sync} = e^{j\left(2\pi\Delta f\frac{(q+lN_t)}{N_{FFT}}+\varphi_0\right)}(\mathbf{h_l} \otimes \mathbf{s_l})_{q-\Delta\tau} \quad \textbf{Eq. 2.3}$$

In the following, the residual timing offset is supposed to be sufficiently small to avoid **inter-symbol interference** (ISI). This is true if the residual timing offset is inferior to the Cyclic Prefix duration: $\Delta\tau < N_{FFT}.CP$

2.3.5.4 Expression of the baseband signal after demodulation

After synchronization, the demodulation is done by applying an FFT on N_{FFT} samples (the CP has been removed).

$$d_{l,k} = FFT\left[\left(r_{l,q}^{sync}\right)_{q=0}^{q=N_{FFT}-1}\right](k) \qquad \textbf{Eq. 2.4}$$

This provides:

$$d_{l,k} = \sum_{q=0}^{N_{FFT}-1} e^{j\left(2\pi\Delta f\frac{(q+lN_t)}{N_{FFT}}+\varphi_0\right)} \sum_{n=-\infty}^{+\infty} h_{l,n} s_{l,q-\Delta\tau-n}\,.\,e^{-j2\pi\frac{qk}{N_{FFT}}}$$

$$d_{l,k} = e^{j(2\pi\Delta fl\frac{N_t}{N_{FFT}}+\varphi_0)} \sum_{n=-\infty}^{+\infty} h_{l,n} \sum_{q=0}^{N_{FFT}-1} s_{l,q-\Delta\tau-n}.e^{-j2\pi q\frac{k-\Delta f}{N_{FFT}}}$$

We replace the expression of $s_{l,q-\Delta\tau-n}$ in function of the sent symbols (Eq. 2.1):

$$d_{l,k} = e^{j(2\pi\Delta fl\frac{N_t}{N_{FFT}}+\varphi_0)} \sum_{n=-\infty}^{+\infty} h_{l,n} \sum_{q=0}^{N_{FFT}-1} \sum_{p=0}^{N_{FFT}-1} c_{l,p}.e^{j2\pi p\frac{q-\Delta\tau-n}{N_{FFT}}}.e^{-j2\pi q\frac{k-\Delta f}{N_{FFT}}}$$

$$d_{l,k} = e^{j(2\pi\Delta fl\frac{N_t}{N_{FFT}}+\varphi_0)} \sum_{n=-\infty}^{+\infty} h_{l,n} \sum_{p=0}^{N_{FFT}-1} c_{l,p}.e^{-j2\pi p\frac{\Delta\tau+n}{N_{FFT}}} \sum_{q=0}^{N_{FFT}-1} e^{-j2\pi q\frac{k-p-\Delta f}{N_{FFT}}}$$

We replace the last sum using the result of the sum of a geometric sequence: $\sum_{q=q_{min}}^{q=q_{max}} e^{jq2\varphi} = e^{j\varphi(q_{min}+q_{max})}.\frac{\sin(\varphi(q_{max}-q_{min}+1))}{\sin(\varphi)}$

$$d_{l,k} = e^{j(2\pi\Delta fl\frac{N_t}{N_{FFT}}+\varphi_0)} \sum_{n=-\infty}^{+\infty} h_{l,n} \sum_{p=0}^{N_{FFT}-1} c_{l,p}.e^{-j2\pi p\frac{\Delta\tau+n}{N_{FFT}}}.e^{-j\pi(k-p-\Delta f)\frac{(N_{FFT}-1)}{N_{FFT}}}.\frac{\sin\left(\pi(k-p-\Delta f)\right)}{\sin\left(\pi\frac{k-p-\Delta f}{N_{FFT}}\right)}$$

$$d_{l,k} = e^{j(2\pi\Delta fl\frac{N_t}{N_{FFT}}+\varphi_0)} \sum_{p=0}^{N_{FFT}-1} c_{l,p}.e^{-j2\pi p\frac{\Delta\tau}{N_{FFT}}}.e^{-j\pi(k-p-\Delta f)\frac{(N_{FFT}-1)}{N_{FFT}}}.\frac{\sin\left(\pi(k-p-\Delta f)\right)}{\sin\left(\pi\frac{k-p-\Delta f}{N_{FFT}}\right)} \sum_{n=-\infty}^{+\infty} h_{l,n}.e^{-j2\pi\frac{pn}{N_{FFT}}}$$

The last sum is the Discrete Time Fourier Transform of the channel impulse response evaluated at sub-carrier p's frequency. Let us define $H_{l,p} \triangleq \sum_{n=-\infty}^{n=+\infty} h_{l,n}.e^{-j2\pi\frac{pn}{N_{FFT}}}$. It corresponds to the channel transfer function affecting the p-th sub-carrier.

The final result of the demodulated symbol expression in presence of residual timing and frequency offsets is:

$$d_{l,k}(\Delta\tau,\Delta f) = e^{j(2\pi\Delta f l\frac{N_t}{N_{FFT}}+\varphi_0)} \sum_{p=0}^{N_{FFT}-1} c_{l,p}.H_{l,p}.e^{-j2\pi\frac{p\Delta\tau}{N_{FFT}}}.e^{-j\pi(k-p-\Delta f)\frac{(N_{FFT}-1)}{N_{FFT}}}.\frac{\sin\left(\pi(k-p-\Delta f)\right)}{\sin\left(\pi\frac{k-p-\Delta f}{N_{FFT}}\right)}$$

Eq. 2.5

This general formula is analyzed in the next section for different synchronization cases. It is coherent with the results present in [Morelli 2007].

2.3.5.5 Particular cases depending on synchronization performances

- $\Delta\boldsymbol{\tau} = \mathbf{0}$ **and** $\Delta\boldsymbol{f} = \mathbf{0}$

For a perfect time and frequency synchronization, the expression of the demodulated signal is

$$d_{l,k}(0,0) = e^{j\varphi_0}.c_{l,k}.H_{l,k}$$ **Eq. 2.6**

This means that we have the initial transmitted symbol affected by the channel frequency response at the given sub-carrier frequency and a random phase offset. This can be easily corrected thanks to channel estimation through pilots and equalization.

- $\Delta\boldsymbol{\tau} \neq \mathbf{0}$ **and** $\Delta\boldsymbol{f} = \mathbf{0}$

In case of perfect frequency synchronization,

$$d_{l,k}(\Delta\tau,0) = e^{j\varphi_0}.c_{l,k}.H_{l,k}.e^{-j2\pi\frac{k\Delta\tau}{N_{FFT}}}$$ **Eq. 2.7**

In addition to the channel distortion already observed in Eq. 2.6, the symbol is affected by a phase shift depending on the sub-carrier index k and the residual timing offset. All these impairments can be corrected during the channel equalization step.

- $\Delta\boldsymbol{\tau} = \mathbf{0}$ **and** $\Delta\boldsymbol{f} \neq \mathbf{0}$

If we only have a perfect time synchronization, we obtain

$$d_{l,k}(0,\Delta f) = e^{j(2\pi\Delta f l\frac{N_t}{N_{FFT}}+\varphi_0)} \sum_{p=0}^{N_{FFT}-1} c_{l,p}.H_{l,p}.e^{-j\pi(k-p-\Delta f)\frac{(N_{FFT}-1)}{N_{FFT}}}.\frac{\sin\left(\pi(k-p-\Delta f)\right)}{\sin\left(\pi\frac{k-p-\Delta f}{N_{FFT}}\right)}$$

We can isolate the terms corresponding to symbol $p = k$, in order to better analyse the meaning of this expression:

$$d_{l,k}(0,\Delta f) = e^{j(2\pi\Delta f l\frac{N_t}{N_{FFT}}+\varphi_0)}\left(c_{l,k}.H_{l,k}.e^{j\pi\Delta f\frac{(N_{FFT}-1)}{N_{FFT}}}.\frac{\sin(\pi\Delta f)}{\sin\left(\pi\frac{\Delta f}{N_{FFT}}\right)} + \sum_{\substack{p=0\\p\neq k}}^{N_{FFT}-1} c_{l,p}.H_{l,p}.e^{-j\pi(k-p-\Delta f)\frac{(N_{FFT}-1)}{N_{FFT}}}.\frac{\sin\left(\pi(k-p-\Delta f)\right)}{\sin\left(\pi\frac{k-p-\Delta f}{N_{FFT}}\right)}\right) \quad \textbf{Eq. 2.8}$$

In this expression, we see that the residual frequency offset Δf creates three types of degradation:

1. an overall phase shift due to the accumulation of the frequency error over the successive OFDM symbols,
2. a degradation of the useful part of the demodulated symbol, affected by a phase shift and an attenuation,
3. some contributions from the symbols transmitted from adjacent sub-carriers. Therefore, when there is bad frequency synchronization, **inter-carrier interferences** appear.

In the rest of this study, we will consider the second case of synchronization states, where $\Delta\tau \neq 0$ and $\Delta f = 0$ (Eq. 2.7). This is realistic with regards to the [van de Beek 1997] synchronization algorithm's performances.

2.4 Typical SNR of a DVB-SH transmission

[DVB-SH 2008-2] provides the required SNR for a few combinations of symbol modulation and coding rate, also called ***modcods*** (Table 4). This required SNR corresponds to a frame error rate of 10^{-5} (ie quasi-error free transmission) and has been obtained thanks to simulations done in a TU6 mobile channel model, for 2 different speeds. The TU6 mobile channel model is an urban propagation model defined by 6 multipaths having a varying amplitude following a Rayleigh distribution and fixed delays. The model details can be found in [DVB-SH 2008-2]. Later, a variation of the TU6 model will be presented (see the TU20 model described in section 3.1.2)

Values for other modcods are not available in the reference document.

Required noise floor levels for handheld receivers are also given in [DVB-SH 2008-2] and recalled in Table 5.

With these 2 parameters (required SNR and the receiver noise floor level), it is possible to know the minimum required power level of the received signal, that has to be reached in a correctly-designed emitter network.

The interesting conclusion of this section is that the received signals will always have a relatively high power. This received power will come from several emitters, as DVB-SH works with an SFN. Depending on the used modcods in the system deployment, ***the minimum SNR will vary between 1 and 11 dB***.

Table 4 - Performance in TU6 for a DVB-SH receiver (FER = 5%) [DVB-SH 2008-2]

Modcod	Required SNR (dB)
QPSK 1/3 (50 kmph)	1.2
QPSK 1/2 (50 kmph)	4.3
16QAM 1/5 (50 kmph)	2.5
16QAM 1/4 (50 kmph)	4.1
16QAM 1/3 (50 kmph)	6.2
16QAM 1/2 (50 kmph)	9.5
QPSK 1/3 (3 kmph)	3.3
QPSK 1/2 (3 kmph)	5.8
16QAM 1/5 (3 kmph)	4.8
16QAM 1/4 (3 kmph)	5.6
16QAM 1/3 (3 kmph)	7.8
16QAM 1/2 (3 kmph)	11

Table 5 - Noise floor level in typical receiver [DVB-SH 2008-2]

Bandwidth B	Noise floor level
1.7 MHz	-107.7 dBm
5 MHz	-102.7 dBm
8 MHz	-100.7 dm

3 Pseudo-range estimation in a mono-emitter system

The positioning strategy chosen in this study is based a geometric positioning method (tri-lateration) in a similar way as what is done in GNSS. Therefore, pseudo-range estimation is one of the main step to achieve position calculation.

The presented pseudo-range estimation method is based on the estimation of the Channel Impulse Response (CIR). The distance between the emitter and the receiver will be derived from the time of arrival of the signal, which can be observed through the peaks present in the CIR. Correct modeling of the CIR is therefore essential for taking a realistic case for the development of pseudo-range estimation techniques. Therefore, this chapter will first present an urban propagation channel model (section 0). This model will permit to understand the behavior of the urban propagation channel and to guide us towards a viable pseudo-range estimation strategy.

The signal processing for positioning strategy follows the following steps (Figure 13):

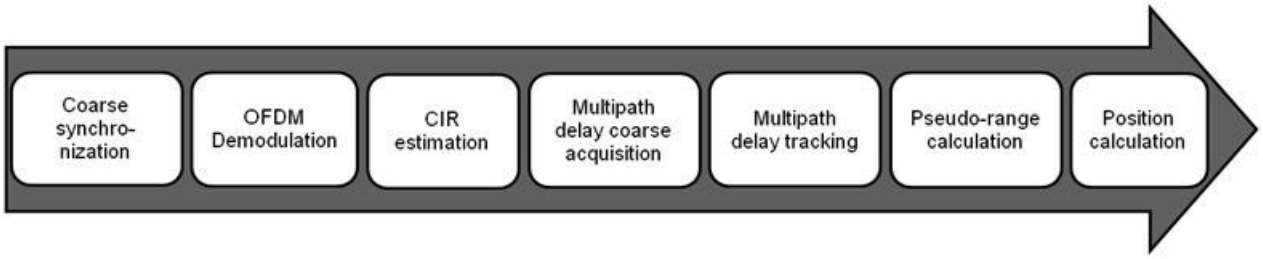

Figure 13 - Receiver signal processing strategy for position calculation

The 2 first boxes are done in a conventional way: coarse synchronization is achieved thanks to the [van de Beek 1995] algorithm and demodulation has been described in section 2.3.5.5.

This chapter describes the following boxes:

- CIR estimation in section 3.2,
- Multipath delay acquisition in section 3.3,
- Multipath delay tracking in section 3.4,
- Pseudo-range calculation, with simulations in section 3.6.

Finally, an adaptation of the multipath delay acquisition and tracking will be presented in section 3.5, anticipating the case of multi-emitter systems that will be covered in chapter 4. This modification consists in using windowing technique in order to reduce sidelobes in the CIR estimation, and therefore avoid potential bias in the delay estimation, and inter-emitter interferences.

Position calculation will be presented in chapter 6.

3.1 The urban propagation channel: a challenge for timing-based pseudo-range estimation

The urban propagation channel presents a lot of challenges for pseudo-range estimation based on timing measurements. Among others, the particularities of the urban propagation channel are [Pérez Fontán 2008]:

- **Signal attenuation dependency to distance (a.k.a pathloss) with large exponential factor**. In free space propagation, the signal power attenuation dependency to distance is in a $1/d^2$ law. In urban environment, due to the presence of obstacles on the path followed by the signal, this dependency follows a $1/d^\alpha$ law, with $\alpha > 2$ in general;
- **Slow fading (a.k.a. shadowing)** of the signal power. Shadowing is due to the presence of large obstacle such as buildings;
- **Fast fading**, which is caused by the close environment of the receiver. The close environment of the receiver create signal replicas coming from all azimuth with a random phase, whose sum creates large signal power variations even for small displacements of the order of the signal carrier wavelength.
- **The presence of different received signal replicas**, which are created by the interaction of the signal with the remote environment of the receiver, typically high-rise buildings or close mountains. These replicas may arrive with delay up to several µs and will appear or disappear with the motion of the receiver;

No complete model has been found in literature with the desired accuracy (a summary of the reviewed urban propagation models is found in Annex B). Therefore, a simplified channel model has been created. This simplified model takes into account realist pathloss and fast fading of the signal power, which will permit to test and validate the developped pseudo-range estimation techniques in a representative propagation channel. Further discussion on the adequation of the model can be found in section 3.1.5. This channel model is a combination of 2 different models well known in the telecommunication field:

- the COST231 Wallfisch Ikegami pathloss model [COST231 1993] described in section 3.1.1,
- the TU20 multipath model [UMTS 2004] described in section 3.1.2.

3.1.1 COST 231 Wallfisch-Ikegami pathloss model

This model [COST231 1993] takes into account some geometric urban environment parameters (building height, street width, etc.) in order to describe the pathloss. It takes into account various urban propagation events, such as multiple diffraction from roofs if several building blocks are present on the path between the receiver and the emitter, diffraction from the last roof before the receiver, dependency on the carrier frequency, etc.

According to [COST231 1993], this model provide goof fitting with measurement campaigns: a mean error of +/- 3 dB and a standard deviation between 4 and 8 dB for the scenarios where the emitter antenna is above the neighbour roofs, which corresponds to our studied case.

The model is based on the following mathematical expression:

$$L = L_0 + L_{rts} + L_{msd} \qquad \text{Eq. 3.1}$$

with the free space loss in dB $L_0 = 32.4 + 20.\log d + 20.\log f_c$

d the distance between the emitter and the receiver in km

f_c the carrier frequency of the transmission in MHz

the rooftop-to-street diffraction and scatter loss L_{rts} in dB:

$$L_{rts} = -16.9 - 10.\log w + 10.\log f_c + 20.\log\left(h_{roof} - h_{MS}\right) + L_{ori}$$

w the street width in meters

h_{roof} the rooftop height in meters

h_{MS} the receiver height in meters

L_{ori} a pathloss term in dB depending on the orientation of the street:

$L_{ori} = -10 + 0.354.\varphi$ for $0° \leq \varphi \leq 35°$

$L_{ori} = 2.5 + 0.075.(\varphi - 35)$ for $35° \leq \varphi \leq 55°$

$L_{ori} = 4 - 0.114.(\varphi - 55)$ for $55° \leq \varphi \leq 90°$

φ is the street orientation with regard to the emitter direction direction

the multi-screen diffraction in dB $L_{msd} = L_{bsh} + k_a + k_d.\log \mathrm{d} + k_f.\log f_c - 9.\log b$

b the building separation in meters

h_{BS} the emitter height in meters

$L_{bsh} = -18.\log\left(1 + h_{BS} - h_{roof}\right)$ for $h_{BS} > h_{roof}$

$k_a = 54$ for $h_{BS} > h_{roof}$

$k_d = 18$ for $h_{BS} > h_{roof}$

$k_f = -4 + 1.5.\left(\frac{f_c}{935} - 1\right)$ for metropolitan centers

The values used in all simulations of this report are:

- $\varphi = 90°$
- $b = 40m$
- $w = b/2 = 20m$
- $h_{roof} = 20m$
- $h_{MS} = 1.5m$
- $h_{BS} = 23m$
- $f_c = 2.2GHz$

The obtained pathloss for these parameters is plotted in Figure 14.

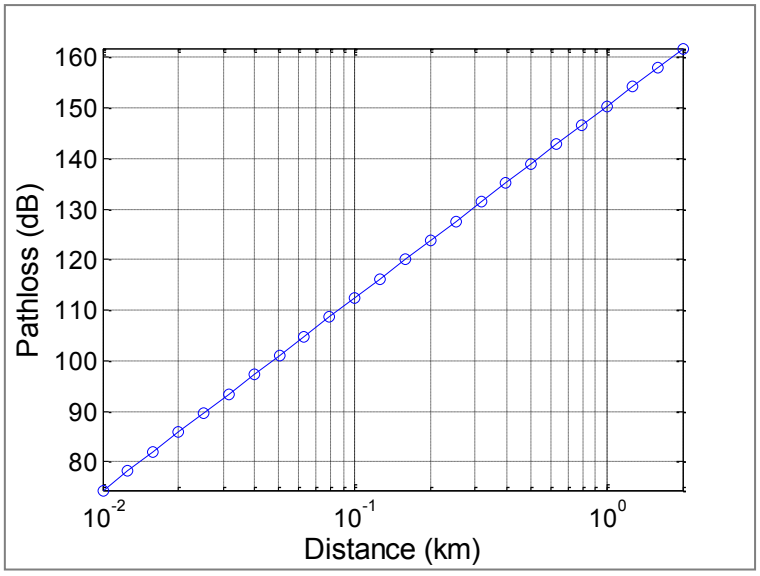

Figure 14 - Pathloss vs distance model used in this study

3.1.2 Description of the TU-20 model

The TU-20 propagation model [UMTS 2004] is used for validating the performances of a mobile communication transmission. It describes a 'typical' propagation environment, where the receiver receives 20 replicas of the signal with fixed delays and varying power.

The power distribution is a Rayleigh distribution and the spectrum of each multipath corresponds to a Jake's spectrum. These 2 characteristics originate from the hypothesis that at a given instant, several copies of the same signal arrives from different azimuths with random phase. The Jake's spectrum is described by Eq. 3.2 and illustrated in Figure 15.

$$S_{Jake}(f) = \frac{1}{\pi f_d \sqrt{1-(f/f_d)^2}} \qquad \textbf{Eq. 3.2}$$

with $f_d = \frac{f_c.v}{c}$, the maximum Doppler frequency;
f_c, the carrier frequency;
v, the speed of the mobile receiver;
c, the speed of light.

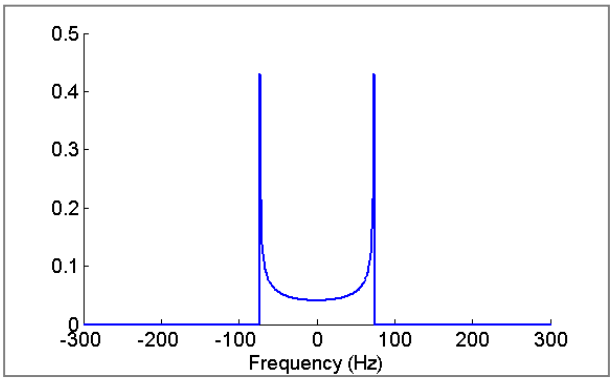

Figure 15 - Jake's spectrum illustration ($f_d = 73\ Hz$)

The delays and average relative power are given in Table 6.

Table 6 - power delay profile for TU-20 multipath model [UMTS 2004]

Multipath number	Relative delay (µs)	Avg relative power (dB)	Doppler Spectrum
1	0	-5.7	Jake
2	0.217	-7.6	Jake

3	0.512	-10.1	Jake
4	0.514	-10.2	Jake
5	0.517	-10.2	Jake
6	0.674	-11.5	Jake
7	0.882	-13.4	Jake
8	1.230	-16.3	Jake
9	1.287	-16.9	Jake
10	1.311	-17.1	Jake
11	1.349	-17.4	Jake
12	1.533	-19.0	Jake
13	1.535	-19.0	Jake
14	1.622	-19.8	Jake
15	1.818	-21.5	Jake
16	1.836	-21.6	Jake
17	1.884	-22.1	Jake
18	1.943	-22.6	Jake
19	2.048	-23.5	Jake
20	2.140	-24.3	Jake

The generation of the taps' amplitude is describes in Figure 16.

A complex Gaussian time series is generated at the desired sampling rate, then filtered to give it the desired Jakes' spectrum. Finally, its amplitude is corrected.

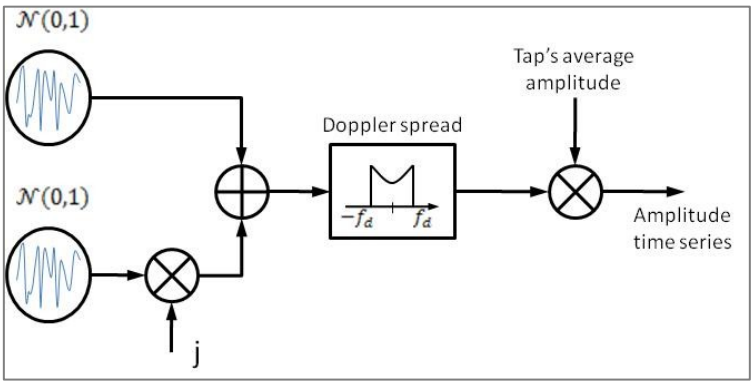

Figure 16 - Rayleigh distributed tap's amplitude generation

3.1.3 Retained CIR model expression

The retained CIR model expression is given by:

$$h_l(\tau) = 10^{\frac{L_{COST}(d_l)}{20}} . \left(\sum_{n=0}^{N_{taps}-1} a_{l,n} . \delta \left(\tau - \frac{d_l}{c} - \tau_n . T_{samp} \right) \right)$$

where l is the OFDM symbol index and corresponds to the time of reception of the l-th OFDM symbol;

d_l is the distance between the receiver and the emitter at the time of reception of the l-th OFDM symbol;

$L_{COST}(d_l)$ is the pathloss provided by the COST 213 Wallfisch-Ikegami pathloss model expressed in dB taken from Eq. 3.1. We will use the notation $l_{COST}(d_l) = 10^{\frac{L_{COST}(d_l)}{20}}$;
$a_{l,n}$ is the complex amplitude of the n-th multipath applied to the l-the OFDM symbol. To simulate the fast fading, it has a Rayleigh distribution and a Jakes spectrum. The amplitude time series is generated as described in Figure 16;
τ_n is the relative delay of the n-th multipath, provided in Table 6. Here, it is normalized by the sampling period of the OFDM signal.

However, assuming good timing synchronization, the observed CIR will have a delay origin at $\tau - \frac{d_l}{c}$. this simplifies the observed CIR expression to the following expression. Eq. 3.3 will be used in the rest of the study.

$$h_l(\tau) = l_{COST}(d_l).\left(\sum_{n=0}^{N_{taps}-1} a_{l,n}.\delta\left(\tau - \tau_n.T_{samp}\right)\right) \quad \textbf{Eq. 3.3}$$

From this CIR expression, we can obtain the Channel Transfer Function (CTF) by doing the FFT of Eq. 3.3:

$$H_l(f) = l_{COST}(d_l).\left(\sum_{n=0}^{N_{taps}-1} a_{l,n}.\exp\left(-j2\pi f\tau_n T_{samp}\right)\right)$$

To relate this expression to the equations of section 2.3.5, we can provide the expression of the CTF at the frequency of the k-th sub-carrier $f = \frac{k}{T_U} = \frac{k}{N_{FFT}.T_{samp}}$:

$$H_l\left(f = \frac{k}{T_U}\right) = H_{l,k} = l_{COST}(d_l).\left(\sum_{n=0}^{N_{taps}-1} a_{l,n}.\exp\left(-j\frac{2\pi k\tau_n}{N_{FFT}}\right)\right) \quad \textbf{Eq. 3.4}$$

We can observe that the CTF varies from one frequency value to another, thus illustrating the frequency selectivity of the channel.

3.1.4 Illustration of CIR time series

Figure 17 shows the aggregate pathloss obtained from a generated CIR time series. The distance between the receiver and the emitter is set to 600m and the speed of the receiver is 10 km/h. In this conditions, the COST231-WI model indicates a pathloss of 142 dB, which corresponds to the mean of this time series.

We can observe pathloss fluctuations due to the fast fading introduced by the TU-20 model. The amplitude of the variations is above 10 dB and they happen very fast.

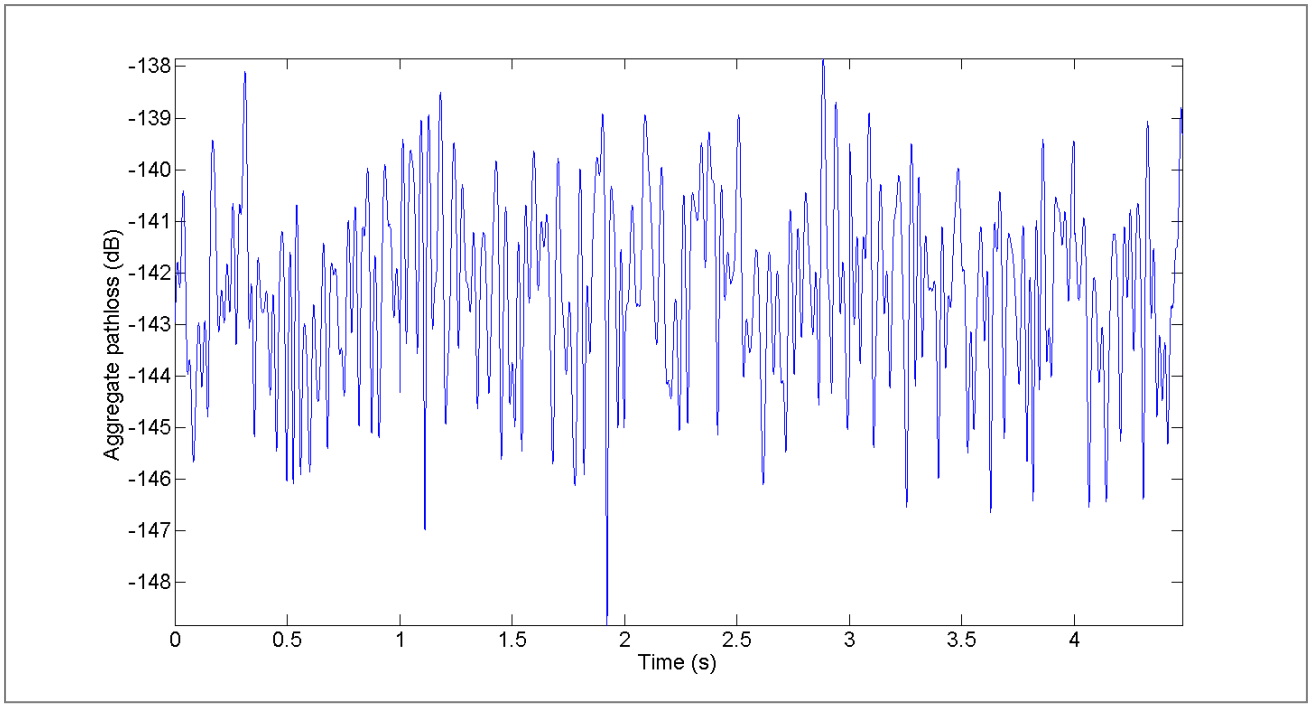

Figure 17 - Illustration of overall pathloss obtained through a CIR time series

Figure 18 and Figure 19 show an illustration of the first tap of the TU-20 models for 2 different speeds when the receiver is at a distance of 600m. The average power of the time series is -147.7 dB, which corresponds to a pathloss of 142 dB from the COST231-WI model, with an additional relative power degradation of -5.7 dB from the first line of Table 6.

As expected, the fading rate depends on the speed of the receiver, accordingly to the width of the Jake's spectrum. Also the amplitude is affected by large fadings, which can reach several tens of dB.

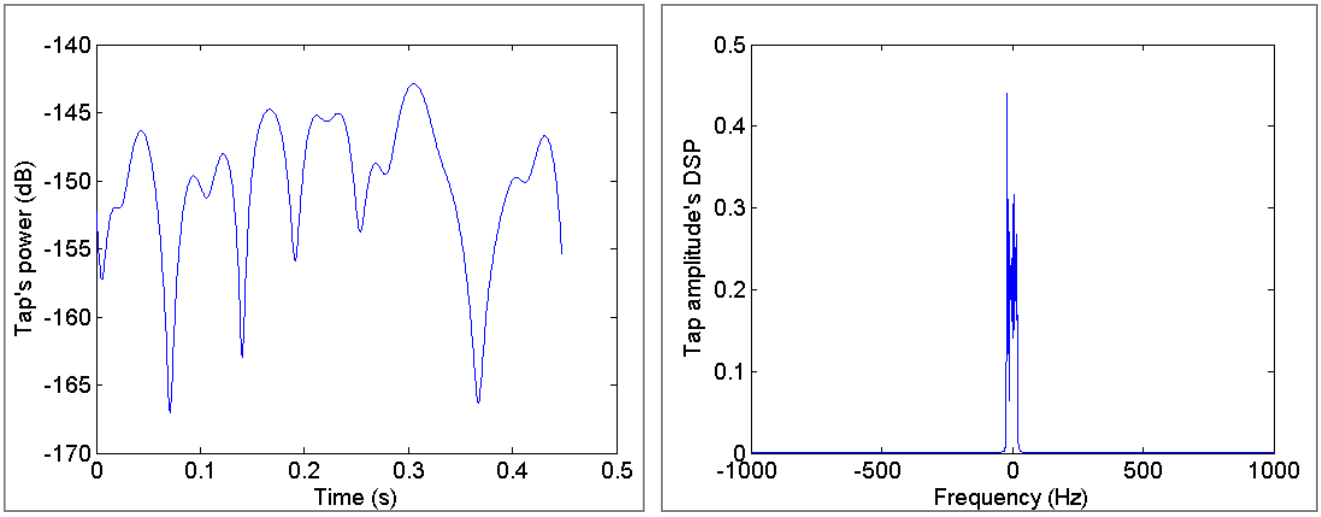

Figure 18 - Illustration of one tap's time series (left) and doppler spectrum (right) at a speed of 10 km/h

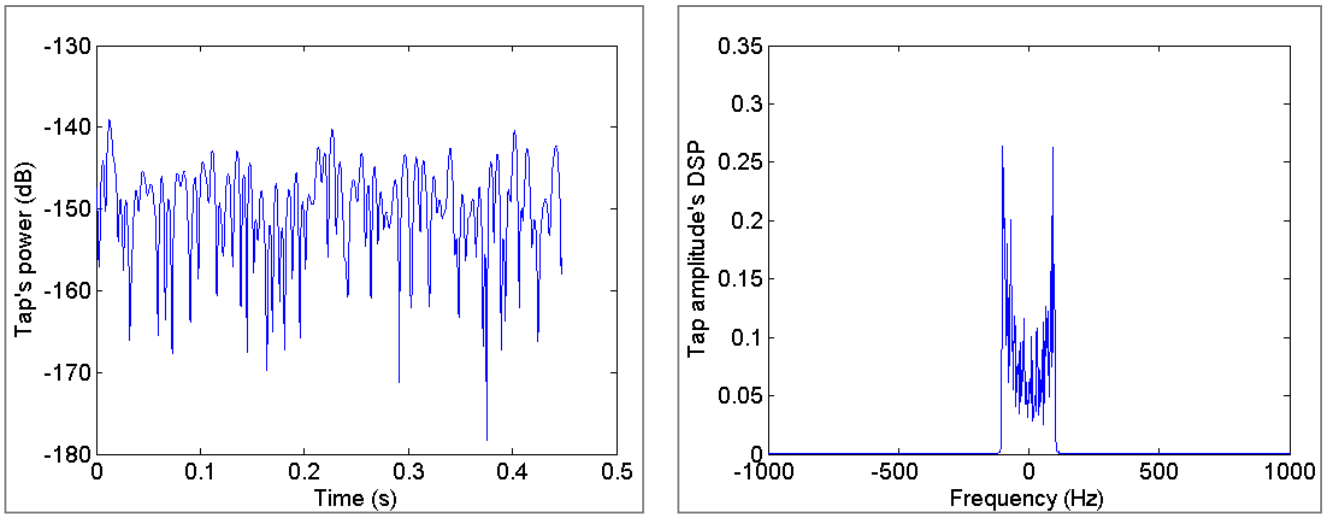

Figure 19 - Illustration of one tap's time series (left) and doppler spectrum (right) at a speed of 50 km/h

Figure 20 shows the CIR and the channel transfer function (CTF) at 2 different instants of the time series.

On the CIR figure, the large delay interval during which multipath exist is shown. The latest signal replica arrives at a delay of 2.14 µs. This creates a frequency-selective channel, as observed on the CTF figure.

The 2 instants of observation are separated by 22.4 ms, which corresponds to a distance of 6.2 cm at a speed of 10 km/h. This illustrates the fact that the channel is rapidly changing.

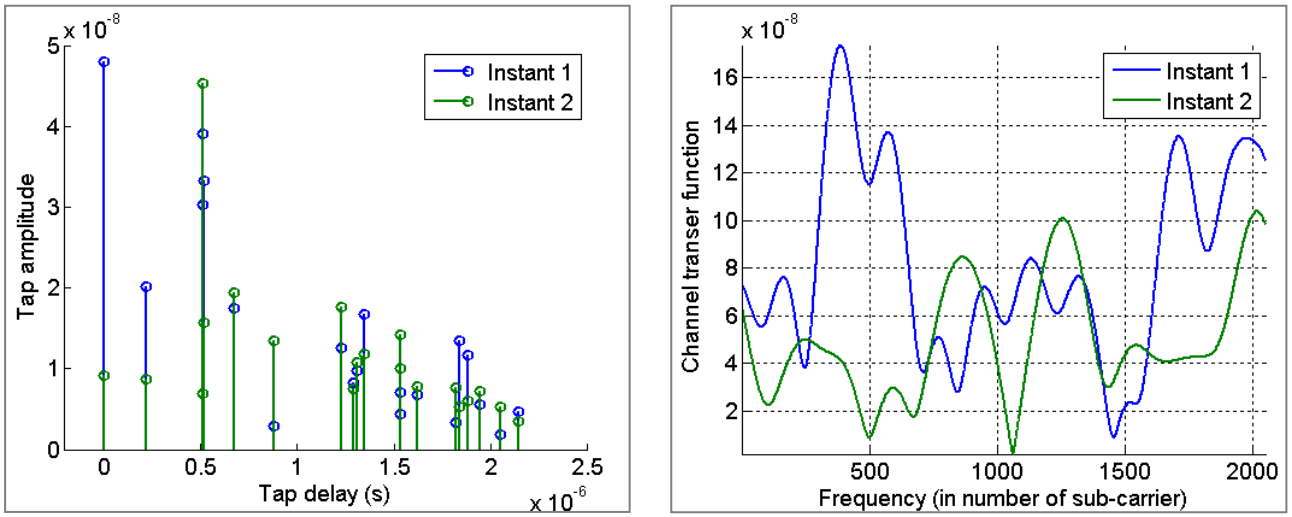

Figure 20 - Illustration of CIR (left) and CTF (right) at 2 different instants, separated by 22.4 µs

Finally, Figure 21 illustrates the evolution of the CTF amplitude in time. The y-axis corresponds to the frequency range normalized by the sub-carrier bandwidth, the x-axis to the time of observation and the color to the amplitude of the CTF.

Again, the frequency selectivity of the TU-20 channel and the fast variation of the CTF are observed: the fading is correlated in the frequency and time dimensions with a limited correlation distance.

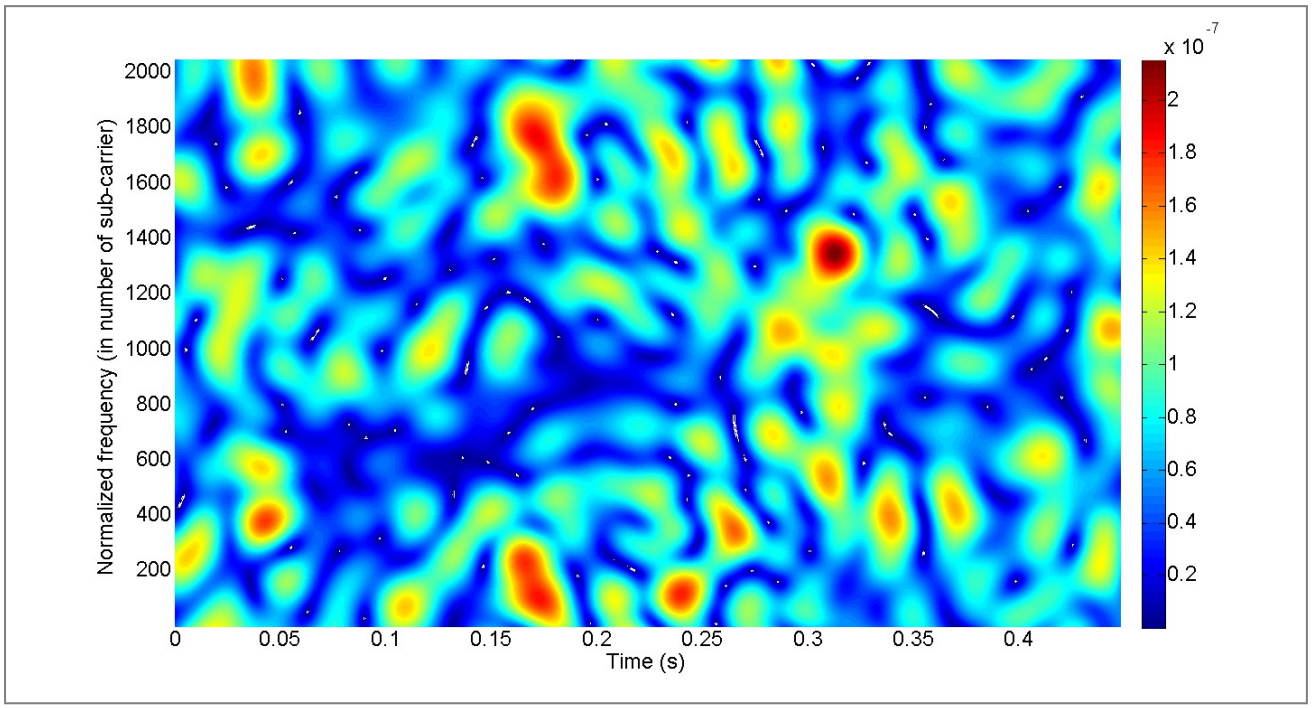

Figure 21 - Time-varying channel transfer function's amplitude

3.1.5 Discussion on the adequation of this model

The presented CIR model enables to test the pseudo-range estimation methods using validated hypothesis, and in particular:

- **a realistic signal power degradation due to the distance** between the terrestrial emitter and the receiver;
- a realistic **time dispersion** or equivalently **frequency selectivity** of the channel by the use of 20 delayed multipaths;
- an adequate **fast fading** of each multipath amplitude, which depends on the receiver's speed.

However, not all the characteristics of an urban propagation channel are taken into account in this simplified model, due to lack of information or for simplification reasons. It lacks notably:

- **The multipath delay variation**. In this model, all multipaths keep the same relative delay, which is not realistic for a mobile receiver over long observation duration. For example, if a receiver gets close to a wall, there should be a group of multipath that sees its delay decreased;
- **The apparition and disappearing of taps**. The receiver always receives 20 signal replicas from the emitter. Some replicas will virtually disappear due to fading, but on a short duration only.

- **No NLOS error**. The first multipath arriving at the receiver is always supposed to follow the LOS path. This does not simulate the fact that the LOS path may be totally blocked. This issue can be mitigated by the fact that in this model, the largest peak in the CIR amplitude will often be toward 0.51 µs, where 3 multipaths arrive at almost the same delay.
- **Shadowing**. It is well accepted that shadowing adds an additional log-normally-distributed attenuation to the signal power, with a standard deviation of ~10dB and a correlation distance of the order of the building block dimensions, e.g. ~30m [Pérez Fontán 2008]. Simulating shadowing would therefore require very large time series, e.g. several *hundreds* of meters travelled during the time series. The size of such time series would have been incompatible with the types of simulations considered in this study.

The weaknesses of the considered model essentially come from the fact that the 2 combined models (COST 231 WI and TU-20) have been created for telecommunication system validation. In particular, the TU-20 model aims at creating the received signal power dynamics that a telecommunication receiver may encounter, in order to validate demodulation, channel equalization, interleaving and/or coding techniques. It is not interested in the fine multipath delay modelling, which would be required for a positioning-related study.

Other urban multipath channel models have been investigated and are presented in "Annex B - Other investigated urban propagation models". However, none of them could completely solve the issues of the model presented in this section. There is clearly a need to research and develop new urban propagation model dedicated to the radionavigation domain.

However, the retained multipath channel model will permit to simulate the estimation of multipath delays in realistic SNR conditions and in fast fading channels. Using this model, solution to these issues will be found in the pseudo-range estimation method. Later on, in Section 4.3, the pseudo-range estimation method will be tested using real channel sounding measurements.

3.2 CIR estimation by correlation

CIR estimation is done by correlating the received signal with a local replica of the expected signal. This local replica is composed of the pilot symbols on the pilot sub-carriers and null symbols elsewhere. The correlation process takes advantage of the FFT demodulation of the received OFDM signal and is achieved by doing the iFFT of the product of the frequency-domain symbols. The correlation process is illustrated by the following block diagram.

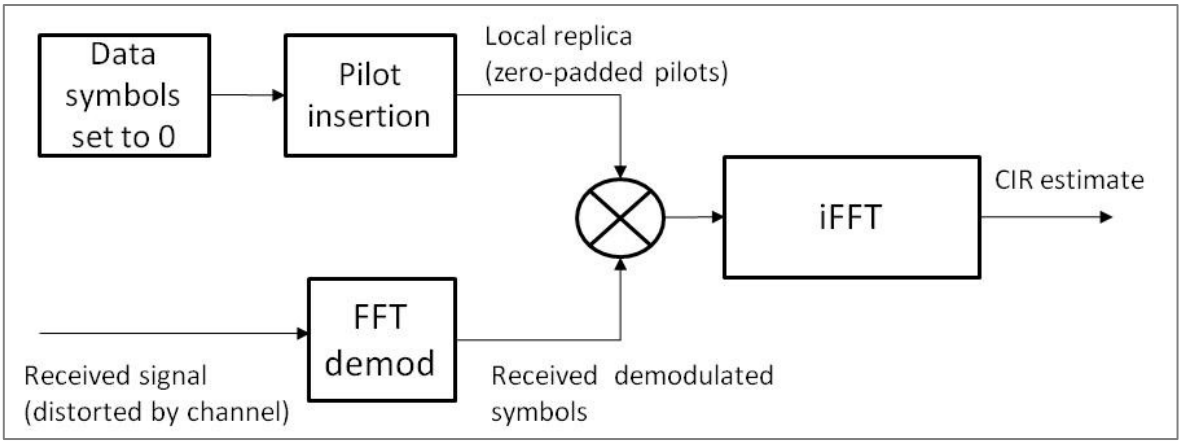

Figure 22 - Correlation operation done to estimate the CIR

The local pilot signal is defined as follows: let us call $\mathcal{P}$ the pilot sub-carrier index space. The expression of the local pilot signal on sub-carrier q of OFDM symbol l is

$p_{l,q} = c_{l,q}$ if $q \in \mathcal{P}$
$p_{l,q} = 0$ on others sub-carriers

The local pilot signal will only use the ***scattered*** pilot symbols. This means that we can use the following index change:

$$q \in \mathcal{P} \Leftrightarrow q = i.P + N_0 \text{ for } i \in [0..N_p]$$

where N_0 is sub-carrier index of the first scattered pilot. This number varies with the OFDM symbol number. It therefore depends on the index l. $N_0 \in \{12, 3, 6, 9\} + N_{guard}$
N_{guard} is the number of null sub-carriers on the lower part of the transmission spectrum, which depends on N_{FFT}
N_p is the number of scattered pilot sub-carriers, which also depends on the FFT size
P is scattered pilot pattern period. $P = 12$ for DVB-SH signals, which means that pilot symbols are inserted every 12 symbols.

3.2.1 Correlation over a single symbol with fine frequency offset hypothesis

In this section, the starting point of these calculations is Eq. 2.7, ie the expression of the demodulated signal under good synchronization hypothesis ($\Delta f = 0$ and small $\Delta\tau \neq 0$). A noise-free transmission is considered, thus dismissing the noise term. The received demodulated symbol on sub-carrier q of OFDM symbol l is

$$d_{l,q} = c_{l,q}.H_{l,q}.e^{-j2\pi\frac{q.\Delta\tau}{N_{FFT}}}$$

There exists a time offset between the local signal and the received signal, which we call Δt, expressed in number of samples.

$$p_{l,q}(\Delta t) = p_{l,q}.e^{-j2\pi\frac{q.\Delta t}{N_{FFT}}}$$

The received pilot symbols is correlated with the local reference signals. As the correlation is done only on the pilot subcarriers, the index q goes through the pilot sub-carriers index subset $\mathcal{P}$ only.

$$R_l(\Delta t) = \frac{1}{N_p}\sum_{q\in\mathcal{P}} d_{l,q}.p^*_{l,q}(\Delta t)$$

After index change and considering that the pilots are BPSK-modulated symbols, $c_k.c_k^* = \sigma_p^2$, where σ_p^2 is the power of the boosted pilots, we obtain

$$R_l(\Delta t) = \frac{\sigma_p^2}{N_p}\sum_{i=0}^{N_{pilots}-1} H_{l,i.P+N_0}.e^{j2\pi\frac{(i.P+N_0).(\Delta t-\Delta\tau)}{N_{FFT}}} = \frac{\sigma_p^2}{N_p}\, e^{j2\pi\frac{N_0.(\Delta t-\Delta\tau)}{N_{FFT}}}\sum_{i=0}^{N_{pilots}-1} H_{l,i.P+N_0}.e^{j2\pi\frac{i.P.(\Delta t-\Delta\tau)}{N_{FFT}}}$$

Let us replace the channel transfer function by its expression:

$$R_l(\Delta t) = \frac{\sigma_p^2}{N_p}\, e^{j2\pi\frac{N_0.(\Delta t-\Delta\tau)}{N_{FFT}}} \sum_{i=0}^{N_{pilots}-1} \sum_{n=0}^{N_{taps}-1} l_{COST}(d_l).a_{l,n}.e^{-\frac{j2\pi(i.P+N_0)\tau_n}{N_{FFT}}}.e^{j2\pi\frac{i.P.(\Delta t-\Delta\tau)}{N_{FFT}}}$$

$$\boxed{R_l(\Delta t) = \frac{\sigma_p^2}{N_p}.\sum_{n=0}^{N_{taps}-1} \alpha_{l,n}(\Delta t).\frac{\sin(\pi\beta.(\tau_n+\Delta\tau-\Delta t))\,)}{\sin\left(\frac{\pi\beta}{N_p}.(\tau_n+\Delta\tau-\Delta t)\right)}} \quad \textbf{Eq. 3.5}$$

where $\alpha_{l,n}(\Delta t) = l_{COST}(d_l).a_{l,n}.e^{-\frac{j\pi(\tau_n+\Delta\tau-\Delta t)}{N_{FFT}}.\left(2.N_0+P.(N_p-1)\right)}$ is a complex factor accounting for the multipath complex amplitude and a phase term depending on many parameters;

$\beta = \frac{PN_p}{N_{FFT}} = 0.832$. It is a constant in the DVB-SH standard, valid for every DVB-SH modes.

For short offset between the local replica delay with regards to the tap delay and the residual time synchronization offset (ie $|\tau_n + \Delta\tau - \Delta t| \ll 1$), the correlation output can be approximated as:

$$R_l(\Delta t) \approx \sigma_p^2.\sum_{n=0}^{N_{taps}-1} \alpha_{l,n}(\Delta t).\mathrm{sinc}(\pi\beta.(\tau_n+\Delta\tau-\Delta t))\,) \quad \textbf{Eq. 3.6}$$

3.2.2 Noise at the correlator's output

If the noise is no longer neglected, the correlator output becomes:

$$R_l(\Delta t) = \frac{\sigma_p^2}{N_p}.\sum_{n=0}^{N_{taps}-1} \alpha_{l,n}(\Delta t).\frac{\sin(\pi\beta.(\tau_n+\Delta\tau-\Delta t))\,)}{\sin\left(\frac{\pi\beta}{N_p}.(\tau_n+\Delta\tau-\Delta t)\right)} + \frac{1}{N_p}\sum_{q\in\mathcal{P}} n_{l,q}.p_{l,q}^*(\Delta t)$$

where $n_{l,q}$ is the noise affecting the q-th sub-carrier of the l-th OFDM symbol. This noise has a variance noted σ_n^2.

Using the central limit theorem, the variance of this noise component can be estimated equal to $N_p.\sigma_n^2$. This noise will affect the various signal processing techniques used in the following.

This noise power can be reduced by averaging the correlation output over several symbol. However, one has to be careful since the channel will also change during the averaging window.

3.2.3 Multipath amplitude estimation thanks to correlation

If the correlation is calculated exactly at one multipath delay τ_k, and noise term of the received signal is neglected, the correlator's output is equal to

$$R_l(\Delta t = \Delta\tau + \tau_k) = \sigma_p^2 . l_{COST}(d_l) . a_{l,k} + \frac{\sigma_p^2}{N_p} . \sum_{\substack{n=0 \\ n \neq k}}^{N_{taps}-1} \alpha_{l,n}(\Delta t) . \frac{\sin\left(\pi\beta(\tau_n + \Delta\tau - \Delta t)\right)}{\sin\left(\frac{\pi\beta}{N_p}(\tau_n + \Delta\tau - \Delta t)\right)}$$ **Eq. 3.7**

In Eq. 3.7, there are 2 terms: the first one corresponds to the amplitude of the k-th multipath, while the other term corresponds to an error introduced by the presence of other multipaths.

If the other multipaths are sufficiently far from the observed delay and not too powerful, the second term should be small compared to the desired one.

3.2.4 Ambiguity of the estimated multipath delay

The multipath delay estimation is the basis for the pseudo-range estimation. By doing this correlation, 2 sources of ambiguity affect a multipath delay, which must be addressed in order to have a precise, unambiguous pseudo-range estimation:

- the repetition of the scattered pilot sequence,
- the periodicity of the CIR estimate.

The scattered pilot sequence repeats itself every 4 OFDM symbols (see Figure 10). This creates an ambiguity on a multipath delay corresponding to 4 OFDM symbol duration.

The correlation operation creates a periodic function, with a period of N_p samples (see Figure 24, right). This creates an ambiguity corresponding to N_p sample duration. It should be noted that the number of symbols can be artificially increased by averaging the correlation coming from 4 consecutive symbols. Since the scattered pilot sequence is different in 4 consecutive symbols, it would be equivalent to do a correlation with $4.N_p$ symbols, as shown in Figure 23. This solution can be used in order to mitigate the effect of ambiguity, since it would multiply by 4 the ambiguity distance due to the periodicity of the correlation function.

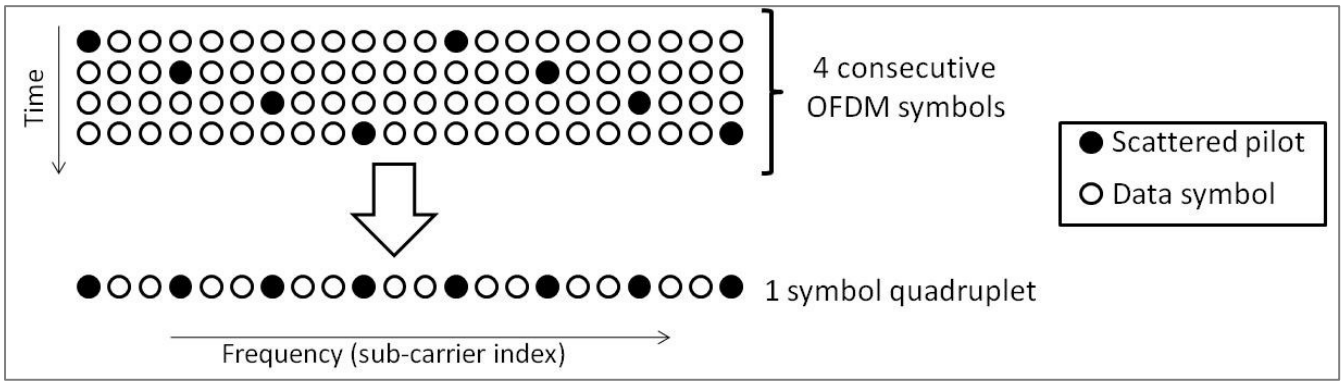

Figure 23 - Artificial scattered pilot increase by averaging several consecutive correlation output

The 2 ambiguity values for every DVB-SH modes are collected in Table 7. For each DVB-SH modes, the most problematic ambiguity is the one created by the periodicity of the CIR estimate. The modes with lower FFT size are and higher bandwidth are more affected by this ambiguity, since they have the lower number of scattered pilot symbols.

If the ambiguity is several time larger than the emitter separation, it can be easily solved at the position computation level. A typical emitter separation would be comprised between 1 and 2 km.; Therefore, DVB-SH modes with value 1K FFT size should be avoided. A more complete study of the impact of the DVB-SH modes on the positioning service is provided in section 7.2.

Table 7 - estimated delay ambiguity for each DVB-SH modes.
The upper value corresponds to the scattered pilot sequence repetition,
while the downer value corresponds to the CIR estimate periodicity.

Mode	CP = 1/4	CP = 1/8	CP = 1/16	CP = 1/32
1K, 1.7 MHz	840,0 km 11,6 km	756,0 km 11,6 km	714,0 km 11,6 km	693,0 km 11,6 km
1K, 5 MHz	268,8 km 3,7 km	241,9 km 3,7 km	228,5 km 3,7 km	221,8 km 3,7 km
1K, 8 MHz	168,0 km 2,3 km	151,2 km 2,3 km	142,8 km 2,3 km	138,6 km 2,3 km
2K, 5 MHz	537,6 km 7,4 km	483,8 km 7,4 km	457,0 km 7,4 km	443,5 km 7,4 km
2K, 8 MHz	336,0 km 4,7 km	302,4 km 4,7 km	285,6 km 4,7 km	277,2 km 4,7 km
4K, 5 MHz	1075,2 km 14,9 km	967,7 km 14,9 km	913,9 km 14,9 km	887,0 km 14,9 km
4K, 8 MHz	672,0 km 9,3 km	604,8 km 9,3 km	571,2 km 9,3 km	554,4 km 9,3 km
8K, 5 MHz	2150,4 km 29,8 km	1935,4 km 29,8 km	1828,6 km 29,8 km	1774,1 km 29,8 km
8K, 8 MHz	1344,0 km 18,6 km	1209,6 km 18,6 km	1142,4 km 18,6 km	1108,8 km 18,6 km

3.2.5 Illustration of the CIR estimation by correlation

3.2.5.1 Ideal correlation peak shape

The correlation expression indicates that the shape of the correlation peak is a sinus cardinalis function for small delays, as predicted by Eq. 3.6 (Figure 24, left). The amplitude of the peak corresponds to the boosted amplitude of the sent symbols ($\sigma_p^2 = 4/3$).

In addition, the correlation output amplitude function is periodic, with a period of N_p samples (Figure 24, right).

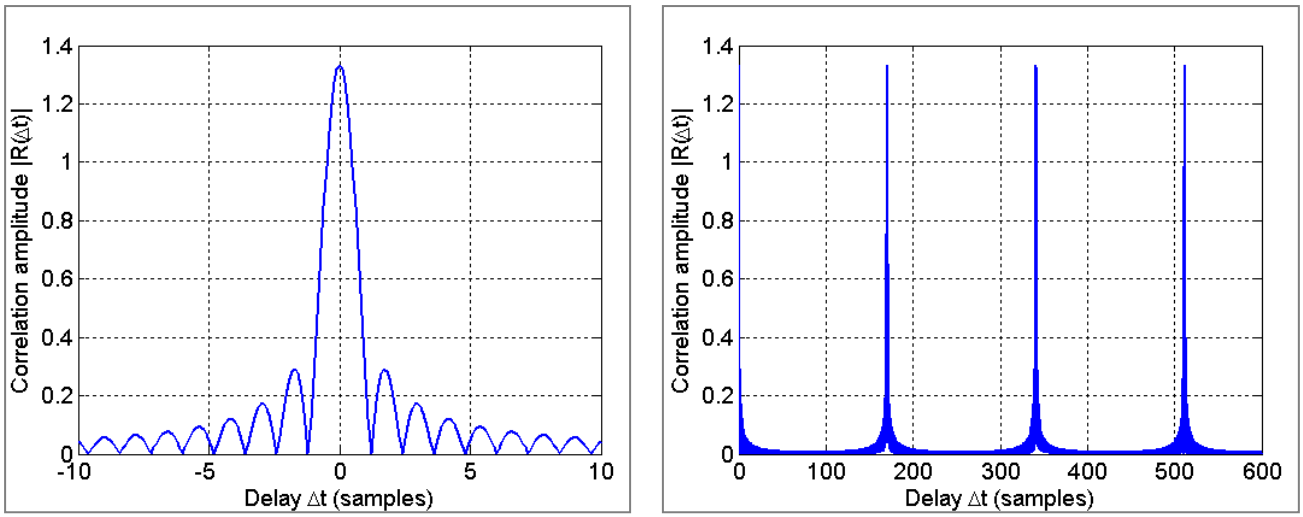

Figure 24 - Correlation amplitude for a single-tap channel. The pulse shape can be approximated by a sinus cardinalis for small delays (left), which repeats itself every N_p samples (right)

3.2.5.2 3-multipath channel estimation

Figure 25 shows the resulting correlation amplitude for a 3-multipath channel. We can observe the presence of large sidelobes in the correlation function, that could potentially (and wrongly!) be considered as multipaths. Also, when the multipaths have a random phase, the resulting correlation amplitude is very affected.

CIR parameter extraction will therefore be difficult in such multipath channel.

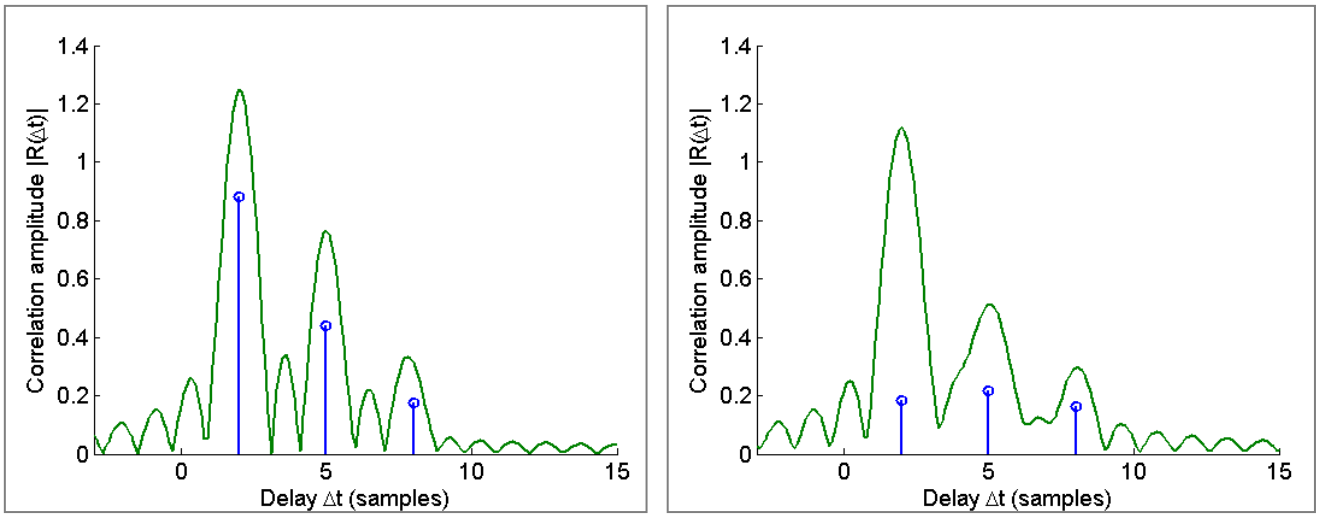

Figure 25 - Illustration of correlation amplitude for a multipath channel. Multpaths are found at delays 2, 5 and 8.T_{samp}. The multipahts have the same phase on the left figure, while their phase is random on the right figure.

3.2.5.3 Illustration of TU-20 channel estimation

The following graphs (Figure 26) shows the power of the correlation output expressed in dB, obtained for the CIR time series described in section 3.1.4 at different SNR. The correlation is calculated over a large delay range (represented on the y-axis) in order to see all 20 multipaths and their sidelobes, and over a duration (represented on the x-axis) long enough to observe large fluctuations of the CIR amplitude (several hundreds of ms).

The position of the peaks of power in this channel time series varies in time. Often, the first multipath has a power inferior to later multipaths. This will be a challenge since it is the first multipath that is desired for the computation of the pseudo-range measurement.

Also, at high SNR, the correlation sidelobes due to the sinc-shaped correlation peak appear clearly. These sidelobes may be wrongly considered as individual multipath, which is a problem for the detection of the earliest significant multipath.

The SNR at which the signal is received is likely to be above 0 dB for the closest emitter. However, viewing the correlation output for low SNR, it should be possible to estimate multipath delay even for remote emitters.

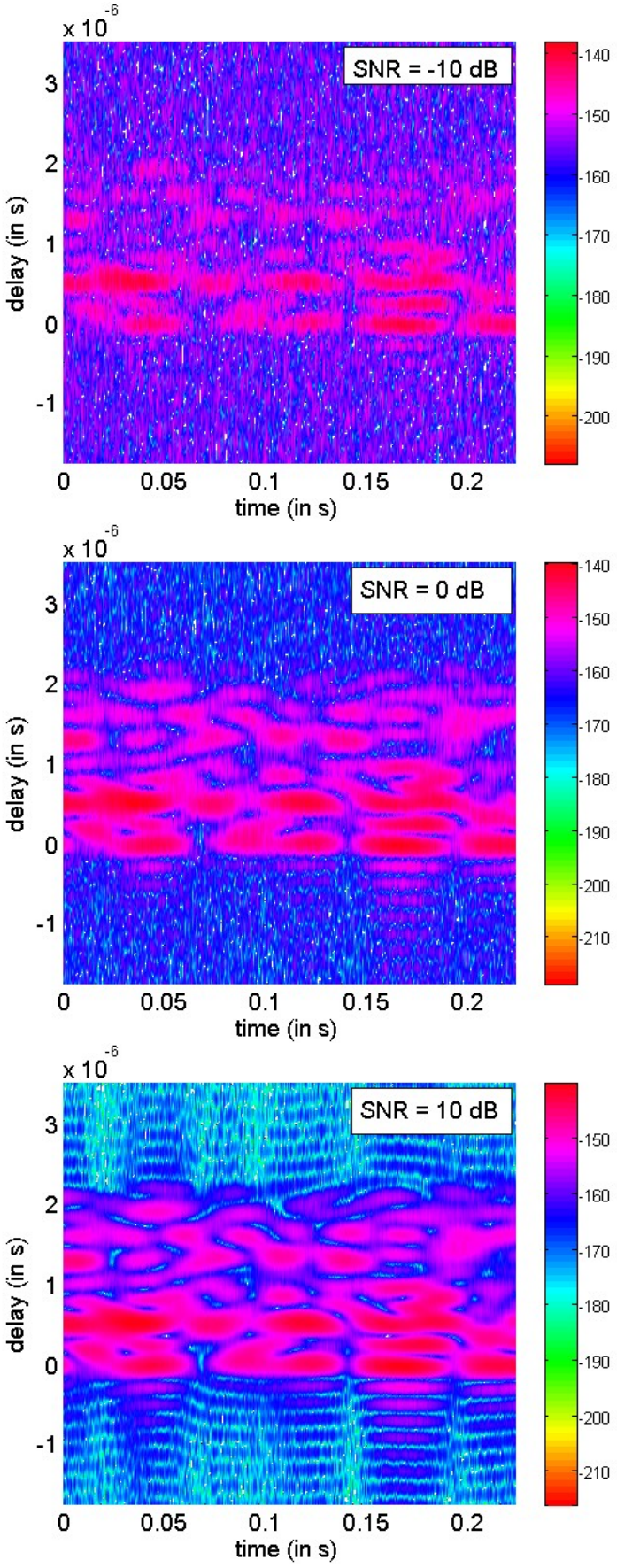

Figure 26 - Illustration TU-20 CIR time series estimation by correlation at different SNR: -10 dB; 0 dB; 10 dB

3.3 Acquisition phase: Matching Pursuit algorithm

The correlation function over a wide range of delay provides an estimate of the CIR as seen in the previous section.

Once the estimate of the CIR is available, some multipath extraction methods can be used. They are generally estimation techniques which aims at finding some parameters (the multipath characteristics), which yield the best matching between a multipath channel model and the (noisy) CIR estimate. Among others, the SAGE [Fleury 1999], ESPRIT [Paulraj 1985] or Matching Pursuit [Cotter 2002] are well-known algorithms.

In this study, the Matching pursuit algorithm has been chosen. This algorithm is well suited to estimate the delay of sparse CIR, ie CIR which is defined over a large delay range with small non-zero support. Therefore, this technique will be well-adapted to CIR encountered in Single Frequency Networks, where the signal replicas coming from different emitters may arrive with large relative delays.

3.3.1 Principle of the Matching Pursuit algorithm

The overall principle of the Matching Pursuit is a variation of the Least Square algorithm. The goal is to find the family ρ_l, φ_l, and τ_l for $l \in [1..L]$ that minimizes the error between a measurement (the CIR estimate vector obtained by correlation) and a model of the multipath CIR:

$$\hat{\rho}_l, \hat{\varphi}_l, \hat{\tau}_l = \arg \min_{\rho_l, \varphi_l, \tau_l} \sum_{k=1}^{K} \left\| \hat{h}(k) - \sum_{l=1}^{L} \rho_l e^{j\varphi_l} f(k - \tau_l) \right\|^2 \quad \textbf{Eq. 3.8}$$

where K is the length of the estimated vector
L is the number of considered multipaths
$\hat{h}(k)$ is the channel impulse response estimates
$f(k)$ is the pulse model of the estimated multipath

Eq. 3.8 can be rewritten using matrix notation:

$$\hat{\rho}_l, \hat{\varphi}_l, \hat{\tau}_l = \arg \min_{\hat{\rho}_l, \hat{\varphi}_l, \hat{\tau}_l} \left\| \hat{\mathbf{h}} - \mathbf{P}\boldsymbol{\beta} \right\|^2 \quad \textbf{Eq. 3.9}$$

where $\hat{\mathbf{h}} = \left[\hat{h}_1, \hat{h}_2, \ldots, \hat{h}_K\right]$ is the vector of the CIR estimates
$\mathbf{P} = [\mathbf{P}_1, \mathbf{P}_2, \ldots, \mathbf{P}_L]$ is a KxL matrix containing the pulse samples for each considered multipath
$\mathbf{P}_l = [f(1 - \tau_l), f(2 - \tau_l), \ldots, f(K - \tau_l)]^T$ is the pulse model for the multipath affected by a delay equal to τ_l
$\boldsymbol{\beta} = \left[\rho_1 e^{j\varphi_1}, \rho_2 e^{j\varphi_2}, \ldots, \rho_L e^{j\varphi_L}\right]^{\mathrm{T}}$ is the vector of the complex amplitude of the L considered multipaths.

The Matching Pursuit algorithm [Cotter 2002] permits to find the delays $\hat{\tau}_l$. The principle is to find iteratively the columns of $\mathbf{P}$ that best matches the CIR estimates (the column index corresponds to

the delay of the taps). After each iteration, the CIR vector is corrected by removing the pulse of the retained path and a new delay is estimated.

The CIR estimate vector $\hat{\mathbf{h}}_\mathbf{0} = [\hat{h}_1, \hat{h}_2, \dots, \hat{h}_K]$ is initiated with the correlation output described in section 3.2.

For each step i, the following operations are done:

- The most probable instant is found:

$$\hat{\tau}_{i+1} = \arg\max_{l} \frac{\left|\mathbf{P}_l^H . \hat{\mathbf{h}}_i\right|^2}{\left\|\mathbf{P}_l^H\right\|^2}$$

- The CIR estimate is corrected by the pulse centered on $\hat{\tau}_i$:

$$\hat{\mathbf{h}}_{i+1} = \hat{\mathbf{h}}_i - \frac{\mathbf{P}_l^H . \hat{\mathbf{h}}_i}{\left\|\mathbf{P}_l^H\right\|^2} . \mathbf{P}_l$$

These steps are looped until a given number of multipath delays have been extracted or the corrected CIR estimate at step i no longer contains any useful signal, ie until $\left\|\hat{\mathbf{h}}_i\right\| < \varepsilon$

The multipath amplitude is estimated by the factor $\frac{\mathbf{P}_l^H . \hat{\mathbf{h}}_i}{\left\|\mathbf{P}_l^H\right\|^2}$.

3.3.2 Application of the algorithm to the studied case

We have decided to use the Matching Pursuit algorithm with the absolute value of the CIR estimate. Indeed, the phase of each multipath is changing very rapidly (with a displacement of the receiver of the order of the cm), and it will therefore be difficult to use this information consistently all along the pseudo-range estimation process.

In this case, the CIR estimate vector is provided by the amplitude of the correlation output over a wide range of delay: $\hat{\mathbf{h}} = [|R_l(0)|, |R_l(T_s')|, \dots, |R_l((N_{corr}-1)T_s')|]$, where $[0, T_s', \dots, (N_{corr}-1)T_s']$ is delay range over which the correlation was calculated. $1/T_s'$ is the sampling rate of the CIR estimate.

The correlation range is chosen to cover the delay range over which a delay may be encountered. Therefore, it should be at least as long as the maximum expected multipath delay.

The pulse shape of one multipath in the correlation output is approximated by a sinus cardinalis function (Eq. 3.6). This pulse model is used to generate the matrix $\mathbf{P}$, with each column being

$$\mathbf{P}_l = \frac{4}{3}\left[sinc(\pi\beta(1-l)T_s'), sinc(\pi\beta(2-l)T_s'), \dots, sinc(\pi\beta(N_{corr}-l)T_s')\right]^T \quad \textbf{Eq. 3.10}$$

For the implementation of this algorithm, we will therefore use the pulse matrix defined as follows:

$$\mathbf{P} = \frac{4}{3}\begin{bmatrix} sinc(0) & sinc(-\pi\beta T_s') & \cdots & sinc(-\pi\beta(N_{corr}-1)T_s') \\ sinc(\pi\beta T_s') & sinc(0) & \cdots & sinc(-\pi\beta(N_{corr}-2)T_s') \\ \vdots & \vdots & & \vdots \\ sinc(\pi\beta(N_{corr}-1)T_s') & sinc(\pi\beta(N_{corr}-2)T_s') & \cdots & sinc(0) \end{bmatrix}$$

where T_s' is the sampling period of the estimated CIR

3.3.3 Simulations of multipath acquisitions using the Matching Pursuit algorithm

3.3.3.1 Delay estimation in an AWGN channel

The algorithm is applied to estimate the delay in an AWGN channel (only one replica of the signal arrives at the receiver), with the DVB-SH signal mode (2K, 1/4, 5 MHz). 2500 acquisitions are launched and statistics are derived from this series of simulations.

The rate of false detection is calculated and defined as follows: a false detection is considered when the estimated delay is more than 1 sample away from the true delay. Indeed, if the delay is estimated within one sample of the true value, it is expected that the tracking phase will be able to keep track of this delay.

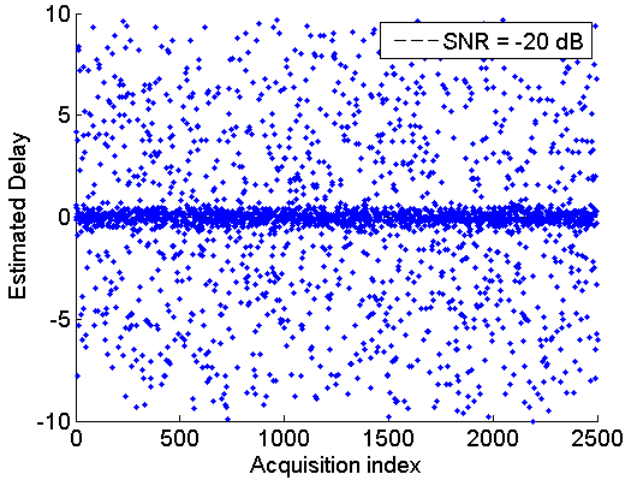

Figure 27 - Illustration of delay estimates obtained by MP for SNR = -20dB

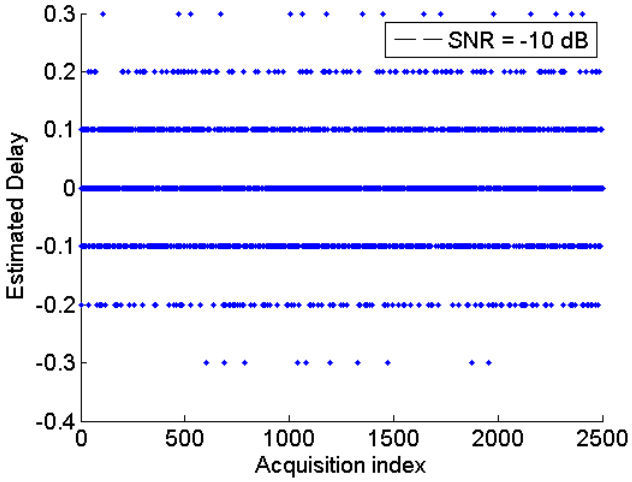

Figure 28 - Illustration of delay estimates obtained by MP for SNR = -10 dB

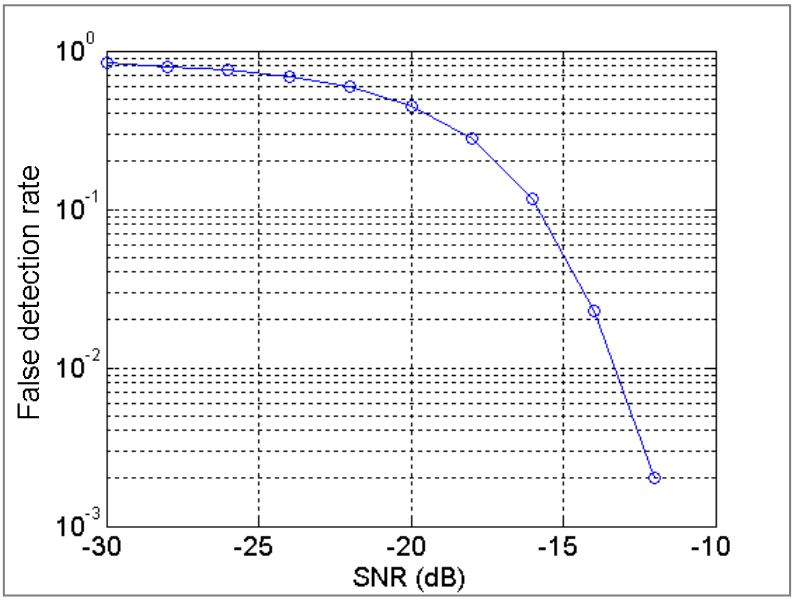

Figure 29 - False detection rate vs SNR

The false detection rate quickly diminishes rapidly with the SNR increase (Figure 29) for SNR above -22 dB. This is coherent with the processing gain of the correlation operation, which is equal to

$G_{corr} = N_{pilots}.4/3 = 142 * 4/3 = 22.7$ dB. Indeed, a correlation peak will be detectable only if the post-correlation SNR is above 0 dB.

Also, it is interesting to see in Figure 28 that the multipath delay is estimated with a resolution equal to the channel estimate sampling duration T_s'. Therefore, the resolution of the delay estimation may be limited by the sampling rate of the CIR estimate, for example due to a design choice aiming at reducing the computational load of the receiver.

3.3.3.2 Delay estimation in a TU-20 channel

In these simulations, the Matching Pursuit algorithm is used for detecting 20 multipaths in the CIR modelled by the TU-20 model. The same CIR realizations shown in section 3.2.5.3 are used.

The Matching Pursuit algorithm is an iterative technique. The first multipath that are estimated are those which brings the most contribution to the CIR estimate. In other words, the Matching Pursuit algorithm estimates the most powerful multipaths first.

In Figure 30, the 10 first detected delays are shown for an SNR between -5 and 10 dB. We can observe that the main multipaths of the estimated CIR are detected, but also that the Matching Pursuit estimates some false delay for low SNR.

In Figure 31, only the 5 first detected delays are shown. This resulting delay estimates are much cleaner, showing that only the most significant multipaths should be kept.

It is also observed that the first multipath delay, which is the desired one for pseudo-range estimation, is not always detected by the Matching Pursuit algorithm, either due to strong fading of this particular multipath, or by the masking effect of other signal replicas.

In order to maximize the chances of using this first signal replica, it seems recommended to start periodic acquisitions (ie a Matching Pursuit algorithm is launched periodically) in order to make sure that the first signal replica is acquired.

3.3.4 Conclusion on the Matching Pursuit algorithm

The Matching Pursuit algorithm is able to provide estimates of the delays of the multipaths present in a CIR for good SNR conditions. However, it has 2 inherent drawbacks:

- the algorithm is very cumbersome: it requires a search computation over a large range of delays and each iteration step requires a large matrix handling.
- the delay estimates do not use the potentially useful information about the multipath delays estimated at previous instants. This latter drawback is also a strength, since it will permit to obtain delay estimates even when no previous information is available.

For these 2 reasons, the Matching Pursuit algorithm is well adapted for a delay ***acquisition*** phase. Multipath delay acquisition will be usefully completed by a delay tracking phase, described in the next section.

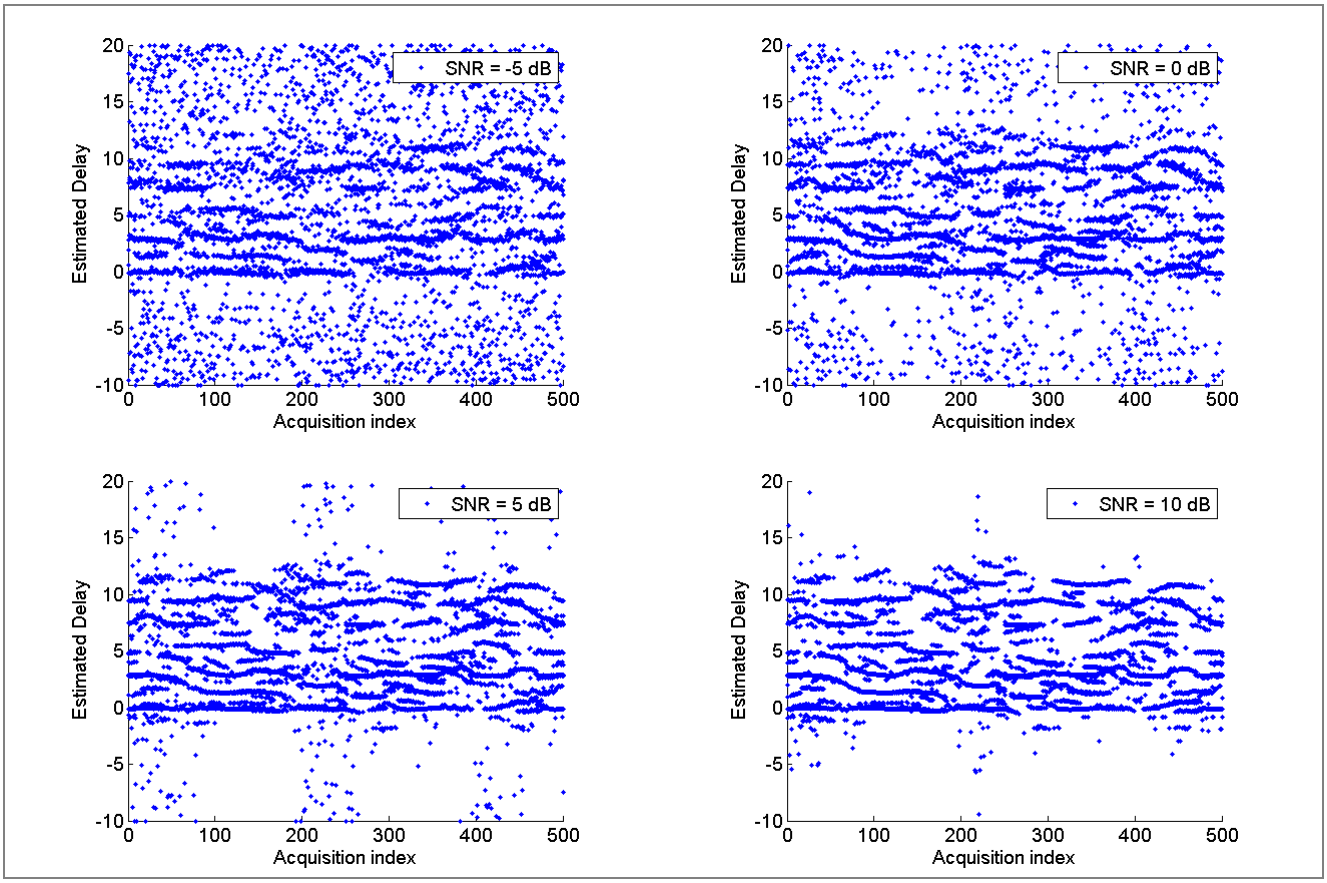

Figure 30 - Delay estimation by Matching Pursuit (10 first estimated multipaths)

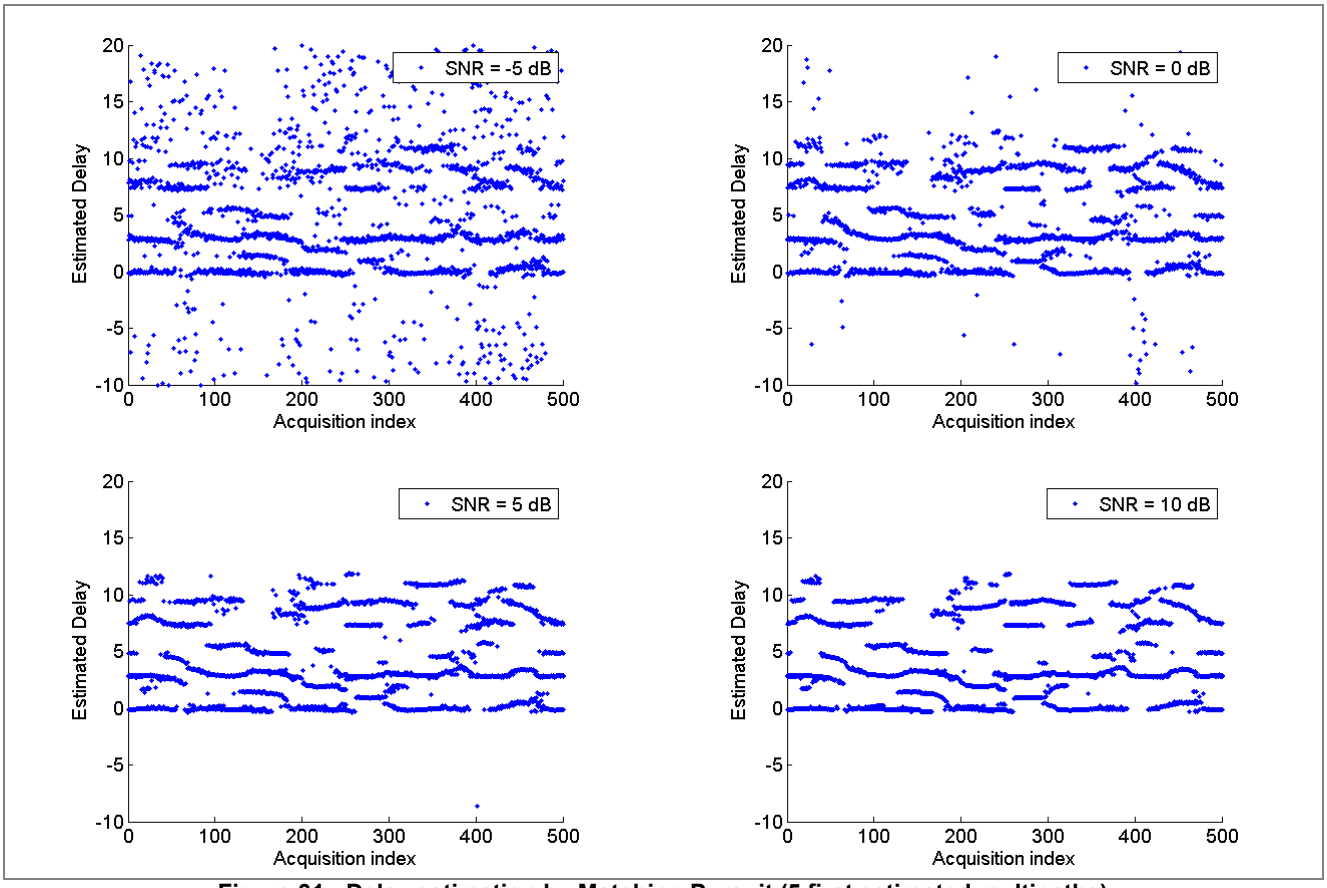

Figure 31 - Delay estimation by Matching Pursuit (5 first estimated multipaths)

3.4 Tracking phase: Delay-Lock Loop

The Matching Pursuit algorithm provides rough delay estimates, which are used to launch a tracking phase using a Delay-Lock Loop (DLL). The DLL will be used to obtain a fine delay estimate, with a much finer resolution than the one obtained previously.

The studied DLL [Yang 1999] (see Figure 32) uses 3 correlators calculating the correlation function at 3 different instants and combines them into a particular discriminator, to obtain the updated value of the delay estimation.

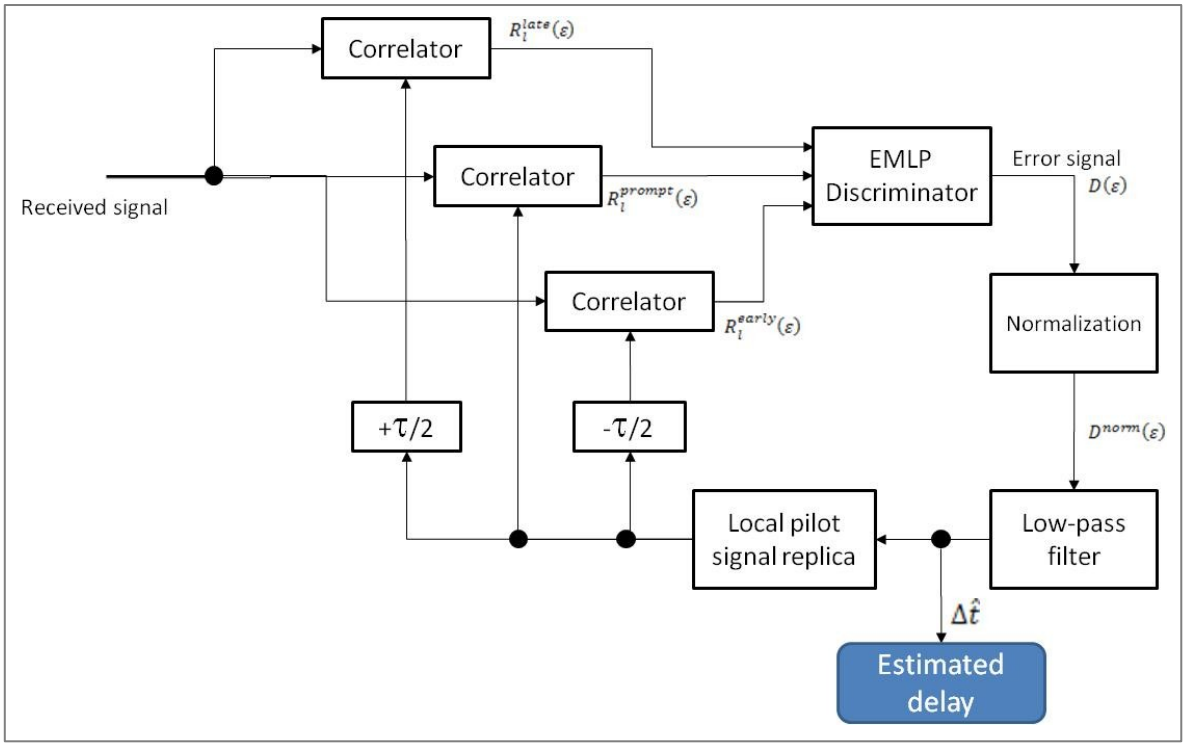

Figure 32 - DLL principle block diagram

3.4.1 Expression of the correlators' outputs for a single tap

3 correlations are achieved:

- one using the incoming signal with a local replica delayed by $\delta/2$. This correlation will be qualified as "early";
- one using the incoming signal with a local replica delayed by $-\delta/2$. This correlation will be qualified as "late";
- one using the incoming signal with a local replica without delay correction. This correlation will be qualified as "prompt".

The parameter δ is called the correlator spacing and is normalized by the sample duration.

Assuming a single-multipath channel and using Eq. 3.6, which supposes a small delay offset between the current estimated delay and the true multipath delay, we can detail the correlators' output as follows:

$$R_l^{early}(\varepsilon) \triangleq R_l\left(\Delta t - \frac{\delta}{2}\right) = \sigma_p^2.\alpha_l.sinc\left(\pi\beta.\left(\varepsilon - \frac{\delta}{2}\right)\right) \quad \textbf{Eq. 3.11}$$

$$R_l^{late}(\varepsilon) \triangleq R_l\left(\Delta t + \frac{\delta}{2}\right) = \sigma_p^2.\alpha_l.sinc\left(\pi\beta.\left(\varepsilon + \frac{\delta}{2}\right)\right) \quad \textbf{Eq. 3.12}$$

$$R_l^{prompt}(\varepsilon) \triangleq R_l(\Delta t) = \sigma_p^2.\alpha_l.sinc(\pi\beta\varepsilon) \quad \textbf{Eq. 3.13}$$

where $\varepsilon \triangleq \Delta t - (\tau_l + \Delta\tau)$ is the offset between the current estimated delay and the true multipath delay. We will call ε the estimation error.

3.4.2 Expression of the discriminator's output

The discriminator used in this DLL is an early minus late power discriminator. The expression of the discriminator's output is

$$D(\varepsilon) = \frac{\left|R_l^{early}(\varepsilon)\right|^2 - \left|R_l^{late}(\varepsilon)\right|^2}{\left|R_l^{prompt}(\varepsilon)\right|^2} = \frac{sinc\left(\pi\beta.\left(\varepsilon - \frac{\delta}{2}\right)\right)^2 - sinc\left(\pi\beta.\left(\varepsilon + \frac{\delta}{2}\right)\right)^2}{sinc(\pi\beta\varepsilon)^2} \quad \textbf{Eq. 3.14}$$

When the tracking error is small, by using first-order Taylor series, [Serant 2010] has demonstrated that

$$\frac{D(\varepsilon)}{\varepsilon} \underset{\varepsilon \to 0}{\longrightarrow} \frac{1 - \frac{\delta}{2}.\pi.\beta.\sin(\pi\beta\delta) - \cos(\pi\beta\delta)}{\pi^2\beta^2\frac{\delta^3}{16}}$$

The discriminator's expression is therefore linear around 0. This calculation can be used to normalize the discriminator, using a constant K_{norm}, so that the discriminator output is equal to the estimation error, as seen in Figure 33.

In the end,

$$\boxed{D^{norm}(\varepsilon) = \frac{1}{K_{norm}}.\frac{\left|R_l^{early}(\varepsilon)\right|^2 - \left|R_l^{late}(\varepsilon)\right|^2}{\left|R_l^{prompt}(\varepsilon)\right|^2}} \quad \textbf{Eq. 3.15}$$

where $K_{norm} = \frac{1 - \frac{\delta}{2}.\pi.\beta.\sin(\pi\beta\delta) - \cos(\pi\beta\delta)}{\pi^2\beta^2.\frac{\delta^3}{16}}$

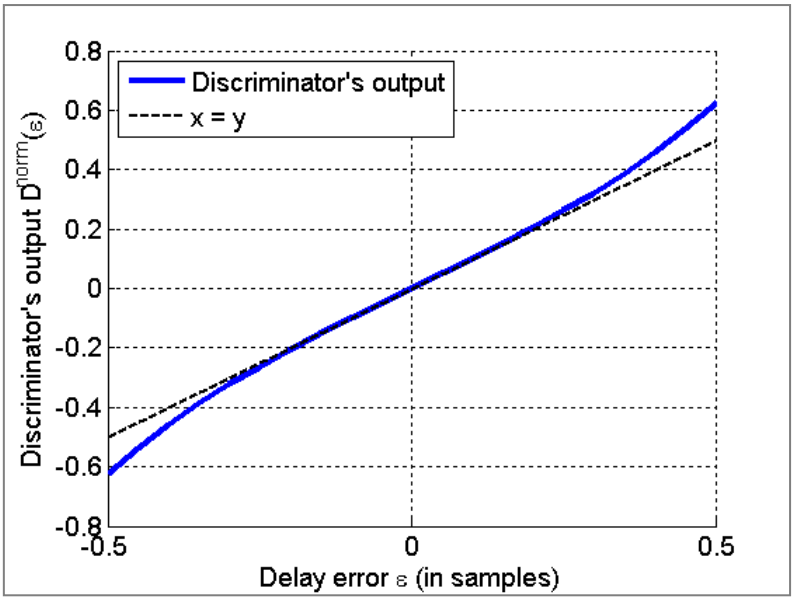

Figure 33 - Curve of the discriminator's output

3.4.3 Tracking loop filter and update of the delay's estimation

The discriminator's output at instant l, named D_l^{norm} is used to update the estimated delay computed at the previous instant.

In order to reduce the noise in the loop, a loop filter is used, according to [Stephens 1995]. Three parameters define the loop: the time between each estimate T_i, the DLL loop order, and noise loop bandwidth B_l.

In this study, $T_i = T_{symb}$ since it is the time between each CIR estimate.

The loop order impacts on the possibility to track highly dynamic inputs.

The noise loop bandwidth B_l has influence on the noise reduction of the output of the loop, and on the ability of the loop to track high dynamic inputs. A high value of B_l means that the loop will be able to track highly dynamic inputs, but the output will be affected by more noise. If B_l is low, the loop will be able to track only low dynamic input, but the nose affecting the output will be lower.

Therefore, B_l has to be chosen so as to find a compromise between the estimated delay dynamics (related to the mobile speed) and the quality of the delay estimate in terms of noise.

Also, the choice of B_l may have an impact on the DLL's robustness against multipath. A high loop bandwidth means that the DLL will likely diverge as soon as the tracked multipath will begin to fade significantly. If the loop bandwidth is reduced, the estimated delay may stay in the linearity zone of the DLL long enough to be able to re-acquire the multipath once the fading is gone. This particularity of the DLL behavior in fading channels would deserve a specific attention which has unfortunately not been given in this PhD study.

3.4.4 Variance of the estimated delay error

Under AWGN hypothesis (no multipath), the variance of the estimated delay can be expressed theoretically. [Serant 2010] describes all the steps to obtain the final result:

$$Var(\Delta\hat{t}) = 2B_l T_{symb} \frac{K_1}{SNR}\left(1 + \frac{K_2}{SNR}\right) \quad \text{Eq. 3.16}$$

where B_l is the DLL equivalent noise loop bandwidth

T_{symb} is the symbol duration and corresponds to the time interval between 2 delay estimates

$SNR = \frac{\alpha^2}{\sigma_n^2}$ is defined as the ratio between the tap's power α^2 and the noise variance σ_n^2

$$K_1 = \frac{9}{4} \cdot \frac{\left(1 - sinc(\pi\beta\delta)\right) sinc\left(\frac{\pi\beta\delta}{2}\right)^2}{N_p . K_{norm}^2}$$

$$K_2 = \frac{9}{32} \cdot \frac{1 + sinc(\pi\beta\delta)}{N_p sinc\left(\frac{\pi\beta\delta}{2}\right)}$$

[Serant 2010] has shown that the influence of the correlator spacing δ is negligible, contrary to the case of classical GNSS signals with rectangular waveforms.

Figure 34 shows the variance of the estimated delay error at the output of the DLL. It considers tracking conditions in a single-tap channel, where the only impairment is thermal noise. The delay's standard deviation is expressed in samples. A numerical application of error's standard deviation for mode (2K 1/4 5MHz) is given in Table 8.

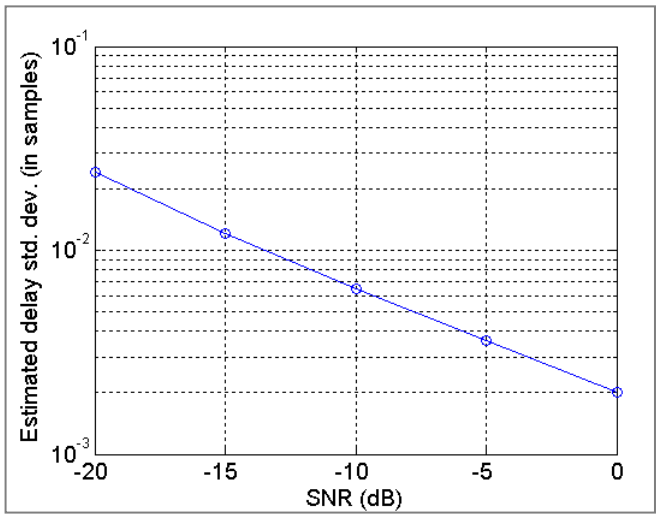

Figure 34 - Tracking loop error standard deviation vs SNR

Table 8 - Tracking loop error's standard deviation vs SNR with $\delta = 1$

SNR (dB)	$Std(\Delta\hat{t})$ (samples)	$Std(\Delta\hat{t}).c.T_{samp}$ for 2K 1/4 5MHz
-20	3.35e-2	1.76 m
-15	1.68e-2	88.2 cm
-10	9.05e-3	47.5 cm
-5	5.01e-3	26.3 cm
0	2.81e-3	14.7 cm

The tracking performances in ideal conditions are very good. Although the AWGN case will rarely be met in urban environment, this result is quite encouraging. Indeed, as seen in section 2.4, typical SNR will generally above 0 dB, thus leaving a large attenuation margin in order to obtain satisfying tracking performances. This means that the proposed pseudo-range method should permit to work in indoor environment or with remote emitters.

3.4.5 Influence of a close multipath on the discriminator's output

The multipath error envelope is often used in order to look at a DLL's sensitivity to multipath. This plot consists of the collection of the discriminator's output for a 2-multipath channel, where the second multipath amplitude is half of the first multipath and its delay takes different values. To have the extreme values of the error, the 2 multipaths are considered in phase and in phase opposition. This analysis is done without noise.

Figure 35 shows the multipath error envelope for the presented DLL

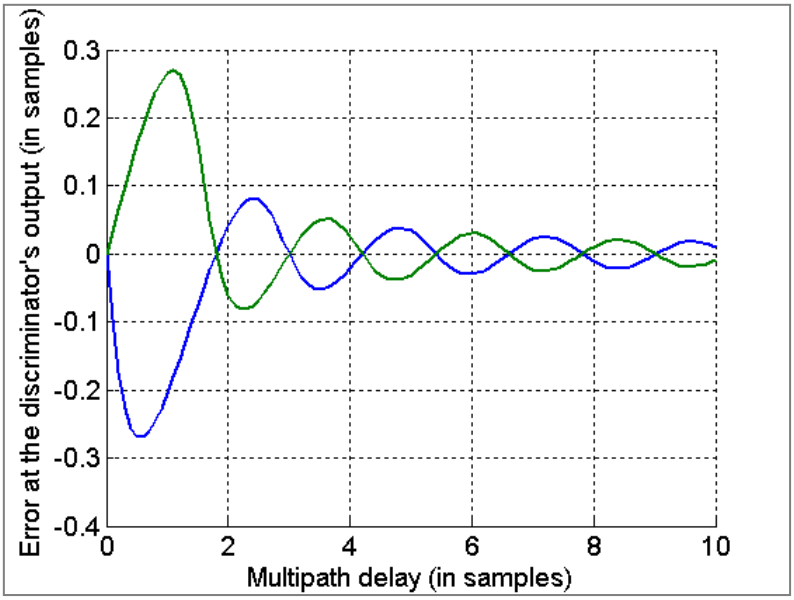

Figure 35 - Multipath error envelope of the proposed DLL with $\delta = 1$

The maximum error is around $0.3T_{samp}$. For the (2K 1/4 5MHz) mode, this relates to about 15m. Also, a multipath has an effect even if it has a long delay, due to the presence of sidelobes in the correlation function.

[Serant 2010] shows that this envelope does not depend on the correlator spacing δ.

3.4.6 Conclusion of the DLL

The DLL is an efficient way to provide precise a delay estimate from an initial rough estimate provided by the Matching Pursuit algorithm. It requires the calculation of the correlation at only 3 different instants. Very good performances are achieved in terms of tracking error variance, with sub-meter error standard deviation for SNR above 0dB.

The influence of the multipath on the DLL output has been studied. Multipath will create a bias even for high relative delays. The case shown in the multipath error envelope consists of 2 multipath of relative amplitude factor equal to 2. This may be a realistic multipath scenario for the case GNSS, where satellite signals are often received with a high elevation angle.

However, in the terrestrial network of emitters, the signals coming from 2 emitters will likely have a relative amplitude factor of several tens of dB. An example of this phenomenon called the Near-Far effect will be shown later in section 4.1.2. Therefore, the other multipath influence is an issue for multipath delay estimation, that can be addressed thanks to the use of windowing techniques, described in the following section.

3.5 Windowing techniques

One of the main issues of the presented delay estimation method is the presence of sidelobes in the CIR estimation. These sidelobes create 2 issues:

1. There is a risk of tracking a sidelobes instead of the main lobe if the DLL is not correctly initialized;
2. In the presence of several multipaths, the delay tracking will be affected even if the relative delay between the multipaths is important. This will be an important issue in terrestrial Single Frequency Network, in which Near-Far effect appears (see section 4.1.2).

In order to reduce these sidelobes, windowing techniques can be used.

3.5.1 Principle of windowing and application to the delay estimation method

Instead of using the correlation described in section 3.2.1, the local replica that is weighted by a window.

$$R_l^{window}(\Delta t) = \frac{1}{N_p} \sum_{q \in \mathcal{P}} c_{l,q} . p_{l,q}^*(\Delta t) . w_{window}(q) \qquad \textbf{Eq. 3.17}$$

where $w(q)$ is the window function.

Two windows have been considered:

- The ***Hamming window***, with the following expression:

$$w_{Ham}(q) = 0.53836 - 0.46164 \cos\left(\frac{2\pi q}{K-1}\right)$$

- The ***Blackman-Harris window***, with the following expression:

$$w_{BH}(q) = 0.35875 - 0.48829 \cos\left(\frac{2\pi q}{K-1}\right) + 0.14128 \cos\left(\frac{4\pi q}{K-1}\right) - 0.01168 \cos\left(\frac{6\pi q}{K-1}\right)$$

where K is the number of non-null subcarriers, as defined in Table 3 in section 2.3.3.

The case without window corresponds to a ***rectangular window***, where $w(q) = 1$.

Figure 36 shows the correlation peak for the different windows. We can observe that compared to the case without window, the Blackman-Harris window strongly attenuates the sidelobes, but in return, its main lobe is larger and lower. The Hamming window stays in-between.

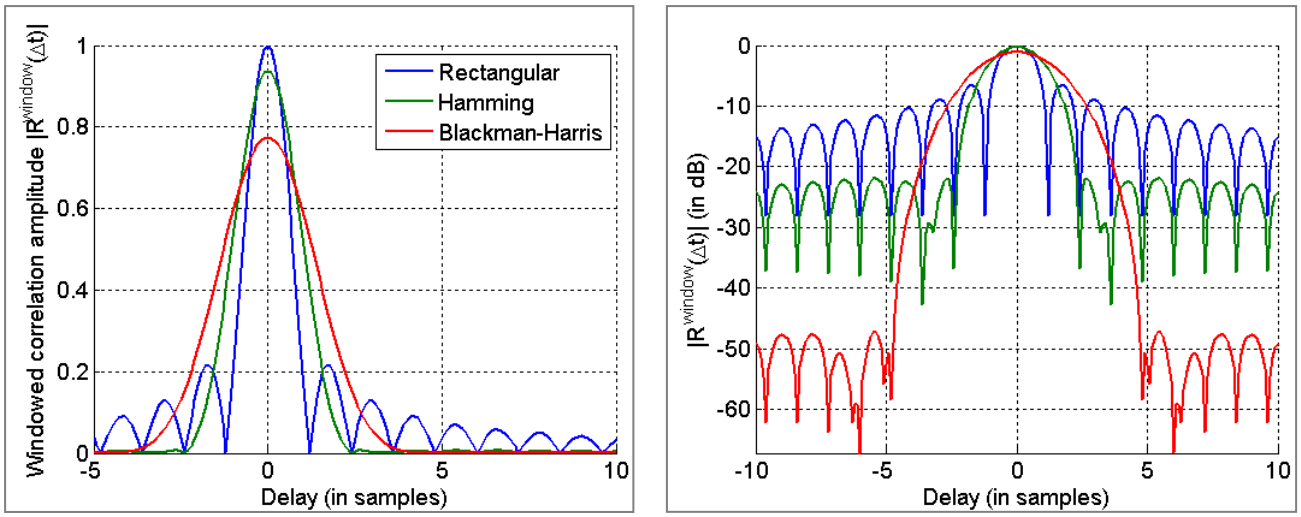

Figure 36 - Correlation peak comparison with windowing techniques

Table 9 quantifies the main lobe widening and amplitude reduction. The main lobe widening factor has been determined so that the main lobe of the windowed correlation would fit the main lobe of a sinc using K_{width}^{window}. This is illustrated in Figure 37 .

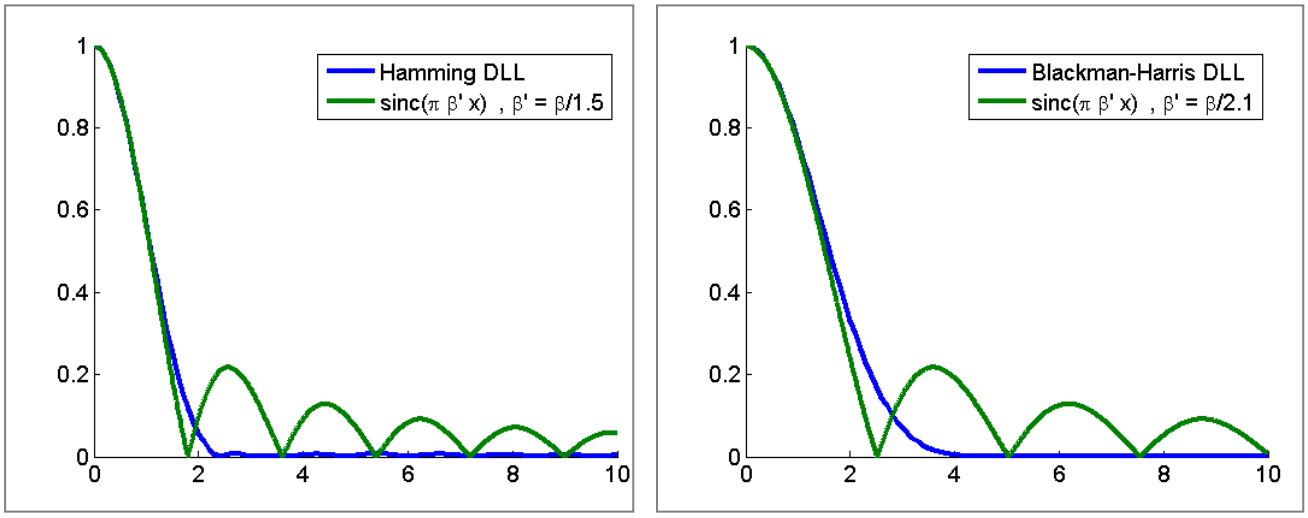

Figure 37 - main lobe widening factor validation for Hamming window (left) and Blackman-Harris window (right)

Table 9 - Correlation degradation quantification due to windowing

Window technique	Main lobe widening factor K_{width}^{window}	Main lobe amplitude K_{amp}^{window}
Rectangular	1	1
Hamming	1.5	0.9374
Blackman-Harris	2.1	0.7744

3.5.2 Application of windowing to CIR estimation

The different windowing techniques are applied to the CIR time series showed in section 3.2.5.3 and plotted in Figure 26.

We can observe (1) the attenuation of the sidelobes for high SNR conditions; (2) the widening of the correlation peaks. This can be a particularly annoying degradation, since 2 multipaths may merge in a single correlation peak. This phenomena is particularly visible for the Blackman-Harris window.

3.5.3 Application of windowing to the delay acquisition

The Matching Pursuit algorithm can be adapted to the use of windowed correlation. In this case, the pulse shape model used to generate matrix **P** (Eq. 3.10) shall take into account the windowing. Since no closed form of the pulse shape has been calculated, the correlator's output expression is used directly to model the pulse shape:

$$\mathbf{P}_l = \frac{1}{N_p}\left[\sum_{q\in\mathcal{P}} c_{l,q}.\,p^*_{l,q}(kT_s').\,w_{window}(q), k \in [-l \ldots N_{corr} - l]\right]^T \qquad \text{Eq. 3.18}$$

Simulations with windowed correlation are done in an AWGN without multipaths. 2500 acquisitions are launched with the DVB-SH signal mode (2K, 1/4, 5 MHz)

As in section 3.3.3, the rate of false detection is calculated (Figure 38) and defined as follows: a false detection is considered when the estimated delay is more than 1 sample away from the true delay.

The windowing technique bring a small degradation, that should not be compromising the acquisition of signals from nearby emitters since encountered SNR should be above 0 dB (see section 2.4).

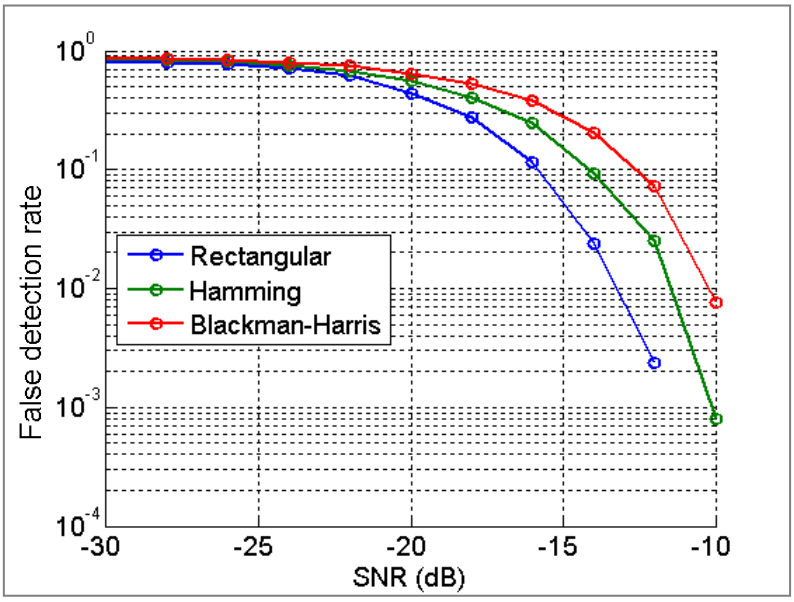

Figure 38 - False detection rate vs SNR for windowed correlation

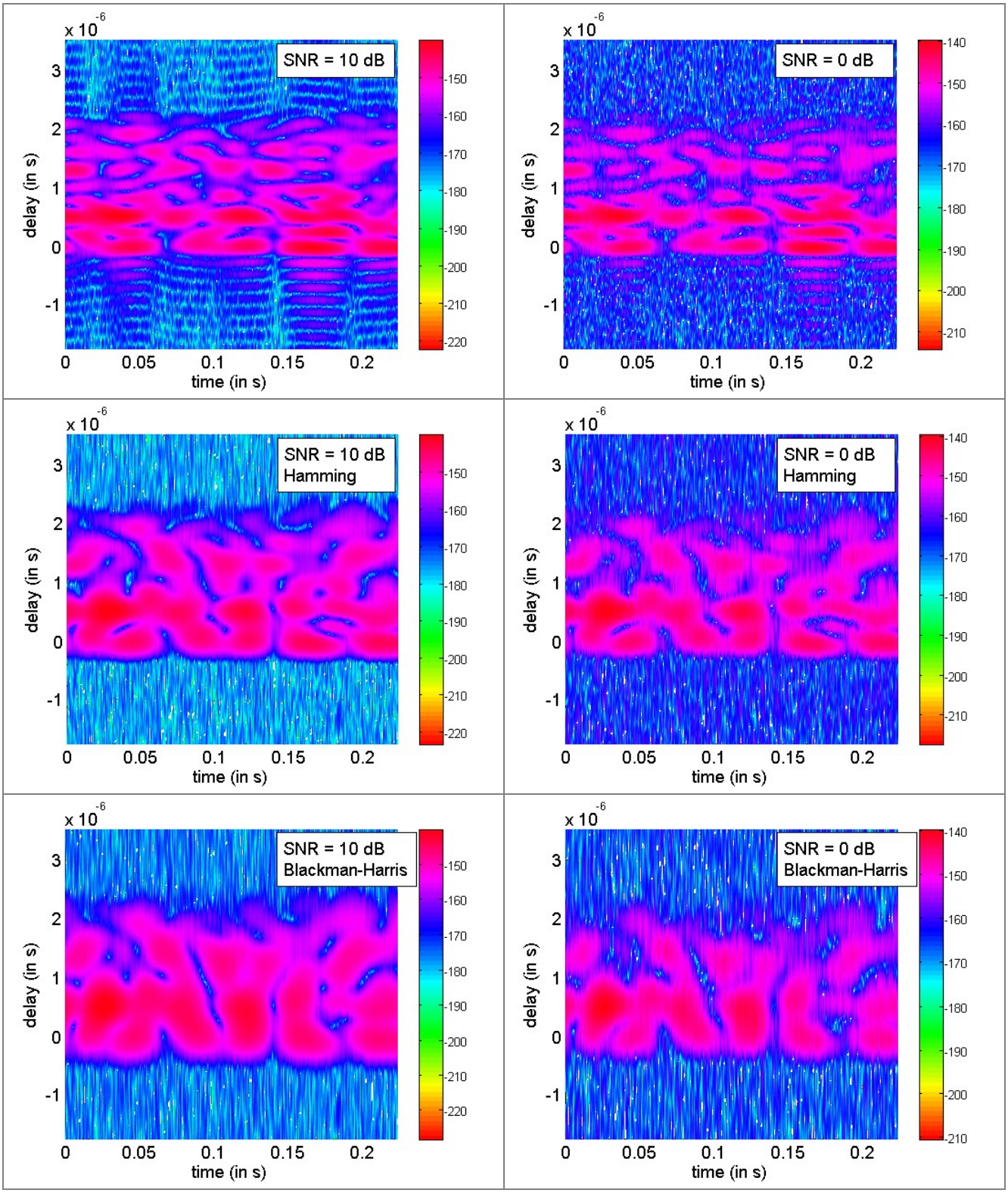

Figure 39 - Illustration TU-20 CIR time series estimation by windowed correlation

3.5.4 Application of windowing to the delay tracking

The tracking error variance formula (Eq. 3.16) from [Serant 2010] and recalled in section 3.4.4 can be adapted to the case of the windowed correlation by approximating the windowed correlation peak by a sinc function with a larger main lobe. To do this, the main lobe widening factors (Table 9) are used.

$$Var^{window}(\Delta\hat{t}) = 2B_l T_{symb} \frac{K_1'}{SNR}\left(1 + \frac{K_2'}{SNR}\right) \qquad \text{Eq. 3.19}$$

where K_1' and K_2' have the same expression as in Eq. 3.16 except that they use β' instead of β;
$\beta' = \beta / K_{width}^{window}$, with K_{width}^{window} the main lobe widening factor. $K_{width}^{Ham} = 1.5$ and $K_{width}^{BH} = 2.1$.

Figure 40 shows the performances of the estimation in tracking conditions for the considered windowing techniques.

The Hamming window creates a degradation equivalent to a 4dB lower SNR compared to the rectangular window, and the Blackman-Harris window brings a 6 dB SNR degradation compared to the rectangular window.

However, the tracking accuracy remains very low for the SNR above -10 dB, keeping this tracking error negligible compared to other error sources.

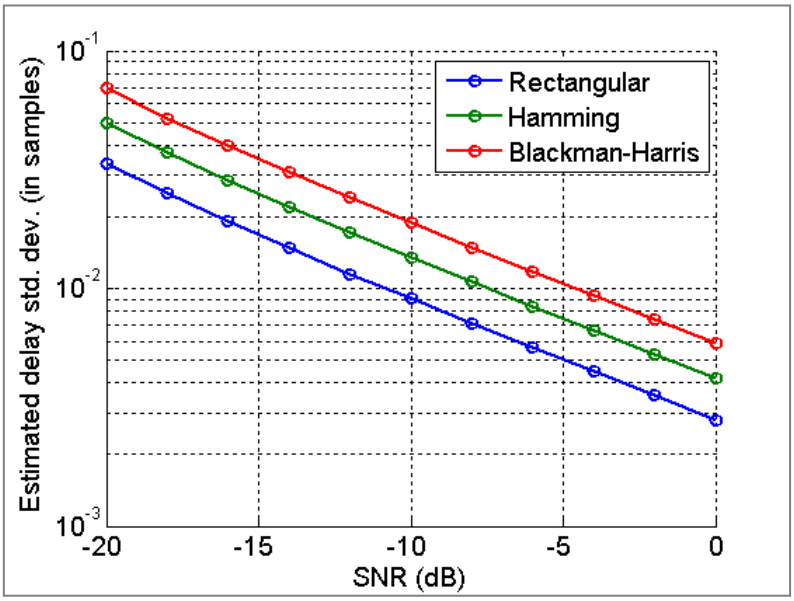

Figure 40 - Estimated delay standard deviation for different window vs SNR

3.5.5 Multipath error envelope for windowed DLL

Finally, the multipath error envelope for windowed DLL is shown in Figure 41.

As expected, the windowed DLLs are more affected by close multipath, due to the larger width of the correlation main lobe.

Also, windowed DLLs are no longer affected by far multipath, due to the removal of sidelobes.

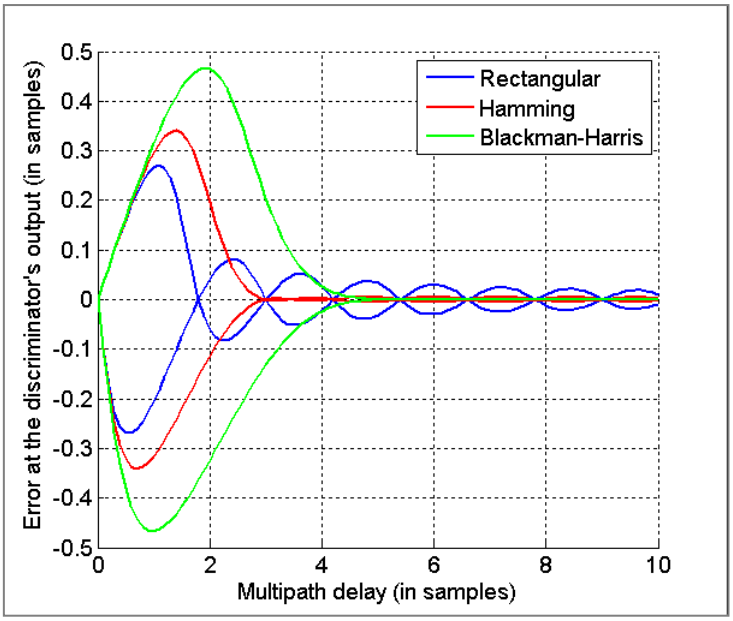

Figure 41 - Multipath error envelope for windowed DLL

3.6 Pseudo-range estimation strategy

The previously-described techniques provides

- a rough multiple multipath delay estimation in a multipath channel (Matching Pursuit algorithm);
- a fine single multipath delay estimation (windowed DLL).

In order to work in urban environment, these techniques have to be combined carefully, taking into account the particularities of the urban propagation channel. Indeed, as described in section 3.1, the urban environments creates several replication of the transmitted signals, each affected by fast fading. These multipaths may appear or disappear as the receiver moves. Finally, the LOS signal, which is required for unbiased pseudo-range estimation, may be blocked or received with a lower power than later multipath. As shown, the urban propagation channel is a huge challenge for pseudo-range estimation.

3.6.1 Pseudo-range estimation strategy overview

Given these constraints and the characteristics of the methods, the following delay estimation strategy is proposed:

1. **Acquisition**: A Matching Pursuit algorithm is run to estimate the main peaks of the correlation function. The multipath amplitude estimation realized by the Matching Pursuit algorithm is used to keep only the most powerful taps.
2. **Tracking**: For each estimated delay, a DLL is launched. Therefore, several DLLs will be running in parallel, which permits to keep tracking a signal even if one multipath disappears.
3. **DLL number limitation**: In order to keep the number of running DLL low, some DLL exclusion schemes are implemented, based on the tracked multipath amplitude, the convergence toward the same multipath or the divergence of the multipath delay.
4. **Periodic acquisition**: A new Matching Pursuit algorithm is launched periodically, in order to maximize the chance of tracking the earliest multipath in case it was not present during the

previous Matching Pursuit run or if it has disappeared since the last Matching Pursuit run. A new DLL will be launched only if the new estimated delay is not too close from an already estimated one.

5. **Pseudo-range computation**: At each estimation instant, the *earliest* estimated delay is used for the pseudo-range estimation. This should minimize the NLOS error.

The overall pseudo-range estimation strategy is summarize in the Figure 42. Additionally, a feedback of the delay estimation towards the demodulator's synchronization process may be added (not shown on the figure), since the delay estimate obtained by this method is expected to give better performances than the conventional synchronization process.

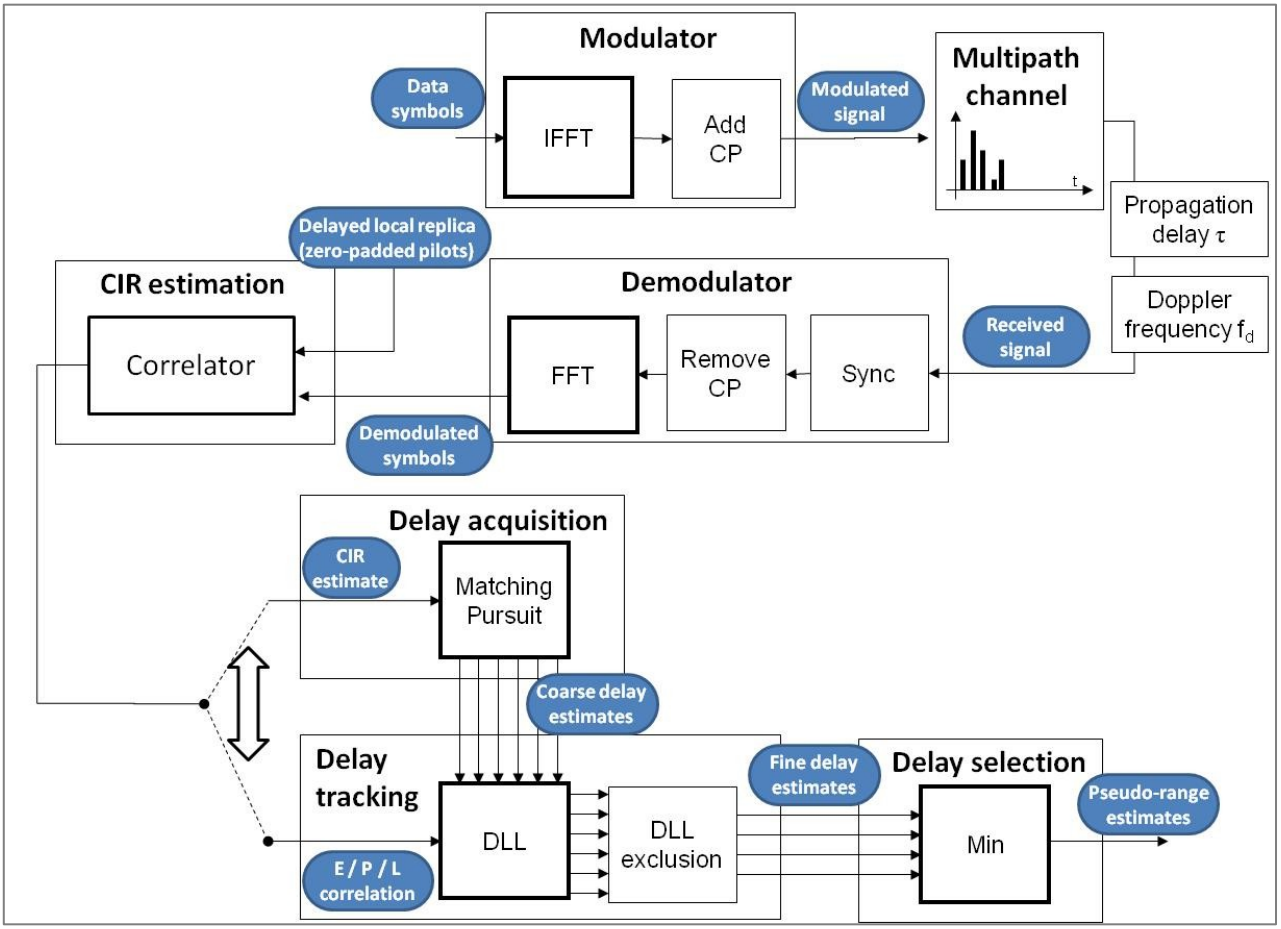

Figure 42 - Overall pseudo-range estimation strategy in a mono-emitter system

3.6.2 Implementation of the pseudo-range estimation strategy

In order to keep the number of running DLL low, some DLL exclusion schemes are set-up. The parameters for the overall delay estimation strategy are:

- Duration between 2 Matching Pursuit run - T_{ACQ}
- Acquisition threshold - γ_{ACQ}
- Tracking threshold - γ_{TRK}
- Window length for average multipath power estimation - T_{avg}
- Window length for converging DLL criteria - N_{Xerror}

- Window length for diverging DLL criteria - $N_{MeanVar}$, γ_{Div}

The present section discusses the choice for the values of these parameters.

3.6.2.1 Duration between 2 Matching Pursuit run - T_{ACQ}

The duration between 2 Matching Pursuit run should be chosen in order to take into account the dynamics of the channel, mainly the apparition and disappearing of a signal multipath. Reducing this time interval will also increase the chance to acquire the first multipath at the expense of extra computation time.

However, no theoretical model have been found for this apparition / disappearing rate of multipath. Different values for T_{ACQ} have been tested through simulations. The results will be presented later, in section 4.3.

3.6.2.2 Acquisition threshold - γ_{ACQ}

The Matching Pursuit algorithm provides the delay and amplitude of several multipaths detected in a CIR estimate. As shown in section 3.3.3.2, the Matching Pursuit algorithm provides some wrongly detected multipath, that can be excluded based on a threshold on the multipath amplitude.

This threshold is set depending on the desired false alarm probabilty and on the power of the received signal.

3.6.2.3 Window length for average multipath amplitude estimation - T_{avg}

In the overall pseudo-range estimation strategy, some DLL are excluded by comparing the tracked multipath amplitude with a threshold. However, this amplitude is affected by fast and deep fading. In order to reduce the depth of these fading the estimated amplitude is averaged over a window of length T_{avg} seconds.

3.6.2.4 Tracking threshold - γ_{TRK}

A DLL is stopped if the averaged prompt correlator, which is an estimator of the tracked multipath amplitude goes below a threshold. This permits to excludes the DLL following low-power multipath or a disappeared multipath.

The tracking threshold has been studied in [Serant 2010]. It mainly depends on the power of the received signal. There is also a trade-off to be made between the availability of the low power multipath delay estimates and their quality.

3.6.2.5 Window length for converging DLL criteria - N_{Xerror}

The criteria for considering that 2 DLLs have converged is the cross-error over a N_{Xerror}-long window:

$$Xerror_{(i,j)}(k) = \sum_{p=0}^{N_{Xerror}-1} \left| \Delta\hat{t}_{k-p}^{(i)} - \Delta\hat{t}_{k-p}^{(j)} \right| \qquad \textbf{Eq. 3.20}$$

where $\Delta\hat{t}_k^{(i)}$ is the estimated delay at instant k provided by DLL i.

2 DLL are considered to be tracking the same multipath delay if the cross-error criteria is below N_{Xerror}. This would correspond to 2 DLL which would have estimated a delay inferior to 1 sample

for a duration of N_{Xerror} OFDM symbols. The duration $N_{Xerror}.T_{symb}$ should be chosen in relation with the converging duration of the DLL.

3.6.2.6 Window length for diverging DLL criteria - $N_{MeanVar}$, γ_{Div}

A DLL output may diverge in case the DLL is not tracking an existing multipath (it was started on noise, or the multipath it was tracking disappeared). In order to detect this case, the mean variation of the estimated delay is calculated for each DLL:

$$MeanVariation(k) = \left| \frac{1}{N_{MeanVar}} \sum_{p=0}^{N_{MeanVar}-1} (\Delta\hat{t}_{k-p} - \Delta\hat{t}_{k-p-1}) \right| \quad \textbf{Eq. 3.21}$$

A DLL is considered to be diverging if its $MeanVariation$ is above a threshold: if $MeanVariation(k) > \gamma_{Div}$. This threshold should take into account the dynamics of the receiver and the length of the considered window $N_{MeanVar}$. This criteria corresponds to a variation of $c.\gamma_{Div}.T_{symb}$ meters in a duration of $N_{MeanVar}$ OFDM symbols. Therefore, it excludes DLL that are moving faster in average than the following speed: $c.\gamma_{Div}/N_{MeanVar}$.

3.7 Simulations

3.7.1 Simulation parameters

The presented pseudo-range estimation strategy is applied to the intense multipath CIR time series presented in 3.1.4. The parameters used for this simulations are presented in 2 parts: Table 10 for the system parameters and Table 11 for the receiver parameters.

The system parameters (DVB-SH mode and emitter EIRP) have been taken from early publication on DVB-SH system deployments [Chuberre]. The noise floor level has been taken from the DVB-SH Implementation Guidelines [DVB-SH 2008-2]. Finally, the average SNR has been calculated from the CIR time series.

The receiver parameters were mainly chosen empirically, based on the comments made in Section 3.6.2. The particular choice of a high noise loop bandwidth B_l of 10 Hz is motivated so as to let the DLLs follow potentially fast varying multipath delays and/or converge quickly toward a significant multipath.

Table 10 - System parameters used in the single-emitter case

N_{FFT}	2048
CP	1/4
B	5 MHz
Emitter EIRP	53.2 dBm
Noise floor level	-102.6 dBm
Average SNR	13.36 dB

Table 11 - Receiver parameters used in the single-emitter case

B_l	10 Hz
T_i	T_{symb} = 448 µs
T_{ACQ}	2000.T_{symb} = 896 ms
T_{avg}	80.T_{symb} = 35.84 ms
γ_{ACQ}	3.16e-8
γ_{TRK}	1e-8
N_{Xerror}	3.$floor(1/(B_l T_i)$ = 669
$N_{MeanVar}$	200.T_{symb} = 89.6 ms
γ_{Div}	1e-4.$N_{MeanVar}$ = 8.96 µs

3.7.2 Simulation results

The results for a non-windowed and Hamming-windowed pseudo-range estimation are presented in the next pages. For each case, the following graphs are shown:

- the estimated delays time series over the estimated CIR time series;
- the pseudo-range error, which is calculated as the delay difference between the minimum estimated delay and the first multipath true delay;
- the cumulative density function of the pseudo-range error;
- the number of active DLL all over the simulation.

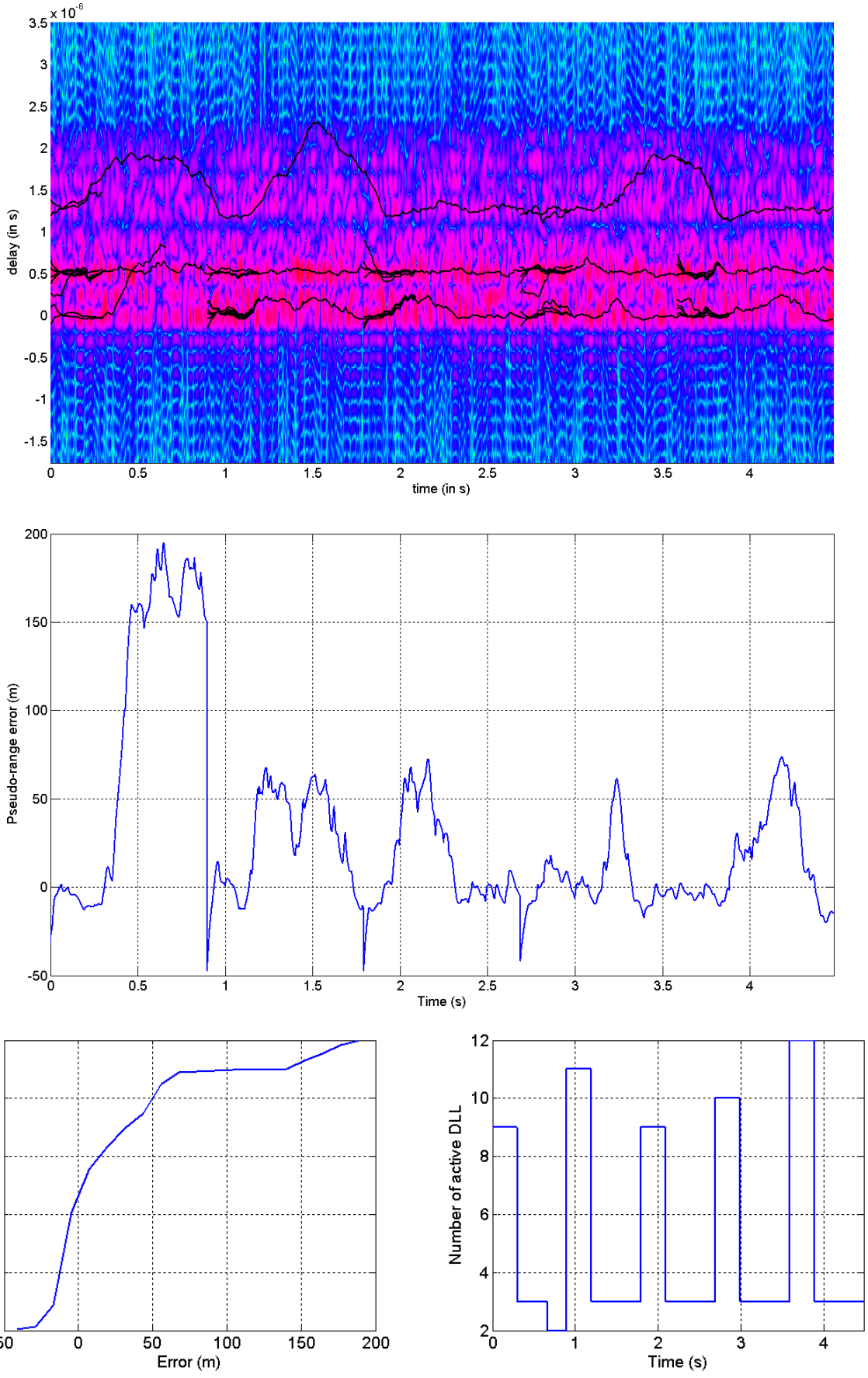

Figure 43 - Rectangular window - Simulation of pseudo-range estimation

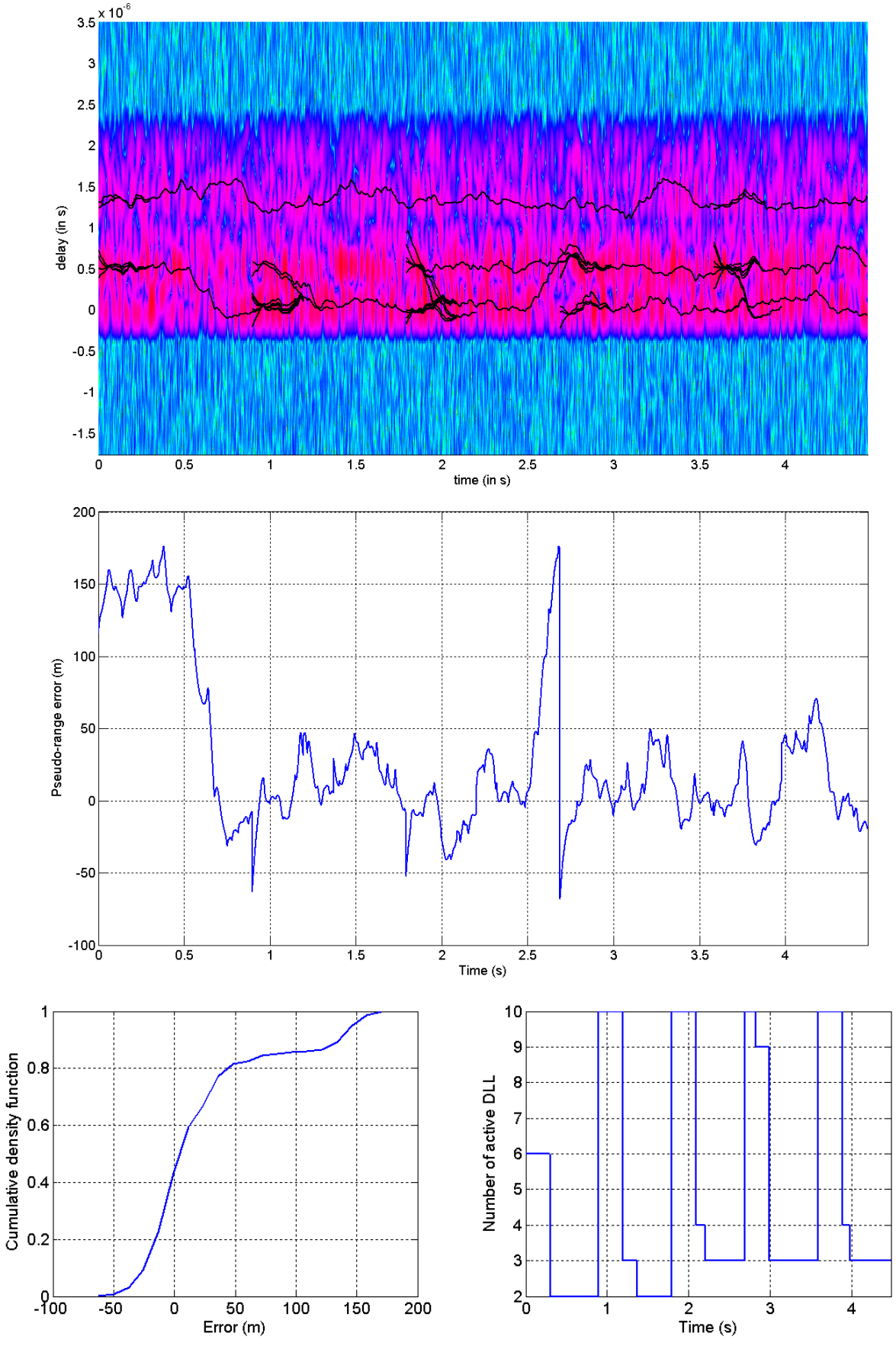

Figure 44 - Hamming window- Simulation of pseudo-range estimation

3.7.3 Simulation analysis

The realized simulations use a very particular CIR model, with 20 multipath with fixed delays and varying amplitude given by the TU-20 model [UMTS 2004]. In particular, this model imposes the presence of 2 close power peaks, with respective delays towards 0 and 0.5 µs. The second power peaks is the most powerful one, therefore providing a challenging case for a ToA-based pseudo-range estimation technique. Also, it shall be reminded that this particular 20 multipath scenario may not be representative of the multipath delay distribution encountered by mobile receiver, as seen in the chosen CIR model discussion in Section 3.1.5.

In the case of non-windowed simulations, the 2 power peaks are clearly distinct, while they are merged in the Hamming-windowed simulations.

In both simulations, the first multipath is lost at some points, and therefore, the estimated delays are locked on the second CIR peak power toward 0.5 µs. This is why the pseudo-range error reaches and stays toward 150m.

The use of periodic Matching Pursuit algorithm permits to re-acquire the first multipath when it has been lost. But it also creates some negative pseudo-range errors due to the initialization of DLLs at a delay before the first multipath. This is observed through the periodic error peaks toward negative values.

The performances of the pseudo-range estimation are summarized in Table 12.

Table 12 - Single emitter pseudo-range error estimation overall performances

Simulation	Mean error (m)	Error standard deviation (m)	Minimum error (m)	Maximum error (m)
No window	29.8	53.0	-47.2	195.0
Hamming window	28.8	54.3	-68.3	176.5

The use of a windowing technique does not degrade particularly the pseudo-range estimation technique. However, the gain of using windowing techniques will be particularly important in the multi-emitter case, in order to mitigate the Near-Far Effect (see Section 4.3).

The mean and standard deviation observed in these simulations may not be very attractive, however the statistics are not very representative due to the frequent leaps of the estimated pseudo-range between the first multipath and the other later peak of power, which create large local pseudo-range errors up to 150m.

In order to observe the performances on stationary parts of this time series (excluding the large error leaps), the same statistics are calculated on 2000 sample-long slices of the error time series (Table 13). Each slice last for approximately 0.9 seconds.

Table 13 - Single emitter pseudo-range error estimation performances for slices of the whole time series

Slice of simulation	Mean error (m)	Error standard deviation (m)	Minimum error (m)	Maximum error (m)
No window - 1	*89.0*	*83.6*	*-47.2*	*195.0*
No window - 2	26.3	27.3	-47.2	67.6
No window - 3	14.12	26.4	-46.6	72.5
No window - 4	3.5	17.3	-41.3	61.6
No window - 5	16.2	26.3	-20.0	73.7
Hamming window - 1	*97.3*	*70.3*	*-63.0*	*176.5*
Hamming window - 2	13.7	18.9	-62.3	47.4
Hamming window - 3	15.9	49.5	-68.2	176.4
Hamming window - 4	5.9	19.3	-67.6	49.4
Hamming window - 5	11.0	26.6	-30.7	70.6

Except for the first slice of signal (in grey in Table 13) where pseudo-range estimation is locked on the second power peak, the mean and standard deviation of the other slices of signal, where the pseudo-range estimation is only affected by close multipaths of about the same amplitude, are much more interesting, varying between 3 to 26m for the error bias and 17 to 50m for the standard deviation.

This shows that if the receiver is able to exclude the large error leaps, it could achieve some interesting pseudo-range estimation performances.

In both simulations, the number of active DLLs remains low (< 11), even with the periodic Matching Pursuit algorithms. This shows that the DLL exclusion scheme is useful and working in order to limit the resources required by the proposed method.

3.8 Conclusion on the pseudo-range estimation in a mono-emitter system

In this chapter, a pseudo-range estimation method has been proposed. It is composed of several steps, recalled in Figure 13.

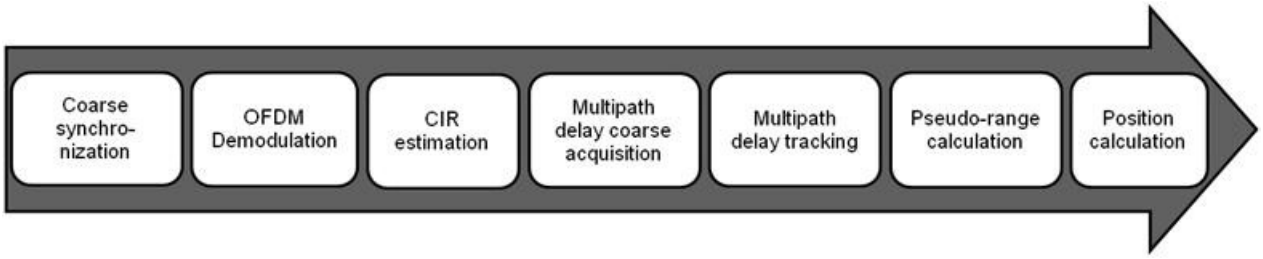

Figure 13 - Receiver signal processing strategy for position calculation

After conventional OFDM signal processing (synchronization and OFDM demodulation), the pseudo-range estimation technique is done in 3 main phases:

- **A delay acquisition phase**, which is based on the CIR estimation by correlation and the Matching Pursuit algorithm
- **A delay tracking phase**, which is based on multiple DLL.
- **A delay selection** for the pseudo-range calculation.

The delay tracking phases may benefit from the use of windowing techniques in order to lower the influence of multipath on the delay tracking.

A strategy combining all the presented different signal processing tools has been set-up, in order to minimize the computational resources required by this pseudo-range estimation technique, notably by determining DLL exclusion processes. This strategy also recommends the launch of periodic acquisitions phases, in order to re-acquire the first path (closest to the desired LOS path) in case it was lost during a fading or shading period.

The proposed pseudo-range estimation method was applied in a TU-20 multipath channel and has provided interesting performances, with a mean pseudo-range error between 3 to 26m and an error standard deviation between 17 and 50m. These performances should be put in relation with the particular channel model used to simulate the multipath environment. Further simulations with more realistic channel models or even measurements on real signals are required in order to characterize more completely the pseudo-range error.

4 Pseudo-range estimation in a multi-emitter system

The previous chapter has described a method for obtaining a pseudo-range from one emitter. However, in order to obtain a position, pseudo-ranges from several emitters are required (at least 3 for 2D positioning).

The DVB-SH system employs a network constituted of several emitters broadcasting the same signal, called a Single Frequency Network (SFN). This particular network configuration raises challenges for emitter discrimination and identification, since the same signal is emitted on the same carrier frequency and in a synchronized way, so that the emitter can recombined the different replicas received from different emitters for more efficient data demodulation thanks to channel equalization techniques.

This chapter proposes a solution to enable emitter discrimination in this context. It will first present the combined CIR (cCIR) encountered in a SFN, and look at the requirements for discriminating emitters (Section 4.1). Then, emitter discrimination methods based on clustering algorithm will be presented (Section 4.2), and finally, simulations of pseudo-range estimation in an SFN will be presented, based on a set of real SFN CIR measurements (Section 4.3).

4.1 Requirements on the combined channel impulse response to enable multi-emitter pseudo-range estimation

The chosen System of Opportunity for positioning makes use of a particular next-generation emitter network, working in a SFN configuration. In this section, it is assumed that the SFN emitters are perfectly synchronized.

4.1.1 Urban propagation channel for several emitters in a SFN

An important clarification has to be made on the terms used in this study. In a multi-emitter system, we will call

- the **Channel Impulse Response (CIR)**, the CIR corresponding to *one* emitter;
- the **combined CIR (cCIR)**, the CIR obtained in the presence of *several* emitters.

The CIR model (Eq. 3.3) can be modified in order to particularize it to a given emitter. For a given emitter i, we can use the following CIR model:

$$h_l^i(\tau) = l_{COST}(d_i).\left(\sum_{n=0}^{N_{taps}^i-1} a_{l,n}^i.\delta\left(\tau - \tau_{l,n}^i.T_{samp}\right)\right) \qquad \textbf{Eq. 4.1}$$

where $h_l^i(t)$ is the CIR complex amplitude of the i-th emitter at the time of the reception of the l-th OFDM symbol and at delay τ;
$l_{COST}(d_i)$ is the pathloss for a travelled distance d_i, corresponding to the distance between emitter i and the receiver. It is determined using the COST 231 Wallfisch-Ikegami pathloss model described in Eq. 3.1 of section 3.1.1;

N_{taps}^{i} is the number of signal replicas in the CIR from emitter i;
$a_{l,n}^{i}$ and $\tau_{l,n}^{i}$ are the complex amplitude and normalized delay of the n-th tap of the CIR from emitter i, at the time indexed by l.

If there are N_{Tx} emitters, the resulting cCIR model will be:

$$h_l(\tau) = \sum_{i=1}^{N_{Tx}} h_l^i(\tau) = \sum_{i=1}^{N_{Tx}} l_{COST}(d_i).\left(\sum_{n=0}^{N_{taps}^{i}-1} a_{l,n}^{i}.\delta\left(\tau - \tau_{l,n}^{i}.T_{samp}\right)\right) \qquad \textbf{Eq. 4.2}$$

In this model, the importance of the distance between the receiver and each emitter has to be emphasized. This distance will impact both the pathloss to each emitter $l_{COST}(d_i)$ and the delay of every multipath, since it mainly comprises the time of flight of the multipath.

4.1.2 Illustration of SFN cCIR and associated issues

For illustration purpose, let us look at a simplified scenario of cCIR obtained in a 3-emitter network. In the following, the fast fading is removed ($a_{l,n}^{i} = 1$) and only 2 multipath per emitter are kept ($N_{taps}^{i} = 2$), with a relative delay of 1 µs ($\tau_{l,2}^{i} - \tau_{l,1}^{i} = 1\ \mu s$).

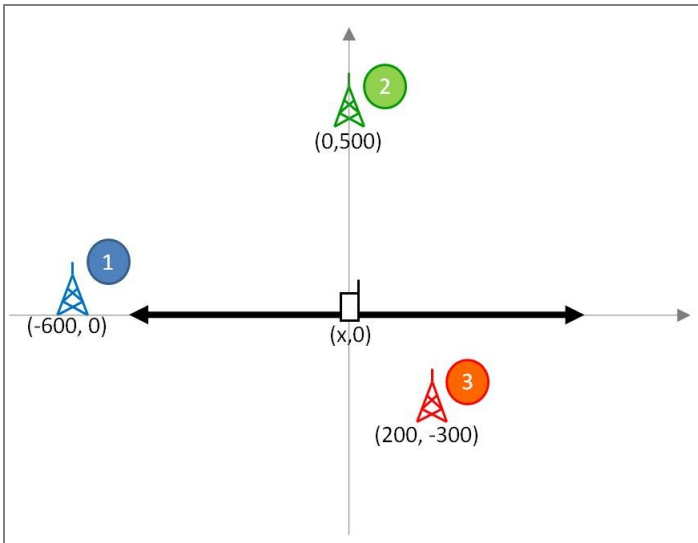

Table 14 - Simplified network scenario

Station	x (m)	y (m)
Tx1	-600	0
Tx2	0	500
Tx3	200	-300
Rx	{-500 ... 500}	0

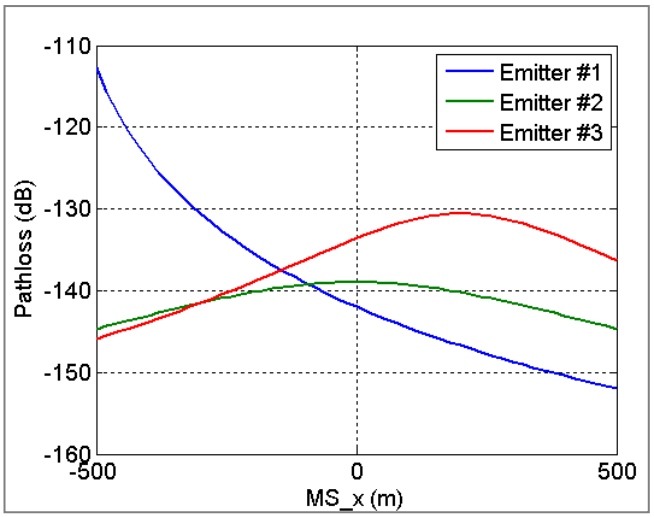

Figure 45 - Pathloss in the simplified SFN scenario

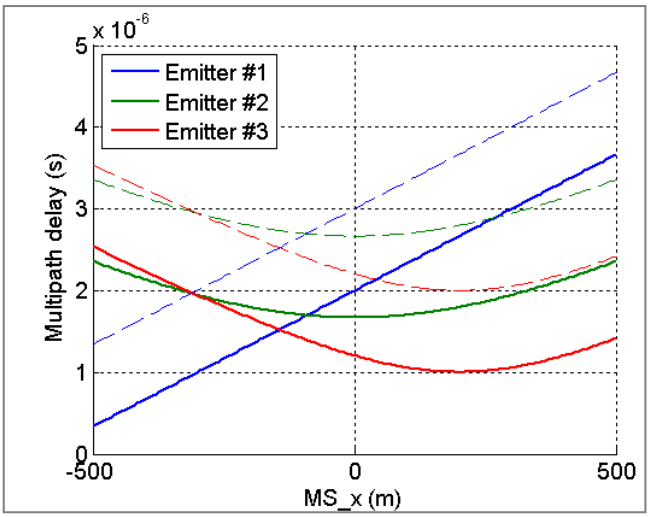

Figure 46 - Multipath delay in the simplified SFN scenario

Figure 45 and Figure 46 show the pathloss and the multipath delay encountered in this simplified scenario. From this illustration, 2 issues related to SFN can be commented:

- ***Near-Far effect***: the relative distance between the receiver and different emitters will greatly vary during the receiver motion. In the considered scenario, on a 1 km-long trajectory, the maximum pathloss variation for an individual emitter is 40 dB. The relative pathloss between 2 emitters is often above 10 dB. This may create inter-emitter interferences, ie a close emitter would mask the signals arriving from more remote emitters.
- ***CIR overlap***: the multipath delay from several emitters have the same value when the receiver is at the same distance to these emitters. This will make the emitter discrimination in the cCIR estimated impossible. This issue is emphasized if the presence of other multipath is considered: for example, a second multipath arriving 1 µs after the first one, illustrated in the dotted line in Figure 46.

Both effect are emphasized by the cCIR estimation process. cCIR estimation is done by a correlation, which turns a dirac of the cCIR into a sinc function in the estimated cCIR vector (see section 3.2). The sidelobes of the sinc function will increase the effect of the Near-Far Effect and of the CIR overlap.

Figure 47 shows the cCIR estimation obtained by correlation technique described in section 3.2 using the (2K 1/4 5 MHz) DVB-SH mode and an aggregate SNR of 20 dB. Sidelobes are greatly "blurring" the cCIR, making it hard to discriminate the different emitters.

Also, remote emitters generates multipath with an amplitude comparable to the sidelobes of nearer emitters, creating an ambiguity on the nature of a peak in the cCIR.

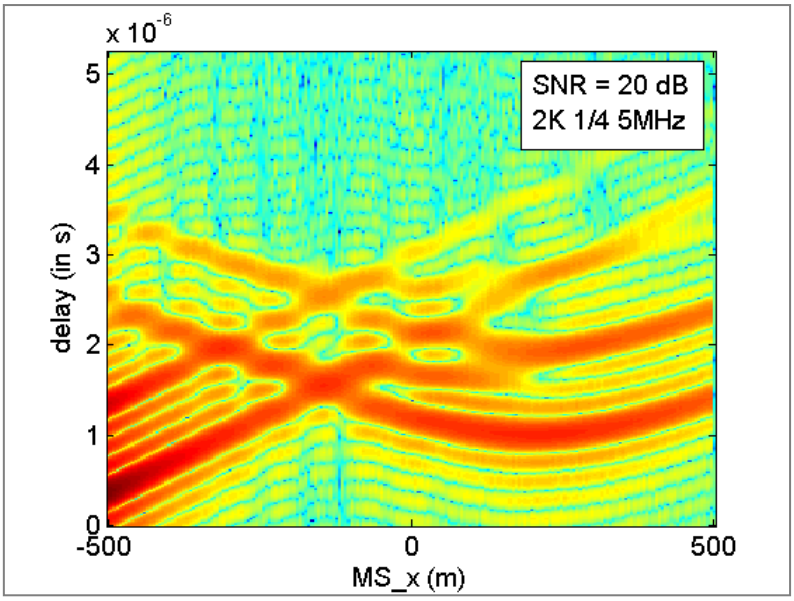

Figure 47 - SFN cCIR estimation in a simplified scenario

4.1.3 Obtaining pseudo-range measurements form an urban SFN cCIR

As presented before, there are 2 main challenges to be addressed in an urban SFN cCIR for emitter discrimination: Near-Far Effect and CIR overlapping.

The Near-Far Effect can be mitigated using ***windowing techniques***, as described in section 3.5. Windowing permits to limit the amplitude of the sidelobes in the cCIR estimation, thus reducing the influence of one emitter over the others.

In order to mitigate the CIR overlapping, the ***introduction of artificial delays*** in the emitters has been proposed [Thevenon 2009-1]. This modification consists in delaying the emission of the signal of each emitter with a predefined artificial delay that can be different for each emitter. This modification should not affect the telecommunication service: as shown in section 2.3.1, an OFDM receiver is able to recombine all received signal replicas as long as their delay is inferior to the Cyclic Prefix duration.

The use of artificial delays is available in the DVB-SH standard, and should therefore impact minimally the system. The associated constraints on the network deployment and on the choice of the OFDM signal parameters are studied in detail in Chapter 7, which provides useful recommandation for operators to adopt the proposed system modification.

In this section, an example is taken for the modification of the simplified SFN scenario. The values of the introduced artificial delays are presented in Table 15. The artificial delay values has been chosen in order to prevent the CIR overlap issue, by preventing the multipath delay to cross each other during the receiver's motion (Figure 48)

Table 15 - Artificial delay values used in the simplified SFN scenario

Emitter	Artificial delay
Tx1	0 µs
Tx2	3 µs
Tx3	6 µs

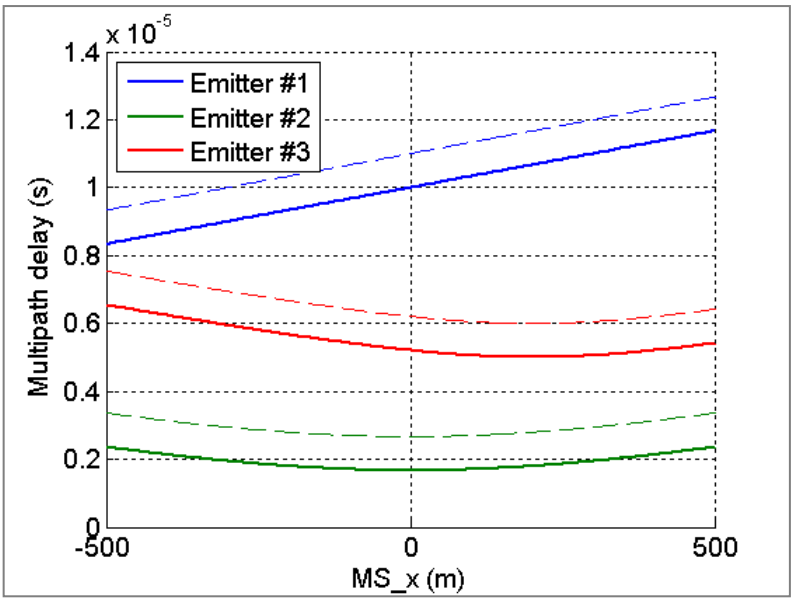

Figure 48 - Multipath delays in the modified SFN scenario after introduction of artificial delays

Figure 49 shows the cCIR estimation obtained by the correlation technique without the use of window technique, while Figure 50 makes use of a Hamming window in order to reduce the sidelobes of the correlation peaks.

For the rectangular window (Figure 49), the Near-Far Effect and the presence of sidelobes in the CIR estimation will affect the detection of the emitters at some points (for MS_x = -500 in this example). Also, even if multipath can be discriminated, the sidelobes of close multipath create some interferences, thus increasing the noise floor - noise + interference floor to be exact - around them.

These issues can be addressed by using windowed correlation, as seen in Figure 50. As expected, the width of the main lobe is wider in the case of windowed correlation, thus potentially degrading the peak location estimation's accuracy.

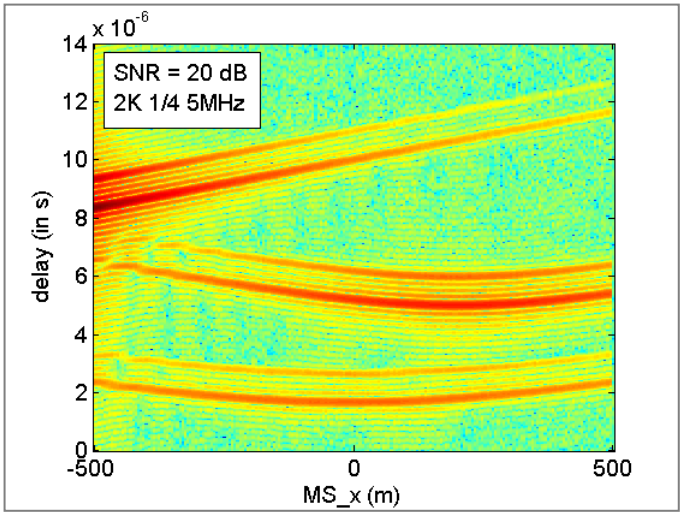

Figure 49 - cCIR estimation in a modified SFN

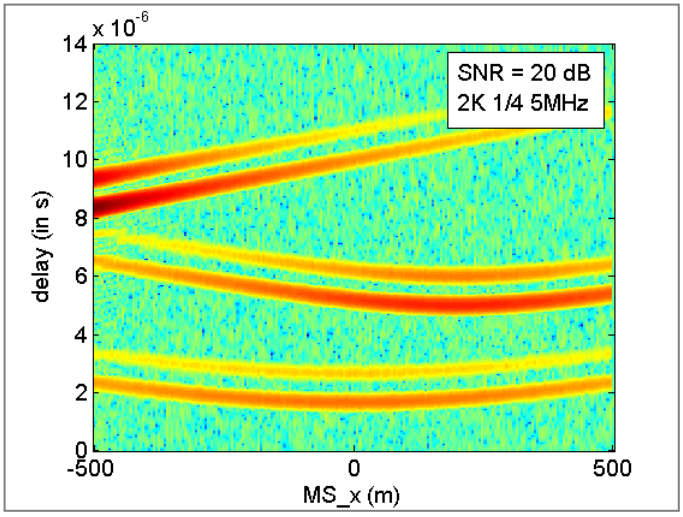

Figure 50 - cCIR estimation using Hamming-windowed correlation in a modified SFN

Once this modification has been brought to the emitters' network, the previously presented delay estimation methodology presented in Chapter 3 can be used. However, an additional step is required, which consists in using a clustering algorithm in order to group the estimated delays by emitter origins. This modification to the pseudo-range estimation method is shown in Figure 51.

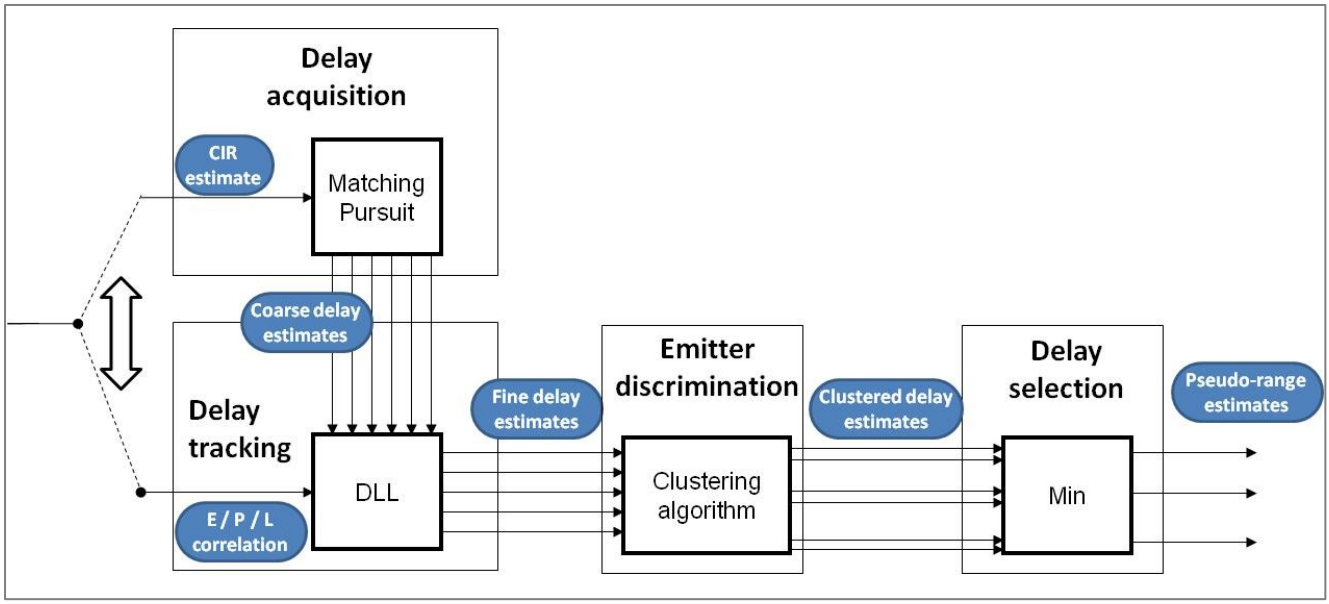

Figure 51 - Delay estimation strategy in the multi-emitter case

4.2 Emitter discrimination in the channel impulse response

All multipaths associated to one emitter should be in the same delay range. For example, the TU20 multipath model presented in section 3.1.2 consider the arrival of multipath with delay up to 2.14 µs, corresponding to obstacles at distances up to 640m. There may be very particular cases creating larger multipath delays, such as far high-rise obstacles (skyscrapers, surrounding mountains) but they will not be considered in this study.

It is therefore possible to cluster the different estimated delays in order to assume that they are associated to the same emitter. To do this, classic clustering algorithms have been used. They have been implemented from the Matlab documentation[10].

4.2.1 Clustering principle

At the input of the emitter discrimination process, several estimated delay time series are available. Each time series is divided into slices, and the average estimated delay over this time slice is calculated. Clustering will be applied to the mean values of the estimated delay, for each slice of time series.

The input of the clustering algorithm is therefore N_{DLL} mean estimated delays noted

[10] http://www.mathworks.it/access/helpdesk/help/toolbox/stats/clusterdata.html

$$\{\overline{\Delta\tau}_1, \ldots, \overline{\Delta\tau}_{N_{DLL}}\}$$

A ***hierarchical cluster tree*** is created from these average value, following these steps:

1. Pairwise euclidian distances are calculated between each mean delay value:
$$d(\overline{\Delta\tau}_n, \overline{\Delta\tau}_m) = |\overline{\Delta\tau}_n - \overline{\Delta\tau}_m|$$
2. A cluster is formed by the two elements having the minimum distance between them. The 2 grouped elements (say elements p and q) are replaced by a new one associated to a new delay value as the mean delay of the 2 grouped elements. $\overline{\Delta\tau}_{\text{new element}} = \frac{1}{2}(\overline{\Delta\tau}_p + \overline{\Delta\tau}_q)$
3. Steps 1 and 2 are repeated until all elements are clustered.

The final clusters are then formed by choosing a threshold on the distance separating 2 branches. In our case, this threshold should be chosen in relation with the expected delay separation between 2 emitters. This threshold should take into account the introduced artificial delay and the maximum delay encountered in a single emitter channel.

Once this threshold is decided, the clusters are determined when 2 branches are separated by a distance above this threshold.

4.2.2 Clustering illustration

The considered scenario is the simplified SFN scenario described in section 4.1.3. It is assumed that every 6 taps have been perfectly estimated at the position MS_x = -455 m (see Figure 52).

6 mean delays (normalized by T_{samp}) are available:

- $\overline{\Delta\tau}_1 = 12.9$
- $\overline{\Delta\tau}_2 = 18.6$
- $\overline{\Delta\tau}_3 = 36.6$
- $\overline{\Delta\tau}_4 = 42.3$
- $\overline{\Delta\tau}_5 = 48.5$
- $\overline{\Delta\tau}_6 = 54.2$

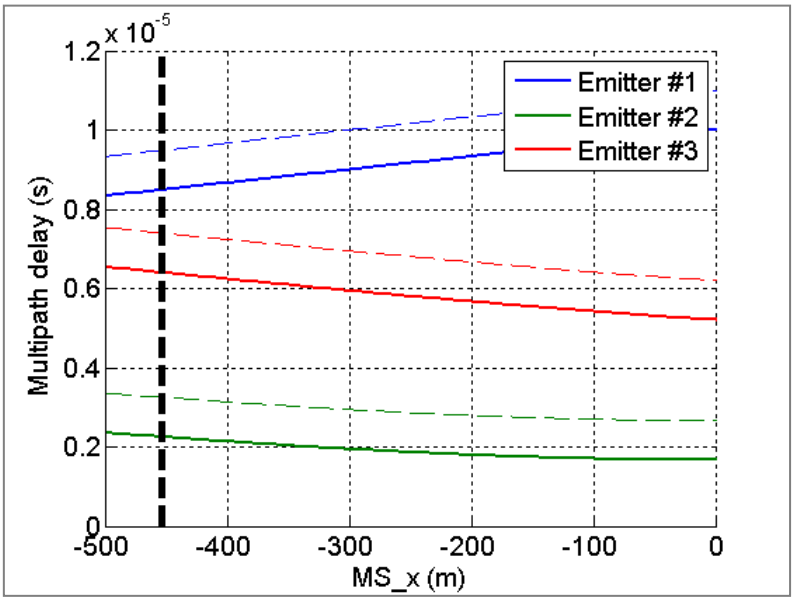

Figure 52 - Multipath delays used for the clustering illustration

Step 1

First, the pairwise euclidian distances between all these estimates is calculated:

$d(\overline{\Delta\tau_1}, \overline{\Delta\tau_2}) = |12.9 - 18.6| = 5.7$
$d(\overline{\Delta\tau_1}, \overline{\Delta\tau_3}) = |12.9 - 36.6| = 23.7$
$d(\overline{\Delta\tau_1}, \overline{\Delta\tau_4}) = |12.9 - 42.3| = 29.4$
$d(\overline{\Delta\tau_1}, \overline{\Delta\tau_5}) = |12.9 - 48.5| = 35.6$
$d(\overline{\Delta\tau_1}, \overline{\Delta\tau_6}) = |12.9 - 54.2| = 41{,}3$
$d(\overline{\Delta\tau_2}, \overline{\Delta\tau_3}) = |18.6 - 36.6| = 18$
$d(\overline{\Delta\tau_2}, \overline{\Delta\tau_4}) = |18.6 - 42.3| = 23{,}7$
$d(\overline{\Delta\tau_2}, \overline{\Delta\tau_5}) = |18.6 - 48.5| = 29{,}9$
$d(\overline{\Delta\tau_2}, \overline{\Delta\tau_6}) = |18.6 - 54.2| = 35{,}6$
$d(\overline{\Delta\tau_3}, \overline{\Delta\tau_4}) = |36.6 - 42.3| = 5{,}7$
$d(\overline{\Delta\tau_3}, \overline{\Delta\tau_5}) = |36.6 - 48.5| = 11{,}9$
$d(\overline{\Delta\tau_3}, \overline{\Delta\tau_6}) = |36.6 - 54.2| = 17{,}6$
$d(\overline{\Delta\tau_4}, \overline{\Delta\tau_5}) = |42.3 - 48.5| = 6.2$
$d(\overline{\Delta\tau_4}, \overline{\Delta\tau_6}) = |42.3 - 54.2| = 11.9$
$d(\overline{\Delta\tau_5}, \overline{\Delta\tau_6}) = |48.5 - 54.2| = 5.7$

Among all these distances, the minimum is found and a cluster with the 2 corresponding elements is created. At this stage, 3 pairs correspond to the minimum distance : (1,2) (3,4) and (5,6).

The pair (1,2) is chosen and grouped into a new element numbered 7, with an associated delay equal to the mean value of the delays of (1,2) : $\overline{\Delta\tau_7} = \frac{1}{2}(\overline{\Delta\tau_1} + \overline{\Delta\tau_2}) = 15.75$

Step 2

The same thing is done with the new element replacing the 2 clustered ones. Therefore 5 mean delays are available and the pairwise euclidian distance is calculated for these 5 elements:

- $\overline{\Delta\tau_7} = 15.75$
- $\overline{\Delta\tau_3} = 36.6$
- $\overline{\Delta\tau_4} = 42.3$
- $\overline{\Delta\tau_5} = 48.5$
- $\overline{\Delta\tau_6} = 54.2$

$d(\overline{\Delta\tau_7}, \overline{\Delta\tau_3}) = 20.85$
$d(\overline{\Delta\tau_7}, \overline{\Delta\tau_4}) = 26.55$
$d(\overline{\Delta\tau_7}, \overline{\Delta\tau_5}) = 32.75$
$d(\overline{\Delta\tau_7}, \overline{\Delta\tau_6}) = 38.45$
$d(\overline{\Delta\tau_3}, \overline{\Delta\tau_4}) = 5{,}7$
$d(\overline{\Delta\tau_3}, \overline{\Delta\tau_5}) = 11{,}9$
$d(\overline{\Delta\tau_3}, \overline{\Delta\tau_6}) = 17{,}6$
$d(\overline{\Delta\tau_4}, \overline{\Delta\tau_5}) = 6.2$
$d(\overline{\Delta\tau_4}, \overline{\Delta\tau_6}) = 11.9$
$d(\overline{\Delta\tau_5}, \overline{\Delta\tau_6}) = 5.7$

Pairs (5,6) and (3,4) have the minimum distance between their elements. The pair (5,6) is chosen and grouped to create element #8 with an associated delay $\overline{\Delta\tau_8} = \frac{1}{2}(\overline{\Delta\tau_5} + \overline{\Delta\tau_6}) = 51.35$

Step 3
Elements (3,4) are grouped into element #9 with associated delay $\overline{\Delta\tau_9} = 39.45$

Step 4
Elements (8,9) are grouped into element #10 with associated delay $\overline{\Delta\tau_{10}} = 45.4$

Step 5
At this stage, there are only 2 left elements (7,10) which are grouped together

The process of the hierarchical cluster tree creation is illustrated in Figure 53.

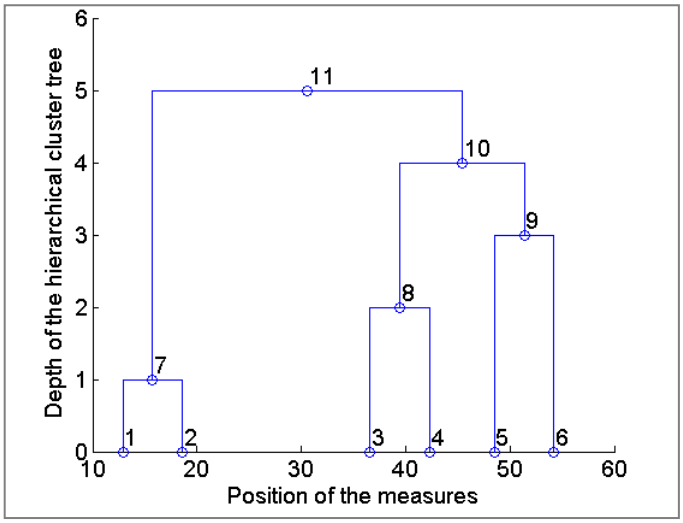

Figure 53 - Illustration Hierarchical cluster tree based on Euclidian distances and mean values

At this stage, all pair elements (delay estimates + created clusters) are sorted by distances:

- $d(\overline{\Delta\tau}_1, \overline{\Delta\tau}_2) = 5.7$
- $d(\overline{\Delta\tau}_3, \overline{\Delta\tau}_4) = 5.7$
- $d(\overline{\Delta\tau}_5, \overline{\Delta\tau}_6) = 5.7$
- $d(\overline{\Delta\tau}_8, \overline{\Delta\tau}_9) = 11.9$
- $d(\overline{\Delta\tau}_7, \overline{\Delta\tau}_{10}) = 29.6$

Then, by choosing a delay threshold, the final clusters can be formed with the desired 'grouping' characteristics.

For this scenario, a threshold of $8.T_{samp} = 1.4\ \mu s$ is appropriate to identify the 3 clusters, because it corresponds to the extent of the delay cluster of a single emitter: the CIR for a single emitter is composed of 2 taps separated by 1 µs. The results of the delay clusters are shown in Figure 54.

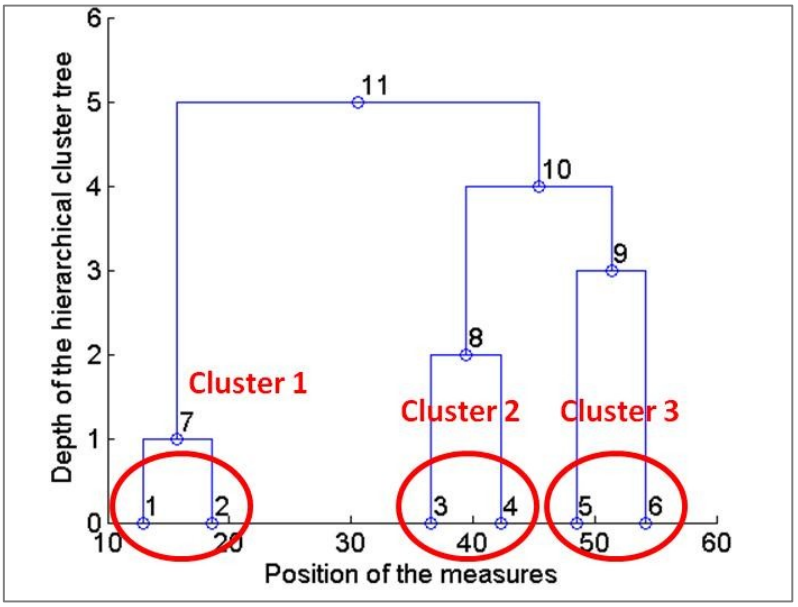

Figure 54 - Clustering results in simplified scenario.

In order to improve the clustering performances, increasing the introduced artificial delay may increase the separation of the different delay clusters, thus favouring the emitter discrimination.

The clustering algorithm may be adapted to different cases by choosing the distance definition between 2 elements, and the associated value attributed to a clustered elements. In this study, the Euclidian distance and the mean value were chosen respectively. No other clustering algorithm was tested.

At the end of this step, several clusters of delays are formed based on their emitter of origin. A pseudo-range can be determined by taking the minimum delay of each cluster in order to be the closest to the LOS path.

4.3 Simulations of pseudo-range estimation in a modified SFN network

4.3.1 Presentation of the CNES cCIR measurements

In order to test the proposed multi-emitter pseudo-range estimation technique, a CIR time series was required. Unfortunately, no adapted SFN channel model was found in the literature, and it was decided to rely on real-world measurements, presented in this section.

In the frame of the S-DMB project (a DVB-SH pre-standardization project), CNES has realized a measurement campaign in urban and sub-urban environments that was used to estimate the propagation channel during the experiment [Lacoste 2009]. The measurements used in this section were made in Auch, France (~20,000 inhabitants) with 2 terrestrial emitters and one helicopter (simulating a satellite) simulating a SFN, and a moving van carrying the receiver. The transmission was done with a carrier frequency at 2.2 GHz in order to characterize the DVB-SH conditions. The path followed by the van during the measurement is shown in Figure 55.

These CIR measurements were made available under the following format:

- The measurements were post-processed in order to remove the measurement tool's noise;
- The measurement sampling rate is 10 Hz;
- The extracted parameters from these measurements are the pathloss and the delay of 6 multipaths for terrestrial emitters. This number of multipaths was chosen due to hardware constraints: the channel emulator using these measurements requires to have 6 taps. If a terrestrial emitter happens to have less than 6 multipaths, then, the amplitude of the absent multipaths is set at a very low value. The satellite emitter has only one tap.

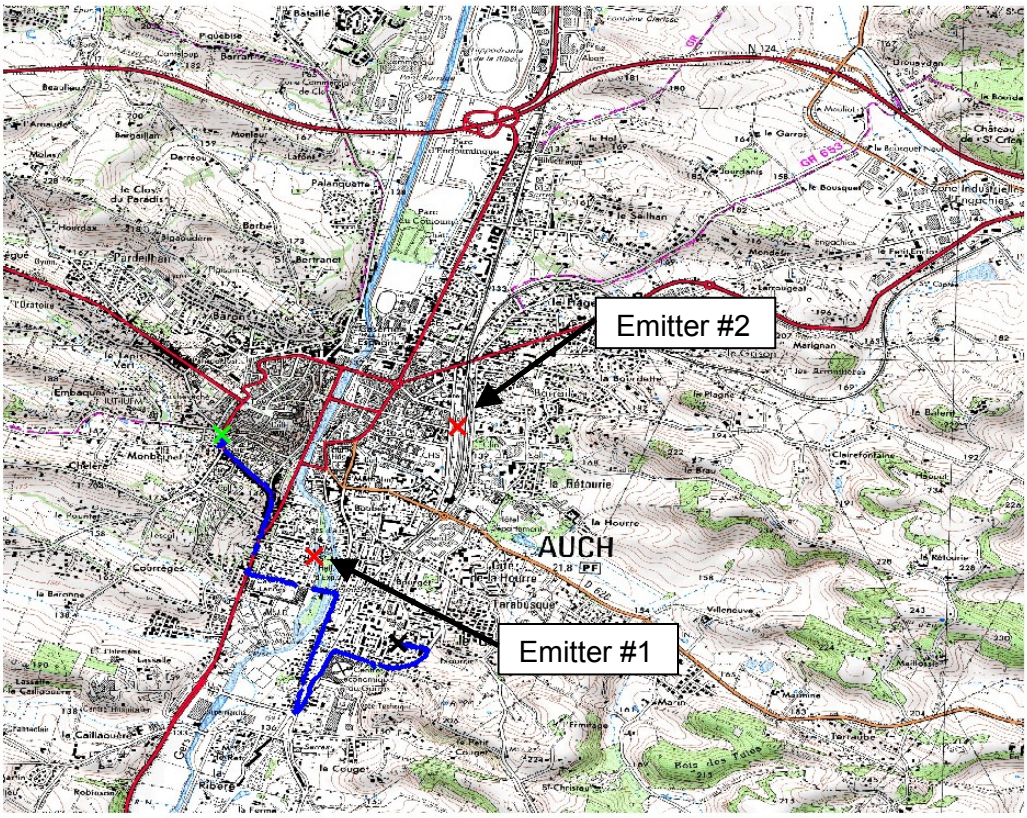

Figure 55 - Path followed by the receiver in blue. The 2 terrestrial emitters are located at the red crosses.

From these parameters, channel time series can be generated via custom-made software with appropriate Rayleigh/Rician-fading, and artificial delay can be introduced between each emitter.

In the following figures, the satellite emitter is plotted in green, while the terrestrial emitters are in red (for emitter #1) and blue (for emitter #2).

In Figure 56, the power of the multipaths is plotted. Aside from the fast fading, huge slow variations of power occur due to the receiver getting close or far to the terrestrial emitter, thus creating Near-Far Effect: the power received from the different emitters may be up to 50 dB apart. The presence of this large Near-Far Effect was one of the criteria for choosing this particular measurement time series among all the ones made by CNES.

As 6 multipaths were required to be present during the whole time series, if less than 6 multipath were detected by the channel sounding process, the remaining multipaths' power was set to a negligible value (-150 dBm). All in all, there are 3 or 4 significant multipaths for each terrestrial emitter.

Also, it should be noted that the LOS signal may not be present in the CNES CIR measurements.

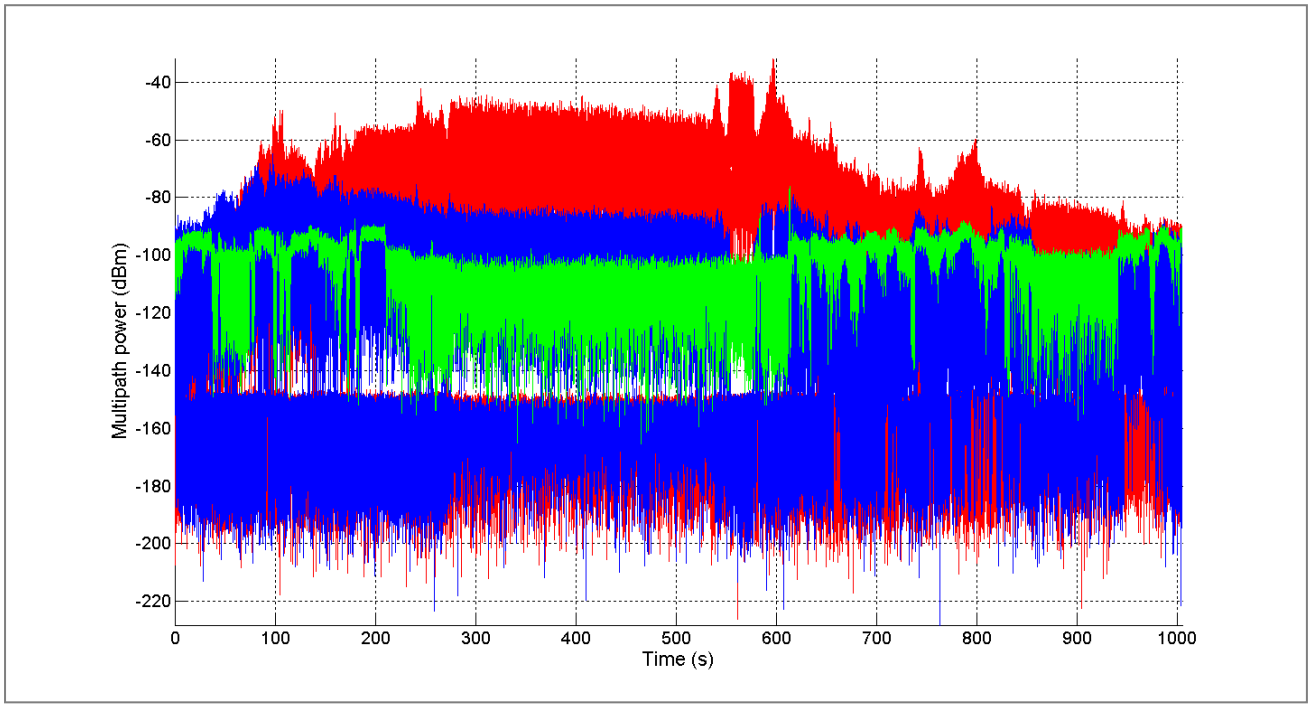

Figure 56 - Multipath power generated from the CNES CIR measurements

In Figure 57 and Figure 58, the delay of the multipaths is plotted. Multipaths whose power is below -120 dB have been put in grey, so that we observe only the most significant multipaths.

The introduction of an artificial delay of 6 µs for the red emitter and 12 µs for the blue emitter permits to avoid the reception of signals from different emitters at the same delay, thus enabling emitter discrimination and identification (Figure 58) compared to the case without artificial delay (Figure 57).

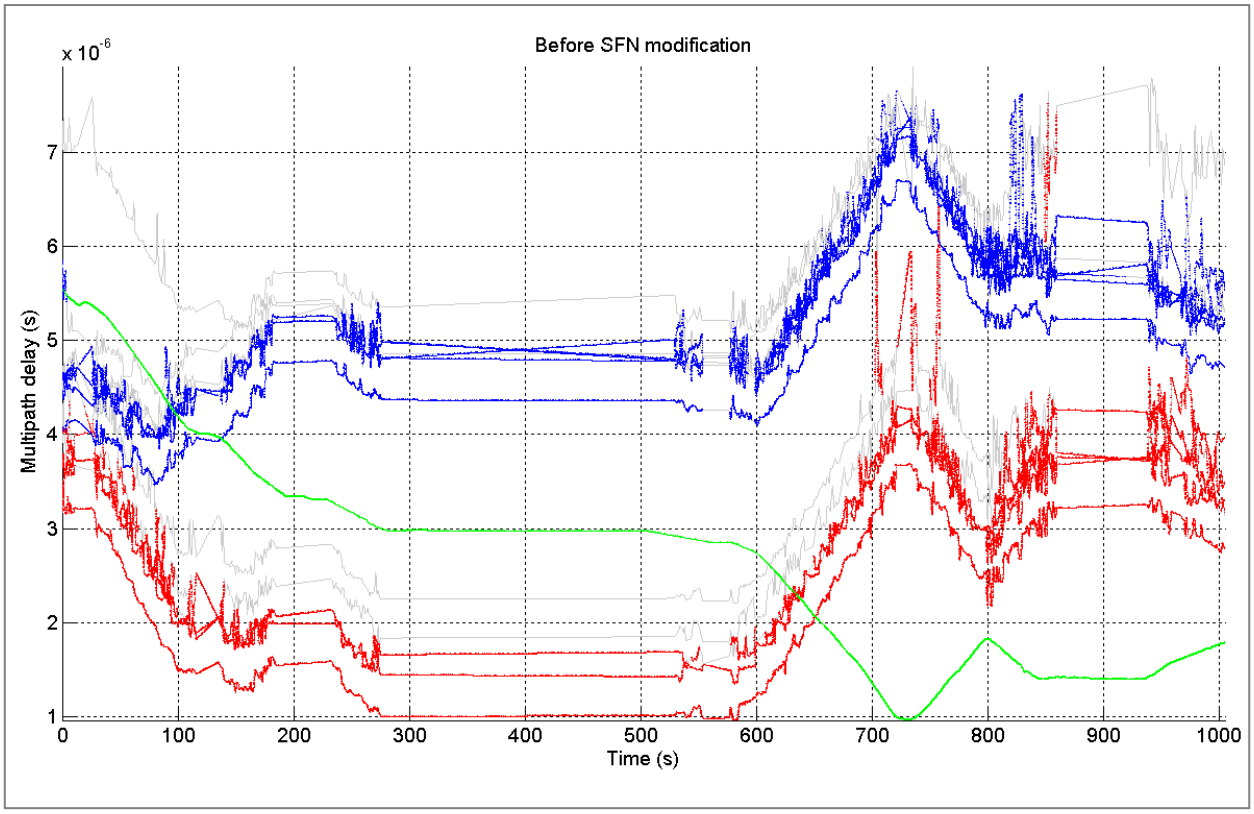

Figure 57 - Multipath delay in the SFN

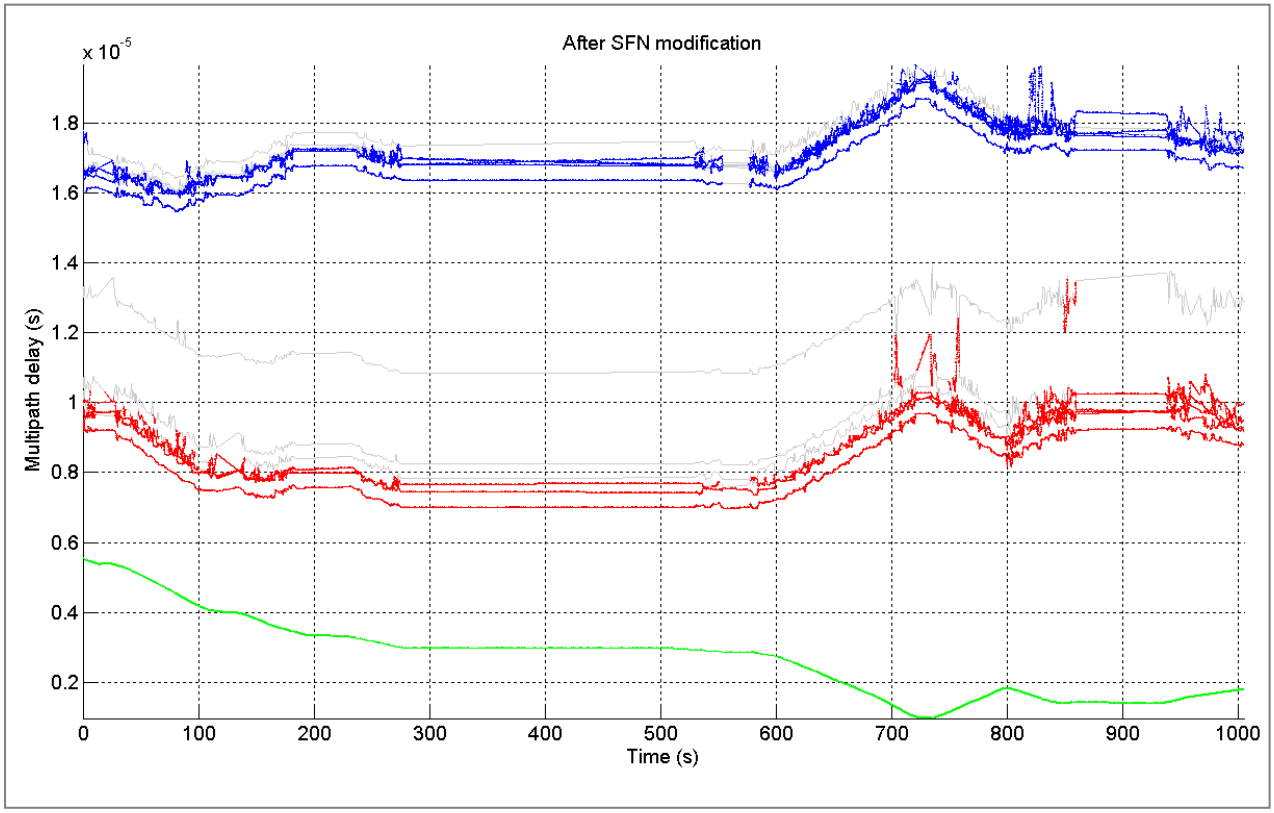

Figure 58 - Multipath delay in the modified SFN after introduction of a 6 µs artificial delay step

4.3.2 Simulation results and analysis

The generated CIR time series has been used to test the pseudo-range estimation and emitter discrimination methods described in chapters 3 and 4 in a realistic case.

The main parameter of the pseudo-range estimation methods that is tested is T**he impact of the windowing technique**. Section 4.1.3 has shown that windowing technique could attenuate the Near-Far effect, and thus improve the tracking conditions by eliminating the influence of emitters on one another. However, windowing also brings a wider correlation peak, which is expected to degrade the pseudo-range estimation accuracy (see section 3.5). The trade-off between the 2 effects will be observed by measuring the pseudo-range estimation performances using the different windowing techniques: rectangular, Hamming and Blackman-Harris windows.

The common parameters in all simulations are summarized in Table 16 for the system parameters and in Table 17 for the receiver parameters. The same system and receiver parameters as in the mono-emitter simulation (section 3.7.1) have been used, except for the acquisition and tracking threshold, which have been adapted to the power of the received multipaths encountered during the measurement, and the acquisition (Matching Pursuit) rate, which has been increased to 14.3 s, in order to reduce the computational load. It has been observed that the increase of the acquisition rate does not change much the behavior of the pseudo-range estimation.

Table 16 - System parameters used in the multi-emitter case (common to simulations #1-4)

N_{FFT}	2048
CP	1/4
B	5 MHz
Emitter EIRP	53.2 dBm
Noise floor level	-102.6 dBm
Average SNR	Between 9.2 and 49.2 dB

Table 17 - Receiver parameters used in the multi-emitter case (common to simulations #1-4)

B_l	10 Hz
T_i	T_{symb} = 448 µs
T_{acq}	$T_{acq} = 32000.T_{symb} = 14.3s$
T_{avg}	$80.T_{symb}$ = 35.84 ms
γ_{ACQ}	1e-6
γ_{TRK}	1e-7
N_{Xerror}	$3.floor(1/(B_lT_i)$ = 669
$N_{MeanVar}$	$200.T_{symb}$ = 89.6 ms
γ_{Div}	1e-4.$N_{MeanVar}$ = 8.96 µs
Clustering threshold	2.5 µs

4.3.2.1 Comparison of cCIR estimation for the different windowing techniques

Figure 59, Figure 60 and Figure 61 on the next page show the cCIR estimation obtained by the use of correlation with different windowing techniques. This technique is described in sections 3.2 and 3.5.2.

On Figure 59, corresponding to the case of a rectangular window, the Near-Far Effect is clearly problematic. The satellite emitter completely disappears in the sidelobes created by emitter #1. Therefore, a period of unavailability should be expected for the satellite emitter in the rectangular window simulation.

The interferences created by the presence of sidelobes also translates into what would be seen as a higher noise floor when acquiring or tracking multipath. One can expect that this will therefore impact the variance of the pseudo-range estimation error for emitter #2 and the satellite emitter due to the high sidelobes coming from emitter #1.

Finally, the presence of strong sidelobes in the cCIR estimation may trigger the acquisition and tracking of a sidelobe in place of a main lobe, due to their comparable amplitudes. This would create a negative bias in the estimated pseudo-range if the tracked sidelobe is earlier than the time of arrival of the first multipath.

This Near-Far Effect issue is still present in the Hamming window simulation Figure 60, while it is completely solved by using a Blackman-Harris window Figure 61. However, the correlation peaks of the windowed cases are wider, and a worse estimation error variance can be expected.

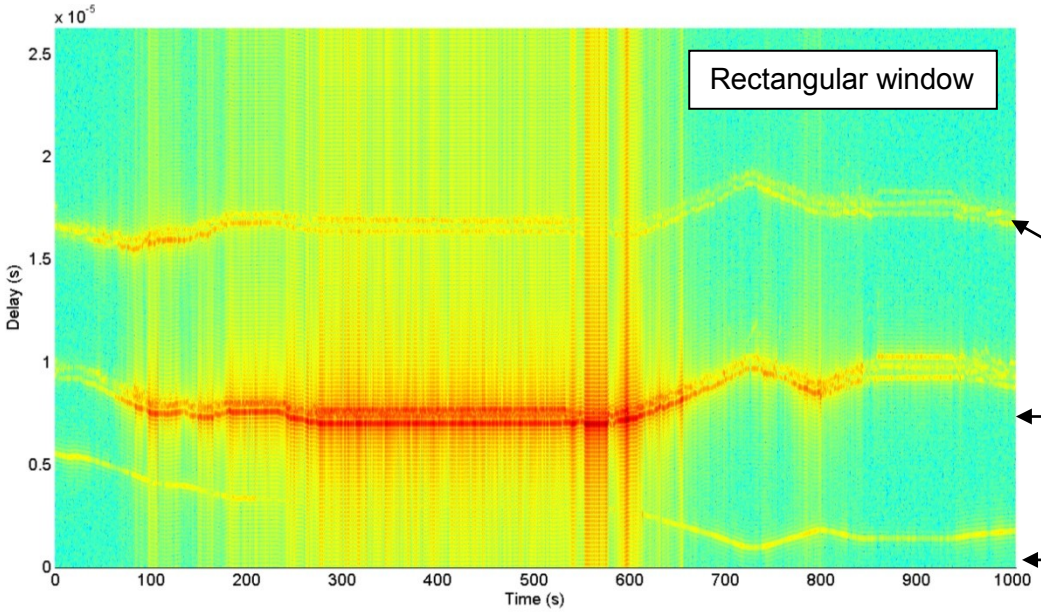

Figure 59 - cCIR estimation of the multi-emitter scenario using a Rectangular window

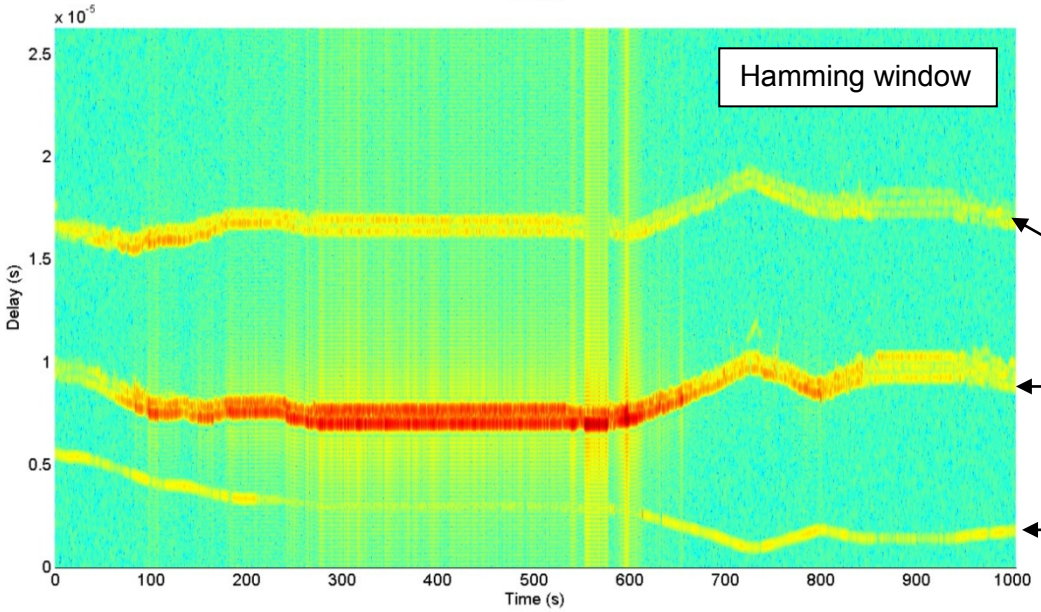

Figure 60 - cCIR estimation of the multi-emitter scenario using a Hamming window

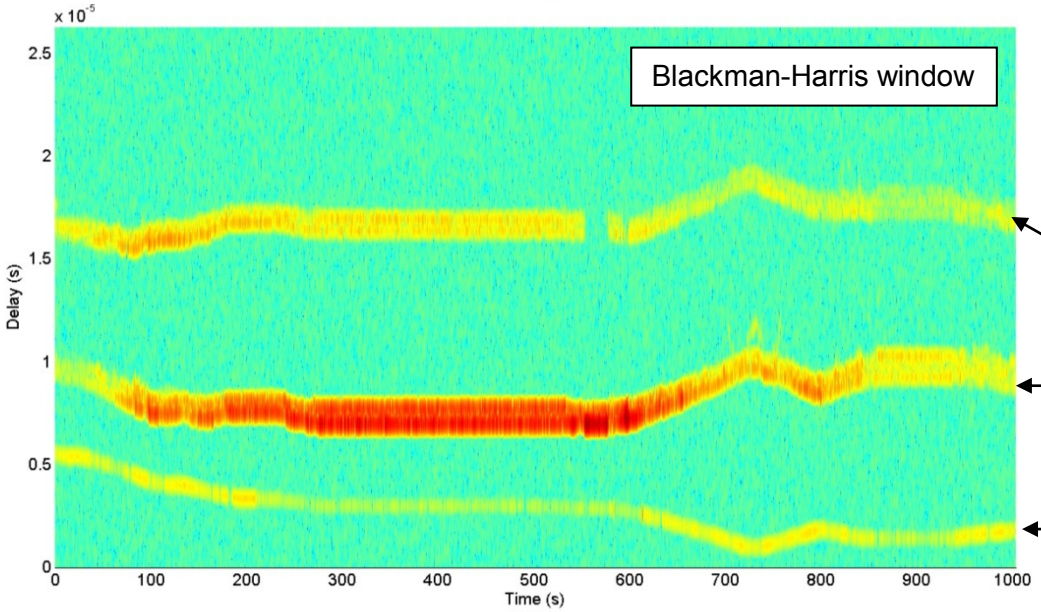

Figure 61 - cCIR estimation of the multi-emitter scenario using a Blackman-Harris window

4.3.2.2 Results of Simulation #1 - Increased time between 2 Matching Pursuit

In this simulation, a rectangular window is used.

The following pages show the simulation results in 2 graphs:

- The first graph (Figure 62) corresponds to the estimated delays during both acquisition and tracking phases after the clustering algorithm. The true delays are plotted in dotted gray lines, while the estimated delays are plotted in plain colored lines. One color corresponds to one emitter.
- The second graph (Figure 63) corresponds to the error between the true delay of each cluster and the selected estimated delay for all 3 emitters. The error is plotted in meters.

In addition to these graphs, the characteristics of the errors (mean errors and standard deviation) are summarized in Table 18.

Table 18 - Pseudo-range error statistics for simulation #1

	Availability (%)	Mean error (m)	Error standard deviation (m)
Emitter #1	100	-185.2	289.0
Emitter #2	100	-9.7	144.3
Emitter #3 (sat)	67.1	11.2	62.8

- The first remarkable result is that **the clustering algorithm is working**: 3 different clusters of estimated delays are created and correspond to the multipaths coming from the different emitters.
- Then, the **tracking of sidelobes** from correlation peaks can be observed, through the parallel lines that appear on the estimated delay time series for emitter #1 and #2. This is particularly problematic if early sidelobes are tracked, ie sidelobes whose delay is inferior to the main lobe of the multipath, because it creates a (large) negative error when the minimum delay of each cluster is chosen. This phenomenon explains the large negative errors affecting the estimated pseudo-distances for emitters #1 and #2, which can reach several hundreds of meters.
- **Brutal leaps of errors occur**, due to the stopping of the tracking of a given multipath or multipath's sidelobe, or when a new acquisition phase finds a new earlier multipath to track. When this occurs, the pseudo-distance uses a new tracked delay, which may be several several µs apart from the previously used tracked delay, thus resulting in leaps of several tens or hundreds of meter for the pseudo-range estimation.
- In the event of good tracking of the same multipath over a large duration, for example for the last 200s of the simulation, the estimation reaches good performances, as shown in Table 19. Emitter #1 is still affected by large error leaps, but for emitters #2 and #3 that are tracked successfully, the estimation performance is very good.

Table 19 - Pseudo-range error statistics for simulation #1 for the last 200s of the simulation

	Mean error (m)	Error standard deviation (m)
Emitter #1	25.7	110.0
Emitter #2	1.2	5.7
Emitter #3 (sat)	0.1	1.4

- Finally, the **Near-Far Effect is problematic** for emitter #3, due to the masking of its multipaths by the signal coming from emitter #1. This results in a high unavailability of the emitter #3's estimated pseudo-range.

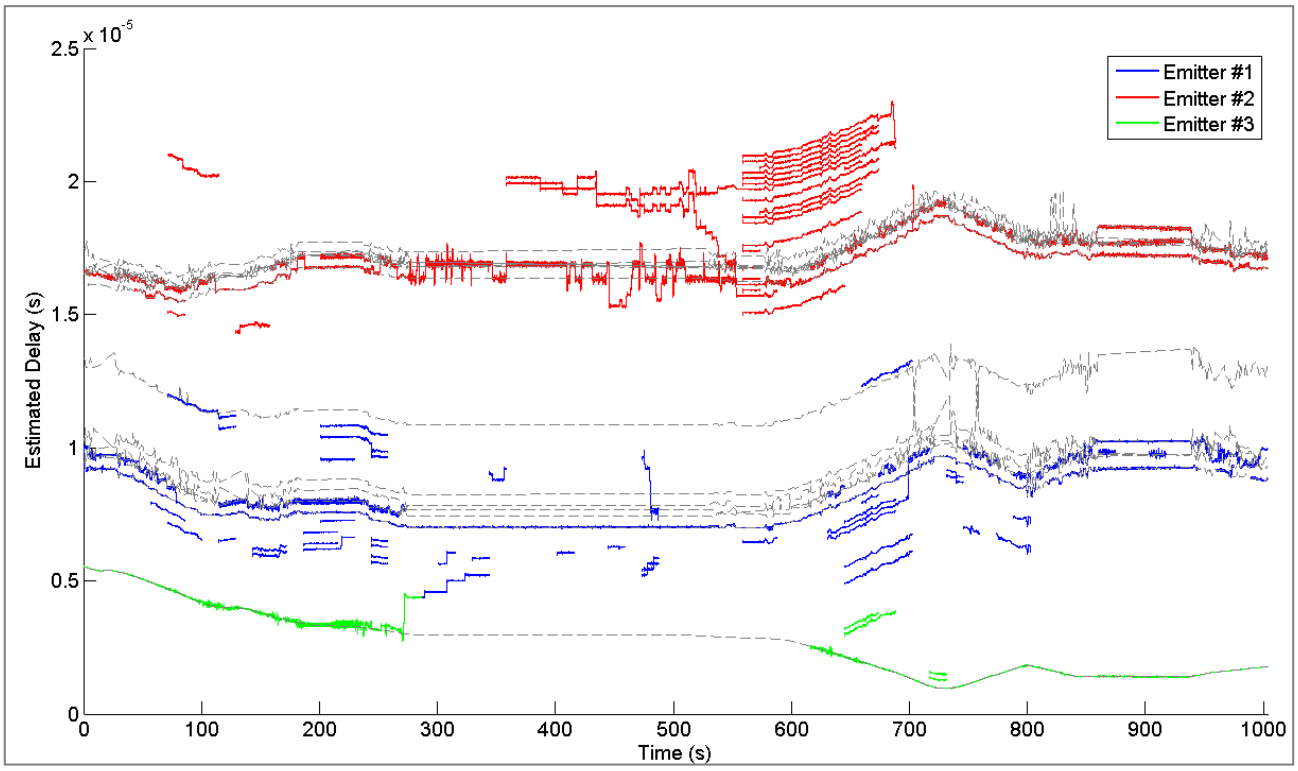

Figure 62 - Estimated delays after clustering for Simulation #1

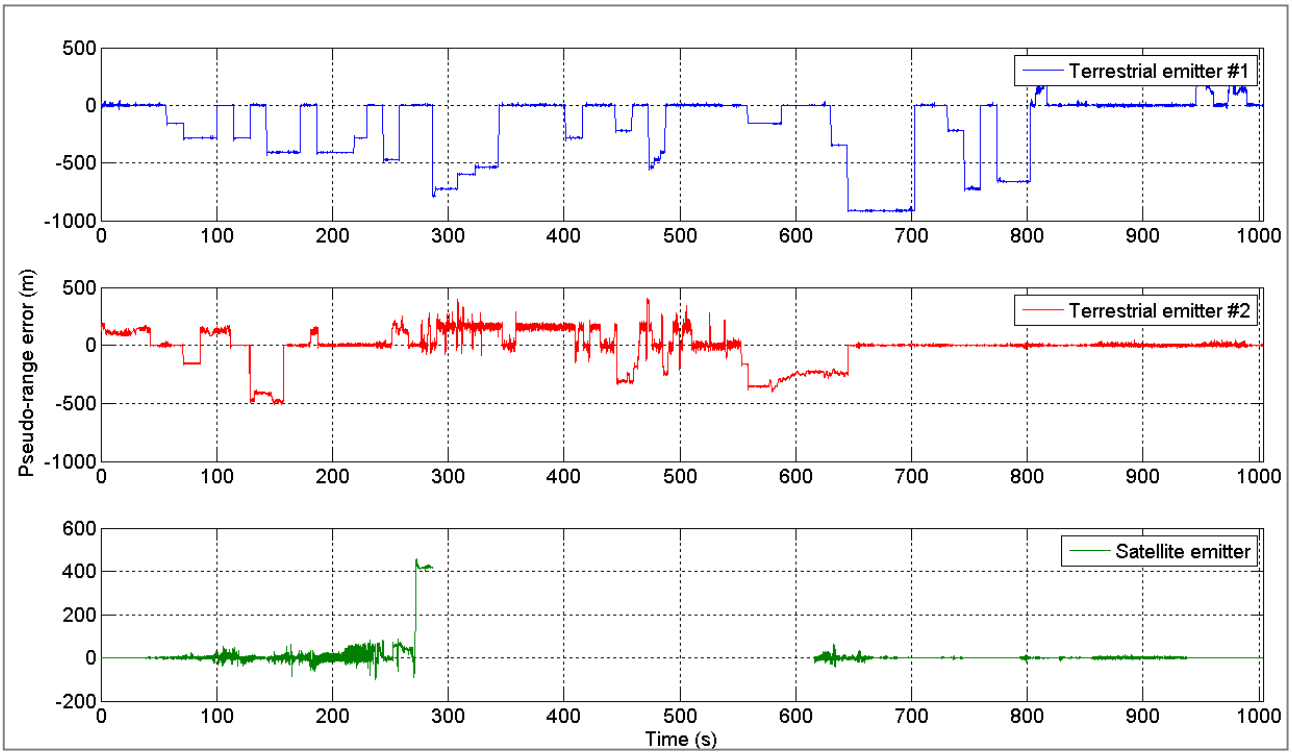

Figure 63 - Pseudo-range errors for Simulation #1

4.3.2.3 Results of Simulation #2 - Hamming window

In order to reduce the impact of the Near-Far Effect on the pseudo-range estimation, this simulation uses the Hamming window.

Table 20 - Pseudo-range error statistics for simulation #2

	Availability (%)	Mean error (m)	Error standard deviation (m)
Emitter #1	100	-150.2	219.1
Emitter #2	100	26.7	61.9
Emitter #3 (sat)	88.6	29.7	169.0

- For emitter #1, **the tracking of early sidelobes is reduced** but still present on a large part of the time series. This lead to a high mean error and standard deviation of the error due to the tracking of early sidelobes. This phenomenon affects only emitter #1, which is the most powerful.
- For emitter #2, **the tracking of a later correlation peak** is still present, but less frequently compared to the rectangular window.
- For emitter #3, **the availability of the pseudo-range is increased** thanks to the reduction of the sidelobes from emitter #1 by windowing. An increase of the error variance can be observed toward the middle of the time series. It corresponds to the increase of the noise floor in the delay range where the tracked peak dwells. This noise floor increase is due to the power received from the sidelobes coming from the powerful emitter #1 (**Near-Far Effect**), which still affects the delay tracking of the satellite emitter, although they are attenuated by the windowing technique.
- If the error statistics are computed over a slice of a time series not affected by large error leaps, ie between 700 and 800s, the pseudo-range estimation performances are improved, as shown in Table 21. Still, on this time span, the pseudo-range from emitter #1 is affected by large positive leaps, leading to poorer performances than for emitter #2 and #3, which reach an almost **null bias and a standard deviation of 2m** for the terrestrial emitter (#2) and **30cm** for the satellite emitter (#3).

Table 21 - Pseudo-range error statistics for simulation #2 between 700 and 800s

	Mean error (m)	Error standard deviation (m)
Emitter #1	29.3	61.3
Emitter #2	0.3	2.0
Emitter #3 (sat)	0.004	0.3

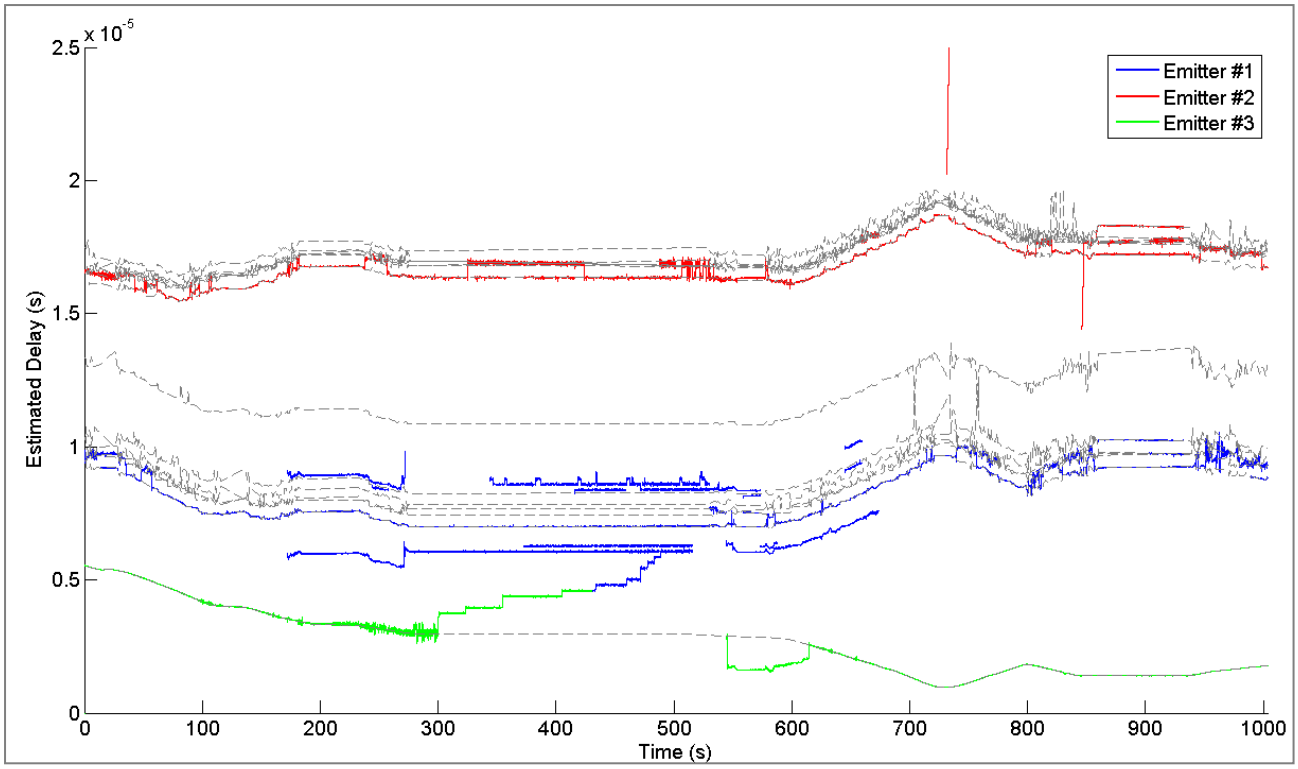

Figure 64 - Estimated delays after clustering for Simulation #2

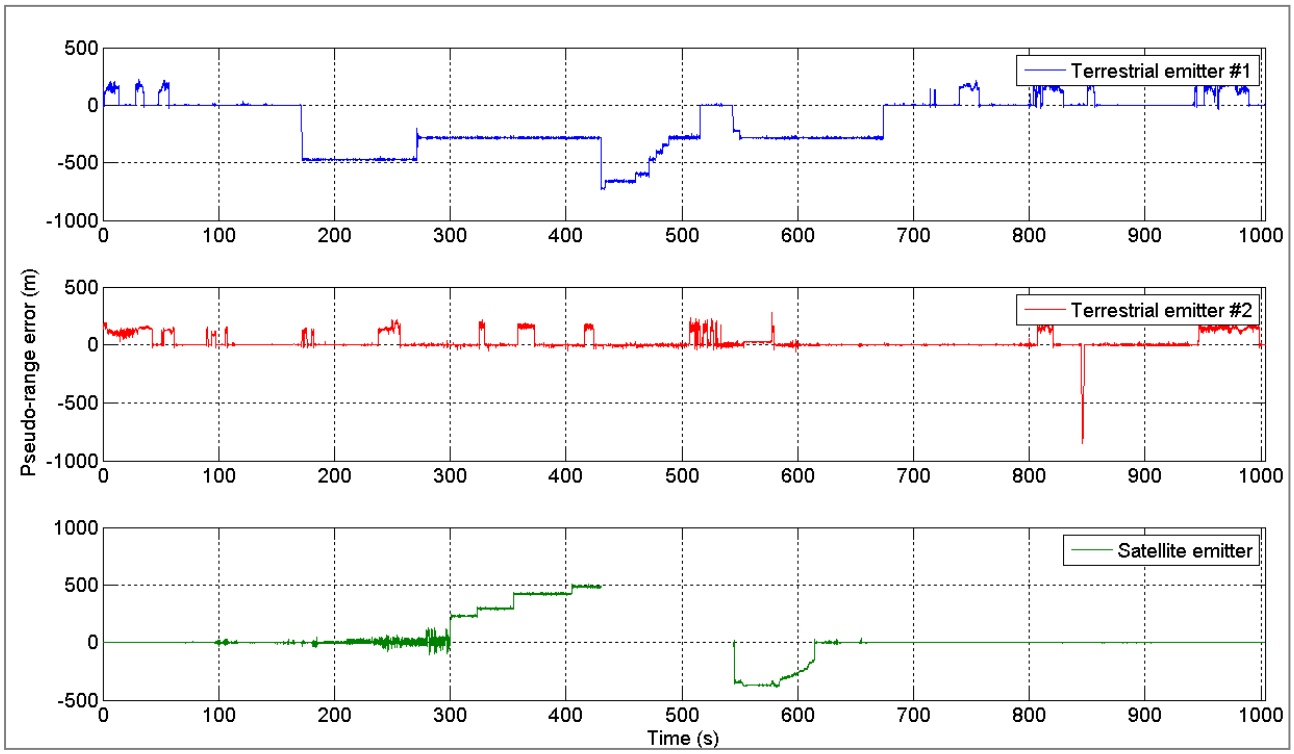

Figure 65 - Pseudo-range errors for Simulation #2

4.3.2.4 Results of Simulation #3 - Blackman-Harris window

This simulation uses a Blackman-Harris window. This window greatly attenuates the sidelobes, but results in a much larger main lobe (see Figure 36 section 3.5.1). Therefore, the mitigation of the Near-Far Effect shall be improved, while the pseudo-range estimation accuracy and sensitivity to close multipath should be degraded.

Table 22 - Pseudo-range error statistics for simulation #3

	Availability (%)	Mean error (m)	Error standard deviation (m)
Emitter #1	98.6	35.0	80.5
Emitter #2	92.9	62.0	79.7
Emitter #3 (sat)	100	80.5	0.9

- The **tracking of early sidelobes is totally solved** by the powerful attenuation of the correlation sidelobes brought by the Blackman-Harris window. This allows to cancel all negative error that were present in the previous simulations.
- The **Near-Far Effect is fully mitigated**, as seen by the complete availability of the pseudo-range estimation coming from the satellite emitter.
- A decrease of the availability of the pseudo-ranges from the terrestrial emitters is observed, but it is due to particular interactions between the acquisition/tracking strategy and the measurements. Aside from these particular conditions, there is no reason why the use of the Blackman-Harris window would decrease the availability of the pseudo-range estimations, compared to the other simulations.
- **Frequent positive error leaps are observed for emitter #2** between 300 and 530s. These leaps are occur because the pseudo-range estimation switches between the first and the second multipath coming from emitter #2. This phenomenon appears in this simulation due to the widening of the main correlation peak by the Blackman-Harris window. Therefore, the peaks are merging into a wide aggregate, which let the DLL switch between the two multipaths accordingly to the encountered fast fading. This issue could be mitigated by decreasing the noise equivalent bandwidth of the DLL.
- If the error is observed in a favorable timespan, e.g. between 600 and 700s, the observed performances are very good, as shown in Table 23. The performances are much improved for emitter #1, thanks to the absence of long tracking period of a later multipath. As for emitter #2 and #3, the performances are slightly degraded compared to simulation #2, due to the fact that the main lobe is wider, and therefore provides a less accurate estimate of the peak location. However, the performances still remain excellent.

Table 23 - Pseudo-range error statistics for simulation #3 between 700 and 800s

	Mean error (m)	Error standard deviation (m)
Emitter #1	4.1	19.6
Emitter #2	2.0	5.6
Emitter #3 (sat)	0.001	0.6

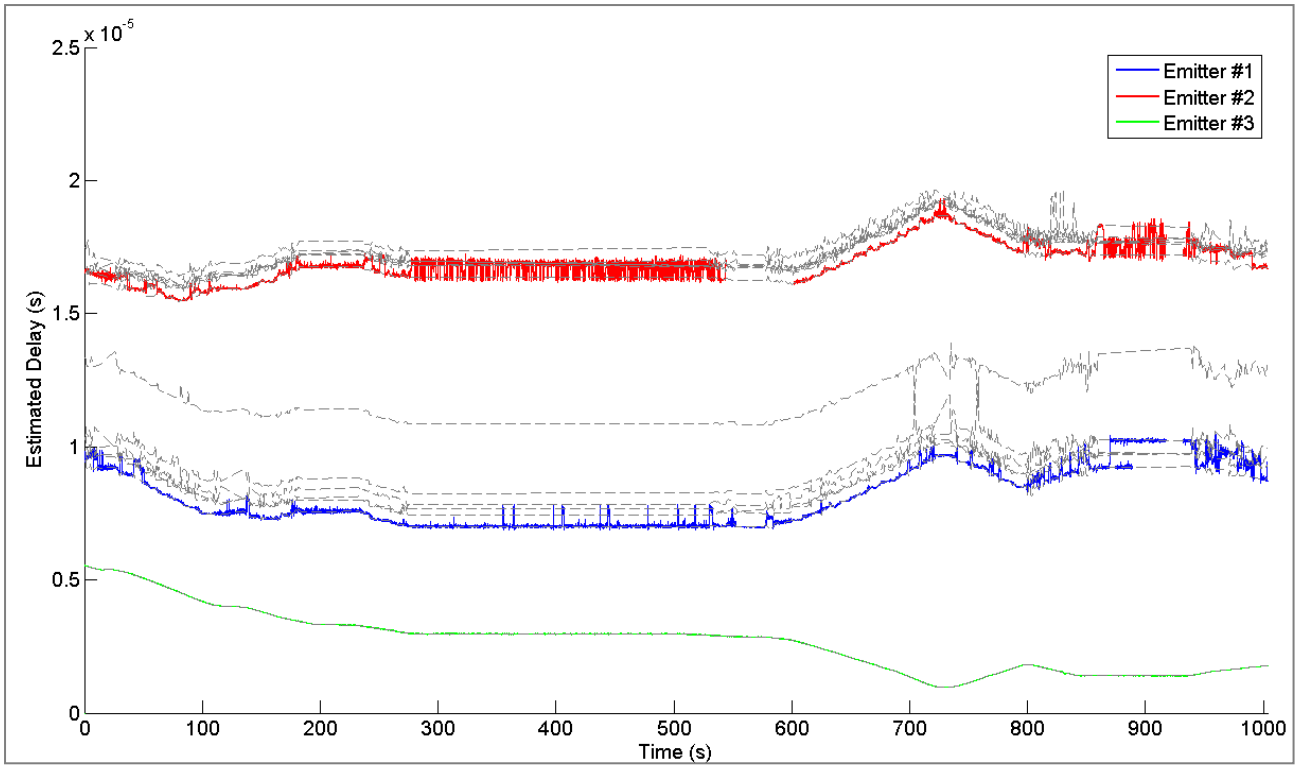

Figure 66 - Estimated delays after clustering for Simulation #3

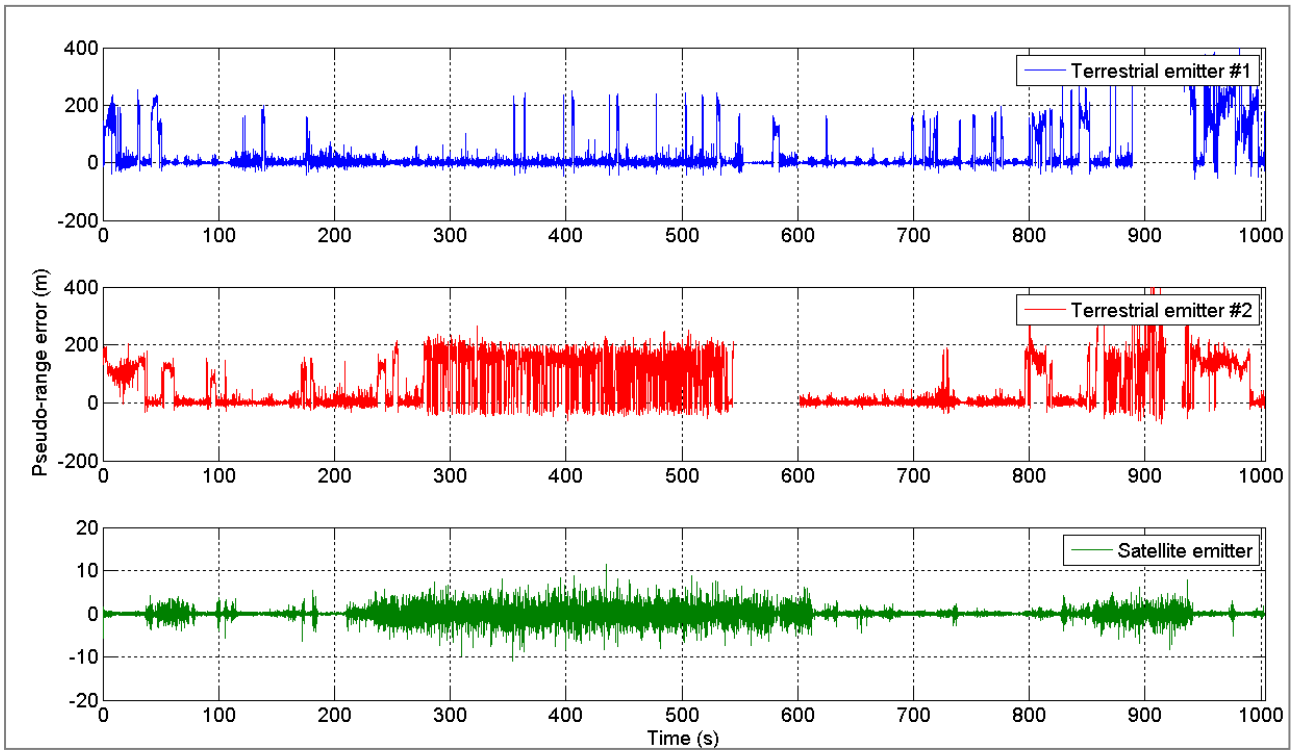

Figure 67 - Pseudo-range errors for Simulation #3

4.3.2.5 Comparison of the performances observed in the simulations

The performances of the pseudo-range estimation for the different simulations are grouped in Table 24. These statistics are calculated over the whole time series.

Table 24 - Comparison of multi-emitter pseudo-range estimation overall performances for the different simulations

	Availability (%)			Mean error (m)			Error standard deviation (m)		
	Simu #1	Simu #2	Simu #3	Simu #1	Simu #2	Simu #3	Simu #1	Simu #2	Simu #3
Emitter #1	100	100	98.6	-185.233	-150.2	35.0	288.951	219.1	80.5
Emitter #2	100	100	92.9	-9.688	26.7	62.0	144.273	61.9	79.7
Emitter #3 (sat)	67.1	88.6	100	11.195	29.7	80.5	62.756	169.0	0.9

These overall statistics may not be fully representative of the typical achievable performances, since the error time series are affected by frequent large leaps, which could be easily detected and hopefully avoided by improving the tracking technique.

In order to have a better hint of the achievable performances, the local error statistics were computed over a carefully chosen timespan of 200s for simulation #1, 100s for simulations #2 and #3, where the pseudo-ranges were not affected by large error leaps. These performances are representative of the achievable performances if a leap-detection and -mitigation technique was successfully implemented. These local statistics are collected in Table 25.

Table 25 - Comparison of multi-emitter pseudo-range estimation local performances for the different simulations

	Mean error (m)			Error standard deviation (m)		
	Simu #1	Simu #2	Simu #3	Simu #1	Simu #2	Simu #3
Emitter #1	25.7	29.3	4.1	110.0	61.3	19.6
Emitter #2	1.2	0.3	2.0	5.7	2.0	5.6
Emitter #3 (sat)	0.1	0.004	0.001	1.4	0.3	0.6

4.4 Conclusion on the pseudo-range estimation in a multi-emitter system

Following the theoretical study and the simulations done with the CNES cCIR measurements, it can be concluded that:

- **The emitter discrimination is perfectly achieved.** This means that the introduced artificial delay values are adequate to the studied case, and that the clustering algorithm does not make any error;
- **Early sidelobe tracking** happens for the rectangular window, thus creating a negative bias in the pseudo-range estimation of strong emitters. This issue is attenuated by the use of the Hamming window and completely solved by the use of the Blackman-Harris window.
- the error time series plots show that the **pseudo-range estimates for terrestrial emitters is affected by leaps between the first multipath and a later one**. This issue is increased by the used of windowing techniques;
- the use of **windowing techniques greatly improves the availability** of pseudo-range estimates for signals received with low power;
- **the best performance is obtained in Simulation #2 (Hamming window)**, where a terrestrial emitter is tracked with a 30 cm bias and an error standard deviation of 2m during 100s, while the satellite emitter is tracked with a 4 mm bias and an error standard deviation of 1m.

However, errors are computed between the first CIR multipath and the first estimated delay. Therefore, errors due to the first multipath arriving through a NLOS path are not observed. This is due to the lack of this information in the CIR measurements. The impact of the NLOS bias is studied in Chapter 6.

Also, the performances have been obtained in only one 1000s simulation, with a particular cCIR. In order to create a complete pseudorange error model, many more simulations in different conditions would be required.

The pseudo-range estimation technique in a multi-emitter scenario could be improved by several means:

- **Detection of pseudo-range estimation leaps.** Errors in the pseudo-range estimation due to the tracking of the wrong multipath results in leaps of the estimated value of *several tens or hundreds* of meters. They could be easily detected, and re-acquisition processes of the lost multipath could be triggered.
- **Adaptive use of the windowing techniques**. The use of strong sidelobe-attenuating window was beneficial in some case (in the presence of sidelobes from other strong emitters) and degrading in some other case (in the presence of close multipaths coming from the same emitter). Therefore, switching from one windowing technique to another would certainly benefit the pseudo-range estimation. The determination of the switching criteria should be quite hard to determine though.
- **Better acquisition techniques**. The tracking of wrong sidelobes in the case of the rectangular window is due to wrong delay acquisition by the Matching Pursuit. In case of better delay estimation during the acquisition phase, this issue may be avoided for strong emitters. Other widely spread CIR extraction parameter techniques beside the Matching Pursuit algorithm are the SAGE [Fleury 1999] or the ESPRIT [Paulraj 1985] algorithms.

- **Loop bandwidth study**. In this study, the only value for the noise loop bandwidth used in the simulation was 10 Hz. Further study may be required to see the impact of the noise loop bandwidth on the pseudo-range estimation. Among other, it is expected that with a low loop bandwidth, a DLL tracking a multipath during a fading period would remain close enough to the multipath delay until the multipath re-appears.
- **Multipath mitigation technique**. Other techniques to mitigate the multipath influence during delay estimation beside windowing techniques could be studied, such as the ones based on the ME-DLL [van Nee 1992][Yang 1999].

5 Emitter identification

After the delay discrimination and the pseudo-range estimation, the receiver has obtained several pseudo-ranges from several emitters. However, in order to calculate its position, the receiver has to know the characteristics of the emitters (position and artificial delay) to associate each pseudo-range with its emitter.

In this chapter, the emitters' characteristics are supposed to be available to the receiver, for example, thanks to a local database loaded in the memory of the handheld receiver, or via an assistance link. Therefore, the remaining task to realize is to associate each pseudo-range with an identified emitter, which we call **emitter identification**.

2 emitter identification techniques have been investigated:

- ***the Watermarking technique***, which a conventional technique, already standardized in some standards using Single Frequency Networks;
- ***the Reverse Positioning technique***, which has been proposed in the frame of this PhD study.

Figure 68 shows the place of the emitter identification process within the receiver's processes. It is placed after the pseudo-range estimation technique, where at this stage, several "anonymous" pseudo-ranges have been estimated, and before the position calculation, which consists in the solving of the position by combining the information between the emitter location and the identfied pseudo-ranges.

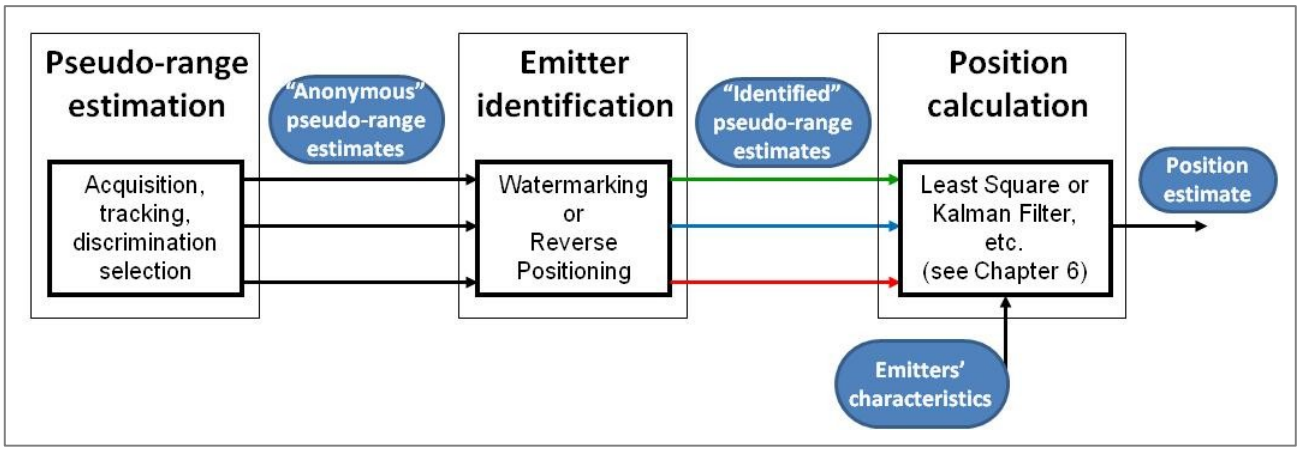

Figure 68 - Position calculation requires pseudo-range estimation and emitter identification

5.1 Watermarking technique

Emitter Watermarking consists in adding an identification signal to the useful DVB-SH signal. This identification signal is a pseudo-random noise sequence transmitted with a very low injection factor on the same signal bandwidth as the DVB-SH signal. This choice of a low-power pseudo-random noise sequence permits to minimize the degradation brought by the identification signal to the useful DVB-SH signal. Additionally, the properties of the pseudo-random noise, notably the high auto-

correlation and low inter-correlation gains, makes this choice a good solution for detection / identification purpose.

This solution has been studied in [Wang 2003] and [Wang 2007], and has been adopted in the ATSC standard (digital TV standard in the US) [ATSC 2007]. The main motivation for developing an emitter identification technique working in a SFN was for the monitoring of interferences by the system operator. Indeed, if interferences are created because of a problem in the SFN deployment, it is useful to be able to identify which emitter is at the origin of the interferences.

5.1.1 Watermarking theory

Emitter identification by watermarking is illustrated in Figure 69. At each emitter, a different watermarking signal is sent, with a low power level compared to the DTV signal power. The receiver receives the signal from different emitters. The emitter detection is done by correlating the received signal with a local replica of the watermarking signal and detecting a peak in the correlation output corresponding to the presence of the tested watermarking signal. As the watermarking signal is synchronized with the DTV signal, no additional synchronization is required: the synchronization information of the DTV signal is also used for the watermarking signal detection.

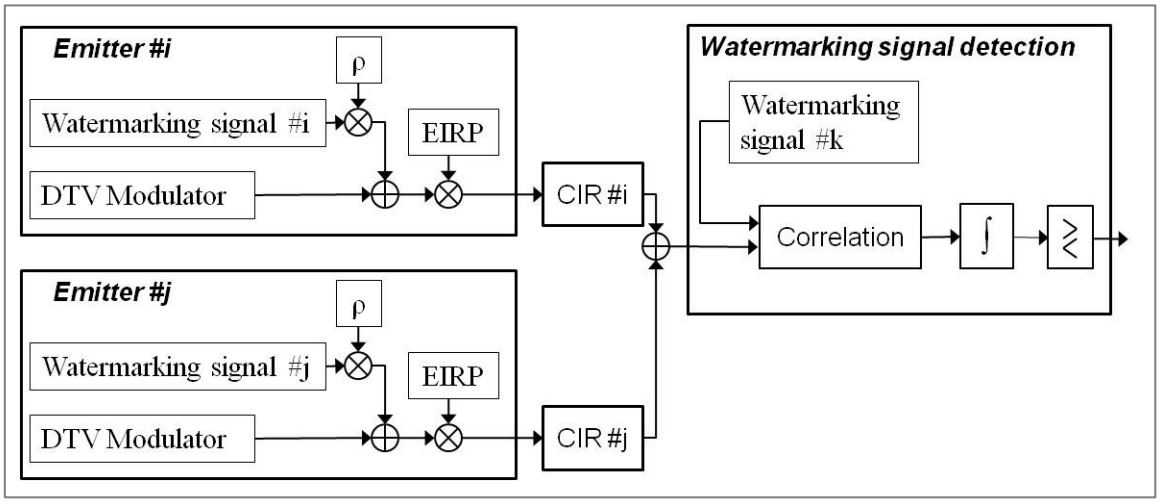

Figure 69 - Principle of emitter identification by watermarking technique

5.1.1.1 Expression in the time domain

Let us consider the addition of the watermarking signal to the emitted DTV signal for a given emitter.

$$s_q^i = s_q + \rho . w_q^i \qquad \text{Eq. 5.1}$$

where s_q is the q-th sample of the ODFM signal: $s_q = \sum_{k=0}^{N_{FFT}-1} c_k . e^{j2\pi \frac{kq}{N_{FFT}}}$, c_k being the sent data and pilot symbols

w_q^i is the q-th chip of the watermarking signal for the i-th emitter, which follows a pseudo-random sequence . [Wang 2003] recommends the use of Kasami sequences.

ρ is the amplitude level of the watermarking signal, called the injection factor. We suppose that the injection factor is identical for every emitter.

If the receiver receives signals from M emitters, then the received signal expression is

$$r_q = \sum_{i=1}^{M} \left(s^i \otimes h^i\right)_q + n_q = \sum_{i=1}^{M} l^i_{COST}.s^i_q + n_q \qquad \textbf{Eq. 5.2}$$

where h^i is the sampled channel impulse response for emitter i. For simplicity, the case of single tap channel without fading and delay is considered. The amplitude of the channel filter is only dependant on the distance between the i-th emitter and the receiver (see section 3.1.1):

$h^i(\tau) = l^i_{COST}\delta(\tau) = 10^{\frac{L^i_{COST}}{20}}\delta(\tau)$

n_q is the gaussian-distributed noise contribution affecting the q-th sample.

This received signal is cross-correlated with a local watermarking signal $\left(w^j_q\right)^*$

$$R_{rw_j}[m] = \sum_{q=0}^{N_{FFT}-1} r_q.\left(w^j_{q-m}\right)^* = \sum_{q=0}^{N_{FFT}-1}\sum_{i=1}^{M} l^i_{COST}.s^i_q.\left(w^j_{q-m}\right)^* + \sum_{q=0}^{N_{FFT}-1} n_w.\left(w^j_{q-m}\right)^*$$
$$= \rho.\sum_{i=1}^{M} l^i_{COST}.\sum_{q=0}^{N_{FFT}-1} w^i_q.\left(w^j_{q-m}\right)^* + \sum_{q=0}^{N_{FFT}-1} s_q.\left(w^j_{q-m}\right)^*\sum_{i=1}^{M} l^i_{COST} + \sum_{q=0}^{N_{FFT}-1} n_q.\left(w^j_{q-m}\right)^*$$

Using the notation $R_{xy}[m]$ for the correlation between the signal x and y taken at instant m, Eq. 5.3 is obtained.

$$R_{rw_j}[m] = \rho.l^j_{COST}.R_{w_jw_j}[m] + \rho.\sum_{\substack{i=1\\ i\neq j}}^{M} l^i_{COST}.R_{w_iw_j}[m] + R_{sw_j}[m].\sum_{i=1}^{M} l^i_{COST} + R_{nw_j}[m] \qquad \textbf{Eq. 5.3}$$

The first term of this sum corresponds to the correlation peak that we want to detect, and the other terms are therefore considered as noise and interference.

The second term corresponds to the cross-correlation of the desired watermarking signal with the other emitted watermarking signal. Due to the cross-correlation properties of the Kasami sequences, this term should be low.

The third term corresponds to the cross-correlation of the desired watermarking signal with the DTV signals coming from all emitters. As the DTV signal is significantly stronger than the watermarking signal, this term will be the most important among the noise and interferences terms. [Wang 2003] and [Yang 1999] suggests some techniques to remove this interference.

Finally, the last term corresponds to the contribution of the receiver's thermal noise to the correlation output. As the noise is uncorrelated with the watermarking sequence, this term will be low.

The watermarking technique consists in detecting the presence of the useful correlation peak, which is drowned in noise and interferences. This is a classical test of Neyman-Pearson.

5.1.1.2 Post-correlation SNIR expression

Let us suppose that the DTV signal and the thermal noise are zero-mean Gaussian random variables. Their power is therefore given by their variance.

From the correlator's output, the post-correlation SNIR can be deduced:

$$\frac{S}{N+I} = \frac{\left(\rho . l_{COST}^{j} .\right)^2 R_{w_j w_j}[m]}{\rho^2 . \sum_{\substack{i=1 \\ i \neq j}}^{M} \left(l_{COST}^{i}\right)^2 . R_{w_i w_j}[m] + Var\left(R_{sw_j}[m] . \sum_{i=1}^{M} l_{COST}^{i}\right) + Var\left(R_{nw_j}[m]\right)} \quad \text{Eq. 5.4}$$

with m chosen as the delay where the correlation peak is found.

After using classic correlation properties of pseudo-random sequences, the following SNIR expression is obtained:

$$\frac{S}{N+I} = \frac{\left(\rho . l_{COST}^{j} . N_{FFT}\right)^2}{N_{FFT} . \rho^2 \sum_{\substack{i=1 \\ i \neq j}}^{M} \left(l_{COST}^{i}\right)^2 + N_{FFT} . Var(s) . \left(\sum_{i=1}^{M} l_{COST}^{i}\right)^2 + N_{FFT} . Var(n)}$$

$$\frac{S}{N+I} = \frac{N_{FFT} . \left(\rho . l_{COST}^{j}\right)^2}{\rho^2 \sum_{\substack{i=1 \\ i \neq j}}^{M} \left(l_{COST}^{i}\right)^2 + \sigma_s^2 \left(\sum_{i=1}^{M} l_{COST}^{i}\right)^2 + \sigma_n^2} \quad \text{Eq. 5.5}$$

where σ_s^2 is the DTV signal power
σ_n^2 is the noise power

5.1.2 Watermarking TxId performance

5.1.2.1 Correlator output's N+I power estimation

In order to set the threshold for detection and false detection probabilities, the power of the noise and interferences σ_{N+I}^2 has to be known. An estimator is proposed in this section.

As shown in Figure 70, the proposed estimator uses a portion of the correlator output to calculate the variance of the signal. The N+I variance should be calculated over a delay range that excludes any correlation peaks due to the presence of signal replica. To do this, we use the correlator output's values at on a delay range starting after the CP duration, since the CP is dimensioned in order to comprise all possible multipath delays.

$$\hat{\sigma}_{N+I}^2 = Var\left(R_{rw_j}[m] \ , \quad m \in [N_{FFT} . CP + 1 \ , N_{FFT}]\right) \quad \text{Eq. 5.6}$$

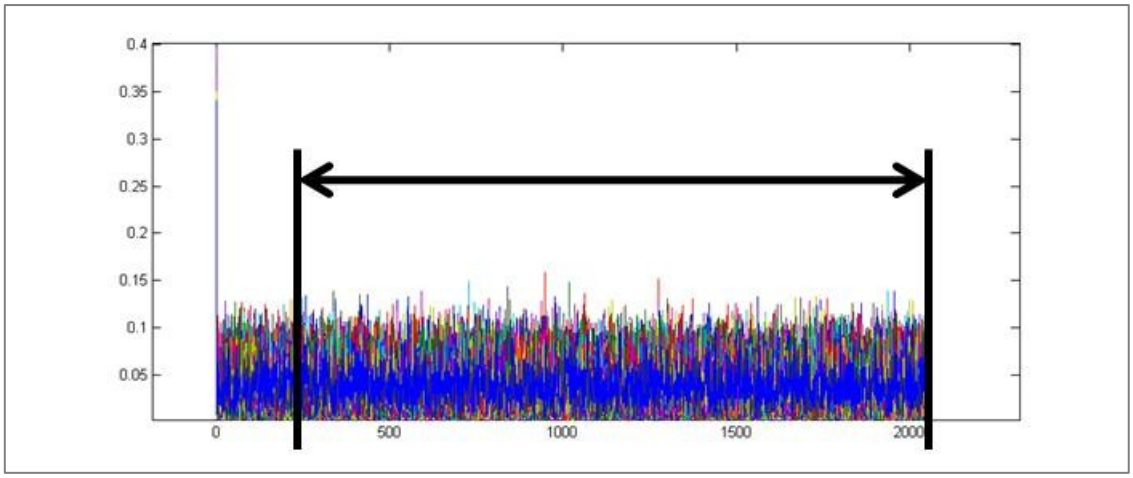

Figure 70 - Watermarking correlator's output. The delay range without the correlation peak can be used to estimate the noise and interference power

5.1.2.2 Determination of the detection threshold

First, the performance of the detection is chosen by setting a wanted false alarm probability. A false alarm occurs when the noise affecting the correlator output exceeds the detection threshold. Therefore, the value of the detection threshold is chosen so as to obtain a wanted false alarm probability

In order to exclude any influence of the phase, the absolute value of the correlator's output is observed. Therefore, the noise term at the output of the correlator follows a Rayleigh distribution (it is the amplitude of 2 Gaussian random variables in quadrature), with a mode equal to $m = \sigma_{N+I}/\sqrt{2}$

The theoretical expression of the cumulative density function of a Rayleigh distribution is

$$P(x < X) = 1 - \exp\left(\frac{-X^2}{2m^2}\right) = 1 - \exp\left(\frac{-X^2}{\sigma_{N+I}^2}\right) \quad \textbf{Eq. 5.7}$$

Therefore, the false detection threshold $X(P_{fa})$ can be determined by setting the probability that the Rayleigh-distributed noise + interference term exceeds the threshold (see Table 26).

$$X(P_{fa}) = \sqrt{-\hat{\sigma}_{N+I}^2 . \ln\left(P_{fa}\right)} \quad \textbf{Eq. 5.8}$$

where P_{fa} is the wanted probability of false alarm.

Table 26 - Detection threshold vs the wanted probability of false detection

Probability of false detection P_{fa}	Correlator's output threshold $X(P_{fa}) = \sqrt{-\sigma_{N+I}^2 . \ln\left(P_{fa}\right)}$
1%	$4.6052 . \sigma_{N+I}$
0.1%	$6.9078 . \sigma_{N+I}$
0.01%	$9.2103 . \sigma_{N+I}$
0.001%	$11.5129 . \sigma_{N+I}$

5.1.2.3 Detection performance

Once the detection threshold is set, the detection probability, which will depend on the power of the received signal, compared to the N+I power, has to be determined. The wanted correlation peak amplitude is the sum of a deterministic value and a complex Gaussian noise term, and therefore follows a Rice distribution, whose cumulative density function is

$$f(x < X, v, m) = 1 - Q_1\left(\frac{v}{m}, \frac{X}{m}\right) \qquad \text{Eq. 5.9}$$

where $v = \sqrt{\rho^2 . EIRP . N_{FFT}^2 . \left(\mathrm{l}_{\mathrm{COST}}^{\mathrm{j}}\right)^2}$ is the peak's deterministic amplitude,

$m = \sigma_{N+I}/\sqrt{2}$ is the noise power on one quadrature component.

$Q_1(\alpha, \beta)$ is the Marcum Q-function.

The Rice factor is defined as $K = v^2/2m^2$, which in the studied case corresponds to the post-correlation SNIR of the watermarking signal $S/(N+I)$.

Figure 71 aims at explaining the detection performances of the watermarking technique. The probability density of the N+I contribution is plotted in blue, while the probability density function of the desired correlation peak is plotted in green.

The dotted line is the threshold required to obtain the desired false alarm probability (in blue), obtained by integrating the N+I amplitude PDF from the false alarm threshold to $+\infty$.

Then, the detection probability is obtained by integrating the peak amplitude PDF from the false alarm threshold to $+\infty$.

The SNR offset the whole green curve, and therefore the detection probability.

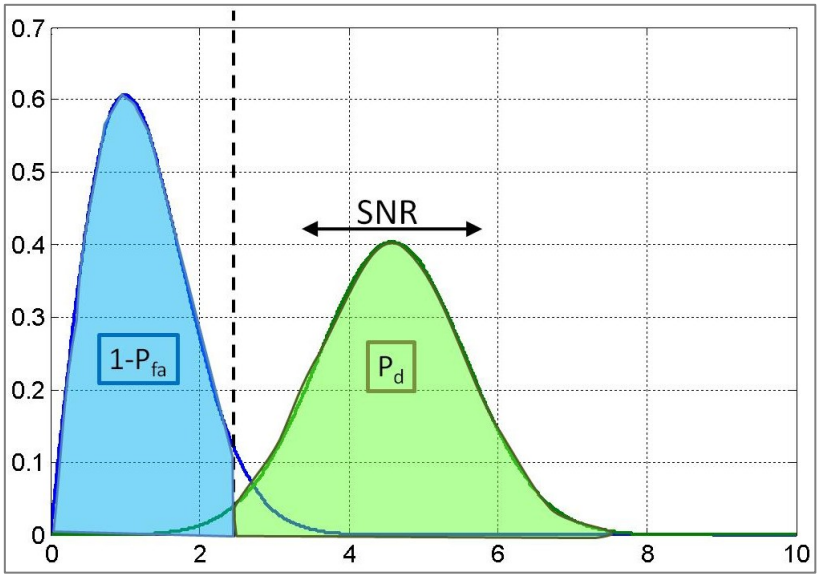

Figure 71 - Illustration of false detection and detection performances of the watermarking technique

Another way to illustrate the relation between the false alarm probability P_{fa}, the detection probability P_{det} and the SNIR is Figure 72, where the P_{det} vs SNIR curve is plotted for different P_{fa}.

The dotted line corresponds to $P_{det} = 0.95$ and the SNR corresponding to a desired P_{fa} are marked at the intersection of the dotted line and the colored curves.

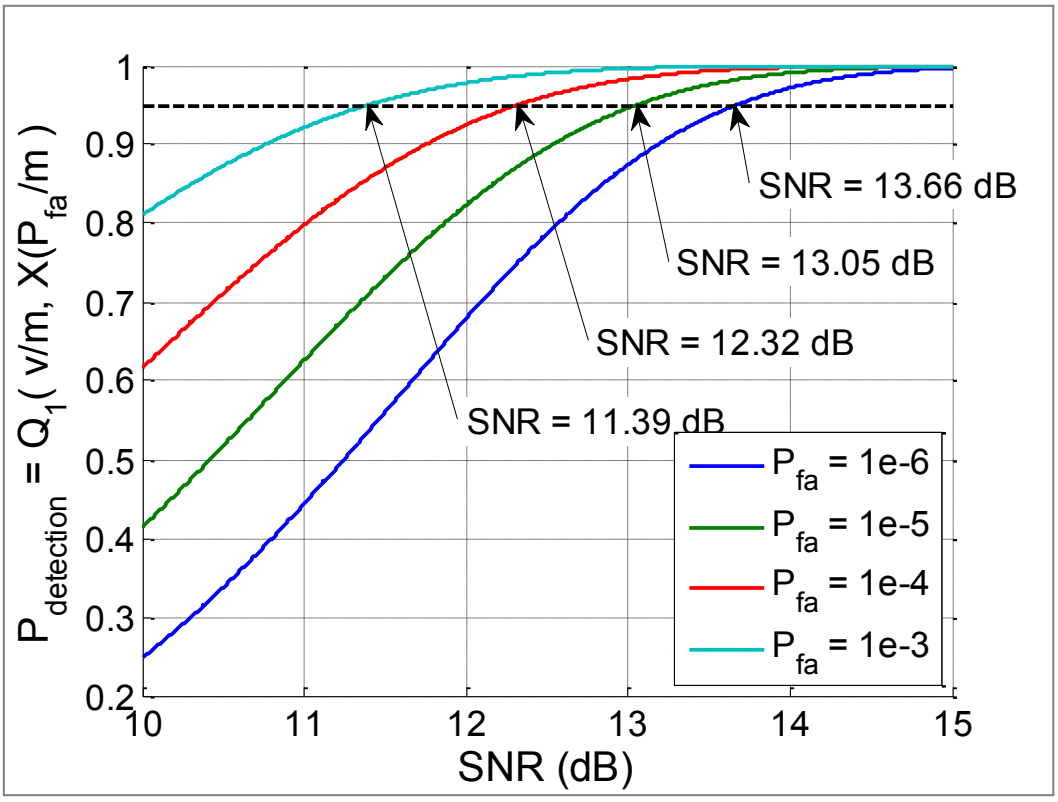

Figure 72 - Relation between P_{fa}, P_{det} and SNR

It can be observed that for a wanted P_{fa} and P_{det}, a single value of post-correlation SNIR corresponds. The following table provides the required post-correlation SNIR for different P_{det} and P_{fa}.

Table 27 - relation between P_{det}, P_{fa} and the required post-correlation SNIR

	$P_{fa} = 10^{-6}$	$P_{fa} = 10^{-5}$	$P_{fa} = 10^{-4}$	$P_{fa} = 10^{-3}$
$P_{det} = 0.9$	13.1830	12.5330	11.7490	10.7590
$P_{det} = 0.95$	13.6620	13.0490	12.3130	11.3900
$P_{det} = 0.99$	14.4950	13.9400	13.2800	12.4610
$P_{det} = 0.999$	15.3410	14.8400	14.2480	13.5210

5.1.3 Relation to system coverage

In the previous section, the relation between the detection performances (both P_{fa} and P_{det}) and the required post-correlation SNIR has been explained, and is summarized in Table 27. The required SNIR can be related to the system coverage thanks to a link budget equation.

For the purpose of this study, the following case will be illustrated:

- $P_{fa} = 10^{-3}$
- $P_{det} = 0.95$
- This results in a required post-correlation SNIR of 11.4 dB.

This required SNIR can be related to the distance between emitter and receiver using Eq. 5.5 and the COST 231 pathloss model described in Section 3.1.1.

Figure 73 and Figure 74 show the resulting SNIR for the emitter placed at coordinates (0,0) with 2 other emitters placed at (1000,0) and (500,866). This particular emitter network deployment forms an equilateral triangle and is the elementary pattern of the classical hexagonal network deployment.

The contour for SNIR = 11.4 dB is plotted in black.

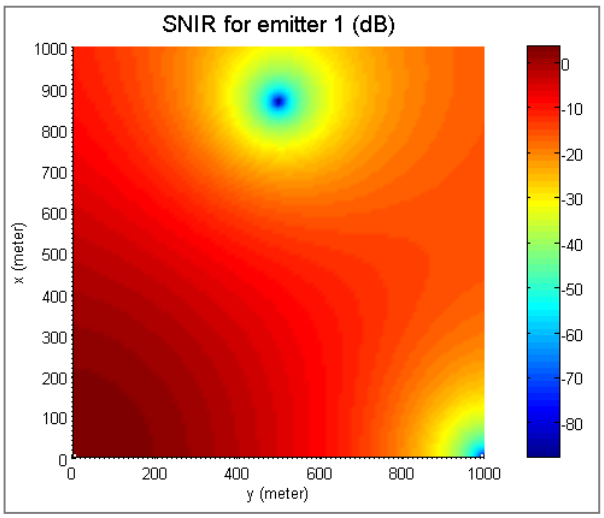

Figure 73 - SNIR map for a 3-emitter SFN

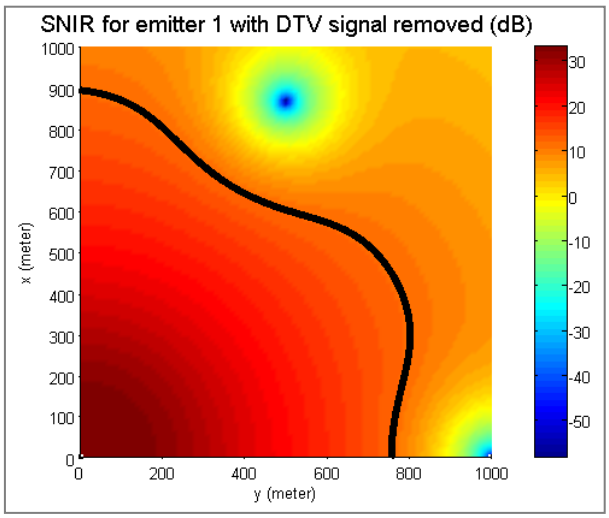

Figure 74 SNIR map for a 3-emitter SFN, with the DTV signal removed

In this case, the SNIR, never exceeds 5 dB over the coverage. With the DTV signal, the noise and interference are always too important, resulting in an empty zone: it is impossible to identify the emitters in this case.

With the DTV signal ideally removed, the plot above shows that at about 200m from another emitter, the noise and interferences are too strong to allow the emitter identification of the emitter placed at (0, 0).

Figure 75 shows the number of emitters that can be identified in an hexagonal network.

The coverage where at least 3 emitters are visible is quite reduced. In the area around one emitter, only one emitter is identifiable. The interferences are too strong to allow the identification of the neighbor emitters. This is a consequence of the Near-Far effect present in dense network of emitters.

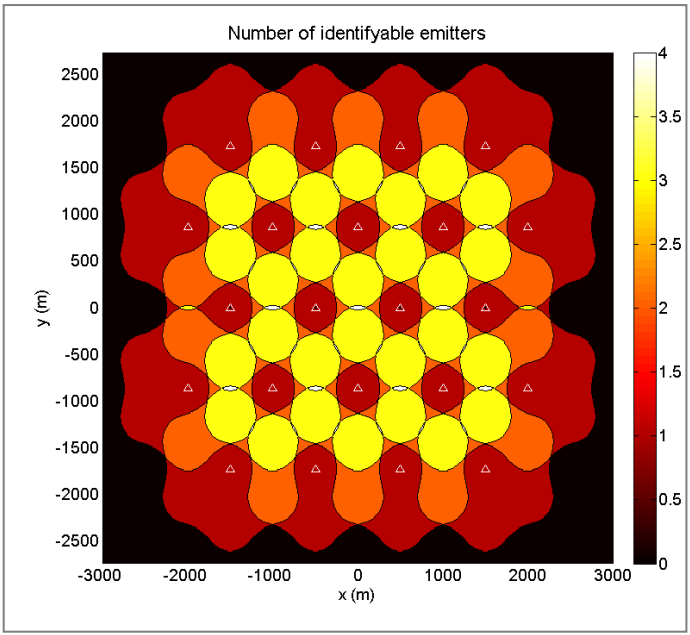

Figure 75 - Number of identifiable emitters with watermarking technique in an hexagonal SFN deployment with a cell radius of 500 m

5.1.4 Conclusion on the watermarking technique for emitter identification

As such, the coverage for emitter identification is not satisfying for localization purpose. In most service coverage, this technique will permit to identify the one or two nearest, strongest emitters, which may be useful for interference monitoring in an SFN. However, for localization purpose, as many emitters as possible have to be identified in order to increase the position accuracy, with a strict minimum of 3 emitters.

Additionally, this technique would require modifications to the emitter network by adding the watermarking signal generator, and modifications to the receiver by adding power-consuming correlators for the emitter identification process only.

The performances of the watermarking technique could be improved by using significantly longer codes (length multiplied by 100 or 1000), therefore increasing the correlation gain and lowering the required SNIR for a desired detection performance. Another solution would be to remove the strongest watermarking signal before searching for other weaker watermarking signal. In any case, the Near-Far Effect would still be a significant issue, with a "jamming" zone around each emitter.

Therefore, emitter identification using watermarking signals does not seem appropriate to our positioning method.

5.2 Reverse positioning technique

In a classical positioning problem, the emitters characteristics and the associated pseudo-ranges are used to determine the position (Figure 76, left). In this section, we propose to use the emitters characteristics (position and artificial delay), an approximate position of the receivers and the anonymous pseudo-ranges in order to identify the pseudo-ranges, ie associate them with an emitter

(Figure 76, right). We have called this technique the emitter identification by **reverse positioning technique**.

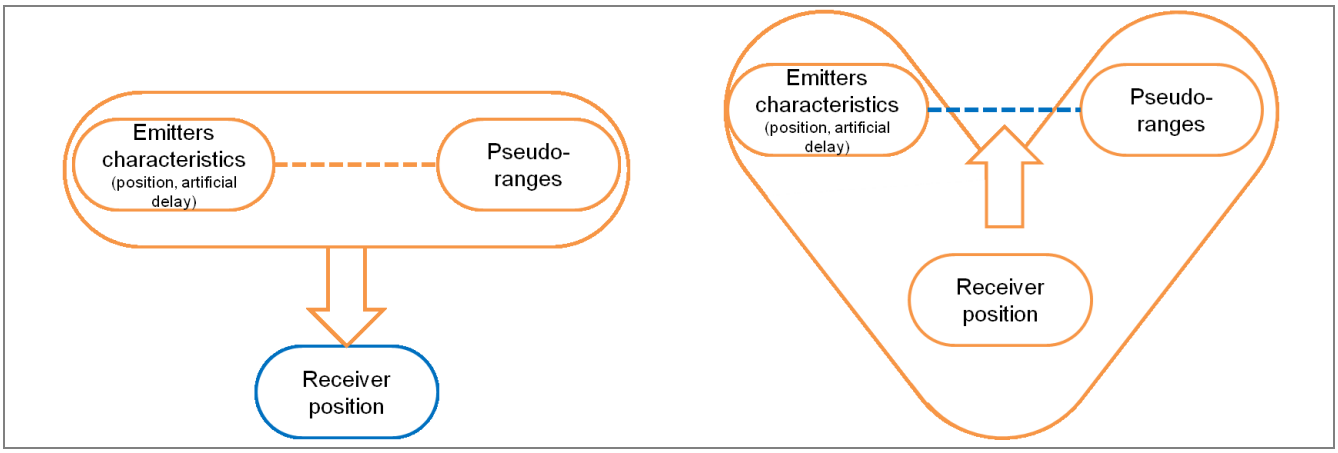

Figure 76 - Direct positioning (left) and Emitter identification by reverse positioning technique (right). In each case, the known data is put in orange, while the unknown is marked in blue.

5.2.1 Principle of the reverse positioning technique

Let us assume that the sensor has collected the measurements

$$\rho_i = h(p, p_i, \tau_i,) + n_i \text{ for } i \in \{\mathbf{Tx}\} \qquad \textbf{Eq. 5.10}$$

with $p = [x, y]^T$ is the position of the sensor,
$p_i = [x_i, y_i]^T$ is the position of the emitter i,
τ_i is the artificial delay of the emitter i,
n_i is the noise affecting the pseudo-range i,
$h(p, p_i, \tau_i) = \sqrt{(x - x_i)^2 + (y - y_i)^2} + c.\tau_i$ is the pseudo-range modeling function,
$\{\mathbf{Tx}\}$ is the ordered set of emitters participating to the measurement,

Let us assume that the sensor knows its approximate position $\hat{p}$. This position can be a position provided by other means of positioning (e.g. Cell ID, a previous GPS position before entering a building, etc.). We call $\hat{p}$ the assistance position.

Through the assistance position, it is assumed that the receiver can determine the set of emitters $\{\mathbf{Tx}\}$ from which a pseudo-range has been received. Calling N_{Tx} is the number of pseudo-ranges, $\{\mathbf{Tx}\}$ consists logically in the set of the N_{Tx} closest emitters to the assistance position.

Let us call $\Sigma(\mathbf{Tx})$ the set of the permutations of $\{\mathbf{Tx}\}$. Among this set, there is one permutation that corresponds to the received pseudo-ranges.

Let us consider a cost function $V(p, \boldsymbol{\sigma})$, which depends on the position p and the permutation $\boldsymbol{\sigma}$ of $\Sigma(\mathbf{Tx})$. It is defined as the norm of the error between the measurements and the pseudo-range model taken at the assistance position $\hat{p}$.

$$V(p, \hat{p}, \boldsymbol{\sigma}) = \sum_{i=1}^{Card(\boldsymbol{\sigma})} \left(\rho_i - \sqrt{(\hat{x} - x_i)^2 + (\hat{y} - y_i)^2} - c.\tau_i\right)^2 \qquad \textbf{Eq. 5.11}$$

If the cost function is calculated for the right permutation, that we name $\overline{\overline{\boldsymbol{\sigma}}}$, and in the case of ideal assistance position and pseudo-range measurements, we obtain $V(p,p,\overline{\overline{\boldsymbol{\sigma}}}) = 0$. Errors on the assistance position and on the pseudo-range will add some contribution to the cost function.

The proposed emitter identification process consists in finding the right permutation of $\{\mathbf{Tx}\}$ that minimizes this cost function.

$$\hat{\boldsymbol{\sigma}} = \underset{\boldsymbol{\sigma}\in\boldsymbol{\Sigma}(\mathbf{Tx})}{\arg\min} V(p,\hat{p},\boldsymbol{\sigma}) \qquad \textbf{Eq. 5.12}$$

5.2.2 Isolation of the correct permutation

Errors in the emitter identification occur when several emitters bring the same contribution to the cost function. In this case, The corresponding permutations will have the same cost function and errors on the measure may force the identification process to chose the wrong permutation.

Let us consider the particular case where all pseudo-range are correctly associated to their emitters except of 2 emitters which are inverted. This error should be the first to appear, ie the most probable and will yield the second lower cost function after the right permutation. Let $\boldsymbol{\sigma}'$ be a permutation where emitter #1 and emitter #2 are respectively and wrongly associated with pseudo-ranges ρ_2 and ρ_1. In this case, the cost function value is:

$$V(p,p,\boldsymbol{\sigma}') = \left(\rho_2 - \sqrt{(x-x_1)^2+(y-y_1)^2} - c.\tau_1\right)^2 + \left(\rho_1 - \sqrt{(x-x_2)^2+(y-y_2)^2} - c.\tau_2\right)^2$$

By replacing ρ_1 and ρ_2 by their noise-free expression depending on the pseudo-range modeling function, this cost function simplifies to:

$$\begin{aligned} V(p,p,\boldsymbol{\sigma}') &= 2.\left(\sqrt{(x-x_2)^2+(y-y_2)^2} - \sqrt{(x-x_1)^2+(y-y_1)^2} + c.(\tau_2-\tau_1)\right)^2 \\ &= 2.\left(d_2 - d_1 + c.(\tau_2-\tau_1)\right)^2 \end{aligned} \qquad \textbf{Eq. 5.13}$$

where $d_i = \sqrt{(x-x_i)^2+(y-y_i)^2}$ is the distance between the sensor position and emitter #i

Let us call $I(p,\hat{p}) = |V(p,\hat{p},\overline{\overline{\boldsymbol{\sigma}}}) - V(p,\hat{p},\boldsymbol{\sigma}')|$ the ***isolation of the right permutation***. This isolation is linked to the probability of making an error in the emitters identification.

If $I(p,\hat{p})$ is large, the 2 likeliest permutations are sufficiently separated so as not to make a mistake.

If $I(p,\hat{p})$ is small, permutation $\boldsymbol{\sigma}'$ may be chosen in place of $\overline{\overline{\boldsymbol{\sigma}}}$.

To begin, the case with the assistance position correct: $\hat{p} = p$ and the pseudo-range perfectly estimated ($n_i = 0$) is considered. Therefore, the isolation reduces to $I(p,p) = |V(p,p,\boldsymbol{\sigma}')|$, since the cost function associated to the right permutation $\overline{\overline{\boldsymbol{\sigma}}}$ is equal to 0.

The isolation of the right permutation is small if $V(p,\hat{p},\boldsymbol{\sigma}')$ is small. The curve $V(p,p,\boldsymbol{\sigma}') = 0$ can have a geometric interpretation: it corresponds to the area of the service coverage where 2 signal replicas arrive at the same time. We will call this area the ***iso-delay zone***.

This iso-delay zone concept can be illustrated by plotting the isolation on the service coverage of a 46-emitter network. The introduced artificial delays are distributed among the emitters according to Figure 77. Here, the emitters are attributed 12 different delays ranging from 0 to 11 times an artificial delay step. This particular network deployment has been chosen since it is extensively investigated in the later section 7.1.2.

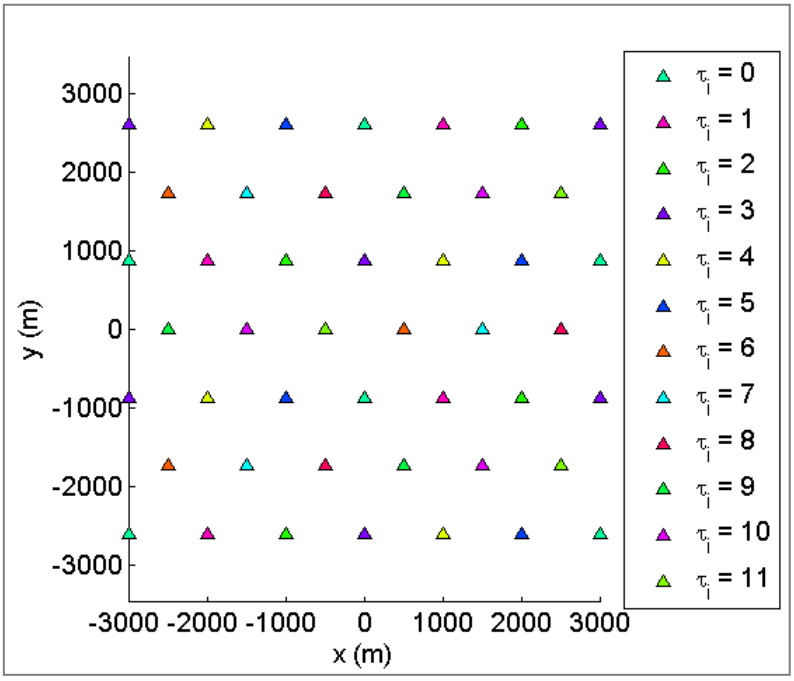

Figure 77 - 12-color artificial delay distribution in an SFN

The 5 closest pseudo-ranges are considered at each point of the coverage, and we assume no error in the assistance position and on the estimated pseudo-ranges. The isolation was limited to a range varying between 0 and 30 dB, in order to have a meaningful display.

In Figure 78, the artificial delay step is set to 0, which means no artificial delay has been introduced in the SFN. The iso-delay zones appear on the symmetry axis of the network, as one could expect.

In Figure 79, the artificial delay step has been set to 2 µs, meaning that each emitter will be affected by an artificial delay ranging from 0 to 22 µs. In this case, the iso-delay zones are much reduced and in shape of hyperbola arcs.

If one would increase the artificial delay step to a value over the propagation time from one emitter to another, there would be no more iso-delay zones. In our example, the emitters are separated by 1000m, so the threshold for the removal of iso-delay zone is an artificial delay step greater than $\frac{1000}{c} = 3.33\ \mu s$.

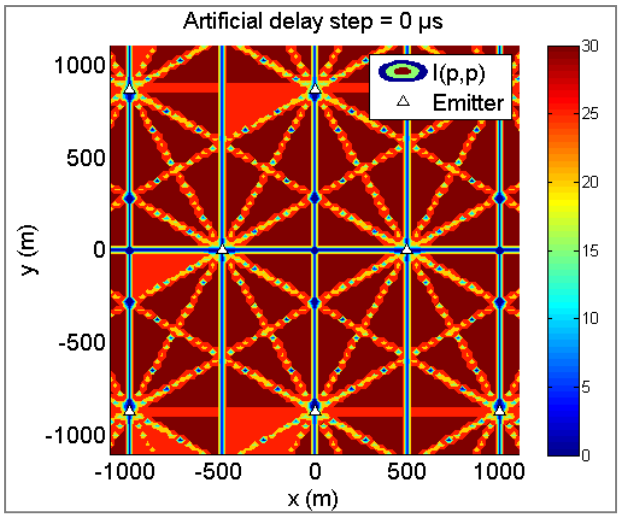

Figure 78 - Isolation over coverage without artificial delay

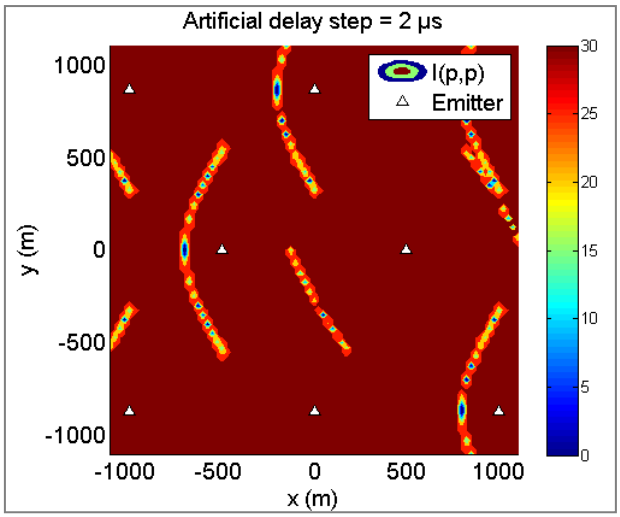

Figure 79 - Isolation over coverage with a 2-µs artificial delay step

With ideal assistance position, ideal pseudo-range estimates and an adequate SFN deployment (ie without iso-delay zones over the service coverage), the reverse positioning method will provide a high isolation of the good permutation, and therefore good identification performances.

5.2.3 Robustness of the reverse positioning technique to errors

Several errors may affect the performances of this technique:

- Error on pseudo-range measurements ρ_i
- Error on assistance position $\hat{p}$
- Error on the tested emitter set $\{\mathbf{Tx}\}$

This section will review the impact of each error, taken individually.

5.2.3.1 Error on pseudo-range measurements ρ_i

Let us assume that each pseudo-range ρ_i is affected by a measurement noise, noted n_i.

In this case, the cost function of the right permutation is:

$$V(p,p,\bar{\bar{\boldsymbol{\sigma}}}) = \sum_{i=1}^{N_{Tx}} n_i^2$$

The cost function of the wrong permutation $\boldsymbol{\sigma}'$ is:

$$V(p,p,\boldsymbol{\sigma}') = 2.\left(n_2 - n_1 + d_2 - d_1 + c.(\tau_2 - \tau_1)\right)^2 + \sum_{i=3}^{N_{Tx}} n_i^2$$

The isolation with noisy pseudo-ranges is:

$$\begin{aligned} I_{noise}(p,p) &= \left| n_1^2 + n_2^2 - 2.\left(n_2 - n_1 + d_2 - d_1 + c.(\tau_2 - \tau_1)\right)^2 \right| \\ &= \left| I(p,p) + n_1^2 + n_2^2 - 2(n_2 - n_1)^2 - 2(n_2 - n_1)\left(d_2 - d_1 + c.(\tau_2 - \tau_1)\right) \right| \end{aligned}$$

Eq. 5.14

The difference between $I(p,p)$ and $I_{noise}(p,p)$ depends on the distribution of the pseudo-range measurement errors.

Simulations with a pseudo-range error following a centered Gaussian distribution with $\sigma = 80$ meters have been run on the service coverage in a modified SFN (Figure 77). This value of pseudo-range error has been chosen in order to reflect the standard deviation simulated in bad conditions with the pseudo-range estimation method proposed in Chapter 3 and 4.

The SFN is modified so as no iso-delay zones are present: the artificial delay step is set to a value superior to the transit time between 2 adjacent emitters, ie it is superior 3.33µs. At each point of the coverage, 100 identification tests are run, with the pseudo-ranges to the 5 closest emitters.

Figure 80 shows the number of wrong identifications out of the 100 identification tests for 2 values of artificial delay step. Some zones are more sensitive to identification errors. They correspond to zones where the pseudo-ranges to 2 emitters are very close, thus creating an ambiguity on the origin of the pseudo-range. The additional noise make this ambiguity more important, thus creating the identification error.

Increasing artificial the delay between the emitters permits to reduce the number of identification errors: from a maximum identification error rate of about 45% for an artificial delay step of 3.4 µs, this maximum error rate goes down to 5% when the artificial delay step is set to 4 µs. However, the vast majority of the area is not affected by identification errors, in both cases.

In view of the pseudo-range estimation error seen in section 3, an error standard deviation of 80m for every pseudo-ranges is clearly a worst case scenario. In reality, the pseudo-ranges from closer emitters will likely have a lower error standard deviation. Even with this challenging hypothesis, the emitter identification technique worked very well.

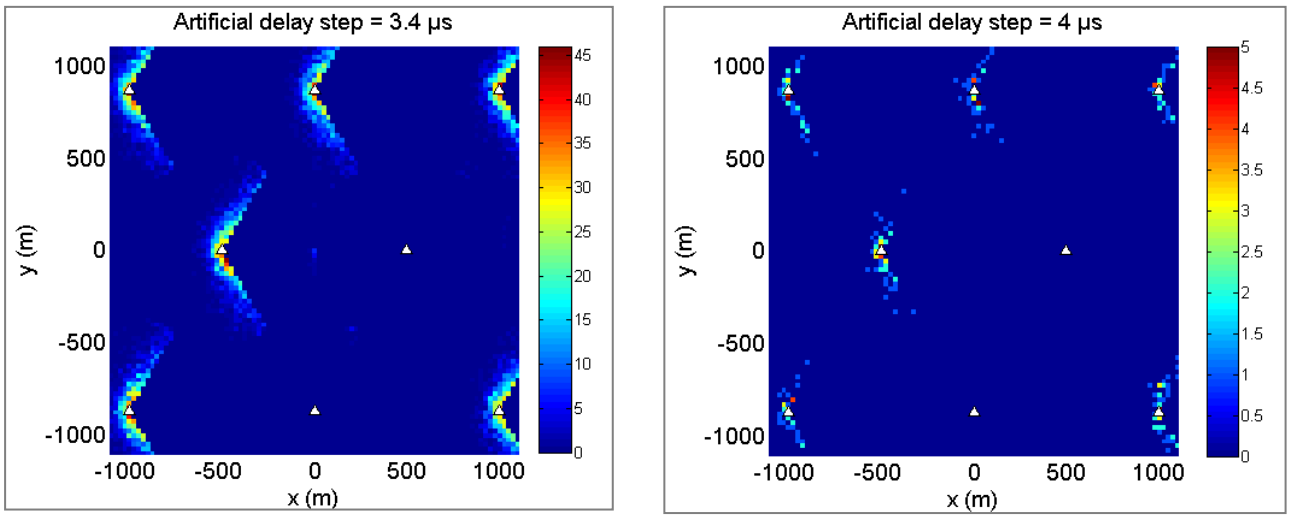

Figure 80 - number of identification errors over coverage due to pseudo-range error for 2 different artificial delay repartition

5.2.3.2 Error on assistance position $\hat{p}$

Let us call ε_x and ε_y the error on the assistance position : $\hat{p} = \left[x + \varepsilon_x\ , y + \varepsilon_y\right]^T$.

Let us call ε_{d_i} the error on the distance between the sensor and the i-th emitter induced by this wrong position.

In this case, the cost function for the correct permutation is:

$$V(p, \hat{p}, \bar{\bar{\boldsymbol{\sigma}}}) = \sum_{i=1}^{N_{Tx}} \left(d_i - \left(d_i + \varepsilon_{d_i}\right)\right)^2 = \sum_{i=1}^{N_{Tx}} \varepsilon_{d_i}^2$$

The cost function of the wrong permutation $\boldsymbol{\sigma}'$ is:

$$V(p, \hat{p}, \boldsymbol{\sigma}') = \left(d_2 - d_1 - \varepsilon_{d_1} + c.(\tau_2 - \tau_1)\right)^2 + \left(d_1 - d_2 - \varepsilon_{d_2} + c.(\tau_1 - \tau_2)\right)^2 + \sum_{i=3}^{N_{Tx}} \varepsilon_{d_i}^2$$

The isolation of the right permutation is

$$\begin{aligned} I(p, \hat{p}) &= \left|\left(d_2 - d_1 - \varepsilon_{d_1} + c.(\tau_2 - \tau_1)\right)^2 + \left(d_1 - d_2 - \varepsilon_{d_2} + c.(\tau_1 - \tau_2)\right)^2 - \varepsilon_{d_1}^2 - \varepsilon_{d_2}^2\right| \\ &= \left|2.\left(d_2 - d_1 + c.(\tau_2 - \tau_1)\right)^2 - 2.\left(d_2 - d_1 + c.(\tau_2 - \tau_1)\right).\left(\varepsilon_{d_1} - \varepsilon_{d_2}\right)\right| \\ &= \left|I(p, p) - 2.\left(d_2 - d_1 + c.(\tau_2 - \tau_1)\right).\left(\varepsilon_{d_1} - \varepsilon_{d_2}\right)\right| \end{aligned} \quad \textbf{Eq. 5.15}$$

The difference between $I(p, \hat{p})$ and $I(p, p)$ depends on the error on the distance to the 2 wrongly associated emitters due to the wrong assistance position.

Simulations with an assistance position error following a centered Gaussian distribution with $\sigma = 100$ meters have been run on the service coverage in a modified SFN. The 100m for assistance position could be a worst case scenario, where only an approximate bad quality assistance position is available, such as one provided by Cell ID in a city for example.

The same artificial delay step as above are considered. At each point of the coverage, 100 identification tests are run, with the pseudo-ranges to the 5 closest emitters.

Figure 81 shows the number of identification errors over the coverage. Here, the error pattern follows the symmetry planes of the network. This is due to the fact that the receiver tests the 5 closest emitters to the (wrong) assistance position. If there is an error on the tested emitter set, there will be an identification error, no matter the value of the artificial delay or isolation of the right permutation. This is why the error pattern is identical for the 2 considered values of artificial delay.

One way to mitigate this mistake is to test the permutation with a higher number of closer emitters than the number of received pseudo-range. This is done in the following section.

Beside this kind of error on the tested emitter set, no identification error seems to occur outside the symmetry planes of the network, due to the error on the assistance position.

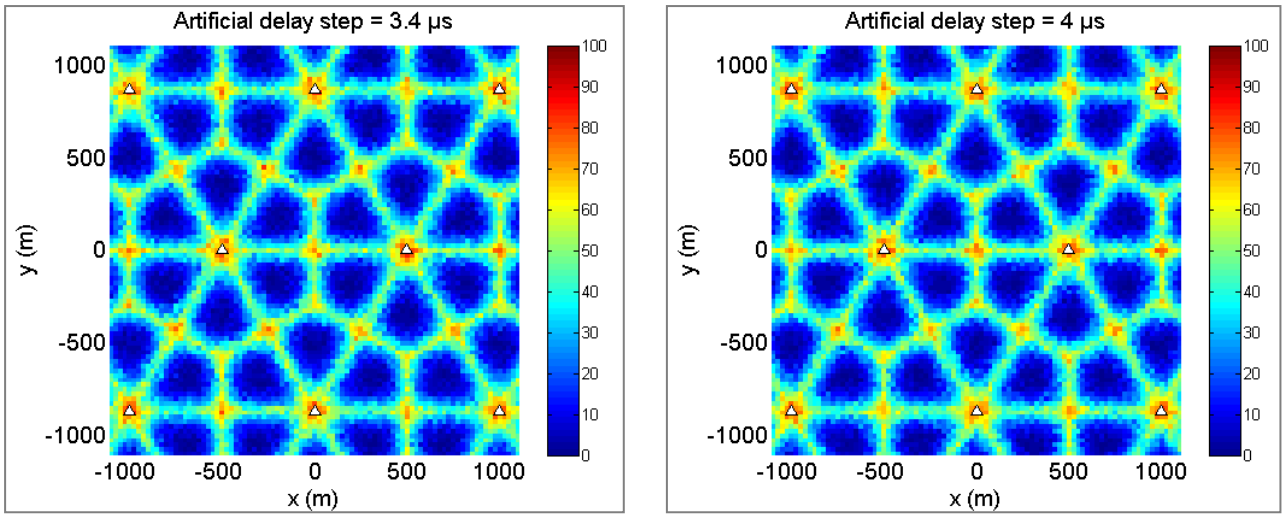

Figure 81 - number of identification errors over coverage due to assistance position error for 2 different artificial delay repartition

5.2.3.3 Error on the tested emitter set $\{Tx\}$

The final type of error that can occur is to use a wrong set of emitters to be tested. This can happen if the error on the assistance position is sufficient to consider the wrong set of N_{Tx} emitters to be tested. It is therefore necessary to consider a larger number of emitters to be tested, in order to avoid this type of error. For example, if a sensor has only discriminated 5 pseudo-ranges, it should try to associate them with the 6 or 7 closest emitters to the assistance position.

This problem is complicated to model, so only simulations have been done to see the impact of such error. The simulation is done by testing the combination of 5 emitters among the 7 closest to the assistance position with an error standard deviation of 100m. For each point of the service coverage, 100 tests were done and the number of wrong emitter identifications is plotted in Figure 82.

It should be noted that this kind of test leads to a combinatory explosion: instead of the $5! = 120$ tests done by testing permutations among the 5 closest emitters, the number of tests raises to $C_7^5.5! = 2520$.

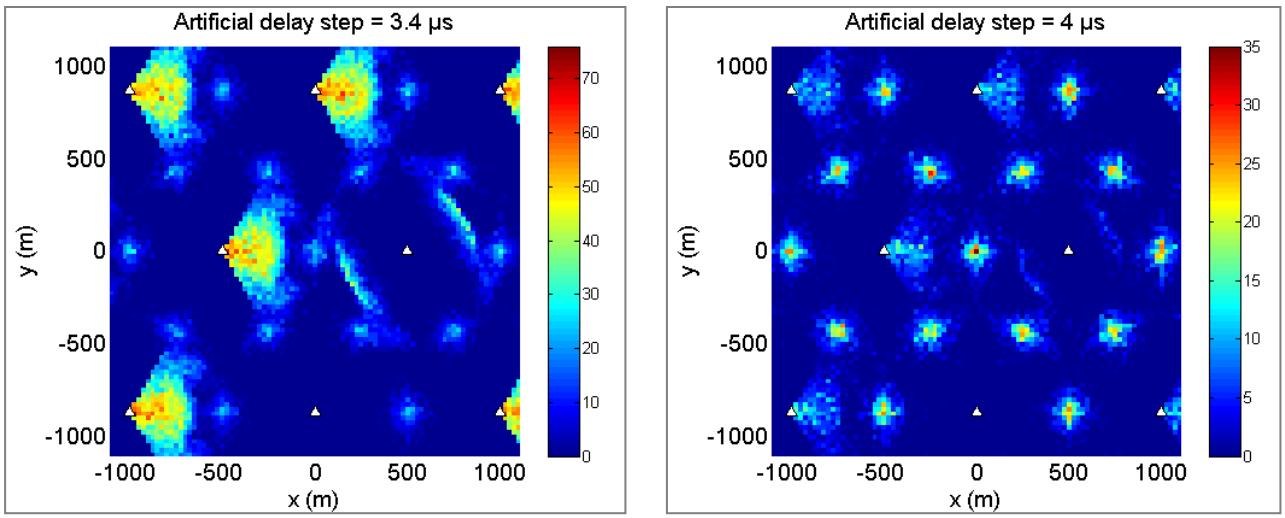

Figure 82 - number of identification errors due to assistance position error and wrong tested emitter set for 2 artificial delay step values (5 out 7 closest emitters)

This kind of error leads to a larger number of false identification. The identification error rate reaches 75% for an artificial delay step of 3.4 µs and 35% for an artificial delay step of 4 µs.

The same simulation was done by reducing the number of received pseudo-ranges to 3, and testing the 5 closest emitters. The results displayed in Figure 83 show a better overall identification performance over the overall coverage, with errors concentrating in the close vicinity of emitters.

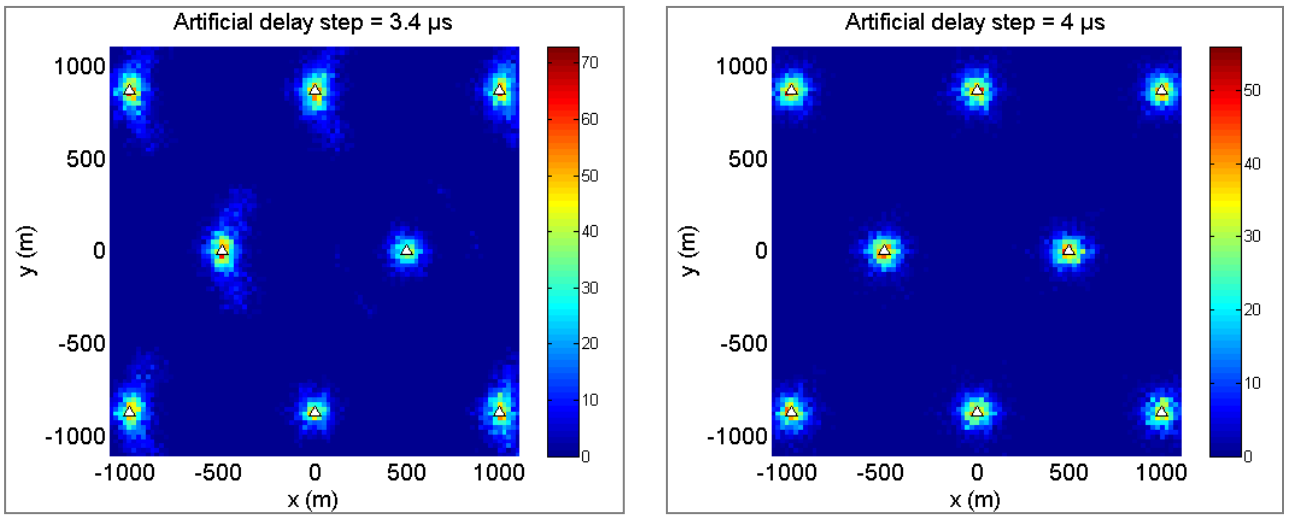

Figure 83 - number of identification errors due to assistance position error and wrong tested emitter set for 2 artificial delay step values (3 out of 5 closest emitters)

5.2.4 Conclusion on the emitter identification by reverse positioning technique

Emitter identification by reverse positioning technique uses the introduced artificial delay in order to find the most probable association of measured pseudo-ranges and emitters. This method requires that the iso-delay zones have been removed from the service coverage of the SFN, thanks to a good attribution of artificial delays among the emitters.

This technique requires an assistance position to work.

The sensibility of this technique to errors on the pseudo-range measurements and the assistance position has been evaluated in a particular SFN deployment. The most important error source is the error on the assistance position, which may lead to associating the measurements with the wrong emitters but also with emitters that are not even present in the neighborhood of the receiver.

This method is subject to combinatory explosion, leading to increased computation time when a high number of pseudo-ranges is received. One way to reduce the number of tests would be to test permutations only on ambiguous emitters. The 1 or 2 closest emitters should be easily and robustly identified from other means, such as the assistance position and the received signal power estimation from the most powerful emitters, and only the remaining emitters would remain ambiguous. This would greatly reduce the number of tests.

Further investigation using other network deployment should also be done in order to see if there is an optimized network configuration or artificial delay attribution that would be more robust to identification error.

5.3 Conclusion on the emitter identification techniques

Watermarking technique for emitter identification in an SFN has been standardized in some countries for network quality monitoring. However, it requires an additional equipment at each emitter. Also, for localization purpose, the possibility to identify a remote emitter in the vicinity of a close emitter is limited due to the Near-Far effect, thus creating a large zone of "self-jamming" around an emitter. Therefore, watermarking is not recommended for emitter identification, or would require large modifications.

Emitter identification by reverse position technique seems the natural emitter identification solution since it has the same constraints required for the emitter discrimination: the removal of iso-delay zones.

The other requirements of this technique are:

- **the knowledge of the emitter characteristics** (position and artificial delay). These data may not change often (the emitters are fixed) and may therefore be available offline, except for the satellite characteristics, which may need frequent updates in order to have the precise orbit position;
- **an assistance position**. An approximate position is required. The quality of this assistance position will impact the wrong identification rate.

This technique seems robust to the errors made on the pseudo-range estimation. This technique should be tested in other cases of network deployment to be able to generalize the reachable performances and also to see if some network deployments yield better identification performances. However, with the hindsight provided by the presented study, this technique yield better results than the watermarking technique.

Therefore, emitter identification by reverse positioning is preferable to the watermarking technique.

6 Position calculation and performances

Once the receiver has associated the estimated pseudo-ranges to identified emitters, it has to combine the pseudo-ranges in order to solve the position unknowns. This section will describe simple, conventional methods to compute the position from estimated pseudo-ranges, so that the performance of the proposed positioning system can be assessed in the position domain.

While the positioning algorithms presently-used are not innovative, one of the main motivations to look at the error in the position domain is to be able to observe the impact of the NLOS bias that cannot be observed in the previously-presented results.

Indeed, one of the main issues of using the CNES SFN CIR measurements to model the propagation channel is the lack of precise knowledge of the NLOS bias, which may be contained in the measurements: the first multipath present in the measurements does not necessarily correspond to the LOS path. However, all the pseudo-range errors calculated in Chapter 4 are computed as the difference between the first estimated multipath delay and the delay of the first tap present in the measurements, since it was the best achievable estimation potentially done using these measurements. However, **a 0m error do not correspond to the LOS signal being estimated**, but rather, the first (NLOS) present multipath being perfectly tracked.

By computing a position using the estimated pseudo-ranges and comparing it with the GPS track recorded during the CNES measurement campaign, it will be possible to assess the impact of the NLOS bias present in the CNES measurements.

The positioning algorithm used in this chapter is the Non-Linear Least Square (NLS) algorithm, which is briefly described in Annex C. Only the 2D position was computed: the clock offset between the receiver and the emitters is assumed constantly null-valued. The position is estimated for every transmitted OFDM symbol (with a rate of $1/T_{symb} = 2250$ Hz), but the shown position is smoothed using a running average over 1s.

6.1 Position calculation using ideal pseudo-range measurements

Figure 84 shows the position computed from a perfect estimation of the delay of the first multipath from each emitter. This means that the pseudo-range measurements used in the NLS algorithm are computed from the delays of the first multipath coming from each emitter.

The norm of the position error is shown in Figure 85. While the trace obtained with the DVB-SH measurements are approximately following the GPS trace, there is a position error which can reach up to 120 m, with a mean absolute error of 24.3 m. The error is induced by potential measurement errors made by the channel sounding device level, and by the NLOS conditions. If the channel sounding measurement errors are considered as negligible, then the remaining source of error is the NLOS bias.

Therefore, it can be concluded that the CNES SFN CIR measurements are heavily affected by NLOS bias. However, this DVB-SH trace should be considered as the best reachable performances with this SFN CIR measurement set.

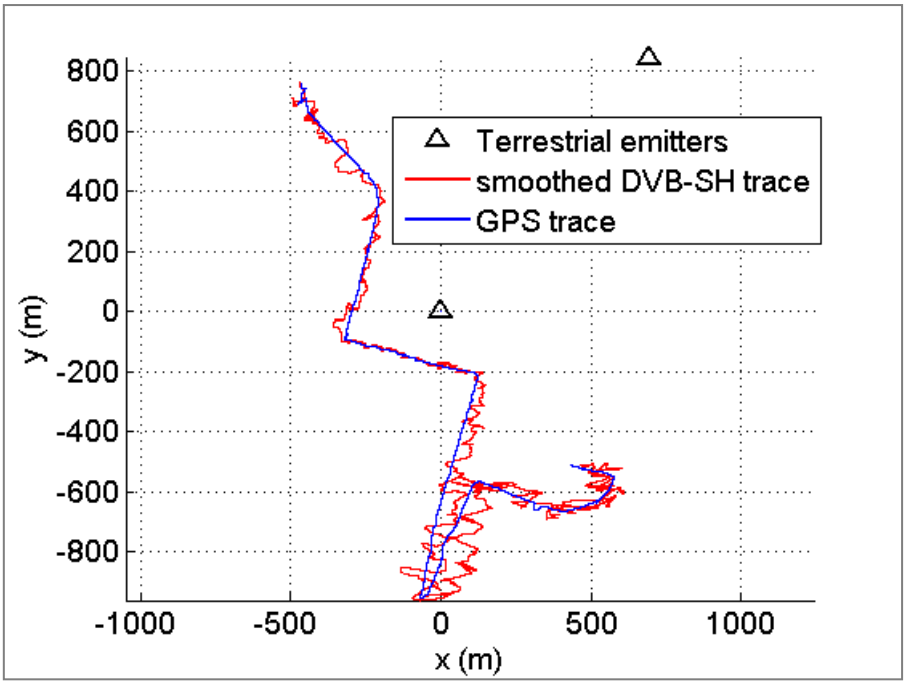

Figure 84 - Estimated and reference trace using perfectly estimated pseudo-range measurements

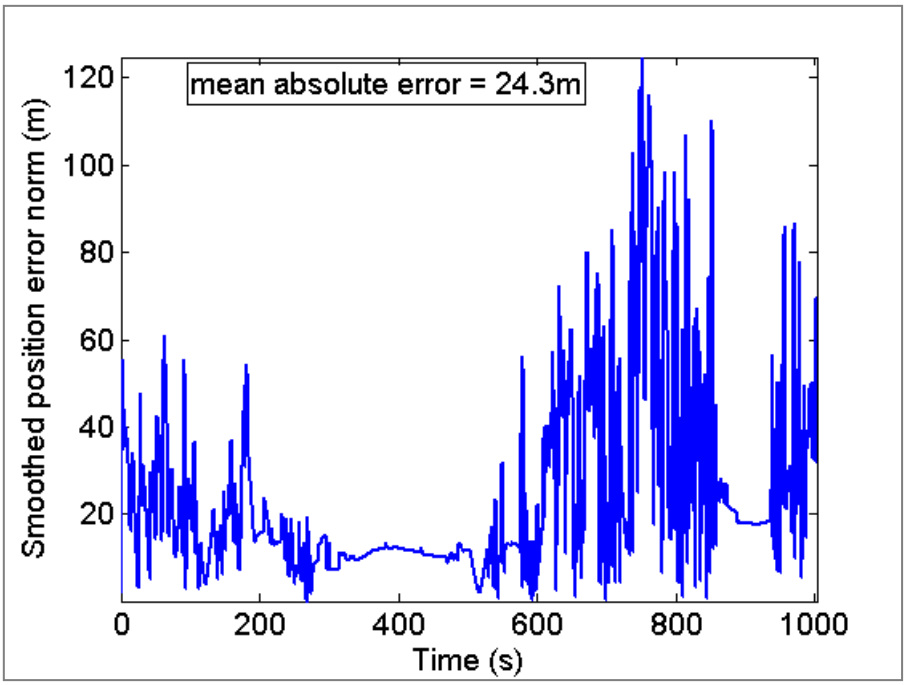

Figure 85 - Position error norm using perfectly estimated pseudo-ranges measurements

6.2 Position calculation using pseudo-range measurements from simulation #3

Figure 86 and Figure 87 show the same results with the pseudo-range estimated with the presented method and using the Blackman-Harris window. Compared to the reference DVB-SH trace, some significant additional errors can be observed towards the beginning, the middle and the end of the

trace. They corresponds to instants where later multipath delays are tracked instead of the first present multipath, thus creating a position error over 100m.

The maximum error reaches 600 m and the mean absolute error is 93.8 m. However, a large contribution of the error appears at the end of the simulated time series. If this period is ignored, the mean absolute error goes down to 63.7m over the first 800s of the simulation. This performances are greatly degraded compared to the simulation using the ideal pseudo-range estimate.

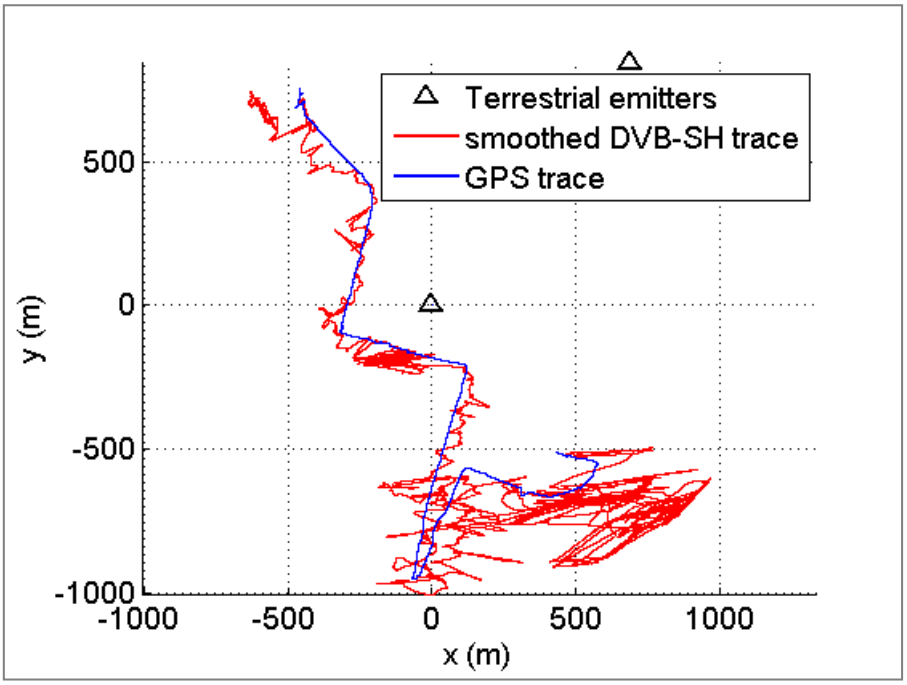

Figure 86 - Estimated and reference trace using estimated pseudo-range measurements using a Blackman-Harris window

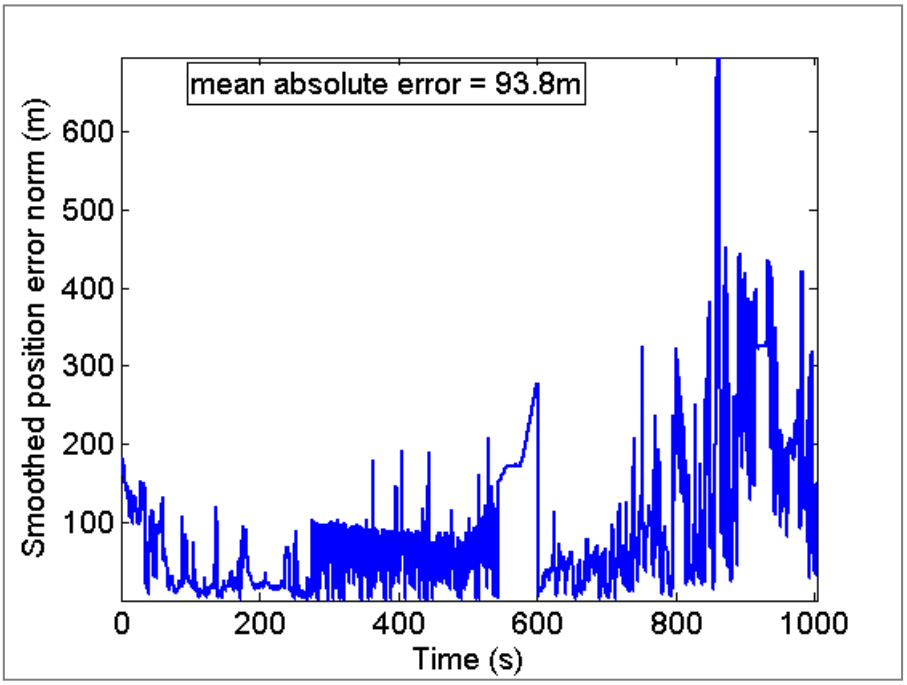

Figure 87 - Position error norm using estimated pseudo-ranges measurements using a Blackman-Harris window

6.3 Position calculation using a combination of pseudo-range measurements from simulations #2 and #3

Finally, Figure 88 and Figure 89 show the same results with the best estimated pseudo-ranges among all presented simulations. Pseudo-range estimates from emitter #1 and #3 are taken from the Blackman-Harris window simulation, while pseudo-range estimates from emitter #2 are taken from the Hamming widow simulation, which is much less affected by later multipath tracking.

The maximum error reaches over 700 m and the mean absolute error is 76.8 m. By calculating the mean on the first 800s of the error time series, a mean absolute error of 41.2 m would be obtained.

In this simulation, the performances are somewhat improved compared to the simulation using Blackman-Harris pseudo-ranges only. This shows the interest of using the right windowing technique, depending on the tracking condition for each emitter.

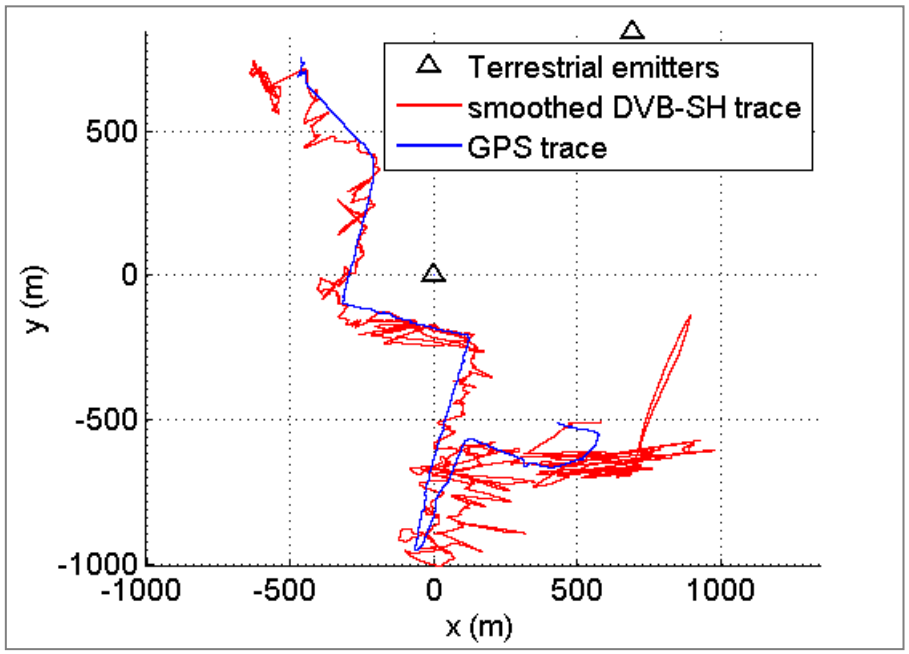

Figure 88 - Estimated and reference trace using best combined estimated pseudo-range measurements

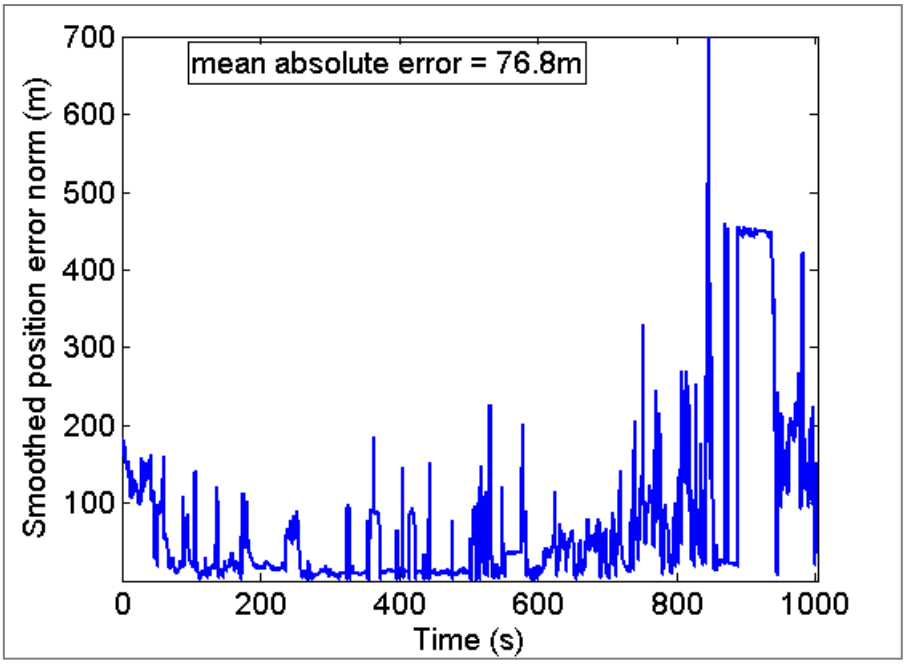

Figure 89 - Position error norm using best combined estimated pseudo-ranges measurements

6.4 Conclusion on positioning performances

This short study of the position-domain error shows the impact of the NLOS conditions on the considered positioning system. Due to the challenging propagation channel between terrestrial emitters and a mobile receiver in urban environment, the best achieved performance is a mean absolute error 41.2m, which would be far less than the positioning accuracy obtained through other urban positioning systems, comprising conventional GNSS.

However, the presented results should be mitigated by several remarks:

- **Only 3 emitters were used** in the simulation. In realistic network deployment, a receiver will likely be able to track the signals from several more emitters, as shown in section 7.1.
- A signal bandwidth of 5 MHz was used, while the DVB-SH standard provisions the use of larger signal bandwidth (up to 8 MHz, as currently employed by the French Digital TV network). Using an **increased signal bandwidth** would lead to increase pseudo-range estimation accuracy, both in terms of error variance and robustness to multipath, and would therefore yield a better final position accuracy.
- **The position error is affected by large sudden leaps**, of several tens or hundreds of meters, which would not be coherent with the receiver dynamics (pedestrian or vehicle) and could be easily detected and mitigated. Including a model of the receiver dynamics, e.g. in a Kalman filter, would permit to increase the position accuracy. Other multipath mitigation techniques could be implemented, such as those mentioned in Table 28.
- **Hybridation with other sources of positioning measurement** would also help mitigating the impact of the NLOS propagation on the position accuracy. Such complementary positioning measurement could come from GNSS measurement or inertial measurements.

Table 28 - Multipath mitigation techniques

Method	Requirements / Issues	References
Pseudo-range variance estimation	• Requires a sufficiently large time series of measurements • Requires noise measurement std dev	[Wylie 1996]
Residual ranking	• Requires a large number of emitters, comprising a sufficient number of LOS emitters (ideally >3) • Combinatory explosion	[Chen 1999]
Maximum likelihood	• Requires parameters of NLOS error and measurement noise distribution parameters	[Cong 2004]
Scattering model fitting	• Requires good estimation of several multipath delay	[Al Jazzar 2002]
Estimation of NLOS error as additional variable	• Requires a large number of emitters (>3)	[Yu 2008]
Kalman tracking	• Requires a good multipath error model to be integrated in the Kalman Filter • Use of Extended or Unscented Kalma Filter required due to the non-linearities created by LOS to NLOS transitions.	[Giremus 2008]

7 Recommendations to operators for providing a navigation service from a DVB-SH system

The method presented for pseudo-range estimation and emitter identification in an SFN requires a modification to the network deployment in order to work. The modification consists in introducing artificial delays at the emission of the signal for neighboring emitters, which results in the removal of iso-delay zones.

Also, every simulations presented in this thesis were realized with the DVB-SH signal mode (2K 1/4 5MHz). However, different signal parameters can be chosen from the DVB-SH standard, and their choice will impact both the positioning and telecommunication performances.

Both the network deployment and the choice of the DVB-SH signal mode are chosen by the operator providing the telecommunication service. This section proposes some elements to help them making these choices and assessing the interest of providing an additional positioning service in terms of expected positioning performances, but also in terms of constraints imposed on the network deployment.

7.1 Recommendations on the SFN deployment

In order to permit emitter discrimination and identification by the proposed methods, the network deployment has to avoid iso-delay zones. The proposed method is the introduction of artificial delays between adjacent emitters. This modification does not impact the telecom service as long as the maximum artificial delay remains in the equalization range of the OFDM mode, which is given by the Cyclic Prefix duration. In addition, artificial delay introduction is already provisioned in the DVB-SH standard.

The considered network deployment in this section consists in a canonical cellular network deployment: the emitters are placed at the corners of adjacent hexagons. Although real-world network deployment will certainly be different, this particular geometry permits to simplify some calculations. Notably the geometry of the network depends on only one parameter: the emitter spacing D.

A purely terrestrial network is assumed. The inclusion of a satellite emitter shall not change radically the presented approach.

In this section, we suppose that the network deployment shall be designed for 4 goals:

1. It should ensure a minimum aggregate SNR over the service coverage to ensure the initial telecommunication service ;
2. It should not create iso-delay zones over the service coverage to permit the positioning service;
3. A minimum of 3 emitters shall be visible at any point of the service coverage. Visibility shall be considered from a positioning point-of-view, ie an emitter is considered as visible if the signal received from it is high enough to permit pseudo-range estimation;
4. The maximum relative delay between any 2 visible emitters shall not exceed the Cyclic Prefix duration at any location of the service coverage.

In this section, a methodology for choosing the network deployment parameters in order to provide both telecommunication and positioning services in a DVB-SH system is proposed. The following hypotheses on the network are done:

- the location of the emitters follows an hexagonal pattern which is defined by a single parameter: the emitter separation D;
- the attribution of artificial delays is done following a re-use pattern with values taken from a set of equally-spaced artificial delays varying between 0 and $(N_{color} - 1).\Delta\tau_{step}$

The methodology for choosing the network deployment parameters aims at respecting both telecommunications and positioning requirements.

This results in the following steps:

1. The emitter separation D is chosen in order to provide a minimum aggregate SNR;
2. The artificial delay step $\Delta\tau_{step}$ is chosen in order to remove intra-cluster iso-delay zones;
3. The re-use factor N_{color} is chosen so as to have enough visible emitters without creating inter-cluster iso-delay zones. This goes in pair with the definition of an SNR threshold for considering the signal received from one emitter for positioning;
4. Choice of the adequate DVB-SH mode (N_{FFT} , CP , B) is made by keeping the modes with the CP duration longer than the maximum observed delay.

The following paragraphs details each of these steps.

7.1.1 Network deployment for telecommunication: minimum aggregate SNR

In order to provide the telecommunication service over a given service area, the network shall provide an aggregate SNR above the demodulation threshold, which mainly depends on the modulation order and the coding rate use for the data. Table 4 in section 2.4 shows the required SNR for different choices of symbol mapping and coding rate.

Let us express the aggregate signal power coming from N_{emit} emitters, supposing the signal variance is equal to σ_s^2. Here, the receiver is supposed to able to recombine perfectly all the received signal replicas, every emitter emits at the same power $EIRP_{tx}$ and the antenna gain of the receiver is called G_{rx}. $l_{COST}(d_i)$ is the pathloss between emitter i and the receiver given by the COST 231 Wallfisch Ikegami model. The received aggregate signal power is:

$$C = \sum_{i=1}^{N_{emit}} C_i = EIRP_{tx}.G_{rx}.\sigma_s^2 \left(\sum_{i=1}^{N_{emit}} l_{COST}^2(d_i) + \sum_{\substack{i,j=1 \\ i \neq j}}^{N_{emit}} l_{COST}(d_i)\, l_{COST}(d_j) \right) \quad \text{Eq. 7.1}$$

For the pathloss model, the COST 231-Wallfisch-Ikegami pathloss model is used with the parameters described in section 3.1.1:

$$l_{COST}^2(d_i)[dB] = -36.3 - 38.\log d_i[m]$$

$$l_{COST}(d_i) = 10^{-1.815}.{d_i}^{-1.9} \quad \text{Eq. 7.2}$$

Supposing a thermal noise at the receiver called N, the aggregate SNR is

$$SNR_{agg} = C/N$$

In order to validate the network deployment for a given telecommunication service, the minimum aggregate SNR shall be above the demodulation threshold called SNR_{req}^{TEL}:

$$\min(SNR_{agg}) > SNR_{req}^{TEL}$$

In an hexagonal network, let us calculate an approximation of the aggregate SNR by taking into account only the 3 closest emitters. In this simpler scenario, the minimum SNR is encountered at the centroid of the triangle formed by the 3 emitters, which is at a distance $D.\sqrt{3}/3$ from each emitter.

The error done by taking into account only the 3 closest emitters instead of more emitters is negligible. In simulations, this error on the aggregate SNR has been observed to be around 0.5 dB by taking into account 46 emitters instead of only 3.

The estimate of the minimum aggregate SNR provided by an hexagonal network is

$$\min\left(SNR_{agg}\right) = \frac{1}{\sigma_n^2}.EIRP_{tx}.G_{rx}.\sigma_s^2.10^{-3.63}.6.\left(D.\frac{\sqrt{3}}{3}\right)^{-3.8} \quad \textbf{Eq. 7.3}$$

Then, by comparing this expression to the required SNR for different modcod, the emitters' EIRP and the emitter separation can be chosen.

The retained EIRP is 53.2 dBm, according to [Chuberre 2006]. The other parameters are:

- $G_{rx} = 0$ dB
- $\sigma_n^2 = -102.7$ dBm
- $\sigma_s^2 = 0.8993$, calculated from the amplitude of the different types of symbols present on the sub-carriers of an OFDM symbol (see section 2.3.3)

Figure 90 shows that an emitter separation $D = 1000m$ permits to use the 16QAM 1/2 modcod with a 13 dB margin on the pathloss. This could correspond to additional pathloss provisioned for indoor coverage. This explain the use of this emitter separation in the previous sections.

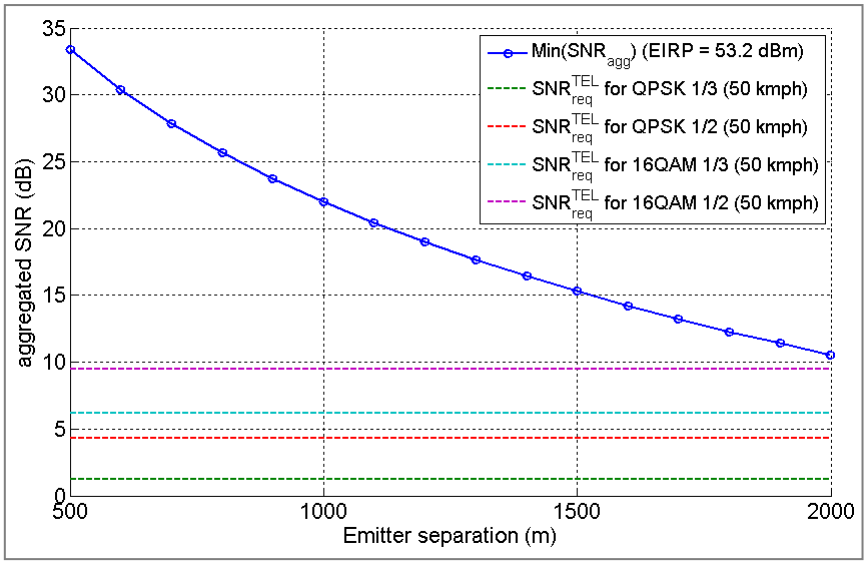

Figure 90 - Aggregate SNR versus emitter separation

7.1.2 Network deployment for positioning: avoidance of iso-delay zones

The aim of this section is to provide recommendations for the introduction of artificial delay in order to avoid iso-delay zones in the service coverage. Chapters 4 and 5 have shown that artificially increasing the relative delay between emitter permits and improves the emitter discrimination and identification processes. However, the maximum delay observed in a cCIR shall remain low enough so as not to degrade the telecommunication service through the presence of inter-symbol interferences.

[Thevenon 2009-1] proposes to use the notion of artificial delay re-use, in a similar way as the frequency is re-used in GSM **cellular networks**. This permits to limit the range of artificial delay required for the system by taking advantage of the limited range of the signal coming from one emitter: if 2 emitters are sufficiently far away from each other, then the same artificial delay can be used for both of them without creating an iso-delay zone in their respective servicing zone.

In such cellular network, each emitter is attributed an artificial delay following a particular pattern that maximizes the distance between 2 emitters having the same attributed artificial delay. We name the number of attributed artificial delay the **number of colors of the pattern or re-use factor** N_{color}.

A group of emitters having every possible attributed artificial delay is called an **emitter cluster**. In the following, the case of a particular cluster with **7 colors** (Figure 91) and **12 colors** (Figure 92) will be studied. These re-use pattern size are quite common in cellular networks.

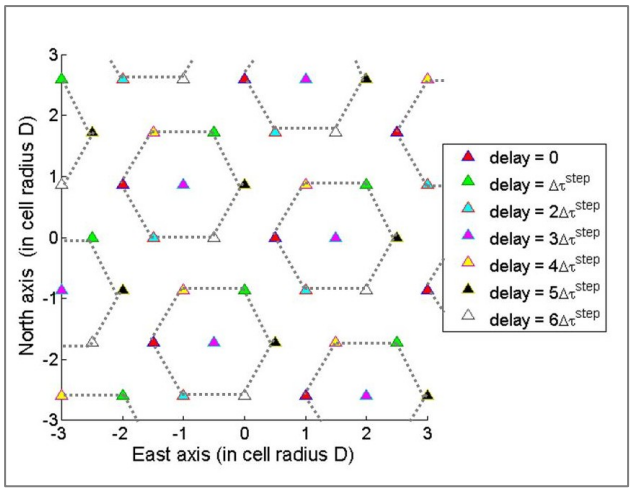

Figure 91 - Hexagonal cellular network with a 7-color reuse pattern

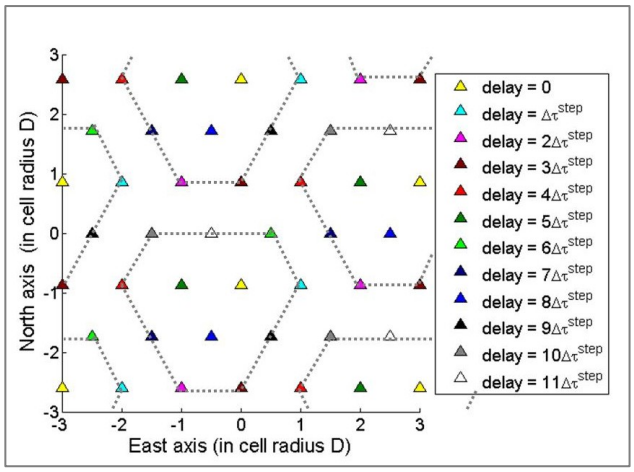

Figure 92 - Hexagonal cellular network with a 12-color reuse pattern

The use of cellular artificial delay re-use creates 2 origins for iso-delay zones:

- ***intra-cluster iso-delay zones***, which are created by emitters of the same cluster;
- ***inter-cluster iso-delay zones***, which are created by emitters of different clusters.

7.1.2.1 intra-cluster iso-delay zones

In order to avoid intra-cluster iso-delay zones, the relative artificial delay between any 2 emitters of the cluster $|\Delta\tau|$ shall be above the propagation time $\Delta d/c$ between these 2 emitters.

$$|\Delta\tau| > \Delta d/c$$

One way to achieve this condition is to take artificial delays that are a multiple of a unitary artificial delay called $\Delta\tau_{step}$, and to take this unitary artificial delay above the propagation time between 2 emitter:

$$\Delta\tau_{step} > D/c$$

Therefore, the emitters of one artificial delay cluster will be attributed artificial delay such as $\{0\ , \Delta\tau_{step}\ , 2\Delta\tau_{step}\ , \dots , (N_{color} - 1).\Delta\tau_{step}\}$.

7.1.2.2 inter-cluster iso-delay zones

In an artificially-delayed hexagonal network, the artificial delay re-use distance is $D.\frac{\sqrt{3N_{color}}}{2}$, where D is the distance between 2 emitters and N_{color} is the number of artificial delay cells per artificial delay clusters. We should note that the larger N_{color} is, the larger the re-use distance is.

Figure 93 illustrates the re-use distance for a cluster size $N_{color} = 7$.

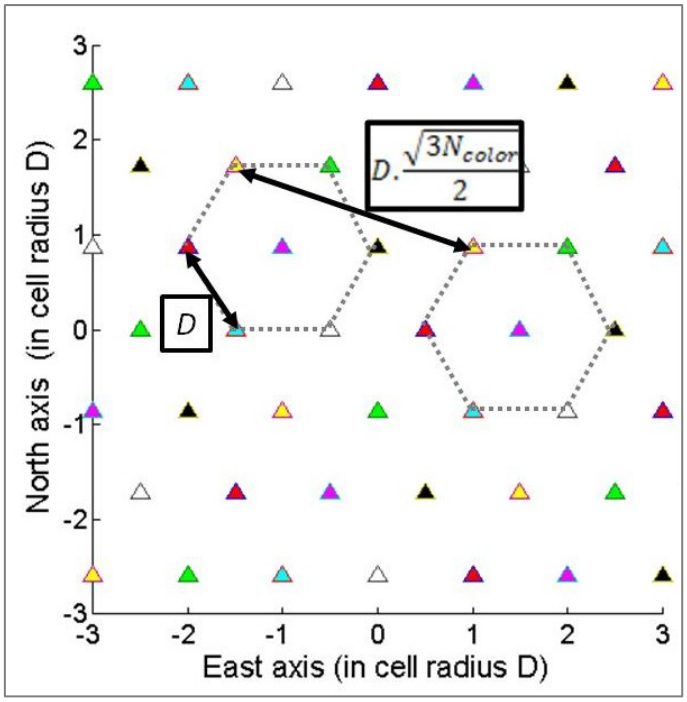

Figure 93 - Re-use distance definition in a 7-color re-use pattern

2 emitters with the same attributed artificial delay will create an iso-delay zone around the bisection of the line joining the 2 emitters. In order to avoid inter-cluster iso-delay zones, the maximum distance at which an emitter shall be considered for pseudo-range estimation is half the re-use distance: $d_{max}^{NAV} = D.\frac{\sqrt{3N_{color}}}{4}$.

Figure 94 shows the number of emitters closer than this distance over the service coverage of an hexagonal network for a re-use pattern of 7 colors and 12 colors. We can see that in both cases, the minimum number of emitters respecting this condition is above 3, thus permitting 2D positioning. It would have not been the case for cellular networks with a lower re-use factor.

It can also be observed that the use of the 12-color re-use pattern largely increases the number of usable emitters for positioning.

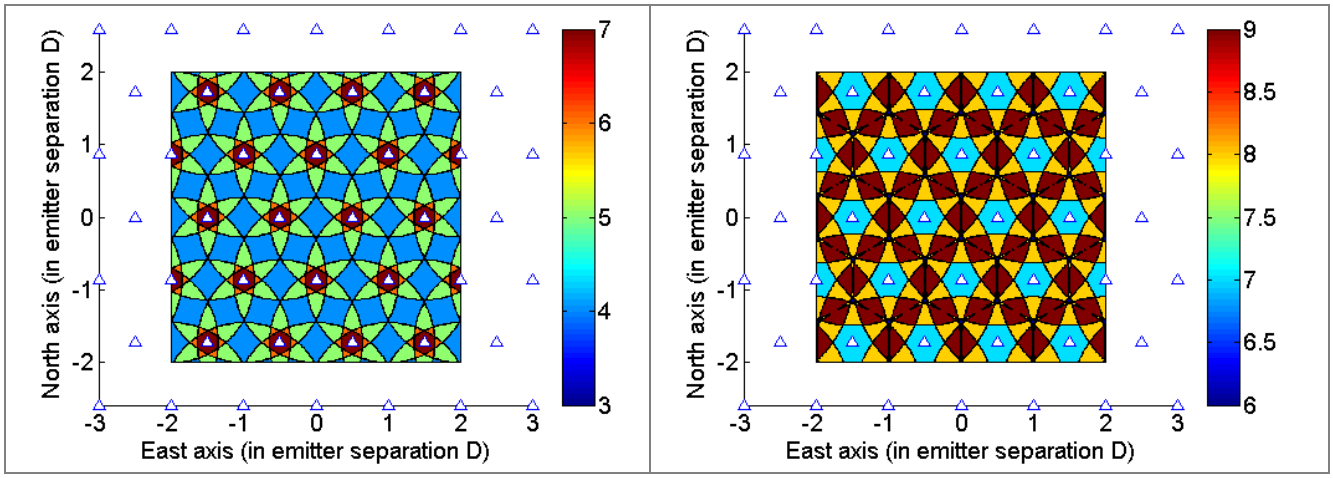

Figure 94 - number of emitters above the navigation SNR threshold in a 7- (left) and 12-color re-use pattern (right)

In order to avoid inter-cluster iso-delay zones issue for the positioning service, the receiver should reject pseudo-ranges coming from the emitters that can create these iso-delay zones, ie all emitters at a distance above d_{max}^{NAV}. This can be done by considering a threshold on the signal power received from an emitter, using Eq. 7.2 for the pathloss (Wallfisch-Ikegami model described in section 3.1.1):

$$SNR_{req}^{NAV} = \frac{\sigma_s^2}{\sigma_n^2}.EIRP_{tx}.G_{rx}.10^{-3.63}.(d_{max}^{NAV})^{-3.8} \quad \text{Eq. 7.4}$$

The SNR threshold can be used in the DLL exclusion schemes, both during acquisition or tracking phases of the pseudo-range estimation method (see section 3.6.2).

However, the pathloss model used to determine this threshold (Eq. 7.2) corresponds to a particular set of geometric urban environment parameters (rooftop height, street width, building separation, etc.) described in section 3.1.1. Therefore, it may be difficult to determine a generic SNR threshold working in every kind of urban environment.

7.1.3 Conclusion on acceptable DVB-SH modes for combined positioning and telecommunication services

In order to avoid inter-symbol interferences, the replicas of the signal should arrive at the receiver within the CP duration. This imposes a limit on the maximum delay affecting replicas of the DVB-SH signal.

The maximum delay affecting a signal depends on 3 parameters:

- the spatial separation between the emitter and the sensor. The maximum of this delay is d_{max}^{NAV}/c
- the artificial delay introduced between 2 emitters. This artificial delay depends on the artificial delay step between 2 delay cells $\Delta\tau_{step}$ and the artificial delay reuse factor (the number of colors). In our case, the maximum artificial delay is $(N_{color}-1).\Delta\tau_{step}$
- The delay introduced by "natural" multipaths encountered in the urban channel. These are of the order of 2 µs, as seen in the TU20 model presented in section 3.1.2.

$$\tau_{max} = \frac{D}{c}.\left(\frac{\sqrt{3N_{color}}}{4} + N_{color} - 1\right) + 2\ \mu s \quad \text{Eq. 7.5}$$

Table 29 shows the value of τ_{max} for $N_{color} = \{7, 12\}$ and $D = \{1000m, 1500m\}$.

Table 29 - Maximum encountered delay in different network deployments

	$D = 1000m$	$D = 1500m$
$N_{color} = 7$	$\tau_{max} = 25.8\ \mu s$	$\tau_{max} = 37.7\ \mu s$
$N_{color} = 12$	$\tau_{max} = 43.7\ \mu s$	$\tau_{max} = 64.5\ \mu s$

Table 30 shows the CP length for each mode, taken from [DVB-SH 2008-1]. Each case is colored if the CP length is below the maximum delay met in the corresponding network deployment. This

means that if a mode is colored in yellow, the CP duration is above 25.8µs and the DVB-SH mode is compatible with a SFN deployment using $N_{color} = 7$ and $D = 1000m$. Also, the compatibility of one mode with a network deployment is inclusive of the network deployments with longer encountered delay. For example, a mode compatible with the SFN deployment using $N_{color} = 12$ and $D = 1500m$, would be compatible with all the SFN deployments, since they all have a lower maximum encountered delay.

Table 30 - CP duration for the different modes. Highlighted modes are compatible with positioning service provision under certain SFN constraints

Mode	CP = 1/4	CP = 1/8	CP = 1/16	CP = 1/32
1K, 1.7 MHz	140 µs	40 µs	35 µs	17.5 µs
1K, 5 MHz	44.8 µs	22.4 µs	11.2 µs	5.6 µs
1K, 8 MHz	28 µs	14 µs	7 µs	3.5 µs
2K, 5 MHz	89.6 µs	44.8 µs	22.4 µs	11.2 µs
2K, 8 MHz	56 µs	28 µs	14 µs	7 µs
4K, 5 MHz	179.2 µs	89.6 µs	44.8 µs	22.4 µs
4K, 8 MHz	112 µs	56 µs	28 µs	14 µs
8K, 5 MHz	358.4 µs	179.2 µs	89.6 µs	44.8 µs
8K, 8 MHz	224 µs	112 µs	56 µs	28 µs

All standardized DVB-SH modes are not able to provide a positioning service as proposed in this PhD study without degrading the telecommunication service. The DVB-SH modes not compatible are those colored in white, corresponding to the modes with the shortest CP duration.

Yet, fortunately, **more than half of the modes would permit to provide a navigation service without interfering with the telecommunication service**.

7.2 Recommendations on the choice of DVB-SH mode

Section 7.1 has showed that some DVB-SH modes permit the introduction of a positioning service in a DVB-SH system without degrading the telecommunication service (see Table 30). The choice of the DVB-SH modes among the potential candidates will have an impact both on the telecommunication and positioning service performances.

7.2.1 Choice of the DVB-SH mode for telecommunication: system throughput

From a telecommunication point of view, the main criteria to monitor is the system throughput, expressed in bits/s. The system throughput does not depend on the FFT size.

Table 31 shows the values of throughput taken from [Tables 7.12 and 7.13 of DVB-SH 2008-2]. Only the values for B = 1.7 MHz and B = 5 MHz are available in this document. The values for a bandwidth of 8 MHz were extrapolated from the 5 MHz values by a scale factor of 8/5. This suppose that OFDM has the same spectral efficiency for the different values of bandwidth, which is realistic, and that coding and interleaving techniques have the same behavior. This last hypothesis is less realistic, so throughput values given in Table 31 for $B = 8\,MHz$ should be considered with precaution.

Table 31 - DVB-SH system capacity for different modcods and DVB-SH signal mode

Modcod	DVB-SH mode		Throughput (Mbps)
	CP	B	
QPSK 1/2	1/4	1.7 MHz	1.074
	1/8		1.194
	1/16		1.264
	1/32		1.302
	1/4	5 MHz	3.357
	1/8		3.730
	1/16		3.950
	1/32		4.069
	1/4	8 MHz	5.371
	1/8		5.968
	1/16		6.320
	1/32		6.510

As expected, the throughput increases with the bandwidth B and decreases with the CP size.

7.2.2 Choice of the DVB-SH mode for positioning: positioning performances

Concerning the impact of the DVB-SH mode on the positioning performance, the tracking error variance formula can be used as a first evaluation criteria of the positioning performance, even if it does not reflect exactly the pseudo-range estimation performance in multipath conditions.

To do this, the [Serant 2010] formula Eq. 3.16, recalled in section 3.4.4, is used. A Blackman-Harris window, a loop bandwidth B_l = 10 Hz and a time between successive estimation $T_i = T_{symb}$ are used. The computed pseudo-range error standard deviations are normalized by the one obtained for DVB-SH mode (2K 1/4 5 MHz). The results are plotted in Table 32.

The main contribution to tracking error comes from the bandwidth of the signal, with an approximate 2 dB gain on the pseudo-range error standard deviation from 5 to 8 MHz.

The error sigma decreases with the CP, but it has only a small influence.

Finally, the FFT size N_{FFT} (though the number of pilots N_p) has almost no influence at high SNR (0 dB), but this influence increases for low SNR (-20 dB): higher N_{FFT} will be better. However, the receiver will unlikely track remote emitters with low SNR in order to avoid inter-cluster iso-delay zones (see section 7.1.2.2), so the influence of N_{FFT} should be considered as negligible.

Table 32 - theoretical relative standard deviation for different DVB-SH mode

DVB-SH mode N_{FFT} , CP , B	$10.log\left(\frac{\sigma_\tau}{\sigma_\tau^{\{2K\ 5MHz1/4\}}}\right)$	
	SNR=0 dB	SNR=-20 dB
1K, 1/4, 1.7 MHz	4,91	4,45
1K, 1/8, 1.7 MHz	4,69	4,22
1K, 1/16, 1.7 MHz	4,56	4,10
1K, 1/32, 1.7 MHz	4,50	4,03
1K, 1/4, 5 MHz	0,02	0,93
1K, 1/8, 5 MHz	-0,20	0,70
1K, 1/16, 5 MHz	-0,33	0,57
1K, 1/32, 5 MHz	-0,39	0,51
1K, 1/4, 8 MHz	-2,01	-0,40
1K, 1/8, 8 MHz	-2,24	-0,62
1K, 1/16, 8 MHz	-2,36	-0,75
1K, 1/32, 8 MHz	-2,43	-0,81
2K, 1/4, 5 MHz	0,00	0,00
2K, 1/8, 5 MHz	-0,23	-0,23
2K, 1/16, 5 MHz	-0,35	-0,35
2K, 1/32, 5 MHz	-0,42	-0,42
2K, 1/4, 8 MHz	-2,05	-1,47
2K, 1/8, 8 MHz	-2,28	-1,70
2K, 1/16, 8 MHz	-2,40	-1,83
2K, 1/32, 8 MHz	-2,46	-1,89
4K, 1/4, 5 MHz	-0,01	-0,67
4K, 1/8, 5 MHz	-0,24	-0,90
4K, 1/16, 5 MHz	-0,37	-1,02
4K, 1/32, 5 MHz	-0,43	-1,09
4K, 1/4, 8 MHz	-2,07	-2,31
4K, 1/8, 8 MHz	-2,29	-2,54
4K, 1/16, 8 MHz	-2,42	-2,67
4K, 1/32, 8 MHz	-2,48	-2,73
8K, 1/4, 5 MHz	-0,02	-1,10
8K, 1/8, 5 MHz	-0,25	-1,33
8K, 1/16, 5 MHz	-0,37	-1,46
8K, 1/32, 5 MHz	-0,44	-1,52
8K, 1/4, 8 MHz	-2,08	-2,90
8K, 1/8, 8 MHz	-2,30	-3,13
8K, 1/16, 8 MHz	-2,43	-3,25
8K, 1/32, 8 MHz	-2,49	-3,32

In order to have a more realistic performance assessment, the pseudo-range estimation method was applied to a slice of the CNES CIR measurements presented in section 4.3.1. Only one emitter was tracked on an approximate duration of 250s. The simulation was done for every mode, except the ones with a bandwidth at 1.7 MHz. The Blackman-Harris windowing technique was used.

Except for some outliers, the performances are mostly defined by the bandwidth of the DVB-SH modes. As expected, high bandwidth provides better error standard deviation, but also a better bias. This is probably due to the higher resolution that permits to discriminate the different multipaths in the CIR estimate, and to track the earliest one.

Outliers are due to the tracking of later peaks in the CIR estimate, thus creating a bias on the pseudo-range estimate.

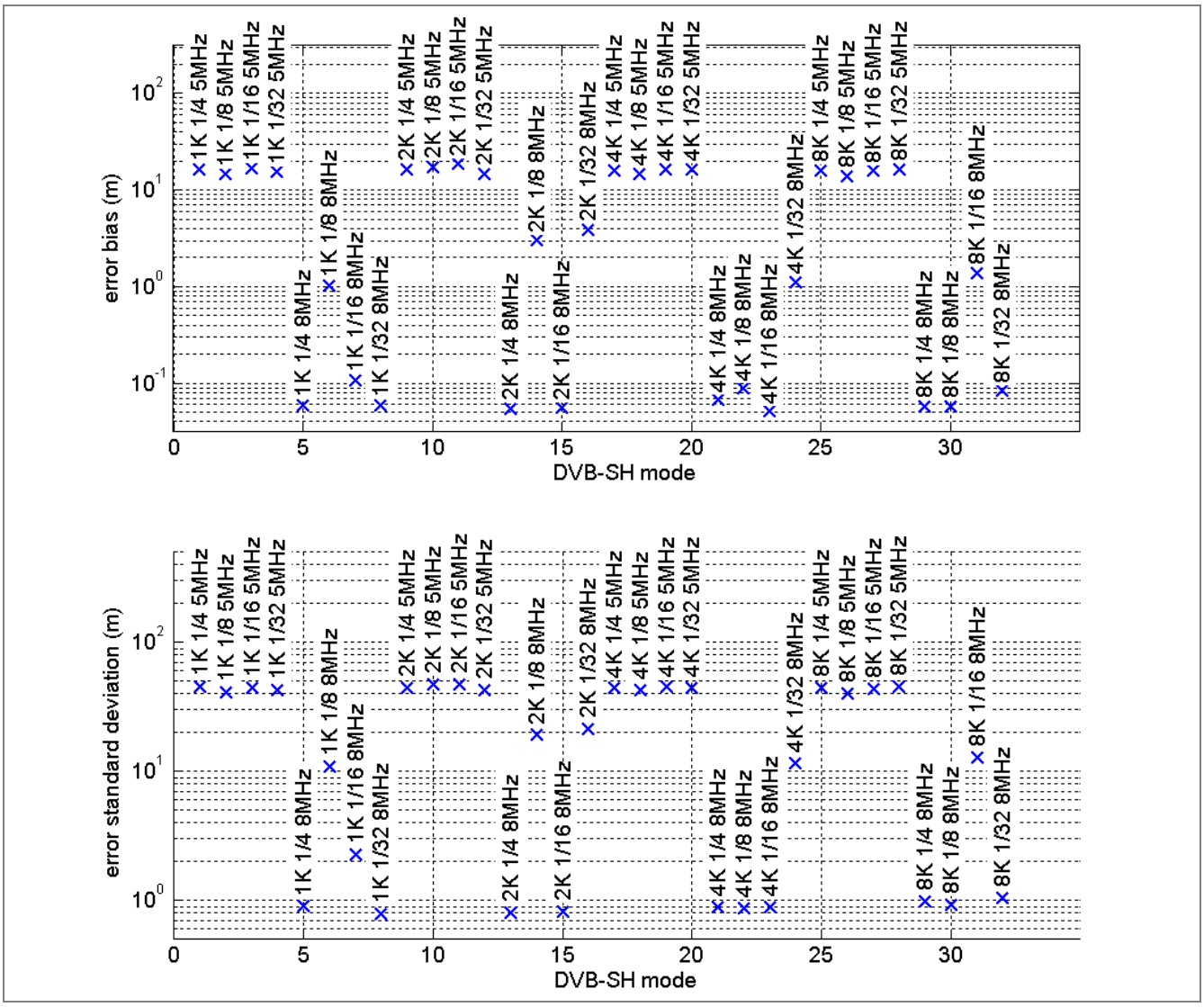

Figure 95 - Simulated pseudo-range estimation performances for different DVB-SH modes

Finally, the DVB-SH mode will also impact the ambiguity on the pseudo-range. In Section 3.2.4, it has been shown that the most problematic effect of ambiguity is due to the CIR periodicity, which depends on the number of scattered pilots. However, by using several consecutive symbols, the

minimum encountered ambiguity distance is 9.2 km for the 1K modes. Depending on the chosen network deployment and introduced artificial delay, the system operator will have to make sure that the maximum encountered delay is lower than the ambiguity distance.

7.3 Conclusion on the combined provision of DVB-SH-based broadcast and positioning services

Figure 96 synthesizes the results of the 2 previous sections on a same graph. The x-axis corresponds to the simulated positioning performances with the x-scale corresponding to the sum of the pseudo-range error mean and one standard deviation of each mode. The y-axis corresponds to the telecommunication performances, with the y-scale corresponding to the system throughput of each mode.

Each DVB-SH mode is placed in this space. The DVB-SH modes permitting both telecommunication and positioning service are plotted with a green circle, while the modes that do not permit a SFN deployment compatible with the proposed positioning method are plotted with a red cross.

On this graph, we can see 2 groups of DVB-SH modes, one allowing high throughput and good pseudo-range estimation accuracy (upper left quadrant) and another group allowing low throughput and bad pseudo-range estimation accuracy (lower right quadrant).

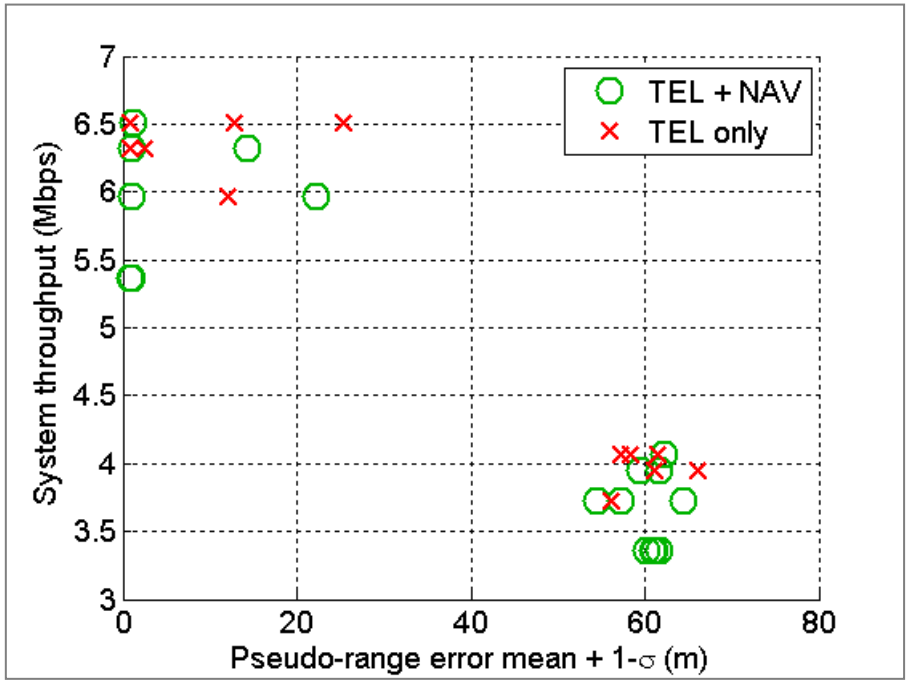

Figure 96 - System capacity vs simulated positioning performances for each DVB-SH mode

The best modes from our point of view are the green circles in the upper-left quadrant. They correspond to the following modes:

- 1K 1/4 8MHz
- 2K 1/4 8MHz
- 2K 1/8 8MHz
- 4K 1/4 8MHz
- 4K 1/8 8MHz
- 4K 1/16 8MHz
- 8K 1/4 8MHz
- 8K 1/8 8MHz
- 8K 1/16 8MHz
- 8K 1/32 8MHz

The validity of this choice of DVB-SH modes are to be mitigated by the fact that the pseudo-range estimation performances have been simulated with only one measurement set, which is not enough to generalize the overall positioning performances. Further studies should be performed in order to characterize the positioning performances in a more general way.

However, this first results should provide an interesting trend on which DVB-SH modes would be preferable. The listed modes will permit to provide the best combined telecommunication and positioning services, the only requirement being a modification on the SFN deployment.

8 Conclusion and perspectives

8.1 Contributions

The goal of this PhD thesis was to assess the feasibility of positioning using a DVB-SH system as system of opportunity.

The DVB-SH system is dedicated to the broadcast of digital TV signals towards mobile users, using the S-band (2.2 GHz). It was chosen because it proposes interesting features enabling tri-lateration-based techniques: the emitters are synchronized, thus permitting timing-based pseudo-range measurements, several emitters are expected to be visible at any point of the main urban centers (including indoor), and the carrier frequency used to transmit the signal is close to other telecommunication bands, thus opening the way to the mutualization of handheld receiver's sub-systems, such as RF front-end and signal processing functions, with the final consequence of receiver cost and power consumption reduction.

However, DVB-SH-based systems also present challenges for positioning, such as (1) the transmission of the signal in urban environment which creates signal power fading, intense multipath and blockage of the LOS signal, (2) OFDM modulation, a wideband modulation technique that had not yet been investigated for positioning purpose and (3) the use of a network of emitters working in SFN configuration, making emitter discrimination and identification challenging.

The main contributions of this study concerns 3 aspects of the positioning problem:

- A signal processing method for estimating pseudo-ranges from DVB-SH signals.
- A system modification to enable emitter identification in an SFN.
- The evaluation of the accuracy of the positioning solution using the proposed methodology

The main development in the *signal processing domain* is the proposition of **a pseudo-range estimation method** based on the tracking of OFDM signals. The overall pseudo-range estimation strategy is adapted to the multipath-intense terrestrial urban propagation channel, where the sensor may receive a varying number of fast-fading replicas of the OFDM signal spread over time.

The method makes use of ***periodic acquisitions*** based on the Matching Pursuit algorithm to improve the chance of acquiring the LOS signal coming from the emitter, and a ***delay tracking*** based on DLL to refine the pseudo-range measurements. The theoretical tracking error in case of LOS conditions is very low, with a standard deviation below 1m for SNR values above 0dB, typically used in DVB-SH deployments.

The use of ***windowing techniques*** allows reducing the influence of the signal coming from other emitters on the delay estimation. This is particularly beneficial due to the Near-Far effect encountered in terrestrial networks, which consists in the masking of remote emitters when the receiver gets close to an emitter.

Simulations using real urban propagation channel measurements have showed that the main source of errors comes from the tracking of NLOS multipaths, with error of several tens or hundreds of meters in the pseudo-range error. If these leaps are detected and taken care of, the residual

standard deviation of the pseudo-range error may be as low as **2m with a negligible bias** as observed in our simulations.

In terms of position accuracy, the simulations using the estimated pseudo-range using the real urban propagation channel measurements and the proposed method, combined with simple position calculation (non-linear least square algorithm) provide a **position RMSE around 40m**. This value takes into accounts the large error leaps in the pseudo-range estimation, and could be lowered to **below 10m** if those leaps are detected and taken care of, and even further lowered if more emitters would be available.

The main contribution at the *system deployment level* is a modification to the SFN deployment permitting **emitter identification in an SFN**. Emitters in an SFN transmit the same signal on the same carrier frequency and in a synchronized way. Therefore, it is difficult for the receiver to know from which emitter the signal replicas are coming from and to distinguish them from multipath created by the environment. The proposed SFN modification makes use of a feature already provisioned in the DVB-SH standard : the introduction of different artificial delays as the identification signature of an emitter.

With this system modification, emitter discrimination becomes possible by using conventional ***clustering*** algorithms on the delay estimates, and emitter identification is permitted thanks to the proposed ***reverse positioning technique***. These techniques shall provide good performances if the network deployment is specifically designed towards the ***eradication of iso-delay zones***. A study has been done in order to provides guidelines for deploying iso-delay-free SFN.

Finally, the different DVB-SH signal parameters provisioned in the standard have been assessed to determine which modes permit to use the proposed methods, and which ones would provide the best telecommunication and positioning performances. These results provide ***useful recommendations to the operators for their choice of DVB-SH system deployment***.

In the end, **several DVB-SH modes are able to provide a positioning service with minimum modification to the system**. First, the signal does not require any modification. Secondly, the network deployment should make use of particular artificial delay distribution, which is a feature already present in the DVB-SH standard and shall not impact the telecommunication service.

8.2 Perspectives

The topic of this PhD study is quite exploratory. We have been able to provide a proof-of-concept for positioning in a DVB-SH system. However, because the goal of this work was to prove the feasibility of DVB-SH positioning, the researched methods and principles may often be improved. Here is a list of potential future works:

- **Complete OFDM signal model**: Some hypothesis on the OFDM transmission model have been made, by assuming no sampling clock offset and no distortion due to the emission or reception filters. The impact of these elements could be studied.
- **Better wideband CIR model dedicated to positioning**: Most existing CIR models have been designed for telecommunication validation purpose. Therefore, they focus primarily on the modeling of the signal power, but do not focus particularly on the fine modeling of multipath delay. As the proposed positioning technique is primarily based on CIR estimation, having a more complete CIR model would help to characterize its performances.
- **Pseudo-range estimation improvement**: The pseudo-range estimation has been studied through 2 main techniques: the Matching Pursuit algorithm and DLL with an EMLP discriminator. Other techniques could be used, such as the SAGE [Fleury 1999] or the ESPRIT [Paulraj 1985] algorithms for CIR parameter extraction, the use of adaptive loop bandwidth / windowing techniques for improving the tracking accuracy, or some multipath-mitigating tracking techniques, based for example on the ME-DLL principle [van Nee 1992].
- **Valid pseudo-range error model**: The proposed method has been applied to a single scenario based on one set of channel-sounding measurements in a particular location. It is difficult to generalize the reachable performances of our method on this single scenario. Having a valid pseudo-range error model is essential for the complete study of DVB-SH positioning, and would require other simulations using more representative measurements (in other types of urban environment for example) or using a more realistic multipath propagation model, or even measurements in an actual deployment of DVB-SH system.
- **Realistic network deployment**: Network planning is a complex task, requiring strong operational research skills. In this study, network planning has been limited to the study of a hexagonal network of emitters, which is barely encountered in real environments. In case of a true network planning, the iso-delay zone suppression by artificial delay attribution may be a more complex task.
- **Emitter synchronization performances**: In this study, a perfectly synchronized network was assumed. However, synchronization performances in SFN should be characterized and their impact on the final position should be assessed. To this end, the participation of a system operator may be precious, to know the emitters' characteristics, and also to assess the feasibility of improving the synchronization of emitters.
- **Position calculation**: The presented position calculation algorithms are very conventional (classic variations of the Least-Square algorithms). Elaborate position calculation (using for example a Kalman filter) would permit to improve the position accuracy. Also, a whole range of multipath-mitigation techniques can be applied at the position calculation level in order to detect, reject or correct pseudo-ranges affected by large bias.
- **Use of antenna diversity**: The relatively high carrier frequency of the DVB-SH signals permits to use multiple antenna in a handheld receiver. This would permit to use smart antenna techniques in order to combat fast fading or to better track the LOS signal. These kind of antenna techniques are currently being investigated in the context of satellite positioning [Konovaltev 2007] and could be applied to DVB-SH positioning.

Finally, the main contributions of this PhD may be applied to other OFDM-based standards or systems using SFN. Therefore, the proposed techniques for positioning may be adapted to various other telecommunication standards, which are summarized in Table 33.

Table 33 - Communication standards that may be compatible with the proposed positioning method

Application	Standard	Modulation	Use of SFN
Terrestrial digital radio / TV broadcasting	DAB Eureka 147	OFDM	SFN
	DVB-T / H / SH	OFDM	SFN
	DMB-T / H	OFDM	SFN
	ISDB	OFDM	SFN
	ATSC	8VSB	SFN
Mobile communication	3GPP LTE	OFDM	Soft Handover
	WiMAX IEEE 802.16	OFDM	Soft Handover
Local Area Network	WiFi IEEE 802.11	OFDM	-
Personal Area Network	WiMedia IEEE 802.15	OFDM	-

MIMO techniques [Kohno 1998] are also increasingly used in mobile communication standards. This technique aims at using the diversity in the signal propagation due to the use of different paths (from different emitters or antenna), different polarization or different frequencies in order to improve the capacity of a communication channel. What is interesting for the point of view of this study, is that MIMO techniques require the use of ***channel sounding techniques***, usually based on the presence of pilots or training sequences. Therefore, these standards provide the opportunity to obtain the CIR estimate by using these sequences dedicated to channel estimation. Once a CIR estimate is obtained, the same pseudo-range estimation techniques presented in this study could be re-used. MIMO techniques are standardized in WiFI, WiMAX and 3GPP LTE, and is still currently a hot topic in research.

With the experienced gained in this thesis, positioning using DVB-SH system, and more generally a whole range of new systems of opportunity, seems promising. The results obtained in this thesis may be improved thanks to identified improvements for future work, and requires the support of system operators or telecommunication service providers in order to fully exploit the potential of opportunistic positioning.

9 References

Al-Jazzar 2002	Al-Jazzar S, Caffery J, You HR. A scattering model based approach to NLOS mitigation in TOA location systems. In: Vehicular Technology Conference, 2002. VTC Spring 2002. IEEE 55th. vol. 2; 2002. p. 861-865 vol.2.
ATSC 2007	Advanced Television Systems Committee. Document A/110B. Synchronization Standard for Distributed Transmission, Revision B. December 2007.
Bahl 2000	Bahl P, Padmanabhan VN. RADAR: an in-building RF-based user location and tracking system. In: Proceedings IEEE INFOCOM 2000. Conference on Computer Communications. Nineteenth Annual Joint Conference of the IEEE Computer and Communications Societies. IEEE; 2000. p. 775-784.
Bingham 1990	Bingham JAC. Multicarrier modulation for data transmission: an idea whose time has come. Communications Magazine, IEEE. 1990; 28(5):5-14.
Chen 1999	Chen PC. A non-line-of-sight error mitigation algorithm in location estimation. In: Wireless Communications and Networking Conference, 1999. WCNC. 1999 IEEE; 1999. p. 316-320 vol.1.
Chuberre 2006	Chuberre N, Bodevin F, Courseille O, Duval R, Dussauby E, Selier C. Unlimited Mobile TV. In: ASMS 2006
Colzi 2008	Colzi E, Lòpez-Risueño G, Samson J, Angeletti P, De Gaudenzi R, Gerner JL. A System-Level Approach to the Feasibility Assessment of GNSS in C-band. In: European Navigation Conference ENC-GNSS 2008; 2008.
Cong 2004	Cong L, Zhuang W. Non-line-of-sight error mitigation in mobile location. Wireless Communications, IEEE Transactions on. 2005;4(2):560-573.
COST231 1993	Digital Mobile Radio Towards Future Generation Systems – COST 231 Final Report. 1993
COST259 2006-1	Molisch AF, Asplund H, Heddergott R, Steinbauer M, Zwick T. The COST259 Directional Channel Model - Part I: Overview and Methodology. Wireless Communications, IEEE Transactions on. 2006;5(12):3421-3433.
COST259 2006-2	Asplund H, Glazunov AA, Molisch AF, Pedersen KI, Steinbauer M. The COST 259 Directional Channel Model - Part II: Macrocells. Wireless Communications, IEEE Transactions on. 2006;5(12):3434-3450.
Cotter 2002	Cotter SF, Rao BD. Sparse channel estimation via matching pursuit with applicaion to equalization. Communications, IEEE Transactions on. 2002;50(3):374-377.
DLR 2005	http://www.kn-s.dlr.de/satnav/
DVB-SH 2008-1	Final draft ETSI EN 302 583 v1.1.0, Digital Video Broadcasting (DVB); Framing Structure, channel coding and modulation for Satellite Services to Handheld devices (SH) below 3 GHz. January 2008
DVB-SH 2008-2	ETSI TS 102 584 v1.1.1. Digital Video Broadcasting (DVB); DVB-SH Implementation Guidelines. December 2008.
E112 2003	Commission Recommendation 2003/558/EC on the processing of caller location information in electronic communication networks for the purpose of location-enhanced emergency call services. Official Journal of the European Union. July 2003.
E911 2000	FCC. 2000. OET Bulletin No. 71 - Guidelines for Testing and Verifying the Accuracy of Wireless E911 Location Systems.
Fernández 1999	Fernández J, Capdevila J, García R, Cabanillas S, Mata S, Mansilla A, et al. Single Frequency Networks for Digital Video Broadcasting. In: ECMAST'99; 1999. p. 120-142.
Fleury 1999	Fleury BH, Tschudin M, Heddergott R, Dahlhaus D, Ingeman Pedersen K. Channel parameter estimation in mobile radio environments using the SAGE algorithm. IEEE Journal on Selected Areas in Communications. 1999 March;17(3):434-450.

Forrester 2009 Forrester C. Forrester's Focus: Solaris Mobile Set-Back. SatMagazine. 2009.

Geomode 2002 McGeough J. Wireless Location Positioning based on Signal Propagation Data. White Paper. 2002.

Gallagher 2009 Gallagher T, Li B, Kealy A, Dempster AG. Trials of commercial Wi-Fi positioning systems for indoor and urban canyons. In: IGNSS Symposium 2009; 2009.

Hegarthy 1999 Hegarthy C, Kim T, Ericson S, Reddan P, Van Dierendonck AJ. Methodology for Determining Compatibility of GPS L5 with Existing Systems and Preliminary Results. In: ION Annual Meeting; 1999.

Hein 2007 Hein G. W., Avila-Rodriguez J.-A., Wallner S., Eissfeller B., Isigler M. and Issler J.-L. A vision on new frequencies, signals and concepts for future GNSS systems, ION GNSS 2007.

Irsigler 2002 Irsigler M, Hein GW, Eissfeller B, Schmitz-Peiffer A, Kaiser M, Hornbostel A, et al. Aspects of C-Band Satellite Navigation: Signal Propagation and Satellite Signal Tracking. In: European Navigation Conference ENC-GNSS 2002; 2002.

ITU RR 2004 International Telecommunication Union - Radio Regulations, Edition of 2004

Kohno 1998 Kohno R. Spatial and temporal communication theory using adaptive antenna array. IEEE Personal Communications. 1998 Feb;5(1):28-35.

Konovaltsev 2007 Konovaltsev A, Antreich F, Hornbostel A. Performance Assessment of Antenna Array Algorithms for Multipath and Interference Mitigation. In: 2nd Workshop on GNSS Signals & Signal Processing - GNSS SIGNALS'2007; 2007.

Lachapelle 2004 Lachapelle G. GNSS Indoor Location Technologies. Journal of Global Positioning Systems. 2004;3(1-2):2-11.

Lacoste 2009 Lacoste F, Carvalho F, Scot G, Ros B. Measurements of the macrocell propagation channel at 2.2 and 3.8 GHz and comparison with some analytical models. In: COST Action IC0802; 2009.

Laine 2007 Laine P. Alcatel-Lucent's proposal for unlimited mobile TV: a hybrid satellite/terrestrial broadcast network based on DVB-SH; 2007.

[Ludden 2000] Ludden B, Lopes L. Cellular based location technologies for UMTS: a comparison between IPDL and TA-IPDL. IEEE VTC 2000.

Mateu 2009 Mateu I, Boulanger C, Issler JL, Ries L, Avila-Rodriguez JA, Wallner S, et al. Exploration of Possible GNSS Signals in S-band. In: ION GNSS 2009; 2009. p. 1573-1585.

Mattsson 2005 Mattsson A. Single frequency networks in DTV. Broadcasting, IEEE Transactions on. 2005 November;51(4):413-422.

Morelli 2007 Morelli M, Kuo CCJ, Pun MO. Synchronization Techniques for Orthogonal Frequency Division Multiple Access (OFDMA): A Tutorial Review. Proceedings of the IEEE. 2007;95(7):1394-1427.

Palmer 2009 Palmer D, Moore T, Hill C, Andreotti M, Park D. Non-GNSS Radio Positioning using the Digital Audio Broadcasting (DAB) Signal. In: ION GNSS 2009; 2009. p. 864-872.

Paulraj 1985 Paulraj A, Roy R, Kailath T. Estimation Of Signal Parameters Via Rotational Invariance Techniques - Esprit. In: Circuits, Systems and Computers, 1985. Nineteeth Asilomar Conference on; 1985. p. 83-89.

Pérez Fontán 2008 Pérez Fontán F, Mariño Espiñeira P. Modeling the Wireless Propagation Channel - A Simulation Approach with Matlab. 1st ed. Wiley; 2008.

[Porcino 2001] Porcino D. Performance of a OTDOA-IPDL positioning receiver for 3GPP-FDD mode. In: 3G Mobile Communication Technologies, 2001. 2001. p. 221-225.

Proakis 2006 Proakis JG, Manolakis DK. Digital Signal Processing (4th Edition). Prentice Hall; 2006.

Rabinowitz 2005 Rabinowitz M, Spilker JJ. A new positioning system using television synchronization signals. Broadcasting, IEEE Transactions on. 2005;51(1):51-61.

Raquet 2007 Raquet JF, Miller MM, Nguyen TQ. Issues and Approaches for Navigation

Using Signals of Opportunity. In: ION NTM 2007; 2007. p. 1073-1080.

Serant 2010 — Serant D, Julien O, Macabiau C, Thevenon P, Dervin M, Corazza S, et al. Development and Validation of an OFDM/DVB-T Sensor for Positioning. In: IEEE/ION PLANS 2010; 2010. p. 988-1001.

Stephens 1995 — Stephens SA, Thomas JB. Controlled-root formulation for digital phase-locked loops. Aerospace and Electronic Systems, IEEE Transactions on. 1995;31(1):78-95.

Thevenon 2008 — Thevenon P, Bousquet M, Macabiau C, Grelier T, Ries L, Roviras D. Regulatory Analysis of Potential Candidate Bands for the Modernisation of GNSS Systems in 2015-2020. In: Satellite and Space Communications. IEEE International Workshop on; 2008. p. 172-175.

Thevenon 2009-1 — Thevenon P, Julien O, Macabiau C, Serant D, Ries L, Corazza S, et al. Positioning principles with a mobile TV system using DVB-SH signals and a Single Frequency Network. In: 2009 16th International Conference on Digital Signal Processing. IEEE; 2009. p. 1-8.

Thevenon 2009-2 — Thevenon P, Julien O, Macabiau C, Serant D, Corazza S, Bousquet M, et al. Pseudo-Range Measurements Using OFDM Channel Estimation. In: ION GNSS 2009; 2009. p. 481-493.

UMTS 2004 — ETSI TR 125 943 v6.0.0 - Universal Mobile Telecommunications System (UMTS); Deployment aspects (3GPP TR 25.943). 2004.

UMTS 2009 — ETSI TR 125 996 v8.0.0 - Universal Mobile Telecommunications System (UMTS); Spacial channel model for Multiple Input Multiple Output (MIMO) simulations (3GPP TR 25.996)

van de Beek 1997 — van de Beek JJ, Sandell M, Borjesson PO. ML estimation of time and frequency offset in OFDM systems. Signal Processing, IEEE Transactions on. 1997;45(7):1800-1805.

van Nee 1992 — van Nee RDJ. The Multipath Estimating Delay Lock Loop. In: ISSTA 92; 1992. p. 39-42.

Venkatachalam 2010 — Venkatachalam M, Etemad K, Ballantyne W, Chen B. Location services in WiMax networks. IEEE Communications Magazine. 2009 Oct;47(10):92-98.

Viterbi 1994 — Viterbi AJ, Viterbi AM, Gilhousen KS, Zehavi E. Soft handoff extends CDMA cell coverage and increases reverse link capacity. IEEE Journal on Selected Areas in Communications. 1994 Oct;12(8):1281-1288.

Wang 2003 — Wang X, Wu Y, Caron B. Transmitter identification using embedded spread spectrum sequences. In: International Conference on Communication Technology Proceedings, 2003. ICCT 2003. vol. 2; 2003. p. 1517-1523.

Wang 2006 — Wang X, Wu Y, Chouinard JY. A new position location system using DTV transmitter identification watermark signals. EURASIP Journal on Applied Signal Processing. 2006;2006.

Wylie 1996 — Wylie MP, Holtzman J. The non-line of sight problem in mobile location estimation. In: Universal Personal Communications, 1996. Record., 1996 5th IEEE International Conference on. vol. 2; 1996. p. 827-831 vol.2.

Yang 1999 — Yang B, Letaief KB, Cheng RS, Cao Z. An improved combined symbol and sampling clock synchronization method for OFDM systems. In: Wireless Communications and Networking Conference; 1999. p. 1153-1157.

Yu 2008 — Yu K, Guo YJ. Improved Positioning Algorithms for Nonline-of-Sight Environments. Vehicular Technology, IEEE Transactions on. 2008;57(4):2342-2353.

Zanier 2008 — Zanier F, Crisci M, Luise M. Signal design criteria and parametric analysis for next generation C-band satellite navigation system. In: European Navigation Conference ENC-GNSS 2008.

[Zhao 2002] — Zhao Y. Standardization of mobile phone positioning for 3G systems. Communications Magazine, IEEE. 2002;40(7):108-116.

Annex A - Regulatory analysis of new positioning service deployment in S and C-band

This section provides a regulatory analysis of the radio-navigation services in S and C-bands.

The frequency allocations are defined in the fifth article of the ITU Radio Regulation document [ITU RR 2004]. This document reviews the allocation of services to the spectrum from 9 kHz up to 1000 GHz. This allocation is decided on a ***regional*** basis (see Figure 97 below). Allocation can be ***primary*** or ***secondary***. Secondary allocations cannot cause harmful interferences to primary services, and cannot claim protection from primary services' interferences.

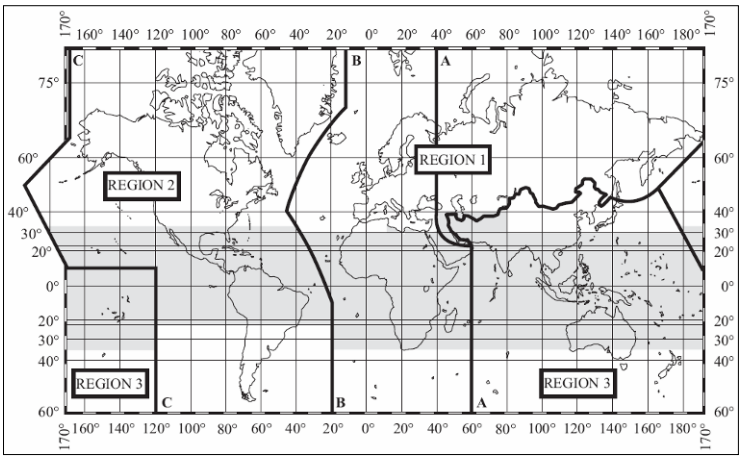

Figure 97 - ITU Region ([ITU RR, 2004], Article 5)

It is also worth noting that each administration (national or regional) have their own table of frequency allocations, since each nation can allocate the spectrum as it wishes over its territory, as long as its stations do not interfere with other nations' stations. Therefore, there may be slight differences between a national table of frequency allocations and the ITU's.

Radiodetermination Satellite Service (RDSS) and Radionavigation Satellite Service (RNSS) are defined in the following way in the [ITU RR 2004] Article 1:

1.9 *radiodetermination*: The determination of the position, velocity and/or other characteristics of an object, or the obtaining of information relating to these parameters, by means of the propagation properties of *radio waves*.

1.10 *radionavigation*: *Radiodetermination* used for the purposes of navigation, including obstruction warning.

1.41 *radiodetermination-satellite service*: A *radiocommunication service* for the purpose of *radiodetermination* involving the use of one or more *space stations*. This service may also include *feeder links* necessary for its own operation.

1.43 *radionavigation-satellite service*: A *radiodetermination-satellite service* used for the purpose of *radionavigation*. This service may also include *feeder links* necessary for its operation.

From these definitions, RNSS and RDSS can be assumed equivalent.

From a regulatory point of view, three possibilities exist to deploy a new satellite positioning service:

(1) Use existing RNSS bands;
(2) Add a new RNSS allocation in an existing band;
(3) Use signals of opportunity.

Service allocations to a given band is a process decided during the ITU's World Radio-communications Conferences (WRC), which take place every 3 or 4 years and gather basically every member state of the United Nations, plus some companies or particular communities (such as the amateur radio-astronomers or the civil aviation).

Concerning solution (1), two downlink RNSS bands already exist in the S- and C-bands. 5010 - 5030 MHz was obtained at the 2000 WRC and confirmed at the 2003 WRC as a worldwide allocation. 2483.5 - 2500 MHz is allocated to RDSS, but only in the ITU Regions 2 (Americas) and 3 (Asia-Pacific).

Possibility (2) has already been encountered for the modernization of GPS and the preparation of Galileo. Indeed, RNSS was added in the 1164 - 1215 MHz band to the existing Aeronautical Radio-Navigation Service (ARNS). Sharing spectrum with an aeronautical service permits to benefit from strong protection criteria against interferences, and to potentially deploy a safety-related RNSS service. Currently, two bands have an exclusive ARNS allocation: 2.7 - 2.9 GHz (used by radars) and 4.2 - 4.4 GHz (used by radio-altimeter) [Hein 2007].

Finally, solution (3) is a radically different way to tackle the issue, since it is a manner to escape from regulatory constraints. Indeed, it is allowed to use telecommunication signals for position determination purpose, as long as the initial telecommunication service remains operational.

An example of mobile telecommunication bands is the IMT2000 frequency allocations. IMT2000 is a global standard, aiming at spreading the 3G and "Beyond 3G" communication technologies. To achieve this, the ITU has accepted to allocate 215 MHz of almost contiguous spectrum in S-band to the Mobile Service (for either terrestrial or satellite systems), in which only IMT2000-approved radio interfaces can be deployed.

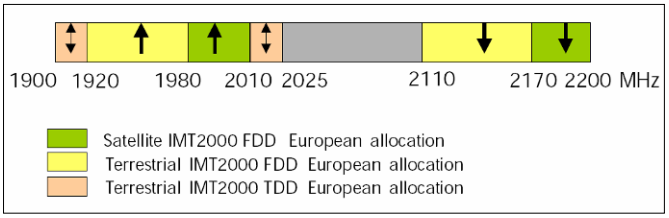

Figure 98 - IMT200 Frequency Allocations

However, virtually any telecommunication bands would be adapted on a regulatory point of view (for example, the 2.4 GHz band, where WiFi stations are deployed).

The initial list of candidate bands and associated systems is summarized below:

- Existing RNSS or RDSS bands
  - 2483.5 - 2500 MHz in Region 2 & 3 only
  - 5010 - 5030 MHz worldwide

- ARNS bands, necessitating a change of allocation
    - 2700 - 2900 GHz used by radars
    - 4200 - 4400 GHz used by radio altimeters
- Telecommunication bands, for use as signals of opportunity.

Further details on each possibility are provided in the following sections.

Existing RNSS bands - C-band: 5010 - 5030 MHz

This existing C-band allocation was obtained at WRC-2000 with other frequency bands attributed to Galileo, but it was not used for the design of the first generation of Galileo, due to technical difficulties, notably a 10 dB loss on the link budget due to higher free space loss and rain attenuations, and increased phase noise affecting the pseudo-range measurement [Irsigler 2002].

There are also strong regulatory constraints affecting the adjacent bands [Zanier 2008]: the aggregate power flux density at Earth surface from all RNSS satellites emitting in this band shall not exceed:

- -124.5 dB(W/m²) in a 150 kHz band in the upper band (5030 - 5150 MHz), where the aeronautical Microwave Landing Systems are used;
- -196.5 dB(W/m²) in a 10 MHz band in the lower band (4990 - 5000 MHz), dedicated to Radio-Astronomy Services.

Moreover, the presence of an RNSS uplink allocation in the adjacent 5000 - 5010 MHz band could cause some interference at the ground stations and the satellites, adding some constraints (isolation between uplink and downlink) to the design of some navigation signals in this band.

At the last WRC in November 2007, this band has been claimed by the Federal Aviation Administration to be used for an Aeronautical Mobile (Route) Service, to deploy a safety-oriented communications between aircraft and the ground. This allocation change is at the agenda of the next WRC which will take place in 2011.

For this reason, interest in this band has improved, and the European Space Agency (ESA) has decided to support specific studies on the use of this band for satellite navigation in its GNSS Evolution Programme.

The challenge of this band is to design a system with more gain, to compensate the link budget loss, while respecting the different interference constraints in the adjacent bands. One solution studied by ESA to regain the power lost during the propagation would be to use more focused beams, which would illuminate different partial region of Earth successively. This technique is called beam-hopping and early performances can be found in [Colzi 2008].

Also, thanks to the shorter wavelength, multiple antennas could be used at the receiver, thus paving the way to the use of smart antenna techniques such as beamforming for satellite tracking or for multipath mitigation in order to improve the link budget [Konovaltsev 2007].

Existing RDSS bands - S-band: 2483.5 - 2500 MHz

RDSS is allocated in this band in ITU region 2 (Americas) and 3 (Asia Pacific) only. That is why this band is used by or planned for regional navigation systems, such as the existing Chinese Beidou or the future Indian Regional Navigation Satellite System. However, at the last WRC'07, European

delegations claimed to consider the extension of this RDSS allocation all over the world. This would imply to study the compatibility with other systems sharing the band, including Globalstar.

Region 1 Table	Region 2 Table	Region 3 Table
2483.5-2500 FIXED MOBILE MOBILE-SATELLITE (space-to-Earth) 5.351A Radiolocation 5.150 5.371 5.397 5.398 5.399 5.400 5.402	**2483.5-2500** FIXED MOBILE MOBILE-SATELLITE (space-to-Earth) 5.351A RADIOLOCATION RADIODETERMINATION- SATELLITE (space-to-Earth) 5.398 5.150 5.402	**2483.5-2500** FIXED MOBILE MOBILE-SATELLITE (space-to-Earth) 5.351A RADIOLOCATION Radiodetermination-satellite (space-to-Earth) 5.398 5.150 5.400 5.402

Table 34 - Frequency allocation in the 2483.5 - 2500 MHz band. ***Excerpt from [ITU RR, 2004] Article 5***

One of the big advantages of this band is that it is either used by telecommunication systems (Globalstar) and close to other telecommunication bands (e.g. UMTS at 2.1 GHz, WiFi at 2.4 GHz). A navigation signal in this band would permit to design simple, cheap mass market receiver providing both telecommunication and navigation services with the same RF head.

ARNS bands – 2.7 - 2.9 GHz and 4.2 - 4.4 GHz

RNSS has already been added to ARNS bands for the modernization of GPS (L5) or for the introduction of Galileo (E5). The sharing with ARNS implies that compatibility must be ensured, so that ARNS systems, often safety-critical for civil aviation, are not disturbed by the new RNSS signals. Some studies in L5 [Hegarthy 1999] have shown the need to reallocate the working frequencies of some ARNS equipment, which is considered reluctantly by the aeronautical community.

Two bands are potentially interesting due to their exclusive ARNS allocation worldwide: the 2.7 - 2.9 GHz (radars) and 4.2 - 4.4 GHz (radio-altimeters) [Hein 2007].

These bands have a very large bandwidth, and the signals used in them are pulsed. This could potentially leave space for compatible extra-wideband navigation signals permitting greater accuracy than today's GNSS planned signals. Also, the new navigation signals would benefit from the strong protection criteria reserved for safety-critical services, which would permit to provide a complementary signal to the current "safety-of-life" navigation signals planned in GPS and Galileo.

Nevertheless, RNSS has been (and will be) generously awarded spectrum at the last WRCs (in 2000 for Galileo and in 2011 with the 2483.5 - 2500 MHz band), whereas ARNS band has often been claimed for other services. In particular, the radar band has been coveted by mobile communication operators, since the pulsed nature of the radar signals makes it non-optimally used (by telecommunication operator's standards). At WRC 2000, that band was discussed to be considered as an extension band for IMT-2000 under agenda item 1.6, but an allocation change was refused.

Currently, no such allocation change is planned in either band. In addition, the need for a new "safety-of-life" signal is currently difficult to justify, since new dedicated signals (GPS L5 and Galileo E5) are going to be introduced in the next few years. These arguments would eliminate the considered ARNS bands from the potential candidates.

The following table summarises the advantages and drawbacks of the considered bands and associated systems.

Band	Advantages	Drawbacks
RDSS / MSS 2483.5 - 2500 MHz	• Possible worldwide allocation in 2011. • Possible synergy with telecommunication service.	• Compatibility with existing telecommunication systems.
RNSS 5010 - 5030 MHz	• Existing worldwide allocation. • Smart antenna techniques.	• Attenuation. • Interference from adjacent RNSS uplink.
ARNS 2700 - 2900 MHz	• Large bandwidth. • Possible Safety-of-Life service. • Pulsed emission of radars.	• Service allocation change required at ITU. • Severe compatibility constraints required by civil aviation.
ARNS 4200 - 4400 MHz	• Large bandwidth. • Possible Safety-of-Life service. • Localised use of radio-altimeter near airports.	• Service allocation change required at ITU. • Severe compatibility constraints required by civil aviation.

Table 35 - Summary of advantages and drawbacks of the considered bands [Thevenon 2008]

Use of Signals of Opportunity - A regulatory bypass

Finally, the last regulatory solution to propose a new positioning service is to employ signals of opportunity. Regulatory issue shall have been addressed during the original service deployment. Therefore, the use of these signals for positioning does not imply any regulatory issue.

This solution is radically different from the previous ones, since it would not tackle the *design of new dedicated navigation signals*, but would focus on the *processing of existing telecommunication signals* for positioning purpose.

Annex B - Other investigated urban propagation models

COST 259 directional channel model

The COST 259 channel model [COST259 2006-1] [COST259 2006-2] was developed in order to provide unified model for directional channel model, as smart antennas is a key technology for 3G and beyond 3G telecommunication systems.

The particularity of this model is its completeness. The following phenomena are simulated:

- a LOS cluster of delay is always visible, and other NLOS clusters may be visible.
- the LOS cluster comprises section where the cluster pathloss in close to the free space loss (corresponding to LOS conditions) and other sections where the pathloss is higher (blockage of the LOS path).
- Cluster shadowing is modelled.
- Cluster delay spread is modelled, with the observed cross-correlation properties with the shadowing
- Cluster angle spread is modelled, both at the receiver and the emitter.
- Different polarization (linear vertical and horizontal) are modelled, with the good correlation properties.

However, the main drawback is the lack of indications to implement the model at multipath component (MPC) level. No clear indication is provided about the number of MPC per cluster and their angle or delay distribution. It is only indicated that the determination of these parameters can be done using uniform distributions (but with which value range?) and shall be done in accordance with the cluster delay spread and angle spread.

This model was implemented from scratch in Matlab. There was some implementation issues:

- the directional side of the model was not implemented. This is not an issue, but rather a downgrading of the model due to the lack of interest in the directional aspect of the propagation channel.
- the cluster interacting objects are placed using a 2D Gaussian distribution, with a standard deviation equal to 100m. This standard deviation is not clearly mentioned in the papers.
- a LOS MPC shall be included in the LOS cluster, with a power provided by the Rice factor. However, the distribution of the Rice factor is not understood from the explanation provided in the papers.
- the MPC delay distribution has been chosen to be a uniform distribution between $\tau_{cluster} + [0\ ;\ 2 * delay\_spread]$. For this reason, the MPC delays are not consistent between 2 realizations of the channel, and the required continuity of the MPC delays is not provided by this implementation.
- correlation distance for shadowing and delay spread are very important (100m), leading to problems for the short time series generation.

3GPP spatial channel model for MIMO simulations

A model similar to the COST 259 model was found and is adopted in the standardization group 3GPP/ETSI [UMTS 2009]. Its goal is the same as the COST 259 model: to provide a complete propagation channel model comprising information about the angle of arrival and departure of the MPCs.

The implementation of this model is similar to the COST 259 one, with more details available in [UMTS 2009]. Notable differences are

- the absence of NLOS clusters. This feature can be included, but on 'switch' basis at the launch of the simulation
- the number of MPC (called sub-path in this model) is specified and set to 120.
- the absence of LOS MPC in the LOS cluster for macro-cells
- slight difference in the various distribution parameters
- the specification of the MPC delay distribution
- the possibility to activate an 'urban canyon' mode
- the lack of correlation distance for shadowing and delay spread time series generation
- the consideration of correlated shadowing for different emitters. An intercorrelation coefficient of 0.5 is specified (which may not be very realistic as shadowing correlation has been observed to be dependent on the azimuth angle between the BS directions)
- no correlation distance is imposed for shadowing and delay spread time series generation.

However, although this model seems better documented, especially for implementation, it still lacks the critical feature that we are searching for: the continuity of MPC delays.

DLR Land Mobile Multipath Channel Model for GNSS

The DLR Land Mobile Multipath Channel Model [DLR 2005] is a Matlab simulator capable of generating propagation channel for navigation applications.

The use of this model was advised by people met at the COST 802 meeting in Toulouse, November 2009. However, further discussions with Mr Steingass, author of this model, have led to the incapacity of using this model:

- the carrier frequency can be upscaled from 1.5 GHz to 2.2 GHz, BUT
- distance between the emitter and the receiver shall be above 4 km
- the elevation angle of the LOS path shall be above 5°.

These 2 last constraints make this simulator inappropriate for our use.

Annex C - Least Square algorithm for position estimation

Non-Linear Least Square position estimation

At the positioning stage, let us assume that M pseudo-ranges have been obtained from different emitters. Each pseudo-range can be expressed as follows:

$$\rho_j = f_i(x,y,b) + n_j = \sqrt{\left(x-x_j\right)^2 + \left(y-y_j\right)^2 + \left(z-z_j\right)^2} + c.\tau_j + b + n_j \qquad \textbf{Eq. 0.1}$$

where j is the emitter index;

(x,y,z) are the coordinates of the receiver. The receiver's height is assumed constant, so only (x,y) are unknown;

(x_j,y_j,z_j) are the known coordinates of emitter j;

$c.\tau_j$ is the known artificial delay of emitter j (τ_j) multiplied by the speed of light c;

b is an unknown common bias affecting all pseudo-ranges. It corresponds to the receiver clock offset with regards to the system clock, and also comprises a common ambiguity term on the distance between the emitters and the receivers. It is considered that all emitters (terrestrial and satellites) are perfectly synchronized, as they are working in SFN configuration;

$f_j(x,y,b) = \sqrt{\left(x-x_j\right)^2 + \left(y-y_j\right)^2 + \left(z-z_j\right)^2} + c.\tau_j + b$ is the pseudo-range modeling function;

n_j is the measurement noise affecting pseudo-range j.

Let us suppose that an approximate position and clock offset of the receiver $(\hat{x},\hat{y},\hat{b})$ close to the actual receiver's are available. It is then possible to linearize the pseudo-range modeling function around this approximate position.

$$f_j(x,y,b) \approx f_j\left(\hat{x},\hat{y},\hat{b}\right) + (x-\hat{x}).\frac{\partial f_j}{\partial x}\left(\hat{x},\hat{y},\hat{b}\right) + (y-\hat{y}).\frac{\partial f_j}{\partial y}\left(\hat{x},\hat{y},\hat{b}\right) + \left(b-\hat{b}\right).\frac{\partial f_j}{\partial b}\left(\hat{x},\hat{y},\hat{b}\right)$$

Let us express the partial derivatives of the pseudo-range modeling function:

$$\frac{\partial f_j}{\partial x}\left(\hat{x},\hat{y},\hat{b}\right) = \frac{\hat{x}-x_j}{\sqrt{\left(\hat{x}-x_j\right)^2 + \left(\hat{y}-y_j\right)^2 + \left(\hat{z}-z_j\right)^2}}$$

$$\frac{\partial f_j}{\partial y}\left(\hat{x},\hat{y},\hat{b}\right) = \frac{\hat{y}-y_j}{\sqrt{\left(\hat{x}-x_j\right)^2 + \left(\hat{y}-y_j\right)^2 + \left(\hat{z}-z_j\right)^2}}$$

$$\frac{\partial f_j}{\partial b}\left(\hat{x},\hat{y},\hat{b}\right) = 1$$

With M pseudo-ranges estimation available, the linear system can be expressed in matrix notation:

$$\mathbf{\Delta\rho} = \mathbf{H}.\mathbf{\Delta p} + \mathbf{n} \qquad \textbf{Eq. 0.2}$$

where $\mathbf{\Delta\rho} = \begin{bmatrix} \rho_1 - f_1(\hat{x},\hat{y},\hat{b}) \\ \vdots \\ \rho_M - f_M(\hat{x},\hat{y},\hat{b}) \end{bmatrix}$

$\mathbf{H} = \begin{bmatrix} \frac{\hat{x}-x_1}{\sqrt{(\hat{x}-x_1)^2+(\hat{y}-y_1)^2+(\hat{z}-z_j)^2}} & \frac{\hat{y}-y_1}{\sqrt{(\hat{x}-x_1)^2+(\hat{y}-y_1)^2+(\hat{z}-z_j)^2}} & 1 \\ \vdots & \vdots & \vdots \\ \frac{\hat{x}-x_M}{\sqrt{(\hat{x}-x_M)^2+(\hat{y}-y_M)^2+(\hat{z}-z_j)^2}} & \frac{\hat{y}-y_M}{\sqrt{(\hat{x}-x_M)^2+(\hat{y}-y_M)^2+(\hat{z}-z_j)^2}} & 1 \end{bmatrix}$. It only depends on geometric factors.

$\mathbf{\Delta p} = \begin{bmatrix} x-\hat{x} \\ y-\hat{y} \\ b-\hat{b} \end{bmatrix}$. It is also called the residual vector.

$\mathbf{n} = \begin{bmatrix} n_1 \\ \vdots \\ n_M \end{bmatrix}$

The solution which minimizes the noise vector is:

$$\mathbf{\Delta p} = (\mathbf{H}^T.\mathbf{H})^{-1}.\mathbf{H}^T.\mathbf{\Delta\rho} \qquad \textbf{Eq. 0.3}$$

This method can be applied iteratively in order let the position estimate converge toward the fitting of the pseudo-range measurements with the pseudo-range model. In the iterative method, the approximate position and clock offset of the receiver uses the updated values obtained by the previous iteration of the algorithm. The number of iterations is generally set by a condition on the residual vector's norm.

Now, let us calculate the variance of the estimator.

$$Cov(\mathbf{\Delta p}) = E[\mathbf{\Delta p}.\mathbf{\Delta p}^T] = (\mathbf{H}^T.\mathbf{H})^{-1}.\mathbf{H}^T.Cov(\mathbf{\Delta\rho}).\mathbf{H}.(\mathbf{H}^T.\mathbf{H})^{-1} \qquad \textbf{Eq. 0.4}$$

where $E[.]$ is the expectation operator.

This relation permits to relate the error variance in the position domain to the error variance of the pseudo-range estimates.

Let us suppose that the error of the pseudo-range estimates is identically Gaussian-distributed and zero-mean, with the same error variance σ_{PR}^2 for each pseudo-range, then $Cov(\mathbf{\Delta\rho}) = I_{MxM}.\sigma_{PR}^2$, where I_{MxM} is the M-sized identity matrix. Eq. 0.4 simplifies to:

$$Cov(\mathbf{\Delta p}) = (\mathbf{H}^T.\mathbf{H})^{-1}.\sigma_{PR}^2 \qquad \textbf{Eq. 0.5}$$

Let us call $\mathbf{D} = (\mathbf{H}^T.\mathbf{H})^{-1}$ and $\mathbf{D}[i,j]$ the term on the i-th row and j-th column of matrix $\mathbf{D}$

In Eq. 0.5, the classical Dilution of Precision (DoP) factors known in GNSS appear: the horizontal 2D position error variance is related to the pseudo-range variance through the Horizontal DoP factor defined by: $HDoP = \sqrt{\mathbf{D}[1,1] + \mathbf{D}[2,2]}$

This comes from the relation:

$$\sigma^2_{position} = \sigma^2_x + \sigma^2_y = (\mathbf{D}[1,1] + \mathbf{D}[2,2]).\sigma^2_{PR} = HDoP^2.\sigma^2_{PR}$$

Figure 99 shows the HDoP map for different number of visible terrestrial emitters. For each point of the coverage, the matrix $\mathbf{H}$ is calculated using the true position and the closest emitters at this point.

All in all, an hexagonal network of terrestrial emitters provides a good HDoP all over the service coverage. The HDoP gets lower (ie better) as the number of visible emitters increases, but it is very good even when only 3 emitters are visible. The DoP would be further improved by the addition of a satellite emitter.

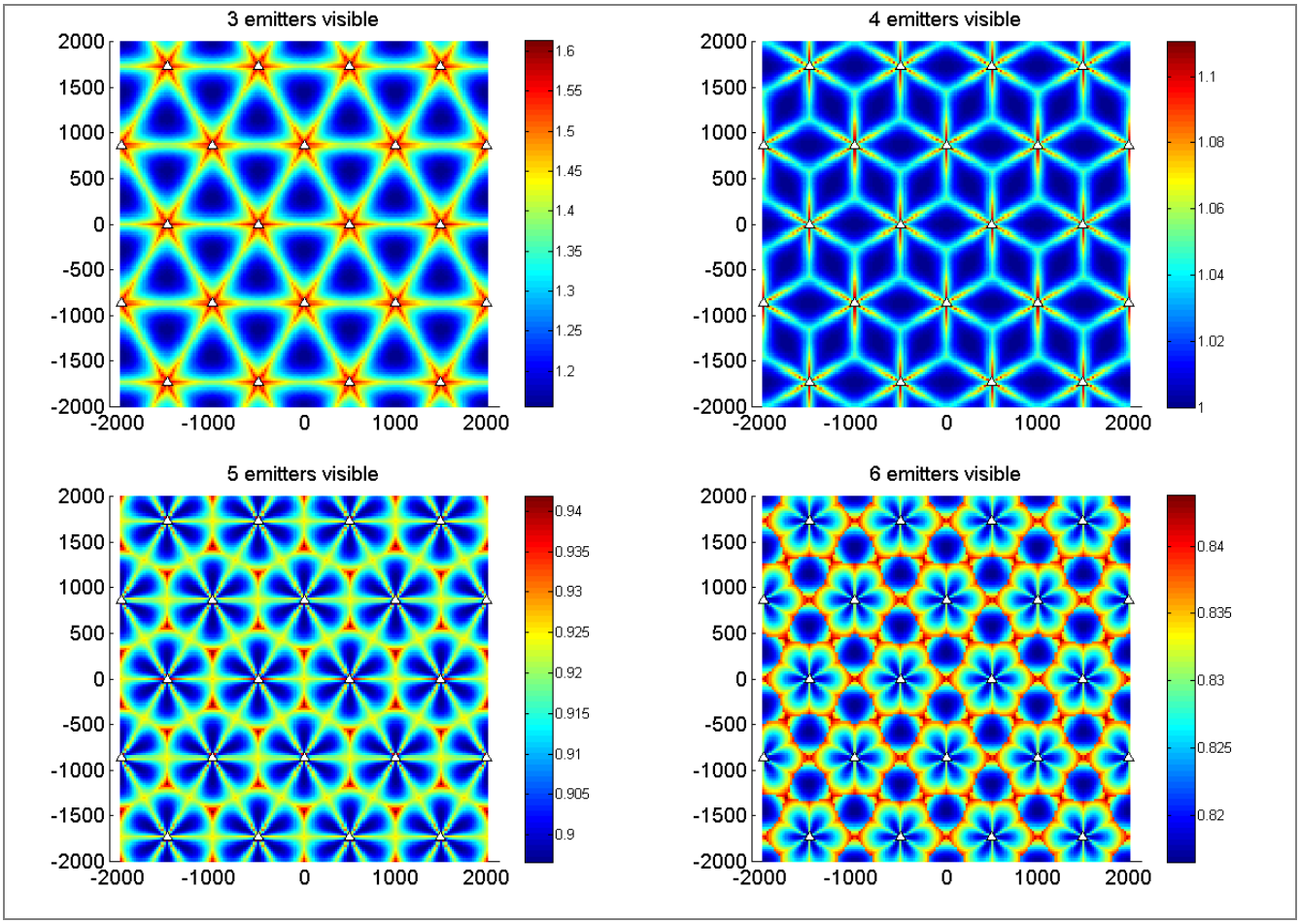

Figure 99 - HDoP cartography for a network of terrestrial emitters

Weighted Non-Linear Least Square position estimation

The Non-Linear Least Square position estimation is well adapted to the case where all pseudo-ranges are affected by a similar measurement noise. However, this situation is not likely to be encountered in a network composed of terrestrial emitters due to the large range of SNR encountered from the different emitters. As seen with the CNES cCIR measurements (see Section 4.3.1), signals from different emitters have been received with a 40 dB power difference.

In this case, the **Weighted Non-Linear Least Square** estimation is preferable.

Let us call the covariance matrix of the noise $\mathbf{R}$. The solution which minimizes the noise vector is the weighted least square estimate:

$$\mathbf{\Delta p} = (\mathbf{H}^T.\mathbf{R}^{-1}.\mathbf{H})^{-1}.\mathbf{H}^T.\mathbf{R}^{-1}.\mathbf{\Delta \rho} \quad \textbf{Eq. 0.6}$$

$$Cov(\mathbf{\Delta p}) = (\mathbf{H}^T.\mathbf{R}^{-1}.\mathbf{H})^{-1} \quad \textbf{Eq. 0.7}$$

To express the pseudo-range error covariance matrix, let us make the following assumptions:

- The noise between different emitters is uncorrelated, so $\mathbf{R}$ is diagonal.
- The diagonal terms corresponds to the error variance of each pseudo-range. We can use the expression from [Serant 2010] quoted in section 3.4.4 and the COST 231 Wallfisch-Ikegami pathloss model [COST231 1993] quoted in section 3.1.1 to calculate these diagonal terms. The Blackman-Harris windowing technique has been considered.
- In order to account for the potential offset between the theoretical formula of the tracking error variance and the reality, an additional 30 dB loss is included in the link budget.

The resulting error standard deviation map is plotted in Figure 100.

The performances are very interesting, with sub-meter accuracy all over the coverage, even when only 3 emitters are considered for position estimation.

However, an important limitation of the considered hypothesis has to be kept in mind: this simulation assumes that the measurement noise affecting the pseudo-ranges is zero-mean and Gaussian. Therefore, pseudo-range errors due to possible NLOS conditions are not considered, which is not realistic for true measurements in an urban environment. However, without a correct NLOS error model, we cannot refine this simulation.

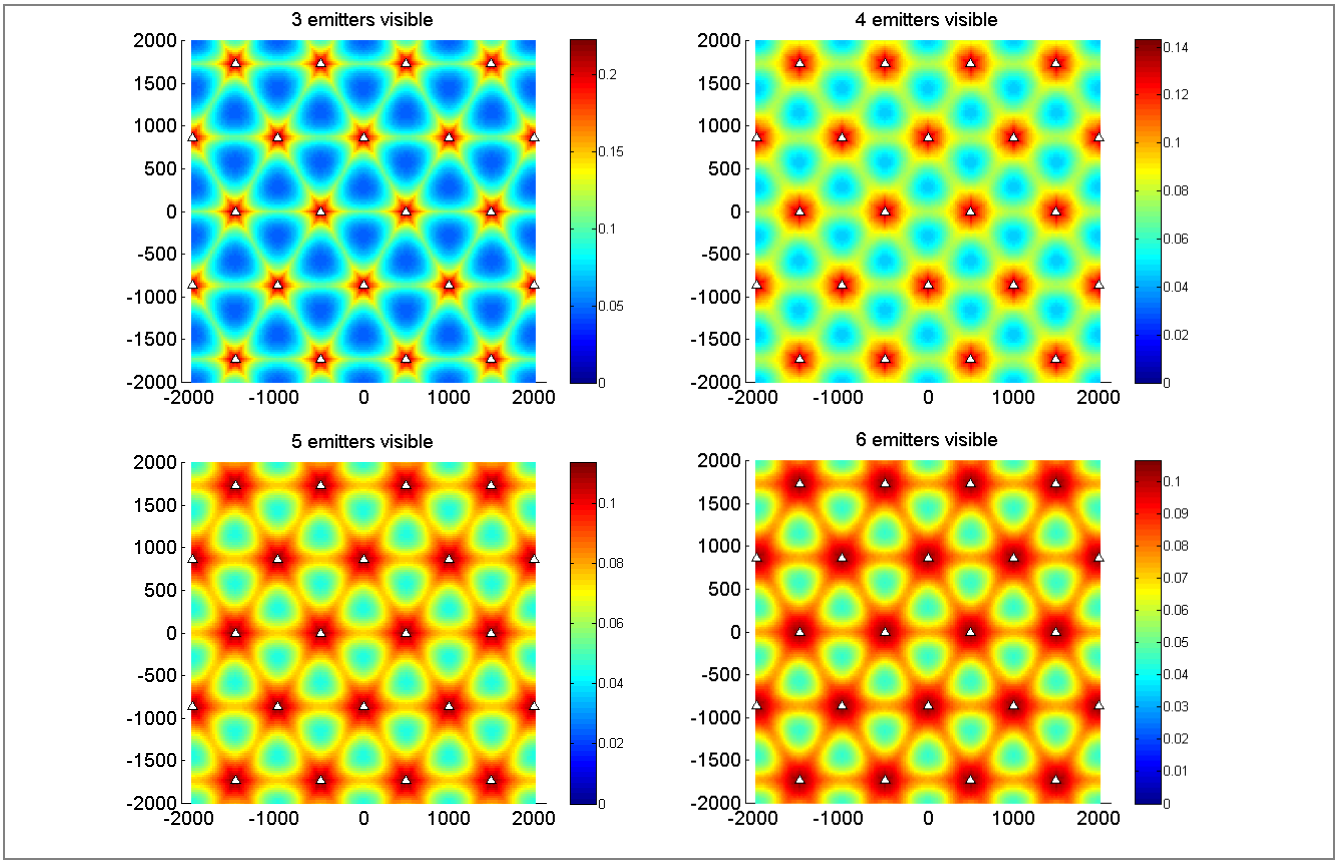

Figure 100 - position error standard deviation cartography obtained by WNLS algorithm in a network of terrestrial emitters

Annex D - French summary of the Thesis

This part is a French summary of the PhD manuscript. **It does not contain any exclusive contents compared to the English part of the manuscript.** It has been written in order to comply with administrative requirements.

D.1. Introduction

Au moment de l'écriture de ce manuscrit (2007-2010), le marché du positionnement est en pleine croissance. Deux raisons principales sont à l'origine de cette croissance :

1. des **réglementations** comme le E-911 américain, qui obligent les opérateurs de téléphonie mobile à pouvoir localiser leur souscripteurs en cas de situation d'urgence. L'équivalent européen devrait voir le jour sous l'appellation E-112.
2. l'explosion des **services liés à la localisation** de l'utilisateur, qui est intimement liée au développement des smartphones. En effet, le nombre de récepteurs GPS vendus dans des smartphones entre 2006 et 2009 a été plus important que le nombre cumulé de récepteurs GPS, tout autres types confondus (aviation, militaire, portable navigation device) depuis la création du GPS.

La majorité de cette croissance se fait dans les centres urbains, où est concentré le marché de masse des utilisateurs. Néanmoins, l'environnement urbain ainsi que l'intérieur des bâtiments représentent des conditions difficile pour le bon fonctionnement des systèmes de navigation par satellite. Cela est dû notamment au blocages des signaux satellites par les immeubles et/ou également aux nombreux multitrajets créés par l'environnement urbain à proximité des récepteurs. Cet environnement crée une dégradation des performances des systèmes de navigation par satellites en termes de disponibilité, précision, continuité et fiabilité.

Différentes pistes ont été poursuivis par les chercheurs afin de permettre le positionnement d'utilisateurs urbains ou à l'intérieur de bâtiments :

- **Des modifications au systèmes de navigation par satellites**. On peut notamment citer (1) des avancées dans le domaine du traitement du signal côté récepteur, tel que l'allongement des durée d'intégration, le développement de nouvelles formes d'ondes robustes face aux multitrajets (BOC), etc. et (2) des mise à jour des systèmes de navigation par satellites au niveau systèmes telles que la mise en place des standards Assisted-GNSS, les récepteurs multi-constellation, la présence de canaux pilotes dans les nouveaux systèmes de navigation par satellites, l'introduction de nouveaux signaux de navigation dans de nouvelles bandes de fréquences, etc. Un résumé intéressant de ce domaine est diponible dans [Lachapelle 2004]
- **D'autres sources de capteurs de positions**
    - **Capteurs inertiels (gyromètres, accéléromètres), magnétomètres, capteurs basés sur la vision.** Ce type de capteurs est complémentaire aux systèmes de navigation par satellites et peut fournir une assistance pour la poursuite des signaux GNSS ou le calcul de la position. Ils peuvent également améliorer la continuité du positionnement dans le cas d'une interruption de réception de signaux GNSS.

- **Les systèmes de radiolocalisation dédiés**. Ces systèmes sont déployés afin de fournir un service de positionnement dans une couverture donnée. Parmi les solutions existantes, on peut citer les pseudolites GNSS, les émetteurs UWB, les bornes RFID, etc. Le principal désavantage de cette solution est son coût important lié au besoin de déployer une infrastructure spécifique pour une couverture de service limitée.
- **Les systèmes ou signaux d'opportunités.** Ce type de solution consiste à exploiter des systèmes ou signaux existants qui n'ont pas été déployés initialement pour fournir un service de positionnement. Ces systèmes sont souvent des systèmes de radio-communication, telles que les systèmes de téléphonie mobile ou de diffusion (radio ou télévision par exemple).

Le sujet de cette thèse s'insert dans cette dernière catégorie.

Les avantages de cette solution sont détaillés dans la liste suivante. Une analyse similaire est disponible dans [Raquet 2007].

- **Disponibilité** : Les signaux d'opportunité sont largement disponibles dans les centres métropolitains, y compris à l'intérieur des bâtiments. C'est en effet dans ces zones que sont concentrés les utilisateurs ciblés par ces services. Cette disponibilité est à mettre en relation avec le **coût réduit** du service de positionnement fourni à travers un tel système, puisque l'infrastructure est déjà déployée pour le service initialement fourni par le système d'opportunité.
- **Diversité des systèmes** : Les systèmes d'opportunité utilisent une grande variété de signaux (modulation, bande passante, fréquence porteuse, etc.) et de déploiement de réseau d'émetteur (réseau UHF pour la TV ou la radio, réseau cellulaire pour la téléphonie mobile, point d'accès à l'intérieur des bâtiments pour les réseaux sans fils, etc.). Si les sources de données de position sont suffisamment décorrélées, cette variété peut se traduire en une sorte de gain de diversité. Par exemple, si un lien satellite est rompu sur une certaine zone, cela pourrait être différent pour une signal provenant d'un émetteur terrestre.
- **Intégration des services de positionnement et de télécommunication** : un même récepteur serait capable de fournir un service de positionnement ainsi que de télécommunication. Cela pourrait permettre l'émergence de nouveaux services hybrides, où les télécommunications aideraient le positionnement (par exemple, grâce au transfert de données d'assistance via le lien télécom, comme dans l'Assisted GPS) ou inversement (par exemple, une assistance du service de positionnement pour la gestion des ressources radio ou la synchronization fine des terminaux). Cela pourrait également permettre le développement d'une plateforme dédiés au services liés au positionnement peu onéreuse, grâce à la mise en commun de sous-systèmes du récepteur, comme la tête RF ou des fonctions de traitement du signal.

Finalement, les systèmes d'opportunité sont complémentaires aux GNSS. En effet, le GNSS restera le moyen de positionnement principal pour les zones péri-urbaines ou rurales, où les systèmes d'opportunité sont généralement moins présents. Au contraire, dans les zones urbaines denses, les systèmes d'opportunités pourront faire valoir leur haute disponibilité pour fournir le service de positionnement. En d'autres termes, les systèmes d'opportunité ne sont pas en compétition directe avec les systèmes de navigation par satellite, mais seront plutôt complémentaires.

Les désavantages, ou plutôt les défis associés à l'utilisation des systèmes d'opportunités sont :

- **Leur conception n'est pas optimisée pour le positionnement** : les performances du service de positonnement seront obtenues à travers une approche "best effort", en tirant le meilleur parti du système d'opportunité existant. En revanche, ces systèmes d'opportunités n'auront pas été conçu pour faire du positionnement, ce qui pourra être illustré au niveau du signal (codes d'étalement de spectre courts, modulation OFDM, etc.) ou au niveau du système (couverture locale par un seul émetteur, pas de synchronisation entre les émetteurs, etc.).
- **Masquage et multitrajets** : la plupart des systèmes d'opportunité envisagés utilisent des émetteurs terrestres. Par conséquent, la transmission du signal entre l'émetteur et le récepteur dans un environnement urbain sera affectée de multitrajets intenses, d'atténuation locale très forte, et sera probablement en transmission sans ligne de visée directe. Cela sera un problème si des principes de positionnement géométriques, tel que la trilatération, sont utilisés.
- **Contraintes vis-à-vis des services de télécommunications** : les modifications au système d'opportunité devraient être réduites au minimum, afin de ne pas interférer avec le service initial du système d'opportunité, et également pour conserver un coût additionnel de déploiement du service de positionnement aussi bas que possible. Cela devrait favoriser l'adoption des solutions proposées par les opérateurs des systèmes d'opportunité.

Parmi d'autres, certains systèmes télécom ont déjà été étudiés pour fournir un service de positionnement: système de télécommunications mobiles 2G et 3G, WiFi, .système de diffusion numérique (TV ou radio). Le détail de l'état de l'art sur ces services se trouve dans la section 1.1.

Dans cette étude, le système d'opportunité choisi est un système basé sur le standard **DVB-SH (Digital Video Broadcasting - Satellite to Handheld)**.

D.2. Modélisation d'une transmission DVB-SH

D.2.1 Introduction au DVB-SH

Le DVB-SH est un standard de l'European Telecommunication Standardisation Institute pour la diffusion de signaux de télévision vers des utilisateurs mobiles en utilisant des signaux dont la fréquence est inférieure à 3 GHz. Le DVB-SH utilise un réseau d'émetteurs hybrides, composé de satellites géostationnaires et d'un réseau d'émetteurs terrestres en zone urbaine, afin de fournir une couverture de service continentale à moindres coûts. Le standard prévoit l'utilisation de plusieurs bandes passantes de signal, allant de 1.7 MHz à 8 MHz) afin de s'accommoder aux contraintes réglementaires des différents pays dans le monde entier. Ce standard est dérivé du DVB-T qui est dédié à la télévision numérique terrestre, et du DVB-SH dédié à la télévision numérique mobile.

Depuis 2008, le standard est fixé au travers de 2 documents [DVB-SH 2008-1] et [DVB-SH 2008-2] permettant de définir les différents aspects de la définition d'un système utilisant ce standard, et ouvrant la voie vers le déploiement commercial du système, ainsi que le développement de récepteurs commerciaux.

En 2010, 2 satellites géostationnaires ont été lancés avec une charge utile dédiée au DVB-SH : ICO GA au-dessus des Etats-Unis, et W2A au-dessus de l'Europe. Néanmoins, aucun réseau terrestre

DVB-SH n'a encore été déployé commercialement, bien que de nombreux tests et démonstrations ont déjà été réalisés.

D.2.2 Architecture d'un système DVB-SH

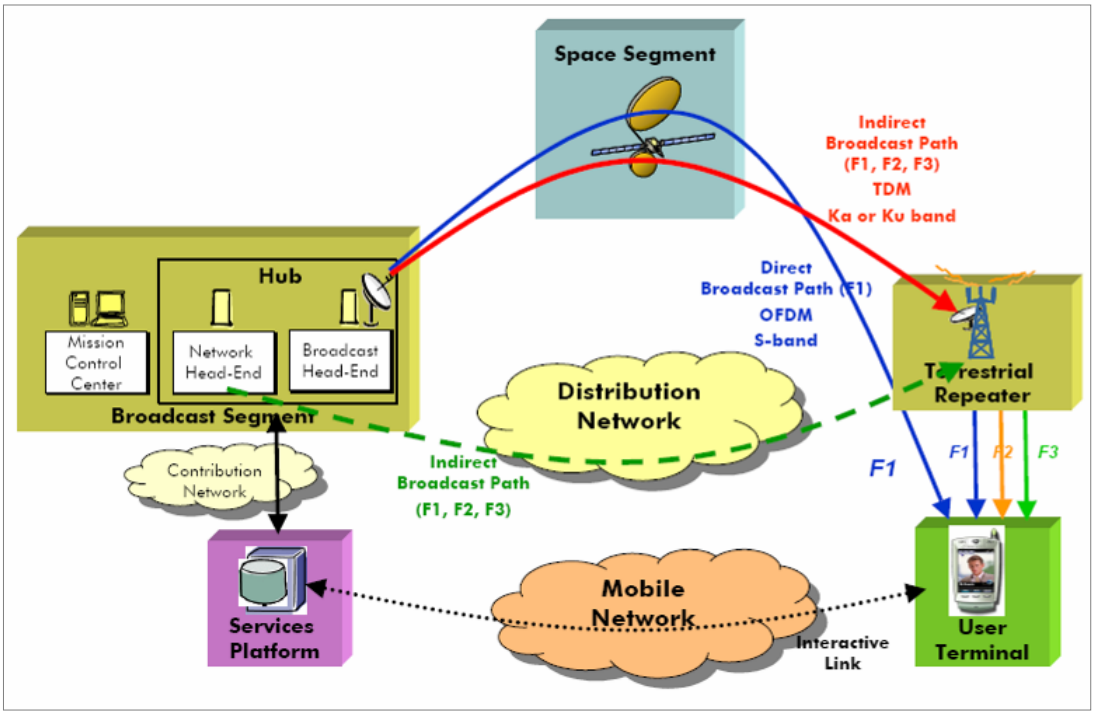

Le schéma ci-dessus illustre l'architecture d'un système DVB-SH. Le système est composé de :

- une **plateforme de service (Service Platform)**, qui réalise l'adaptation des contenus et agrège les programmes télévisuel et d'autres services média dans des flux de services IP (pour *Internet Protocol*).
- un **segment de diffusion (Broadcast Segment)**, qui distribue les flux de services IP vers les émetteurs satellites ou terrestres.
- un **satellite géostationnaire (Space Segment)** dédié (tel que W2A, placé à 10°E et opéré par Solaris Mobile Ltd, un joint venture entre Eutelsat et SES Astra), qui amplifie et convertit les signaux radio de la bande Ka/Ku vers la bande S. Ces signaux en bande S sont directement transmis aux terminaux et fournissent une couverture continental à moindre prix pour les zones rurales et semi-urbaines.
- un **réseau d'émetteurs terrestres (Terrestrial Repeater)**, qui reçoit les données à transmettre du segment de diffusion soit par une liaison par satellite ou via un réseau terrestre IP, et les transmet sur des signaux en bande S aux terminaux dans des zones où la couverture satellite est dégradée, comme les zones urbaines denses ou à l'intérieur des bâtiments.
- les **terminaux utilisateurs (User Terminal)**, qui peuvent décodés les signaux DVB-SH et qui peuvent être également capable de décoder des signaux de téléphonie mobile.

Un réseau DVB-SH européen utiliserait la bande appelée "MSS 2GHz" (pour *Mobile Satellite Services*) entre 2170 et 2200 MHz pour le lien descendant qui sera disponible à travers tout l'Europe en mai 2009. Cette bande de fréquence est bien plus haute que celle utilisée dans les

systèmes de diffusion traditionnel : par exemple, la télévision numérique terrestre française utilise des fréquences allant de 470 à 850 MHz. L'utilisation de ces fréquences plus hautes permet de réduire la taille des antennes, favorisant ainsi l'utilisation du DVB-SH dans des récepteurs mobiles. De plus, la proximité de cette bande avec d'autres bandes télécom (la 3G utilisent les bandes 1.8 et 2.1 GHz) permet la mutualisation de sous-systèmes du récepteurs entre les différents services, comme la tête RF ou des fonctions de traitement du signal.

D.2.3 Principe d'un réseau d'émetteurs mono-fréquence

Dans un système DVB-SH, les émetteurs peuvent fonctionner dans une configuration de réseau mono-fréquence (*Single Frequency Network* en anglais). Un SFN est un réseau où tous les émetteurs diffusent :

- le même signal,
- sur la même fréquence porteuse,
- de manière synchronisée.

Par conséquent, un récepteur dans un SFN recevra plusieurs répliques retardées du même signal. Tant que le récepteur est capable de gérer ces multitrajets (par exemple, en utilisant des technique d'égalisation de canal), cette configuration de réseau permettra d'augmenter la puissance du signal utile reçu par le récepteur, améliorant ainsi les conditions de réception du signal. Si les multitrajets sont trop intenses (par exemple, si le retard des répliques dépasse la capacité d'égalisation du récepteur), ces répliques créeront des interférences. Il est donc important que le déploiement d'un SFN prenne en compte les performances d'égalisation du récepteur afin d'éviter des interférences intra-système.

Le lecteur est invité à lire [Mattsson 2005] ou la section 2.2.2 de ce manuscrit, qui décrivent les contraintes et les bénéfices associés à l'utilisation de SFN dans un réseau de diffusion.

D.2.4 description de l'interface air du DVB-SH

Le standard DVB-SH comprend 2 modes de transmission :

- un mode OFDM (Orthogonal Frequency Division Multiplexing), basé sur le standard DVB-T avec quelques modifications. Ce mode peut être utilisé sur les transmissions satellites et terrestres.
- un mode TDM (Time Division Multiplexing), basé sur le standart DVB-S2. Ce mode n'est utilisé que sur les transmission satellites.

Le mode de transmission le plus populaire est le premier, car il se traduit par un récepteur plus simple, où un seul démodulateur est utilisé pour réceptionner les signaux terrestres et satellite. C'est ce mode de transmission qui est considéré dans cette étude.

Le standard spécifie uniquement le signal transmis [DVB-SH 2008-1] et laisse l'implémentation du récepteur libre. Le schéma bloc du transmetteur pour les 2 modes de transmission est montré dans la figure suivante.

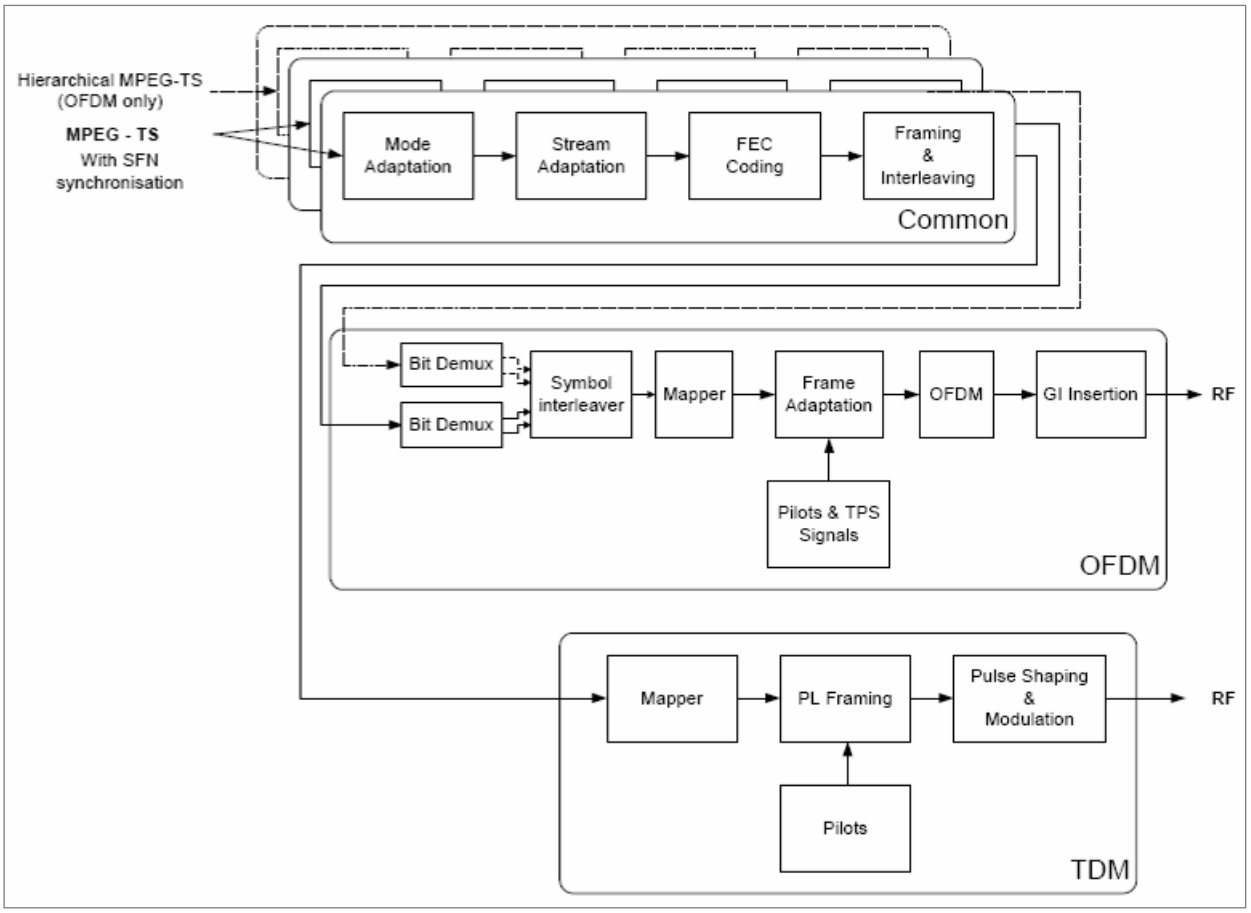

Une grande partie du document [DVB-SH 2008-1] est dédiée à l'encapsulation, au formattage, au codage et à l'entrelacement des flux de données. Différentes en-tête sont incluses, et le codage canal est effectué en utilisant un turbo-code avec un rendement allant de 1/5 à 2/3.

Le signal transmis est un signal utilisant le principe de l'OFDM. L'OFDM est un modulation robuste aux multitrajets. C'est donc un choix intéressant de modulation dans un système utilisant un réseau SFN. Pour des détails sur le principe de l'OFDM, le lecteur est invité à se reporté à la section 2.3.1 de ce manuscrit ou à [Bingham 1990].

Dans le standard DVB-SH, la forme d'onde OFDM est définie par 3 paramètres :

- $\boldsymbol{N_{FFT}}$ - la taille de la FFT utilisée pour la modulation et la démodulation du signal. Ce paramètre peut prendre les valeurs {1024, 2048, 4096, 8192}.
- $\boldsymbol{CP}$ - la taille du préfixe cyclique qui est utilisé comme intervalle de garde pour éviter les interférences inter-symboles crées par l'arrivée de réplique du signal retardé. Ce paramètre peut prendre les valeurs {1/4, 1/8, 1/16, 1/32}.
- $\boldsymbol{B}$ - la bande passante de la transmission. Ce paramètre peut prendre les valeurs {1.7, 5, 8} MHz.

Le triplet formé par ces paramètres est appelé **mode DVB-SH** dans cette étude. Comme indiqué, le standard prévoit l'utilisation de nombreux modes pour fournir aux opérateurs une flexibilité dans le déploiement d'un système DVB-SH.

Dans une transmission OFDM, les symboles sont transmis en parallèle sur N_{FFT} sous-porteuses. Il y a différents types de sous-porteuses :

- **Null** - correspondant à des sous-porteuses où la valeur des symboles transportées est mise à 0. En pratique, ces sous-porteuses Null servent de bande de garde pour limiter les interférences hors-bande du signal OFDM.
- **Data** - correspondant aux sous-porteuses transportant le signal TV. Les symboles transmis sont modulés par une modulation d'amplitude en quadrature à 4 ou 16 états.
- **Transmission Parameter Signaling** (TPS) - ces sous-porteuses transportent de l'information de signalisation sur la transmission en cours. Par exemple, le taux de codage canal, l'ordre de la modulation d'amplitude en quadrature des symboles Data, etc.
- **Pilot** - ces sous-porteuses sont modulées par un séquence pseudo-aléatoire binaire modulée en phase. L'amplitude des symboles pilotes est amplifiée d'un facteur 4/3 comparée aux symboles TPS. Il y a 2 sortes de symboles pilotes : les pilotes continus et les pilotes dispersés (voire la figure ci-dessous pour la répartition de ces 2 sortes de pilotes). Les pilotes sont utilisés pour les opération de synchronisation et d'égalisation du canal.

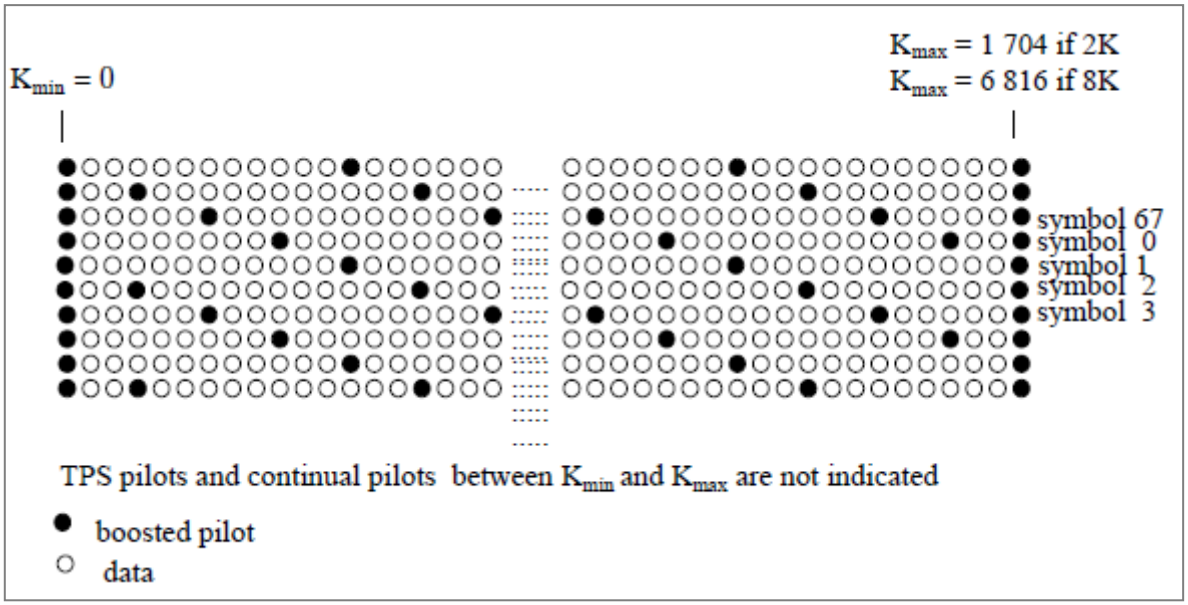

2.5 Modèle du signal OFDM transmis

L'ensemble de l'étude utilise le modèle de transmission suivant.

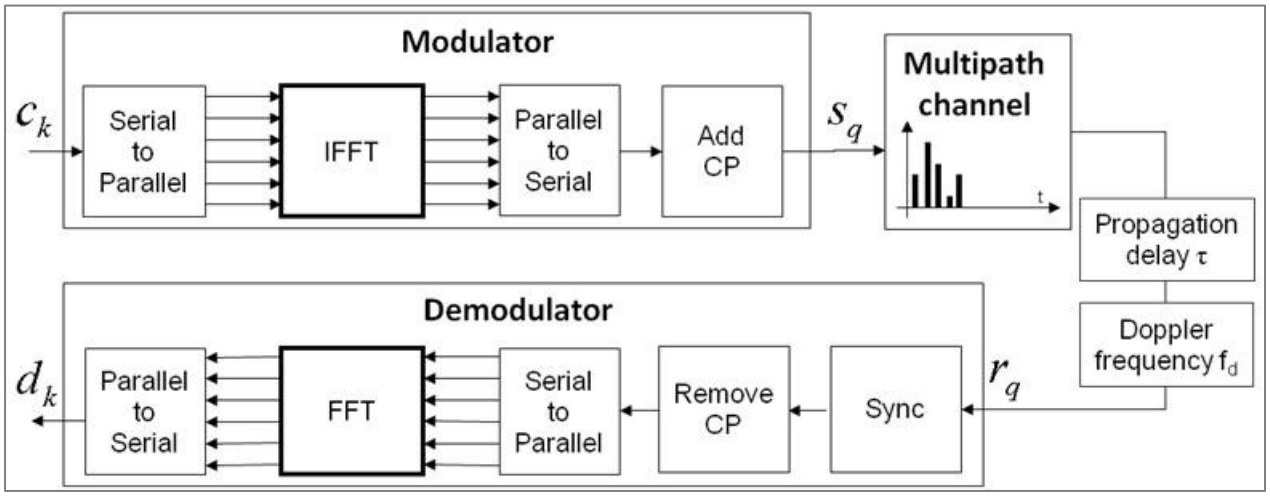

Ce modèle fait les hypothèses simplificatrices suivantes :

- absence de biais d'horloge d'échantillonnage,
- absence de filtre d'émission ou de réception,
- absence de distorsion du spectre dû à l'effet Doppler.

Après un certain nombre de calculs détaillés dans la section 2.3.5 de ce manuscrit, l'expression du signal démodulé dans des conditions de synchronisation fréquentielle parfaite est :

$$d_{l,k}(\Delta\tau, 0) = e^{j\varphi_0}.c_{l,k}.H_{l,k}.e^{-j2\pi\frac{k\Delta\tau}{N_{FFT}}}$$

où $d_{l,k}(\Delta\tau, 0)$ est la valeur du symbole démodulé sur la sous-porteuse k du symbole OFDM l, reçu avec une erreur résiduelle de synchronisation temporelle $\Delta\tau$;
$c_{l,k}$ est la valeur du symbole initialement transmis sur la sous-porteuse k du symbole OFDM l;
$H_{l,k}$ est la réponse fréquentielle du canal de propagation sur la sous-porteuse k à l'instant de transmission du symbole OFDM l;
φ_0 est une phase initiale aléatoire quelconque.

Cette équation sera le point de départ des méthodes présentées au cours de cette étude.

D.3. Estimation de pseudo-distance dans un système mono-émetteur

La stratégie de positionnement retenue dans cette étude est basé sur le principe de positionnement géométrique de la tri-latération, comme utilisé dans les systèmes GNSS. Par conséquent, une des étapes principales du positionnement est l'estimation de pseudo-distances.

La méthode d'estimation de pseudo-distance proposée est basé sur l'estimation de la réponse impulsionnelle du canal (RIC) de propagation. La distance entre l'émetteur et le récepteur sera dérivée du temps d'arrivée des différentes répliques du signal, qui seront observés à travers des pics présent dans la RIC. Par conséquent, une modélisation fine du RIC en environnement urbain est essentielle afin d'adapter les techniques d'estimation de la pseudo-distance à un cas réaliste.

Les différentes étapes de la technique de positionnement proposée sont décrites dans la figure suivante.

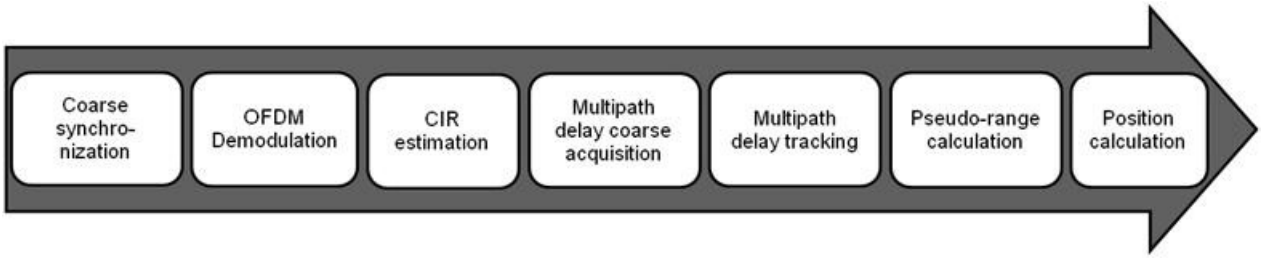

Les 2 premières étapes sont réalisées de manière conventionnelles, notamment via l'utilisation de techniques présentes dans les récepteurs OFDM classique.

Ce chapitre décrit les étapes suivantes :

- l'estimation du canal
- l'acquisition du retard des multi-trajets
- la poursuite du retard des multi-trajets
- le calcul de la pseudo-distance.

Le calcul de la position sera étudié dans un chapitre ultérieur.

D.3.1 Estimation du canal par corrélation

La RIC est estimée en calculant la corrélation du signal reçu avec un réplique local du signal attendu. Cette réplique locale n'est composée que des symboles pilotes sur les sous-porteuses pilotes, les autres sous-porteuses étant mises à une valeur nulle. La corrélation est calculée en utilisant des FFT et iFFT, ce qui utilise avantageusement l'opération de FFT réalisée pour démoduler le signal OFDM. Le schéma suivant montre le procédé de calcul de la corrélation.

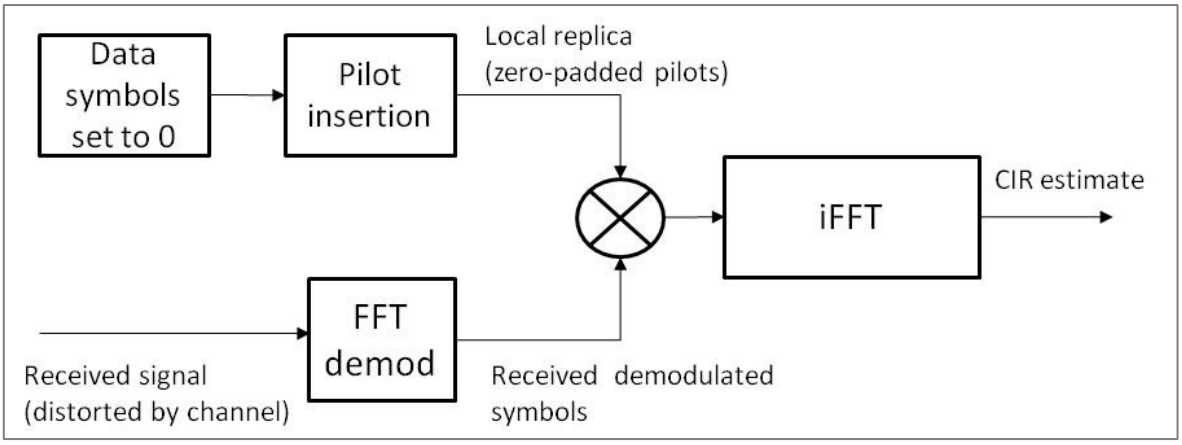

Après divers calculs détaillés dans la section 3.2 de ce manuscrit, on obtient la formule suivant décrivant la sortie de la corrélation :

$$R_l(\Delta t) = \frac{\sigma_p^2}{N_p}. \sum_{n=0}^{N_{taps}-1} \alpha_{l,n}(\Delta t). \frac{\sin(\pi\beta.(\tau_n + \Delta\tau - \Delta t)))}{\sin\left(\frac{\pi\beta}{N_p}.(\tau_n + \Delta\tau - \Delta t)\right)}$$

avec $R_l(\Delta t)$ la sortie du corrélateur lorsqu'il existe un retard Δt entre la réplique locale et le signal reçu à l'instant de réception du l-ième symbole OFDM;
$\alpha_{l,n}(\Delta t)$ un facteur complexe représentant notamment l''amplitude complexe du n-ième multitrajet;
N_{taps} le nombre de multitrajets présents dans le canal;
N_p est le nombre de symboles pilotes utilisés pour calculer la corrélation;
$\beta = 0.832$ est une constante dans le standard DVB-SH, indépendantes du mode DVB-SH utilisé;
σ_p^2 est la puissance des pilotes.

Dans le cas où la réplique locale n'est que très légèrement décalée par rapport au signal reçu, donc dans un cas de synchronisation acceptable $|\tau_n + \Delta\tau - \Delta t| \ll 1$, la corrélation peut être approximée par :

$$R_l(\Delta t) \approx \sigma_p^2 . \sum_{n=0}^{N_{taps}-1} \alpha_{l,n}(\Delta t) . \mathrm{sinc}(\pi\beta . (\tau_n + \Delta\tau - \Delta t)))$$

A travers cette expression, on peut conclure que la sortie du corrélateur est égale à un facteur près à la RIC convoluée par la fonction $\mathrm{sinc}(\ \ )$. Il s'agit donc d'une estimation du canal de propagation. Plus de détails et d'illustrations peuvent être trouvées à la section 3.2 de ce manuscrit.

3.2 Acquisition des retards des multitrajets par l'algorithme Matching Pursuit

A partir de l'estimation du canal de propagation obtenue par l'opération de corrélation, des méthodes d'extraction de paramètres des multitrajets peuvent être appliquées. Parmi d'autres, on peut notamment citer SAGE [Fleury 1999], ESPRIT [Paulraj 1985] ou Matching Pursuit [Cotter 2002].

Dans cette étude, le Matching Pursuit a été choisi. Cet algorithme est adapté à l'estimation du retard des multitrajets dans une RIC où les multitrajets sont fortement espacés, comme c'est le cas dans un SFN.

Le principe de l'algorithme est de minimiser l'erreur quadratique entre des mesures (le vecteur d'estimation du RIC obtenu par corrélation) et un modèle de multitrajets :

$$\hat{\rho}_l, \hat{\varphi}_l, \hat{\tau}_l = \arg \min_{\rho_l, \varphi_l, \tau_l} \sum_{k=1}^{K} \left\| \hat{h}(k) - \sum_{l=1}^{L} \rho_l e^{j\varphi_l} f(k - \tau_l) \right\|^2$$

où K est la longueur du vecteur d'estimation;
L est le nombre de multitrajets considérés;
$\hat{h}(k)$ est l'estimée de la RIC à l'instant d'échantillonnage k;
$f(k)$ est la valeur du modèle d'un multitrajet à l'instant k.

En utilisant des notation matricielle, on peut ré-écrire la formulation précédente :

$$\hat{\rho}_l, \hat{\varphi}_l, \hat{\tau}_l = \arg \min_{\hat{\rho}_l, \hat{\varphi}_l, \hat{\tau}_l} \left\| \hat{\mathbf{h}} - \mathbf{P}\boldsymbol{\beta} \right\|^2$$

où $\hat{\mathbf{h}} = [\hat{h}_1, \hat{h}_2, \dots, \hat{h}_K]$ est un vecteur contenant toutes les estimée de la RIC;
$\mathbf{P} = [\mathbf{P}_1, \mathbf{P}_2, \dots, \mathbf{P}_L]$ est une matrice KxL contenant les échantillons des modèle de multitrajet à différents instants;
$\mathbf{P}_l = [f(1 - \tau_l), f(2 - \tau_l), \dots, f(K - \tau_l)]^T$ est le modèle de multitrajet ayant un retard égal à τ_l;

$\boldsymbol{\beta} = \left[\rho_1 e^{j\varphi_1}, \rho_2 e^{j\varphi_2}, \ldots, \rho_L e^{j\varphi_L}\right]^{\mathrm{T}}$ est le vecteur comprenant les amplitudes complexes des L multitrajets considérés.

L'algorithme Matching Pursuit permet de trouver les délais $\hat{\tau}_l$. Plus de détails et d'illustrations sont présents dans la section 3.3 de ce manuscrit.

D.3.3 Poursuite des retards de multitrajets par boucle à verrouillage de phase

Après avoir acquis des estimations grossières du retard des principaux multitrajets présents grâce à l'algorithme Matching Pursuit, une phase de poursuite du retard de ces multitrajets est lancée à l'aide de boucles à verrouillage de phase (DLL, pour *Delay-Lock Loop* en anglais).

La DLL étudiée [Yang 1999] utilise 3 corrélateurs calculant la fonction de corrélation à 3 instants différents et les combinant afin d'obtenir une mise à jour des retards estimés. Le schéma ci-dessous illustre le principe de la DLL utilisée.

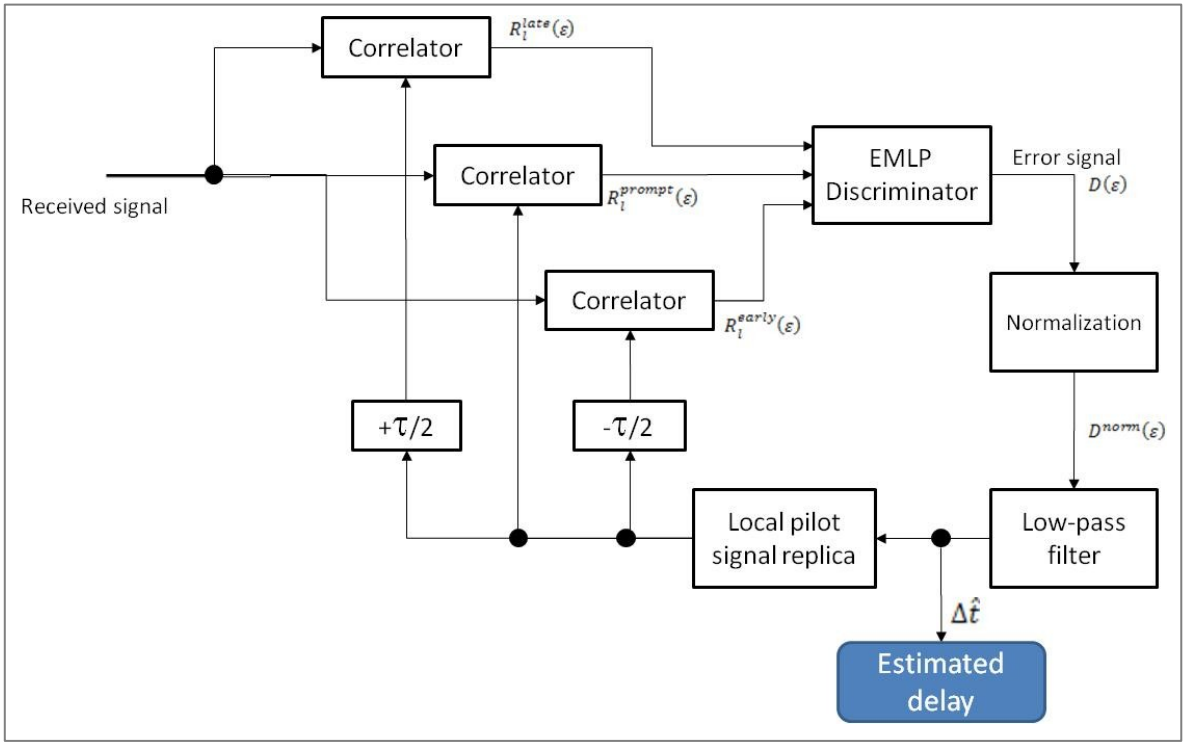

Le discriminateur utilisé dans cette DLL est de type "*Early minus Late Power*". Après normalisation, l'expression à la sortie du discriminateur dans le cas d'un multitrajet isolé est :

$$D(\varepsilon) = \frac{\pi^2\beta^2\frac{\delta^3}{16}}{1-\frac{\delta}{2}.\pi.\beta.\sin(\pi\beta\delta)-\cos(\pi\beta\delta)} \frac{sinc\left(\pi\beta.\left(\varepsilon-\frac{\delta}{2}\right)\right)^2 - sinc\left(\pi\beta.\left(\varepsilon+\frac{\delta}{2}\right)\right)^2}{sinc(\pi\beta\varepsilon)^2}$$

où δ est l'espacement entre les corrélateurs Early et Late.

La sortie du corrélateur est passé dans un filtre de boucle, défini en accord avec [Stephens 1995]. Ce filtre de boucle est défini par 3 paramètres : le temps en chaque estimé T_i, l'ordre de la boucle de la DLL et la bande de bruit de la boucle B_l.

La variance de l'erreur d'estimation du retard en sortie de boucle est donnée par la formule suivante [Serant 2010] :

$$Var(\Delta\hat{t}) = 2B_l T_{symb} \frac{K_1}{SNR}\left(1 + \frac{K_2}{SNR}\right)$$

où SNR est le rapport de puissance entre le multitrajet et le bruit du récepteur;

$K_1 = \frac{9}{4}.\frac{(1-sinc(\pi\beta\delta))sinc\left(\frac{\pi\beta\delta}{2}\right)^2}{N_p.K_{norm}^2}$

$K_2 = \frac{9}{32}.\frac{1+sinc(\pi\beta\delta)}{N_p sinc(\frac{\pi\beta\delta}{2})}$

En traçant la variance de l'estimateur en fonction du SNR, on observe des performances d'estimation inférieur au mètre pour des SNR supérieur à -15 dB. Or dans un système DVB-SH typique, on peut s'attendre à ce que le SNR reçu soit supérieur à 0 dB dans le pire des cas. Cela signifie que l'on peut espérer utiliser des émetteurs lointains pour faire des mesures de retards, et que cette méthode marchera à l'intérieur des bâtiments.

D.3.4 Techniques de fenêtrage

Un des principaux problèmes de la méthode présentées est la présence de lobes secondaires dans l'estimation de la RIC. Ces lobes secondaires sont à l'origine de 2 problèmes :

1. Il y a un risque de poursuivre un lobe secondaire au lieu du lobe principal si la DLL n'est pas correctement initialisée;
2. En présence de plusieurs multitrajets, la poursuite d'un retard sera affectée par ces multitrajets même si un retard relatif important existe. Cela sera un problème notable dans le cas des SFN, où l'effet Proche-Lointain apparaît. Cet effet est expliqué ultérieurement.

Afin de réduire ces lobes secondaires, des techniques de fenêtrage peuvent être utilisées. Dans ce cas, lors du calcul d'une corrélation, la réplique locale est pondérée par une fenêtre :

$$R_l^{window}(\Delta t) = \frac{1}{N_p}\sum_{q\in\mathcal{P}} c_{l,q}.p_{l,q}^*(\Delta t).w_{window}(q)$$

où $w(q)$ est une fonction de fenêtrage.

Deux fenêtres ont été considérées :

- la **fenêtre de Hamming**

$$w_{Ham}(q) = 0.53836 - 0.46164\cos\left(\frac{2\pi q}{K-1}\right)$$

- la **fenêtre de Blackman-Harris**

$$w_{BH}(q) = 0.35875 - 0.48829\cos\left(\frac{2\pi q}{K-1}\right) + 0.14128\cos\left(\frac{4\pi q}{K-1}\right) - 0.01168\cos\left(\frac{6\pi q}{K-1}\right)$$

où K est le nombre de sous-porteuse non-nulles dans le signal DVB-SH reçu.

Le cas sans fenêtrage est équivalent à une **fenêtre rectangulaire** : $w(q) = 1$.

La figure suivante montre la forme du pic de corrélation pour les différents fenêtrages.

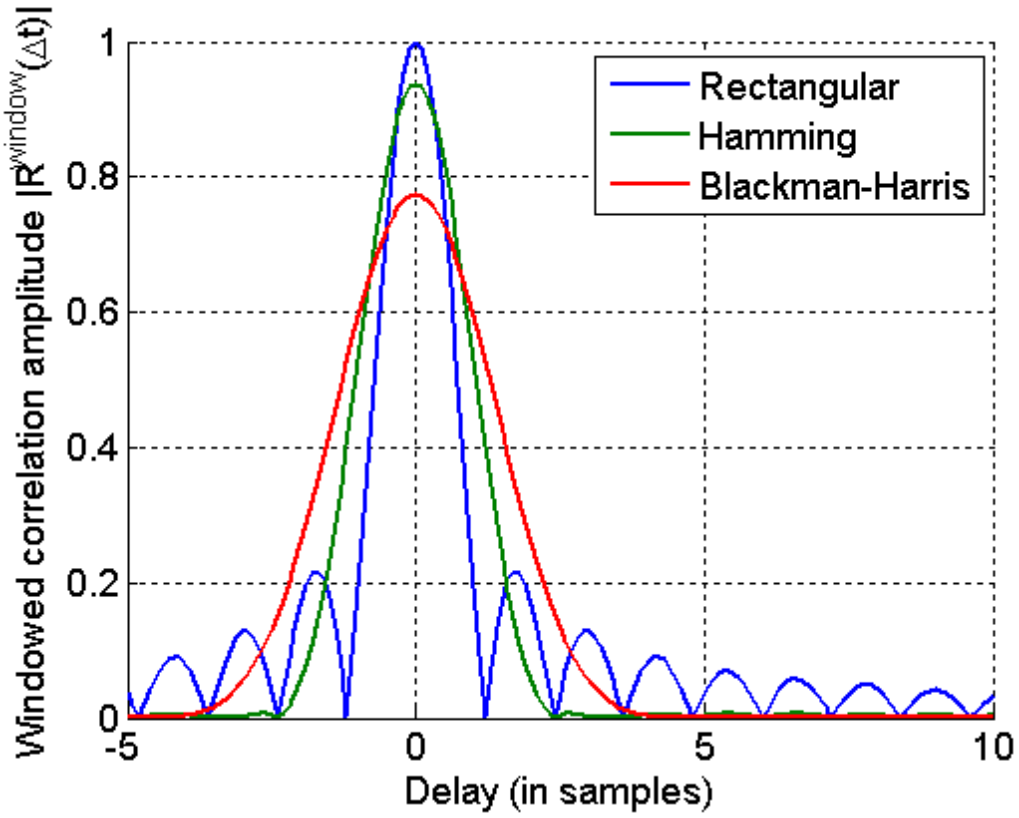

L'utilisation d'une fenêtre diminue les lobes secondaires au prix d'un élargissement du lobe principal. Cela aura notamment un impact sur la précision de la poursuite du pic de corrélation par la DLL, comme démontré dans la section 3.5 de ce manuscrit.

D.3.5 Stratégie d'estimation de la pseudo-distance

Les techniques précédemment décrites permettent d'obtenir :

- une estimation grossière du retard des multitrajets dans un canal multitrajet (algorithme du Matching Pursuit);
- une estimation fine du retard des multitrajets (DLL fenêtrée)

Afin de fonctionner en environnement urbain, l'utilisation de ces techniques doit prendre en compte les particularités du canal de propagation urbain : la présence de plusieurs répliques du signal reçu affectées d'évanouissements profonds et rapides, l'apparition ou la disparition de ces répliques lors du mouvement du récepteur, le blocage du signal LOS. Ces particularités créent un véritable défi pour l'estimation de la pseudo-distance en environnement urbain.

Afin de prendre en compte ces particularités, la stratégie d'estimation de pseudo-distance suivante est proposée :

1. Acquisition : l'algorithme Matching Pursuit est déroulé afin d'estimer les principaux piques de la fonction de corrélation. Une estimation de l'amplitude de ces piques est également réalisée grâce au Matching Pursuit, afin de ne conserver que le retard des répliques les plus significatives en termes de puissance.
2. Poursuite : pour chaque retard estimé lors de la phase précédente, une DLL est lancée. Par conséquent, plusieurs DLL fonctionneront en parallèle à chaque instant.
3. Exclusion de DLL : afin de garder le nombre de DLL bas, des processus d'exclusion de DLL sont implémentés. Une DLL est arrêtée en fonction de l'amplitude du multitrajet poursuivi, de la convergence du retard d'un multitrajet vers un multitrajet déjà poursuivi, ou de la divergence de la poursuite du multitrajet.
4. Acquisition périodique : un nouvel algorithme Matching Pursuit est lancé périodiquement afin de maximiser les chances de poursuivre la réplique du signal arrivant le plus tôt (et donc la plus proche du signal LOS), au cas où elle n'était pas présente lors du Matching Pursuit précédent, ou si elle avait été perdue lors de la phase de poursuite.
5. Calcul de la pseudo-distance : à chaque instant, la pseudo-distance estimée est calculée en prenant en compte le retard du multitrajet le plus faible. Cela devrait minimiser l'erreur due à la poursuite d'une réplique NLOS.

Cette stratégie d'estimation de la pseudo-distance est montrée dans la figure ci-dessous. Plus de détails sur l'implémentation de cette stratégie peuvent être trouvés dans la section 3.6.2 de ce manuscrit.

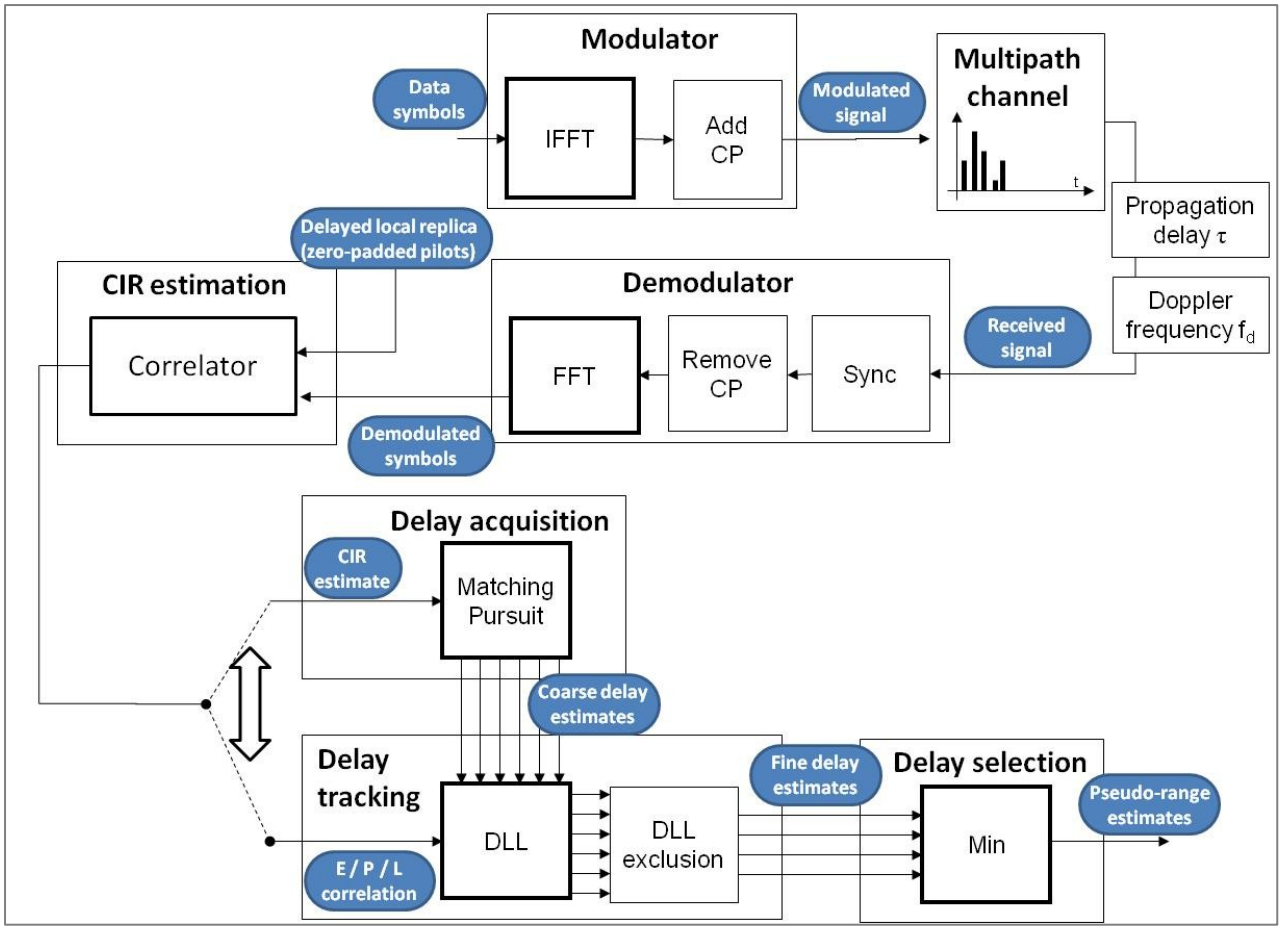

Des résultats de simulation de cette stratégie sont montré dans la section 3.7 de ce manuscrit.

D.3.6 Conclusion sur l'estimation de pseudo-distance dans un système mono-émetteur

Dans ce chapitre, les différentes étapes de la méthode d'estimation de pseudo-distance proposée ont été exposée. Elles sont rappelées dans le schéma suivant :

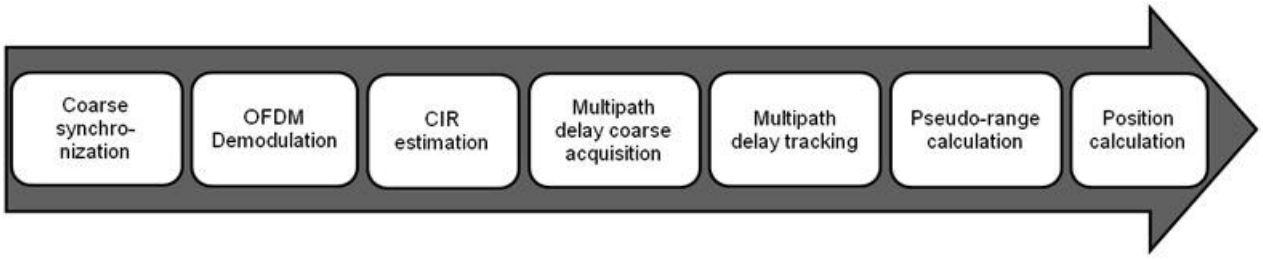

Après des traitements conventionnels du signal OFDM (synchronisation et démodulation par FFT), l'estimation de pseudo-distance est réalisée en 3 étapes :

- **Une phase d'acquisition des retards**, basée sur l'estimation de la RIC par corrélation et l'algorithme Matching Pursuit
- **Une phase de poursuite des retards**, basée sur l'utilisation de DLL multiples

- **Une phase de sélection des retards** pour le calcul de la pseudo-distance.

La phase de poursuite des retard peut bénéficier de l'utilisation de technique de fenêtrage afin de diminuer l'influence des multitrajets sur la poursuite.

Une stratégie de combinaison des ces différents outils de traitement du signal a été mise en place afin de minimiser les ressources nécessaires pour réaliser l'estimation de pseudo-distance, mais également pour prendre en compte les particularités du canal de propagation urbain. Elle consiste notamment à relancer de manière périodique des phases d'acquisition afin de poursuivre le plus souvent possible un signal proche du chemin de visée direct.

La méthode proposée a été appliquée à un modèle de canal urbain (TU-20) et a donné de résultats intéressant, avec une erreur moyenne sur l'estimation de la pseudo-distance entre 3 et 26m, et un écart-type de l'erreur entre 17 et 50m. Ces performances doivent être mis en regard du modèle de canal de propagation très particulier qui a été utilisé. Des simulations supplémentaires avec un canal de propagation plus réaliste ou sur des signaux réels sont nécessaires afin de mieux caractériser l'erreur sur la pseudo-distance estimée.

D.4. Estimation de la pseudo-distance dans un système multi-émetteur

Le chapitre précédent a décrit une méthode afin d'obtenir la pseudo-distance d'un émetteur. Toutefois, afin d'obtenir une position, les pseudo-distances de plusieurs émetteurs sont nécessaires (au moins 3 pour une position 2D).

Le système DVB-SH utilise un réseau d'émetteurs particulier appelé Single Frequency Network (SFN). Ce réseau d'émetteurs crée des difficultés pour la discrimination et l'identification des émetteurs, puisque le même signal est émis sur la même fréquence porteuse et de manière synchronisée par chaque émetteur.

Ce chapitre propose une solution pour permettre la discrimination d'émetteurs dans ce contexte. Les difficultés de discrimination des émetteurs dans un SFN seront présentées dans un premier temps, suivi d'une solution pour permettre cette discrimination. Une technique de discrimination basée sur un algorithme de clustering sera présentée. Enfin, des résultats de simulation d'estimation de pseudo-distance dans un SFN seront montrées, utilisant des mesures de RIC dans un SFN réel.

D.4.1 Condition requise sur la réponse impulsionnelle du canal de propagation pour permettre l'estimation de pseudo-distance dans un cas multi-émetteurs

Dans cette section, on suppose que les émetteurs sont parfaitement synchronisés. Les problèmes associés à l'utilisation d'un SFN sont de 2 types :

- **l'effet Proche-Lointain** (Near-Far effect en anglais) :la distance relative entre le récepteur et les différents émetteurs du réseau varie grandement au cours du déplacement du récepteur. Notamment, il peut arriver que l'on se retrouve proche d'un émetteur alors qu'on est loin d'un autre. Dans ce cas, l'émetteur proche masquera les signaux arrivant des émetteurs plus lointains.

- **le chevauchement des RIC** : les multitrajets arrivant de plusieurs émetteurs peuvent arriver simultanément au récepteur. Cela rend la discrimination des émetteurs impossibles car le récepteur ne pourra pas savoir de quel émetteur provient une réplique.

Ces 2 phénomènes sont amplifiés par le processus d'estimation de la RIC par corrélation, qui transforme un dirac de la RIC du SFN en un sinus cardinal dans l'estimation de la RIC. Les lobes secondaires du sinus cardinal augmentent à la fois l'effet Proche-Lointain et le chevauchement des RIC.

Ces phénomènes sont illustrés dans l'image suivante, qui montre la sortie de l'estimation de canal au cours du temps dans un scénario où le récepteur se déplace dans un réseau à 3 émetteurs. A certains endroits, il est difficile voire impossible d'attribuer un pics de corrélation à un émetteur particulier.

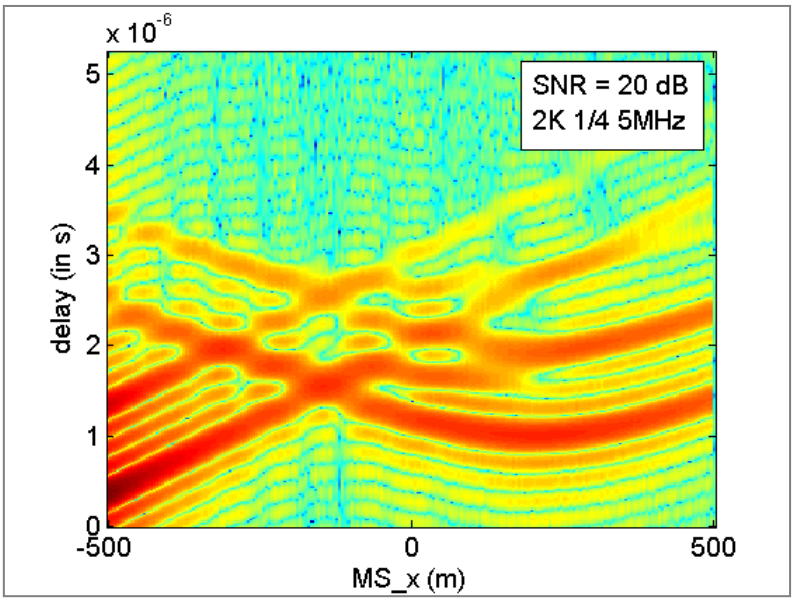

Une solution pour diminuer l'effet Proche-Lointain est d'utiliser des techniques de fenêtrage, telles que présentées dans le chapitre précédent. Le fenêtrage va effectivement diminuer les lobes secondaires dans l'estimée de canal, réduisant ainsi l'influence d'un émetteur sur les autres.

Afin de résoudre le problème du chevauchement des RIC, l'introduction de retards artificiels à l'émission des signaux a été proposée [Thevenon 2009-1]. Cette modification consiste à retarder l'émission du signal avec un retard différent pour chaque émetteur. Cette modification ne devrait pas affecter le service de diffusion de la télévision, car comme vu précédemment, un récepteur OFDM est capable de recombiner des répliques retardées du même signal, tant que le retard des répliques est inférieur à la capacité d'égalisation du récepteur, donnée par la durée du préfixe cyclique dans le cas des signaux OFDM.

L'utilisation des retards artificiels est également prévue dans le standard DVB-SH et peut donc être appliquée sans modification majeure du standard.

Pour illustrer l'apport de ces techniques, les 2 images suivantes sont utilisées. Sur l'image de gauche, un retard artificiel différent pour chaque émetteur a été appliqué, ce qui permet de séparer

les pics de corrélation provenant des différents émetteurs. On peut néanmoins observer qu'au début de la trajectoire, il y a encore un chevauchement des RIC.

Sur la figure de droite, une fenêtre de Blackman-Harris a été appliquée à la corrélatoin, réduisant ainsi les lobes secondaires des pics de corrélation. On peut observer que cela résout le problème de chevauchement des RIC rencontré au début du déplacement sur la figure de gauche.

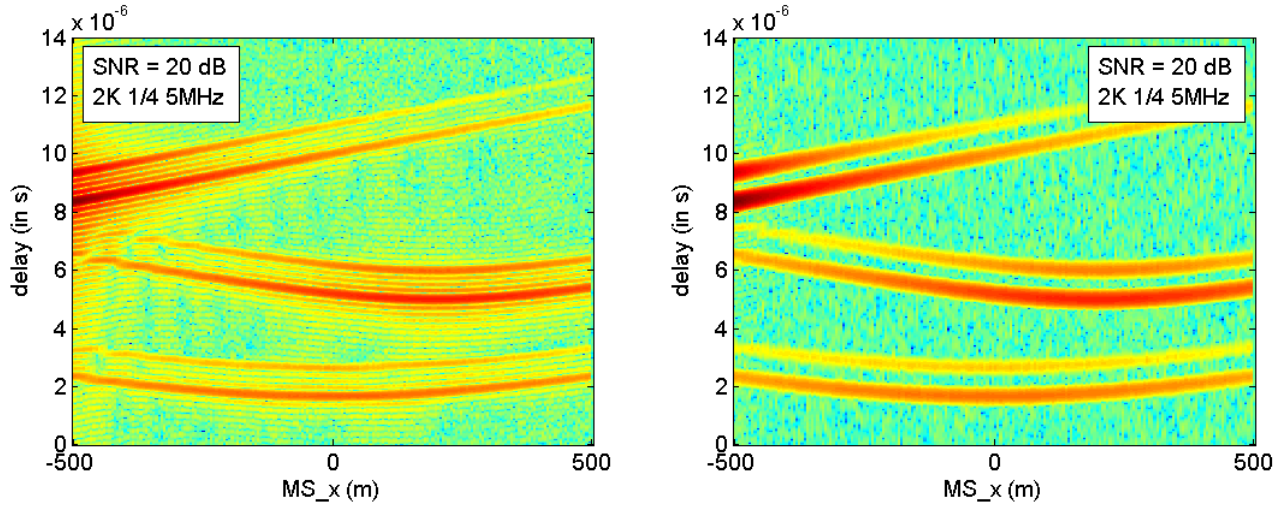

L'introduction de retard artificiel est une modification qui s'effectue au niveau du système. Une fois que le réseau d'émetteur a été modifié, la méthode d'estimation des pseudo-distance présentée dans le chapitre précédent peut être utilisée, en ajoutant une étape supplémentaire permettant la discrimination des émetteurs avant de passer à la phase de sélection du retard pour le calcul de la pseudo-distance. Cette étape supplémentaire est montrée sur le schéma suivant.

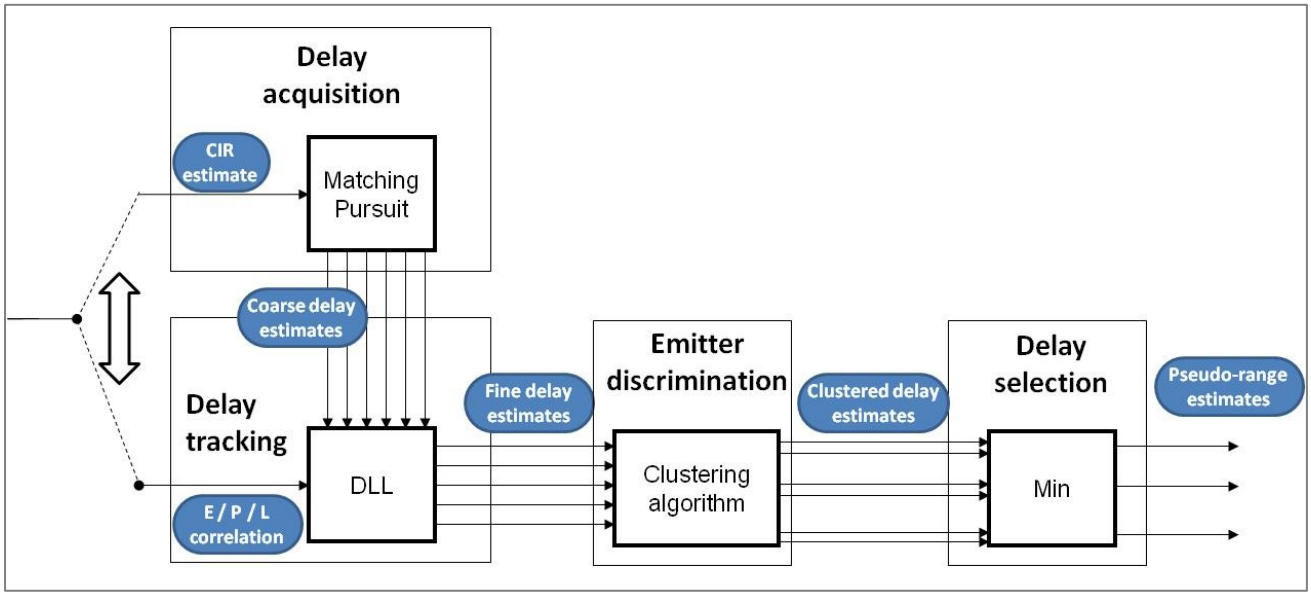

D.4.2 Discrimination des émetteurs dans la réponse impulsionnelle du canal

Tous les multitrajets associé au même émetteur devrait arriver au récepteur dans une plage de retard restreinte. Cela vient du fait que la plupart des multitrajets arrivant au récepteur sont crée par l'environnement proche du récepteur, à quelques dizaine voire centaine de mètres du récepteur, se traduisant par des retards de multitrajet de l'ordre de la micro-seconde.

Il est donc possible de regrouper les différents retards estimés en différents groupes appartenant à différents émetteurs. Afin de réaliser cette étape, des algorithmes de clustering classiques ont été utilisés. Ils sont décrits et illustrés en détail dans la section 4.2 de ce manuscrit.

D.4.3 Simulation de l'estimation de pseudo-distances dans un SFN modifié

Afin de tester la technique proposée d'estimation de pseudo-distance dans un cas multi-émetteurs, une série temporelle de RIC rencontrée dans un SFN est nécessaire. Malheureusement, aucun modèle de canal de propagation SFN satisfaisant n'a été trouvé dans la littérature. Il a donc été décidé d'utilisé des mesures faites en environnement réelles.

Ces mesures ont été réalisées par le CNES dans le cadre du projet S-DMB (une étude de pré-standardisation du DVB-SH). Les mesures utilisées ont été réalisée à Auch, en France (environ 20000 habitans) avec 2 émetteurs terrestres et un hélicoptère simulant une transmission satellite. Les différents émetteurs émettaient des signaux à 2.2 GHz de manière synchronisées, afin de simuler un SFN, et un camionnette se déplaçant en ville a réalisé la mesure du sondage de canal.

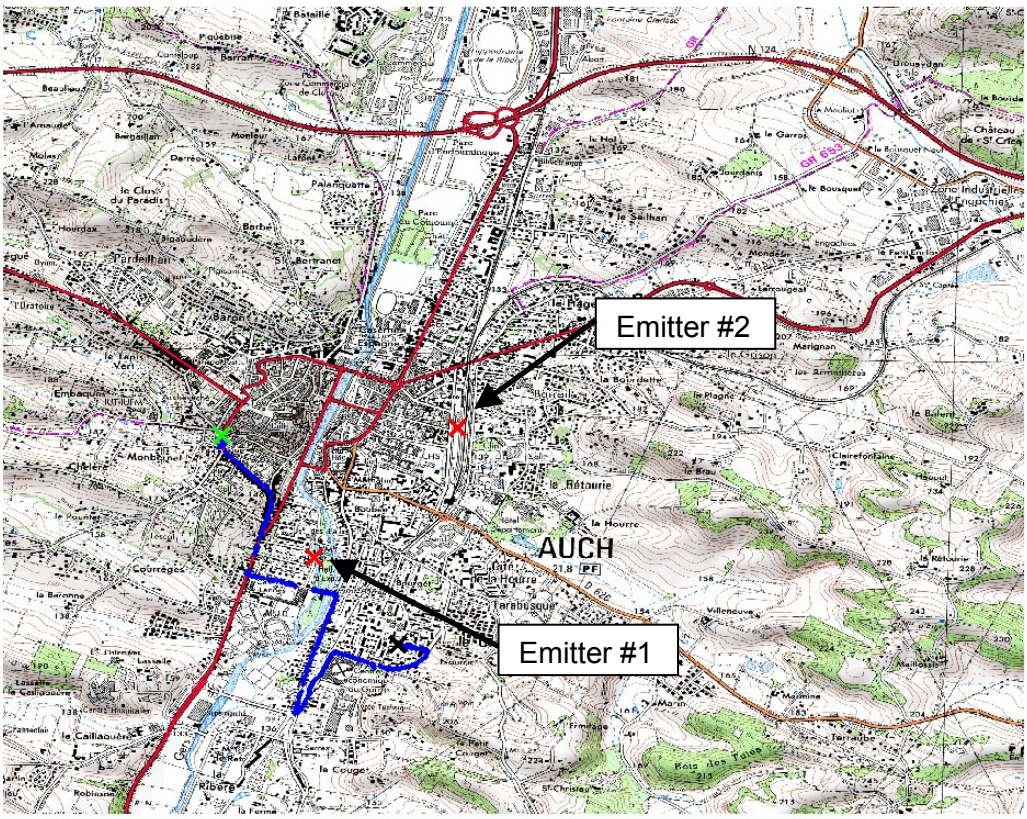

Après application d'un retard artificiel adéquat, le retard des différents multitrajets mesurés suive la courbe suivant.

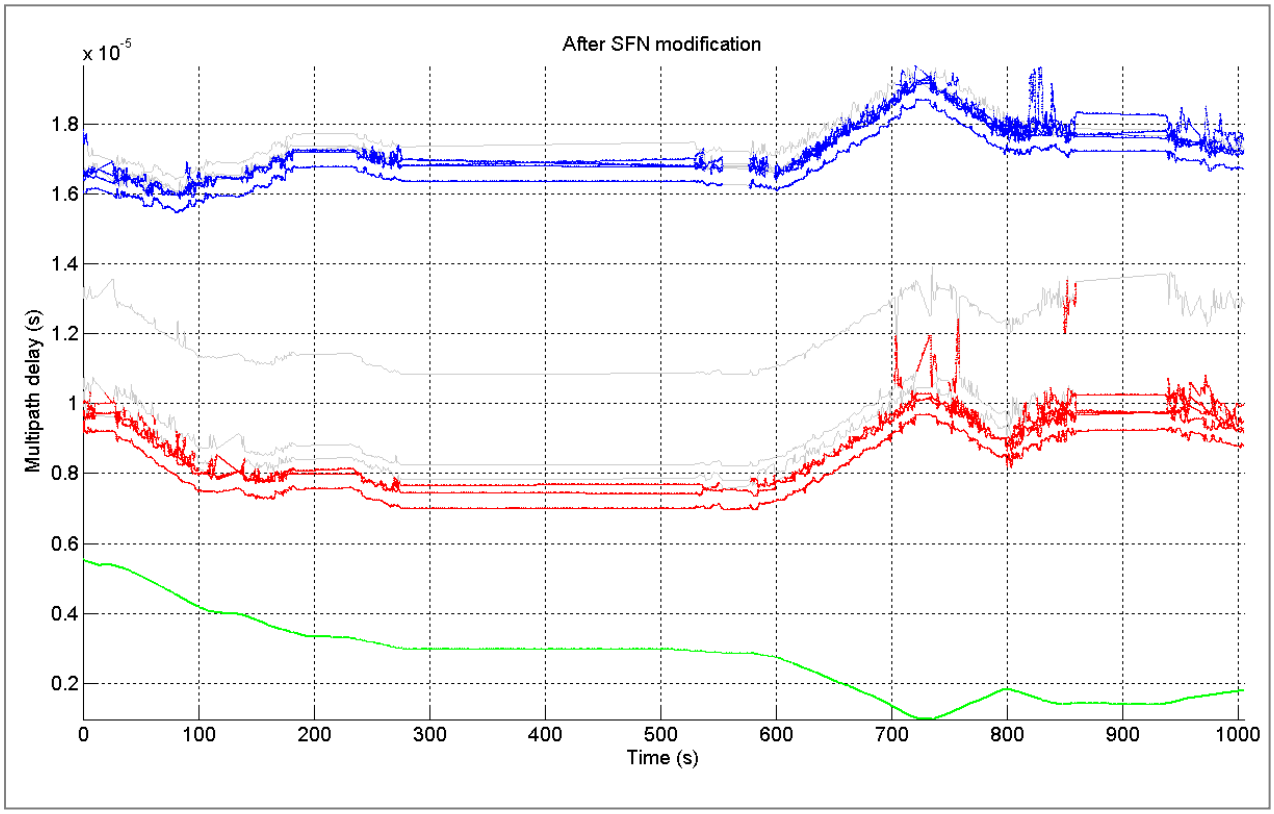

Ce canal a été appliqué à un signal OFDM, et la technique d'estimation de pseudo-distance proposée a été appliquée. L'impact de la technique de fenêtrage est étudié à travers 3 simulations.

Les paramètres communs aux 3 simuluations sont résumés dans les tableaux 16 et 17 du manuscrit.

L'image de l'estimée de canal par corrélation est montrée ci-dessous pour les 3 fenêtres étudiées. On peut observer qu'avec la fenêtre rectangulaire, l'effet Proche-Lointain est problématique pour la poursuite de l'émetteur #3 (l'émetteur satellite) et devrait affecter également l'émetteur #2 à travers les lobes secondaires très élevés provenant de l'émetteur #1.

L'utilisation de fenêtrage permet de résoudre ce problème d'effet Proche-Lointain. Néanmoins, l'élargissement du lobe principal par le fenêtrage devrait dégrader la précision de la détection du pic de corrélation, ainsi qu'augmenter la sensibilité des DLL dans le cas de multitrajets proche.

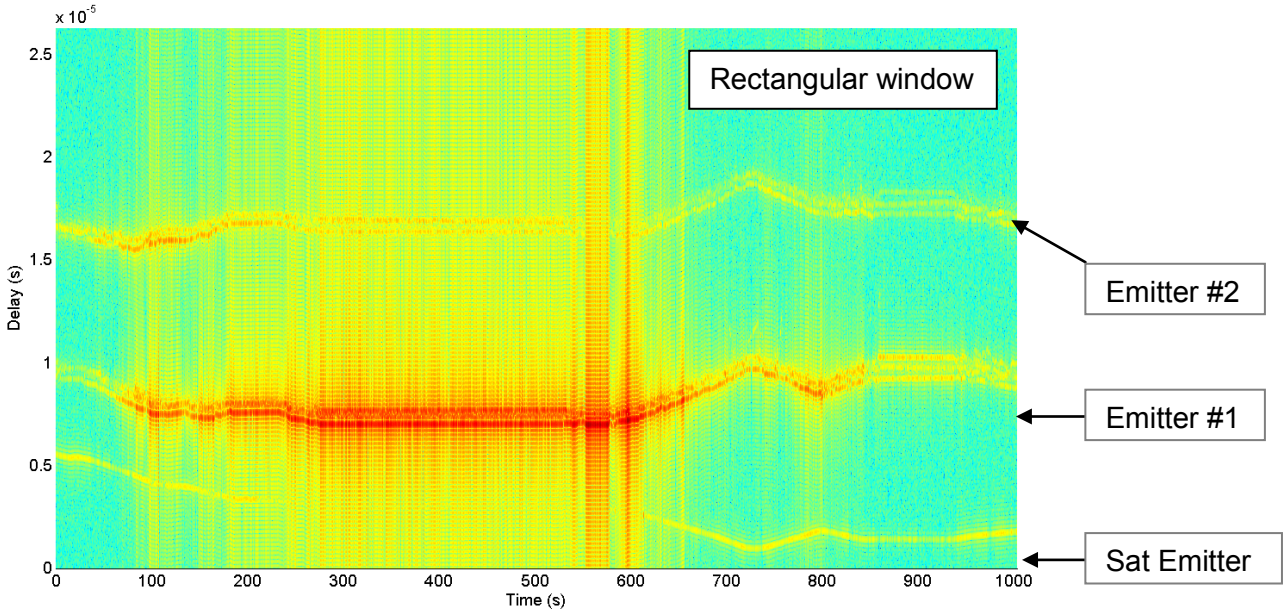
x 10^-5
Rectangular window
Emitter #2
Emitter #1
Sat Emitter
Delay (s)
Time (s)

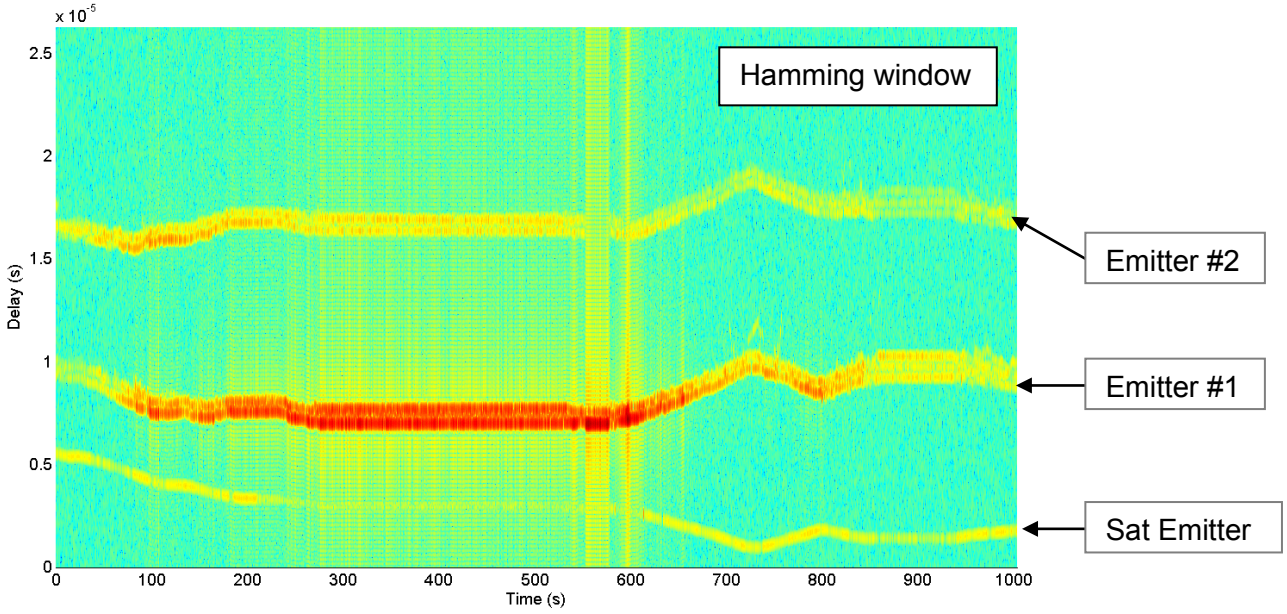
x 10^-5
Hamming window
Emitter #2
Emitter #1
Sat Emitter
Delay (s)
Time (s)

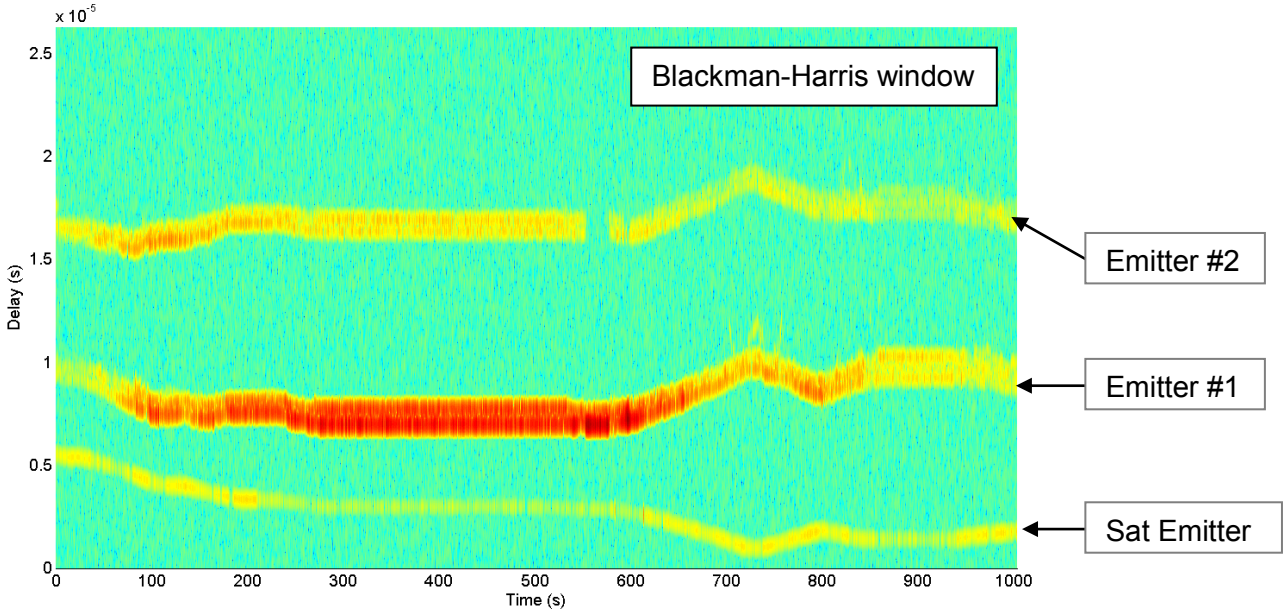
x 10^-5
Blackman-Harris window
Emitter #2
Emitter #1
Sat Emitter
Delay (s)
Time (s)

Les résultats détaillés de chaque simulation se trouvent dans la section 4.3.2. On peut résumer les principaux résultats de la façon suivante :

- La discrimination des émetteurs fonctionnent correctement. Les algorithmes de clustering permettent de différentier les multitrajets provenant des différents émetteurs.
- L'effet Proche-Lointain affecte la disponibilité de l'émetteur #3 dans le cas des simulation #1 et #2. L'utilisation de la fenêtre de Blackman-Harris permet de s'affranchir de ce problème.
- Pour les simulations #1 et #2, les pseudo-distances estimées des émetteurs terrestres sont souvent affectées d'une large erreur négative due à la poursuite d'un lobe secondaire présent en avance par rapport au lobe principal du pic de corrélation. Ce problème est résolu par l'utilisation de la fenêtre de Blackman-Harris.
- Les pseudo-distances estimées des émetteur terrestres sont souvent affectées par des sauts vers des valeurs supérieures. Cela correspond à des phases de la poursuite où des multitrajets proches et significatif sont présents, et où la poursuite du pic de corrélation passe d'un multitrajet à l'autre. Ce phénomène est accentué par l'utilisation de la fenêtre de Blackman-Harris, à cause de l'élargissement du lobe principal de la fonction de corrélation induit par l'utilisation du fenêtrage.
- D'un point de vue quantitatif, les pseudo-distances estimées sont parfois affectées d'erreurs de plusieurs dizaines voire centaines de mètres. Néanmoins, sur des portions de la série temporelle étudié, l'estimation de pseudo-distance présente des performances intéressantes. Le tableau suivant récapitule les statistiques d'erreur sur l'estimation des pseudo-distances pour les différentes simulations, sur une tranche de 100s.
  Dans la simulation #3, on peut observer des biais inférieurs à 5m et des écart-type d'erreur inférieur à 20m pour le cas de l'émetteur le plus difficile à traiter.

Comparaison des performances d'estimation des pseudo-distances dans le cas multi-émetteurs

	Mean error (m)			**Error standard deviation (m)**		
	Simu #1	Simu #2	Simu #3	Simu #1	Simu #2	Simu #3
Emitter #1	25.7	29.3	4.1	110.0	61.3	19.6
Emitter #2	1.2	0.3	2.0	5.7	2.0	5.6
Emitter #3 (sat)	0.1	0.004	0.001	1.4	0.3	0.6

D.4.4 Conclusion sur l'estimation de la pseudo-distance dans un système multi-émetteurs

La technique d'estimation dans un système multi-émetteurs proposée a été testé dans un cas réaliste utilisant des mesures de canal de propagation d'un système SFN réel. Bien qu'affecté d'erreurs particulières, la technique proposée semble viable et les performances obtenues intéressantes, comme indiqué dans l'analyse des résultats de simulations dans le paragraphe précédent.

Néanmoins, l'erreur sur l'estimation de pseudo-distance est calculée comme l'écart entre le premier retard estimé et le retard du premier multitrajet provenant d'un émetteur présent dans les mesures. Or les mesures fournies ne donnent pas d'information sur le fait que le premier multitrajet corresponde au signal LOS. La caractérisation de l'erreur NLOS ne peut donc pas être faite à ce niveau, mais sera étudié dans un chapitre ultérieur.

Par ailleurs, les performances ont été obtenues sur une simulation d'une durée de 1000s, dans un canal de propagation particulier. Afin d'avoir un modèle valide d'erreur des pseudo-distances, d'autres simulations sont nécessaires.

Enfin, la technique d'estimation des pseudo-distances pourrait être améliorer par plusieurs moyens :

- **Détection des sauts dans l'estimation des pseudo-distance.** Les sauts affectant l'estimation des pseudo-distances sont de l'ordre de plusieurs dizaines voire centaines de mètres. Ils pourraient facilement être détectés, et un processus de ré-acquisition pourrait être lancé à ce moment.
- **Utilisation adaptative des techniques de fenêtrage.** L'utilisation d'une fenêtre à forte atténuation des lobes secondaires est bénéfique dans certains cas (en présence d'un brouillage d'un émetteur voisin dans le cas d'un effet Proche-Lointain), mais apporte des dégradations dans d'autres cas (en présence de multitrajets proches provenant du même émetteurs). Par conséquent, le passage d'une technique de fenêtrage à une autre pourrait améliorer l'estimation de pseudo-distances.
- **De meilleures techniques d'acquisition.** La poursuite de lobes secondaires au lieu du lobe principal est due à une mauvaise initialisation des DLL faite par l'algorithme Matching Pursuit. D'autres techniques d'extraction des paramètres de la RIC pourraient être testés, comme les algorithmes SAGE [Fleury 1999] ou ESPRIT [Paulraj 1995].
- **Etude de l'impact de la bande des DLLs.** Dans cette étude, la seule valeur de bande de boucle a été 10 Hz. Des études ultérieures sont nécessaires afin de déterminer l'impact de la bande de boucle sur la performance de l'estimation des pseudo-distances. En plus d'une variance théorique de l'estimateur plus faible, la réduction de la bande de boucle pourrait apporter une robustesse plus importante contre les multitrajets ou les fadings.
- **Technique de mitigation des multitrajets.** D'autres techniques de mitigation des multitrajets pourraient être étudiées, telle que la ME-DLL [van Nee 1992][Yang 1999].

D.5. Identification des émetteurs

Après la discrimination des multitrajets en fonction de leur émetteurs d'origine et l'estimation des pseudo-distances, le récepteur a à sa disposition plusieurs pseudo-distances "anonymes", i.e. pour lesquelles il ne connaît pas l'émetteur d'origine. Or, il a besoin d'associer les pseudo-distances anonymes à des émetteurs afin de calculer sa position. C'est ce que cette étude nomme **l'identification des émetteurs**.

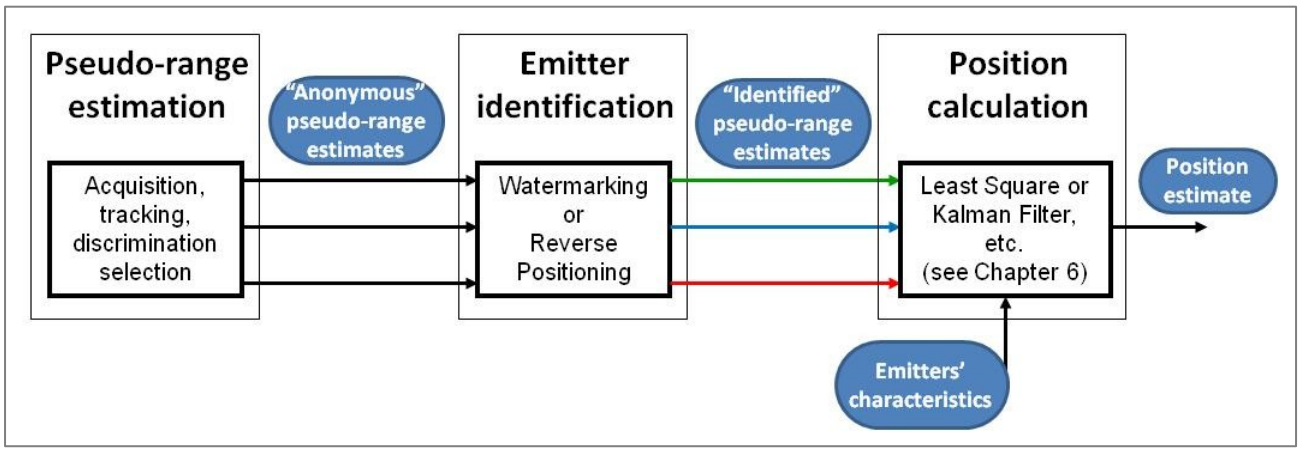

Dans ce chapitre, on suppose que les caractéristiques des émetteurs (positions et retards artificiels) sont connus du récepteur. Cela peut être le cas grâce à une base de données dans la mémoire du récepteur ou accessible via un lien télécom.

Deux techniques d'identification des émetteurs ont été étudiées :

- **la technique de Watermarking**, qui est une technique conventionnelle et déjà standardisée dans certains standards utilisant un SFN;
- **la technique de Positionnement Inversé**, qui est proposée dans le cadre de cette étude.

D.5.1 Identification des émetteurs par Watermarking

La technique de Watermarking consiste à introduire un signal d'identification émis dans la même bande que le signal utile (ici, le signal de télévision). Le signal d'identification est un séquence pseudo-aléatoire transmise avec une puissance très faible afin de ne pas dégrader la démodulation du signal utile. Chaque émetteur contient son propre signal d'identification.

Cette technique a été étudiée dans [Wang 2003] et [Wang 2007], et a été adoptée dans le standard américain de télévision numérique [ATSC 2007].

La section 5.1 de ce manuscrit décrit l'étude qui a été faite dans le cadre de cette thèse. Les principales étapes de cette étude sont :

1. La modélisation du signal transmis par chaque émetteur
2. Le traitement du signal reçu pour l'identification des émetteurs
3. L'expression des performances de détection en fonction de la distance entre le récepteur et un émetteur
4. La détermination de la couverture du réseau sur laquelle un récepteur sera capable d'identifier plusieurs émetteurs.

La conclusion sur cette technique de Watermarking est qu'elle n'est pas satisfaisante pour les besoins liés à un service de localisation. En effet, les signaux d'identification sont grandement affectés par l'effet Proche-Lointain, ce qui rend impossible l'identification d'émetteurs lointains lorsque le récepteur est proche d'un émetteur.

Des traitements particuliers pourraient pallier à ces limitations. Néanmoins, cela augmenterait encore les modifications nécessaires pour déployer le service de localisation, rendant son adoption par les opérateurs encore plus coûteuse. Nous jugeons donc que l'utilisation de signaux de Watermarking n'est pas appropriée à la méthode de positionnement proposée.

D.5.2 Identification des émetteurs par technique de Positionnement Inversé

La deuxième technique d'identification des émetteurs propose d'utiliser les caractéristiques des émetteurs (position et retard artificiel), un position approximative du récepteur et les pseudo-distances anonymes pour identifier les pseudo-distances, c'est-à-dire les associer avec un émetteur.

La section 5.2 de ce manuscrit décrit en détail cette technique, qui est basé sur la définition d'une fonction de coût à minimiser. Cette fonction de coût est définie comme la différence quadratique entre les pseudo-distances anonymes et un modèle des pseudo-distances reçues (comprenant les retards artificiels) par un émetteur placé à la position approximative. Cette fonction de coût est calculée pour chaque permutation possible d'association entre pseudo-distances anonymes et

émetteurs. Grâce à la valeur importante des retards artificiels, seule une association minimise la fonction de coût, si l'on a pris soin d'éviter les zones iso-retards sur la couverture de système.

Les performances de cette technique sont évaluées par simulation dans un cas simple de SFN hexagonal, et la sensibilité aux différentes sources d'erreurs est estimée.

La principale source d'erreur est l'erreur faite sur la position d'assistance fournie au récepteur. De plus, une autre limitation de la méthode présentée est l'explosion combinatoire se produisant lorsqu'un grand nombre de pseudo-distances sont reçues. Cette explosion combinatoire pourrait être réduite en prenant en compte la puissance des signaux reçus pour chaque pseudo-distance, qui lèverait l'ambiguité sur un certain nombre de combinaison à tester.

Néanmoins, sous certaines hypothèses qui semblent acceptables, cette technique produit d'excellent résultats d'identification des émetteurs.

D.5.3 Conclusion sur les techniques d'identification des émetteurs

La technique de Watermarking est une technique d'identification des émetteurs déjà connue et standardisée, et utilisée notamment pour l'identification d'un émetteur proche dans un SFN. Néanmoins, cette technique n'est pas adaptée à l'identification de plusieurs émetteurs.

La technique de Positionnement Inversée est une technique proposée dans le cadre de cette étude. Elle est la technique d'identification des émetteurs la plus naturelle pour la méthode de positionnement proposée dans cette étude, puisqu'elle nécessite les mêmes contraintes que pour la discrimination des émetteurs, à savoir l'exclusion de zones iso-retards dans le SFN. Les autres pré-requis de cette technique sont 1) la connaissance des caractéristiques des émetteurs (position, retard artificiel) et 2) un position approximative du récepteur.

La technique du Positionnement Inversé fournit de bonnes performances dans les simulations effectuée, et est bien adaptée à la méthode de positionnement proposée dans cette étude. Elle est donc préférable à la technique de Watermarking.

D.6. Calcul de la position et performances dans le domaine des positions

Une fois que le récepteur a estimée les pseudo-distances et les a associées à des émetteurs, il doit les combiner afin de calculer sa position. Ce chapitre illustre les performances obtenues par la méthode proposée dans le domaine des positions. La position est calculée en utilisant un algorithme des moindres carrées non-linéaire, décrit dans l'annexe C. Cela permet notamment d'estimer l'impact des erreurs dues au biais NLOS qui n'est pas observable en regardant l'erreur sur les pseudo-distances uniquement, puisque la référence de pseudo-distance utilisée peut être elle-même affectée d'un biais NLOS.

Ce phénomène est illustré en calculant la position à partir de mesures de pseudo-distances idéales, c'est-à-dire en prenant le premier retard présent dans les mesures pour calculer la position.

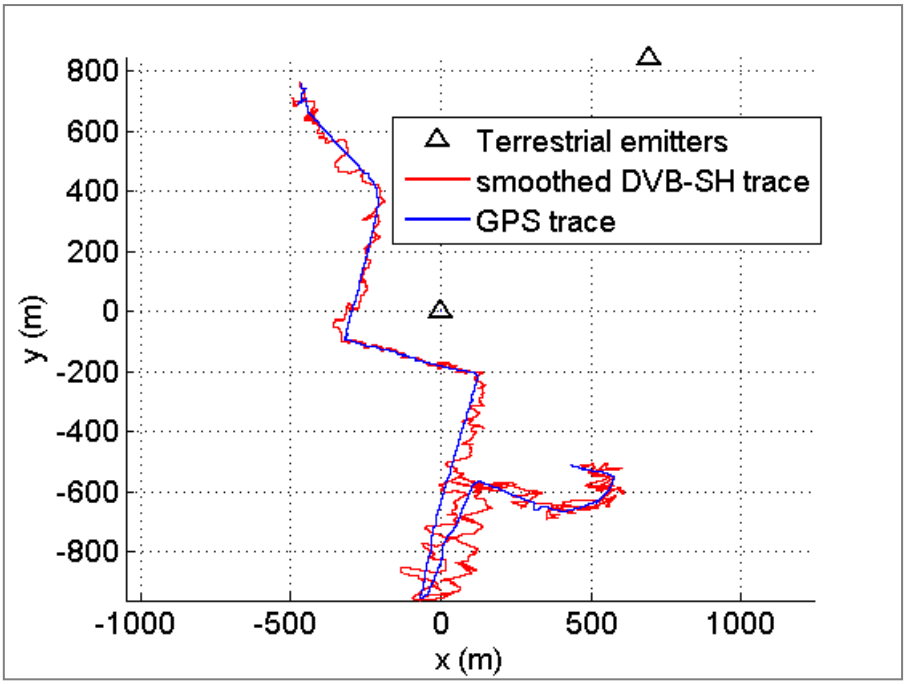

On peut observer les écarts importants de la position avec la trajectoire de référence, donnée ici un récepteur GPS utilisé lors de la collecte des mesures du sondage de canal.

Les sections 6.2 et 6.3 montrent les positions obtenues en utilisant les pseudo-distances estimées avec la méthode proposée. Les erreurs d'estimation apporte des dégradations supplémentaires.

Les meilleures performances de position sont une erreur absolue moyenne de 41.2m, obtenues en utilisant une combinaison de pseudo-distances estimée à l'aide de différentes méthode de fenêtrage. Bien que ces performances soient limitées comparées à d'autres systèmes de positionnement urbain, il faut noter que :

- **Seuls 3 émetteurs** ont été utilisés dans les simulations. Dans un SFN réaliste, un récepteur sera susceptible de poursuivre des signaux provenant de plus d'émetteurs.
- Une bande de transmission de 5 MHz a été utilisée, alors que le standard DVB-SH prévoit l'utilisation de bande plus large (jusqu'à 8 MHz). **L'utilisation d'une bande plus large** améliorerait les performances d'estimation des pseudo-distances, ce qui se traduirait par une meilleure performance dans le domaine des positions.
- **La position estimée est affectée par des sauts importants**, de plusieurs dizaines voire centaines de mètres, ce qui n'est pas cohérent avec la dynamique du récepteur (piéton ou véhicule) et pourrait donc être aisément détecté et mitigé. L'inclusion d'un modèle de la dynamique du récepteur, par exemple dans un filtre de Kalman, permettrait d'améliorer la précision de positionnement.
- **L'hybridation avec d'autres sources de positionnement** permettrait également de diminuer l'impact des la propagation NLOS sur la précision de positionnement. Par exemple, on pourrait hybrider la méthode de positionnement proposée avec des mesures GNSS ou inertielles.

D.7. Recommandations aux opérateurs pour la fourniture d'un service de navigation à partir d'un système DVB-SH

Le chapitre 7 du manuscrit fournit des recommandations aux opérateurs, notamment sur

- le **déploiement du SFN**, en termes de SNR minimum rencontré sur la couverture, et afin d'exclure les zones iso-retards par l'introduction de retards artificiels et la ré-utilisation des retards artificiels;
- le **choix du mode DVB-SH**, qui aura un impact à la fois sur la capacité du lien télécom (en termes de débit), et sur la précision du positionnement (en termes de variance d'estimateur et de robustesse contre les multitrajets)

D.8. Conclusion et perspectives

Le but de la thèse a été d'évaluer la possibilité d'un positionnement utilisant un système DVB-SH comme système d'opportunité.

Le DVB-SH est un standard de diffusion de la télévision numérique vers les récepteurs mobiles. Il a été sélectionné comme système d'opportunité notamment car il utilise un réseau d'émetteurs synchronisés (appelé SFN), qui permet l'utilisation de mesures de temps d'arrivée pour déterminer la pseudo-distance entre le récepteur et un émetteur. De plus, ce type de réseau d'émetteurs devraient être suffisamment dense pour permettre l'acquisition de pseudo-distance provenant de suffisamment d'émetteurs pour pouvoir calculer une position. Enfin, la fréquence centrale utilisée par le DVB-SH est proche d'autres bandes télécom, ouvrant la possibilité de partager des sous-systèmes du récepteur (tête RF, fonctions de traitement du signal) entre les service de communication et de positionnement, avec pour conséquence finale une réduction du coût et de la consommation électrique du récepteur.

Néanmoins, l'utilisation du DVB-SH présente également des défis à relever. La transmission de signaux à partir d'émetteurs terrestres dans un environnement urbain se traduit par d'intenses et abruptes atténuations de la puissance du signal, des multitrajets nombreux et un blocage récurrent du signal LOS. Par ailleurs, la modulation OFDM utilisée dans le DVB-Sh n'a pas encore été étudiée pour faire du positionnement. Enfin, l'utilisation du réseau en configuration SFN soulève des problèmes pour la discrimination et l'identification des émetteurs.

Les principales contributions de la thèse concernent 3 aspects du problème de positionnement :

- une méthode de traitement du signal pour estimer des pseudo-distances à partir de signaux DVB-SH;
- un modification au niveau système et une technique récepteur pour permettre l'identification des émetteurs dans un SFN;
- l'évaluation des performances de la solution de positionnement utilisant la méthode proposée.

De nombreuses pistes d'améliorations et de travaux futurs sont identifiés à la fin du chapitre 8.

Interface air pour systèmes de navigation en bande S :
Etude détaillée des signaux OFDM

Le positionnement en environnement urbain est un domaine de recherche actif, de par la croissance des services grand public liées la localisation, et à cause de réglementations émergentes liées aux situation d'urgence (E911). En environnement urbain ou à l'intérieur des bâtiments, il est communément admis que les systèmes de positionnement basés sur des satellites ne sont pas suffisants pour fournir une position précise, fiable et de manière continue. Des techniques de positionnement alternatives sont donc développées afin de remplacer ou compléter les systèmes de positionnement par satellite.

Cette thèse étudie la possibilité de fournir un service de positionnement utilisant un futur système de diffusion de télévision vers les mobiles basé sur le standard DVB-SH. Le principal attrait de ce système pour du positionnement est sa bonne couverture en milieu urbain, ainsi que l'utilisation d'un réseau d'émetteurs synchronisés. Il est donc possible d'employer des mesures de temps d'arrivée des signaux afin de réaliser une triangulation pour calculer la position d'un récepteur. Afin de fournir ce service innovant, des techniques spécifiques d'estimation de pseudo-distance et d'identification d'émetteurs ont été développées dans le cadre de cette thèse.

Le principal résultat de cette étude est d'avoir montré la faisabilité du positionnement utilisant un système DVB-SH, ne nécessitant que de légères modifications du système qui n'apportent aucune dégradation au service de diffusion TV. De premières simulations ont montré une précision de positionnement autour de 40m en utilisant des mesures réalistes de canal de propagation urbain.

Mots clés : OFDM, Positionnement urbain, Réseau iso-fréquence, signaux d’opportunité

S-band air interfaces for navigation systems :
A focus on OFDM signals

Positioning in urban or indoor environment is a hot topic, either due to regulations such as the E911 or due to the extension of location-based services targeting the mass market concentrated in metropolitan areas. In deep urban or indoor areas, it is generally recognized that satellite-based positioning systems are not suitable (alone) to provide a continuous, reliable and accurate position to the user. Therefore, alternative positioning techniques may be useful to complement or replace satellite positioning in these environments.

This study investigates the possibility of using a mobile TV system based on the DVB-SH standard as system of opportunity for positioning. The main interests of using this system are its good coverage in urban environment and its use of a synchronized network of emitter. It is therefore possible to use Time of Arrival measurements in order to compute a receiver's position using the trilateration principle. In order to provide this innovating service, specific techniques have been developped, in particular a pseudo-range estimation technique and a emitter identification technique.

The main result of this study is the proof of concept of positioning a receiver in urban environment using the DVB-SH system, that requires only slight system modification without degrading the initial TV broadcasting service. The proposed method is simulated using realistic channel sounding measurements and provides a mean positioning error around 40m.

Keywords : OFDM, Urban positioning, Single Frequency Network, Signals of Opportunity